

Functional Dynamics of Protein-Ligand Interactions

Dissertation
zur Erlangung des Doktorgrades
der Naturwissenschaften

vorgelegt beim Fachbereich
Chemische und Pharmazeutische Wissenschaften (FB 14)
der Johann Wolfgang Goethe-Universität
in Frankfurt am Main

von
Tanja Mittag
aus Mainz

Frankfurt 2004
(DF1)

vom Fachbereich Chemische und Pharmazeutische Wissenschaften (FB 14) der Johann Wolfgang Goethe-Universität als Dissertation angenommen.

Dekan:	Prof. Dr. Harald Schwalbe
Gutachter:	PD Dr. Ulrich Günther
	Prof. Dr. Harald Schwalbe
Datum der Disputation:	

Danksagung

Mein Dank gilt Herrn PD Dr. Ulrich Günther, der mich schon früh in meinem Studium für die Möglichkeiten der NMR-Spektroskopie im Allgemeinen und für Bindungsmechanismen von SH2-Domänen im Speziellen begeisterte. Ich danke ihm für die intensive Betreuung, für die Einblicke in seine analytische Denkweise und für die Möglichkeit zum selbständigen Arbeiten. Ich wünsche ihm und seiner Familie in Birmingham alles Gute.

Für die unerwartete dafür aber umso mehr geschätzte Unterstützung und Förderung danke ich herzlich Herrn Prof. Dr. Harald Schwalbe, der mich durch sein Engagement, seine Effizienz und seine Menschlichkeit beeindruckt. Vielen Dank für die Übernahme des Zweitgutachtens!

Herrn Prof. Dr. Heinz Rüterjans danke ich für die stete Unterstützung im Studium und während meiner Diplom- und Doktorarbeit, für die Förderung, die ich durch ihn erfahren habe, für einen Arbeitsplatz in seiner Arbeitsgruppe und für interessante Gespräche. Außerdem verdanken wir ihm maßgeblich die Existenz und die Ausstattung des NMR-Zentrums.

Herrn Prof. Dr. Volker Dötsch danke ich für einen Platz in seiner Arbeitsgruppe, für die gute Arbeitsatmosphäre, für sein Interesse und für seine Unterstützung.

Außerdem ein herzliches Dankeschön allen Mitgliedern der Arbeitsgruppen Rüterjans und Dötsch für die gute gemeinsame Zeit, für die produktive Zusammenarbeit, für eine freundschaftliche Atmosphäre, und für all die gemeinsam verbrachten Stunden, die das Leben so Lebenswert machen. Herrn Dr. Frank Löhr danke ich für seine Hilfe bei NMR-Experimenten, Sigrid Fachinger für ihre wunderbare Organisation, sowie Dr. Wesley McGinn-Straub für hilfreiche Vorschläge zu meiner Arbeit. Besonders danke ich auch Christina Fischer, Alexander Koglin und Marc-Michael Blum für ihre Freundschaft, für gute Gespräche und für ihre Unterstützung bei der Arbeit und im privaten Bereich. Ich freue mich auf Euren Besuch in Kanada!

I thank Prof. Dr. Brian Schaffhausen, Prof. Dr. Gian-Luigi Rossi and Prof. Dr. Lorella Franzoni for successful, interesting and instructive collaborations. I am particularly thankful to my dear friend Lorella, whose hospitality I could enjoy in Parma for three beautiful weeks in October 2003.

Bei meinen Eltern und meiner ganzen Familie bedanke ich mich für ihre immerwährende Unterstützung während meiner gesamten Ausbildung und darüber hinaus. Eure Liebe hat mich erst zu der gemacht, die ich heute bin. Außerdem möchte ich meinen Freunden danken, deren Zuneigung, Verständnis und Vertrauen in mich mir auf meinem Weg geholfen haben.

Am innigsten danke ich meinem Mann Roland, der mich seit Jahren mit seiner Liebe unterstützt, immer für mich da ist, wenn ich ihn brauche, der mir jedoch auch die nötige Freiheit für meine Arbeit gibt, und sich sogar von mir auf einen fremden Kontinent entführen lassen wird. Ich danke Dir von ganzem Herzen!

Contents

1	Zusammenfassung	7
2	Introduction	14
3	Dynamic Processes on the μs-ms Time Scale	15
3.1	New Methodologies involving Relaxation Dispersion Analysis	16
3.1.1	Characterizing Structural Transitions Using Relaxation Dispersion Analysis	16
3.1.2	Discrimination of Two-site Exchange from Complex Exchange Phenomena	17
3.2	Line Shape Analysis	18
3.3	Non-NMR Techniques	19
4	Chemical Exchange	21
4.1	Theoretical Background	21
4.1.1	McConnell Equations	24
4.1.2	Multi-site Exchange	26
4.1.3	Recursive Formula	28
4.1.4	Closed Analytical Expression for Two-site Exchange	28
4.2	Numerical Simulation of Relaxation Dispersion Curves	29
4.2.1	Comparison with the Analytical Expression	31
4.3	Analysis of Experimental Relaxation Dispersion Data	32
4.4	Line Shape Analysis of NMR Signals	32
4.4.1	Line Shapes for Binding Processes	35
4.5	Relaxation Dispersion for Complex Kinetic Models	38

<i>CONTENTS</i>	5
5 Proteins Used as Model Systems in this Work	41
5.1 SH2 Domains	41
5.1.1 Structure and Specificity of SH2 Domains	41
5.1.2 SH2 Function and Mechanisms of Signal Transduction	43
5.1.3 Tandem SH2 Domains	44
5.2 Phosphatidylinositide 3-kinase	45
5.2.1 Role of PI3K in Cellular Regulation	47
5.3 Polyoma Middle Tumor Antigen	48
5.4 The Cellular Retinol-Binding Protein	48
5.4.1 Functions of Cellular Retinol-Binding Proteins in the Cell	49
5.4.2 Retinol Binding to CRBP	49
6 Summary of Publications	52
6.1 Direct Observation of Protein-Ligand Interaction Kinetics	52
6.2 Probing Src Homology 2 Domain Ligand Interactions by Differential Line Broadening	53
6.3 Tracing Kinetic Intermediates during Ligand Binding	55
6.4 Novel Insights into the Mechanism of Retinol Binding by Cellular Retinol-Binding Protein	56
6.5 Freezing of Conformers of the Cellular Retinol-Binding Protein by Retinol	56
6.6 Complex Interaction of the N-SH2 Domain with a Doubly Phosphory- lated Peptide	57
7 Achievements of this Work and Outlook	60
8 Unpublished Results	63
8.1 Complex Interaction of the N-SH2 Domain with a Doubly Phosphory- lated Peptide	63
8.1.1 Results and Discussion	63
8.1.2 Conclusions	70

<i>CONTENTS</i>	6
References	71
9 Appendix	85
9.1 Abbreviations, Symbols, and Units	86
9.2 Matlab Script for the Numerical Simulation of Relaxation Dispersion Curves	88
10 Publications	89

1 Zusammenfassung

Funktionelle Dynamik von Protein-Liganden-Wechselwirkungen

Für das Verständnis der biophysikalischen Eigenschaften von Biomakromolekülen ist sowohl die Kenntnis ihrer Struktur als auch deren zeitliche Veränderung wichtig. Hochaufgelöste Strukturen von Proteinen in verschiedenen funktionellen Zuständen bestätigen, dass Funktion und Dynamik von Proteinen eng gekoppelt sein können. Wechselwirkungen von Proteinen und Liganden gehen oft mit erheblichen Konformationsänderungen einher. Die Strukturen des apo-Proteins und des Komplexes mit dem Liganden beantworten viele Fragen, indem sie Bindungsstellen und -oberflächen aufzeigen. Allerdings zeigen sie uns nur ein statisches Bild der Wechselwirkung. Auch wenn die Strukturen des freien Proteins und des Komplexes bekannt sind, weiß man oft wenig über den Übergang zwischen beiden.

Die Untersuchung dynamischer Vorgänge in Proteinen und ihrer biologischen Relevanz wurde durch methodische Fortschritte in der NMR-Spektroskopie belebt. In den letzten Jahren konzentrierten sich Dynamikstudien hauptsächlich auf den Mikro- bis Millisekunden (μs -ms) Zeitbereich, denn viele wichtige biologische Prozesse wie katalytische Umsetzungen, Ligandenbindung und -lösung, korrelierte Bewegungen großer Proteinsegmente und -domänen finden mit Geschwindigkeitskonstanten von $10^3 - 10^6 \text{ s}^{-1}$ statt. Dynamik im μs -ms Zeitbereich kann mittels Linienformanalyse von NMR-Signalen (Binsch, 1968; Sandström, 1982; Rao, 1989; Lian and Roberts, 1993; Günther and Schaffhausen, 2002) oder Relaxationsdispersionsuntersuchungen, die sich in Carr-Purcell-Meiboom-Gill- (CPMG) (Carr and Purcell, 1954; Meiboom and Gill, 1958) und $T_{1\rho}$ - Experimente (Deverell *et al.*, 1970; Szyperski *et al.*, 1993; Zinn-Justin *et al.*, 1997; Mulder *et al.*, 1998) gliedern, charakterisiert werden.

Die theoretischen und experimentellen Grundlagen zur *Relaxationsdispersion* wurden vor Jahrzehnten etabliert (Carr and Purcell, 1954; Meiboom and Gill, 1958; Carver and Richards, 1972; Jen, 1978). Neue Isotopen-Markierungsstrategien für Biomakromoleküle sowie Fortschritte in der heteronuklearen NMR-Spektroskopie ermöglichen es, chemischen und konformationellen Austausch des Proteinrückgrats (Loria *et al.*, 1999a,b; Tollinger *et al.*, 2001; Wang *et al.*, 2001a; Ishima *et al.*, 2004) und der Seitenketten (Mulder *et al.*, 2001b, 2002) genau und zuverlässig zu charakterisieren. Deshalb konnten mit Hilfe von Relaxationsdispersionsexperimenten allosterische Prozesse (Volkman *et al.*, 2001), Protein-Liganden-Wechselwirkungen (Feher and Cavanagh, 1999; Mulder *et al.*, 2001a; Evenäs *et al.*, 2001; Mittag *et al.*, 2003b) und auch enzymatische Katalyse (Eisenmesser *et al.*, 2002) untersucht werden. Allerdings ist die Charakterisierung komplizierter Austauschprozesse noch immer schwierig. Den meisten Untersuchungen lag bisher die

Annahme eines Zwei-Zustands-Modells zur Erklärung des chemischen Austauschs zugrunde.

Eine zu CPMG-Experimenten komplementäre NMR-Methode zur Untersuchung kinetischer Prozesse ist die *Linienformanalyse von NMR-Signalen*, eine etablierte Technik zur Untersuchung chemischen Austauschs in kleinen Molekülen. Die Analyse von Signalen zweidimensionaler Spektren (z. B. ^1H - ^{15}N -HSQC-Spektren) ermöglicht die aminosäurespezifische Charakterisierung von Austauschparametern in Proteinen. Um Protein-Liganden-Wechselwirkungen zu studieren, kann man Serien von Spektren für steigende Ligandenkonzentrationen aufnehmen und die Verschiebung und Form der Signale untersuchen. Aus diesen Linienformen können kinetische Raten und Informationen über *Bindungsmechanismen* abgeleitet werden (Chan and Reeves, 1972; Binsch, 1975; Rao, 1989; Günther and Schaffhausen, 2002; Günther *et al.*, 2002).

Das Ziel dieser Arbeit war, die funktionelle Dynamik von Proteinen bei der Bindung von Liganden zu charakterisieren und das Potential von Relaxationsdispersions- und Linienformanalyse bei dieser Problemstellung zu vergleichen. Als Modellsystem diente dazu zunächst die Wechselwirkung der *N-terminalen SH2-Domäne* ('Src Homology 2 domain') der Phosphatidylinositol 3-Kinase (PI3K) mit Phosphopeptiden. SH2-Domänen vermitteln Protein-Protein-Wechselwirkungen in Signaltransduktionprozessen durch die spezifische Bindung phosphorylierter Tyrosinreste (pTyr) in bestimmten Peptidsequenzen, wobei die drei Aminosäurereste C-terminal zum pTyr für die Spezifität der Wechselwirkung entscheidend sind.

Zunächst wurde der *Effekt der Ligandenbindung auf die μs -ms Dynamik der N-SH2-Domäne* untersucht. Zu diesem Zweck wurden CPMG-Experimente für die Amidstickstoffkerne des Proteinrückgrats bei zwei verschiedenen Magnetfeldern (11,7 T und 16,4 T) durchgeführt (Mittag *et al.*, 2003b). Als Ligand diente ein Peptid von acht Aminosäuren Länge mit der Sequenz der Bindungsstelle des Middle Tumor Antigens (EEEpYMPME-NH₂, im Folgenden als MT8 bezeichnet) für die Phosphatidylinositol-3-Kinase (PI3K). Der Einfluss der Ligandenbindung auf die Mobilität war durch Experimente bei verschiedenen Ligandenkonzentrationen zugänglich: (1) Das freie Protein, (2) der N-SH2:MT8-Komplex und (3) eine Probe der N-SH2-Domäne, die 1/20 der für die vollständige Sättigung nötige Peptidkonzentration enthielt, wurden untersucht. Die Relaxationsdispersionkurven wurden für jeden Aminosäurerest individuell für ein Modells für Austausch zwischen zwei Zuständen ausgewertet. Die freie N-SH2-Domäne zeigte limitierten konformationellen Austausch auf der ms-Zeitskala in der EF- und in der BG-Schleife. Dies sind zwei Regionen des Proteins, die die Aminosäurereste C-terminal des pTyrs koordinieren und die Spezifität der Wechselwirkung vermitteln.

Relaxationsdispersionsexperimente in der Gegenwart von 1/20 Äquivalent MT8 zeigten

ausgeprägten chemischen Austausch im zentralen β -Faltblatt, in der EF- und in der BG-Schleife und in der pTyr-Bindungstasche. In Gegenwart geringer Konzentration eines hochaffinen Liganden entspricht die Austauschrate näherungsweise der Geschwindigkeitskonstante der Dissoziation. Interessanterweise variieren die Geschwindigkeitskonstanten für verschiedene Aminosäurereste der N-SH2-Domäne. Diese Unterschiede der Geschwindigkeitskonstanten der Dissoziation können als lokale Lebenszeiten des Komplexes und damit als unterschiedliche lokale Affinitäten interpretiert werden. Außerdem konnten komplexere Austauschphänomene als der typische Ein-Schritt-Bindungsmechanismus $P+L \rightleftharpoons PL$ in der EF-Schleife und in Teilen des β -Faltblatts nachgewiesen werden. Die aus Titrationsexperimenten bekannte Differenz der chemischen Verschiebung des freien und des komplexierten Proteins konnte für einige Aminosäurereste nicht zur Interpretation ihrer Relaxationsdispersionskurven herangezogen werden. Dies zeigt, dass der durch kleine Mengen Peptids initiierte chemische Austausch nicht vollständig auf Bindung und Lösung des Peptids zurückzuführen ist, sondern zusätzlich auf konformationellen Austausch des Proteins. Die Austauschpartner des freien Proteins sind wahrscheinlich Konformere, die bei der Wechselwirkung mit dem Liganden gebildet werden und gering populierte Intermediate auf dem Reaktionsweg darstellen. Der 1:1-Komplex aus N-SH2 und MT8 ist konformationell stabil. Größere Austauschbeiträge sind nur für einige Aminosäurereste der BG-Schleife beobachtbar.

Die Untersuchung bestätigte die Schlüsselrolle einiger Aminosäurereste der EF- und der BG-Schleife zusammen mit Resten des β -Faltblatts. Die Geschwindigkeitskonstanten der Aminosäurereste des zentralen β -Faltblatts, deren Seitenketten in die Richtung der EF- und der BG-Schleife zeigen, sind sehr ähnlich, was die Möglichkeit korrelierter Bewegungen dieser wichtigen Segmente nahelegt.

Die Wechselwirkung der N-SH2 Domäne mit MT8 wurde außerdem mittels Linienformanalyse von Signalen aus ^1H - ^{15}N -HSQC-Spektren untersucht, die für steigende Konzentrationen des Liganden aufgenommen wurden (Günther *et al.*, 2002). 37 Aminosäurereste, deren Signale sich bei der Wechselwirkung sukzessive verschoben, konnten analysiert werden. Die erhaltenen Geschwindigkeitskonstanten variierten für verschiedene Positionen im Protein und zeigten eine gute Übereinstimmung mit Raten aus Relaxationsdispersionsexperimenten. Zur Interpretation der Linienformen von Aminosäureresten der α -Helix B, einzelner Reste der BG-Schleife und der gesamten α -Helix A konnte ein Zwei-Zustands-Modell herangezogen werden. Dagegen wiesen die Signale einiger Reste des zentralen β -Faltblatts, der EF-Schleife und der BG-Schleife für mittlere Ligandenkonzentrationen Schultern auf. Die Komplexität der Linien lässt sich mit einem parallelen Bindungsmechanismus erklären.

Um zu untersuchen, ob die beobachteten Effekte spezifisch für die Bindung von MT8 waren, wurden Wechselwirkungen der N-SH2-Domäne mit pTyr und einem acht

Aminosäure langen Peptid untersucht, das von der Sequenz des PDGF Rezeptors ('platelet derived growth factor receptor', SVDpYVPML-NH₂) abgeleitet ist. Interessanterweise führte nur die Wechselwirkung mit MT8 und dem PDGFr-Peptid zu einem Konformeren-Gleichgewicht während der Bindung. In der Mutante I381Y ist Position β D5, die zu einem großen Teil die Spezifität der SH2-Domäne bestimmt, von Isoleucin zu Tyrosin mutiert. Die resultierende Präferenz für hydrophile Peptidsequenzen führt zu einem Affinitätsabfall gegenüber MT8. Die im Wildtyp bei der Bindung eines hochaffinen Liganden induzierten Intermediate werden offensichtlich weder bei der Wechselwirkung mit Phosphotyrosin ($K_D \approx 1$ mM) noch bei der Bindung eines Phosphopeptids an die niedriger affine Mutante I381Y hervorgerufen. Möglicherweise trägt das Fehlen dieser Intermediate sogar zu der verringerten Affinität bei. Von dieser Hypothese ausgehend, zeigt die Mutante P427L, die eine Mutation im β G-Strang aufweist und eine um drei Zehnerpotenzen verringerte Affinität gegenüber MT8 besitzt, ein überraschendes Verhalten. Signale aus Titrationspektren der P427L SH2-Domäne mit MT8 weisen eine ungewöhnlich starke Komplexität mit je vier bis fünf Signalkomponenten auf. Außerdem scheinen die Geschwindigkeitskonstanten der Dissoziation mit Werten zwischen 100 s^{-1} und 1000 s^{-1} einer mikromolaren Affinität zu entsprechen. Im Vergleich zur Wildtyp N-SH2-Domäne und der Mutante I381Y könnte die Assoziations-Geschwindigkeitskonstante durch eine niedrige Verfügbarkeit bindender Konformere verringert sein. Müssen unproduktive Wechselwirkungen wieder gelöst werden, bevor es zu einer endgültigen Bindung kommt, verringert auch dies die scheinbare Geschwindigkeitskonstante der Assoziation.

Die beobachteten Linienformen belegen, dass die Bindung von Phosphopeptiden an die N-SH2-Domäne Umlagerungen im Protein bewirkt, die für den Bindungsprozess essentiell sind. Langsame Prozesse in Schleifen und angrenzende Regionen bestimmen die Geschwindigkeitskonstante der Wechselwirkung.

Eine Fehlerabschätzung der erhaltenen Geschwindigkeitskonstanten der Dissoziation zeigt, dass der Fehler hauptsächlich durch die relativ geringe Änderung der Linienformen bei der Variation der Rate bestimmt wird. Der Einfluss des Signal/Rausch-Verhältnisses auf den Gesamtfehler beträgt nur wenige Prozent. Dagegen reagiert der Fehler sehr sensitiv auf das Verhältnis der Austauschrate zur Differenz der chemischen Verschiebungen.

Mit dieser Publikation wurde die Linienformanalyse als Methode zur Untersuchung von Protein-Liganden-Wechselwirkungen etabliert. Die Analyse von 2D-Proteinspektren erlaubt dabei, einzelnen Aminosäureresten spezifisch verschiedene kinetische Modelle zuzuordnen. Für eine quantitative Analyse ist ein ähnlicher Bereich an Austauschraten zugänglich wie bei CPMG-Experimenten. Jedoch bietet die Linienformanalyse mechanistische Information und die Möglichkeit, kinetische Intermediate direkt zu visualisieren.

Darüberhinaus wurden die Bindungseigenschaften der Mutante P395S untersucht (Mittag

et al., 2004b). Eine Mutation der Position 395 in der EF-Schleife der N-SH2-Domäne von Prolin zu Serin verändert die Spezifität für die Sequenz der Phosphopeptide. Obwohl die EF-Schleife bekanntermaßen mit der dritten Aminosäure C-terminal zum pTyr (Position +3) wechselwirkt, ändert sich die Spezifität für die Position +1. Die Affinität für die Sequenz des PDGF-Rezeptors (relevante Sequenz pYVPM) bleibt erhalten, während MT8 (pYMPM) nur noch mit geringer Affinität gebunden wird. Die Linienformanalyse der Signale aus ^1H - ^{15}N -HSQC-Spektren der P395S SH2-Domäne für steigende Konzentrationen der beiden Liganden enthüllte unterschiedliche Bindungsmechanismen der Phosphopeptide. Die Bindung von MT8 verläuft über einen Zwei-Schritt-Mechanismus. Zunächst erfolgt ein typischer Bindungsvorgang, der bei Liganden/Protein-Konzentrationsverhältnissen von 0.7-0.9 zum Aufbau des Signals eines Intermediates führt. Dieser Zustand ist allerdings relativ instabil, wie seine hohe Dissoziations-Geschwindigkeitskonstante bestätigt. Zur Bildung des Endprodukts der Titration, des P395S-MT8-Komplexes, bedarf es eines weiteren Bindungsvorgangs. Da die Wechselwirkung mit einer 1:1-Stöchiometrie stattfindet, muss es nach dem unproduktiven ersten Bindungsvorgang zu einer Lösung der Wechselwirkung mit nachfolgender Wiederverwendung des Liganden kommen. Die Bildung des stabilen Intermediats für relativ hohe Peptid/Protein-Konzentrationsverhältnisse stellt eine kinetische Barriere für die Umwandlung zum Produkt dar und ist als eine Ursache für die verminderte Affinität zu nennen.

Auch das PDGFr-Peptid wird über einen Zwei-Schritt-Mechanismus gebunden; jedoch erfolgt die Umwandlung in ein bindendes Konformer hier bereits bei geringen Liganden/Protein-Konzentrationsverhältnissen von ca. 0.1. Dies äussert sich in einem auffälligen ersten Titrationsschritt, der sich in der Änderung der Intensität und der chemischen Verschiebung deutlich von den nachfolgenden Schritten unterscheidet. Ab einem Konzentrationsverhältnis von 0.1 gleichen die Linienformen denen eines typischen Ein-Schritt-Bindungsvorgangs. Eine erste Wechselwirkung zwischen P395S und PDGFr-Peptid führt zu einer Umlagerung des Proteins oder zur Stabilisierung eines Konformers eines bereits im freien Zustand vorliegenden Gleichgewichts. Das Intermediat besitzt eine hohe Lebensdauer. Die Zugabe des Liganden scheint die Aktivierungsenergie zur Umwandlung des freien Proteins in das bindende Konformer zu verringern.

Bemerkenswerterweise ist für die P395S-Mutante der N-SH2-Domäne ebenfalls die Bildung mehrerer Konformere bei der Wechselwirkung mit dem höher affinen Liganden, nämlich dem PDGFr-Peptid, in Schlüsselpositionen des Proteins zu beobachten. Im Falle der Bindung von MT8 zeigen nur wenige Aminosäurereste in sehr mobilen Schleifenregionen komplexe Linienformen. Die Untersuchung des unterschiedlichen Bindungsverhaltens der P395S SH2-Domäne bezüglich zweier in der Sequenz nur leicht abweichender Peptide zeigt die Möglichkeit auf, dass Spezifität nicht nur strukturell, sondern auch

kinetisch kontrolliert wird.

Um das Potential der verwendeten NMR-Techniken an einem weiteren Protein zu demonstrieren, wurde das Protein *CRBP* ('*cellular retinol-binding protein*') und seine Wechselwirkung mit dem spezifischen Liganden *Retinol* untersucht (Mittag *et al.*, 2003a). *CRBP* gehört zur Familie der intrazellulären Lipid-Bindungsproteine ('intracellular lipid binding proteins', iLBPs), Speicher für hydrophobe Liganden in der Zelle, die als gemeinsames Strukturmotiv ein β -Fass aus zwei je fünfsträngigen, antiparallelen β -Faltblättern aufweisen. Ein Helix-Turn-Helix-Motiv verschließt eine Seite des Fasses, wodurch eine vom Solvens abgeschlossene Kavität entsteht, in der der hydrophobe Ligand gebunden wird. Strukturen von apo- und holo-*CRBP* weisen sehr ähnliche geschlossene Konformationen auf, die keinen Aufschluss über den Ort und den Mechanismus des Eintritts von *Retinol* geben. Die Schleifenregionen des Fasses sind auf einer schnellen Zeitskala im Pikosekunden- bis Nanosekundenbereich flexibel. Dagegen ergaben Relaxationsdispersionsexperimente eine hohe Mobilität im Millisekundenbereich im gesamten β -Faltblatt. Die höchsten Austauschbeiträge als auch die größten strukturellen Abweichungen, die sich als größte Unterschiede der chemischen Verschiebungen der austauschenden Zustände niederschlagen, sind dagegen in der α -Helix II, in der Verbindungsregion der beiden α -Helices und in der β C- β D-Schleife zu finden. Die höchste Millisekunden-Mobilität ist in der Region zu finden, in der aufgrund von Vergleichen mit Strukturen anderer iLBPs die Portalregion vermutet wird.

Die Untersuchung des Bindungsvorgangs von *Retinol* an *CRBP* mittels Linienformanalyse ergab einen komplexen Bindungsmechanismus, der mehrere sequentielle Schritte beinhaltet (Mittag *et al.*, 2004a). Zunächst erfolgt eine initiale, unspezifische Wechselwirkung von *Retinol* mit Aminosäureresten auf der Oberfläche von *CRBP*. In einer erweiterten Portalregion führt diese Interaktion zu einer Umwandlung der im freien Protein vorhandenen Millisekunden-Dynamik zu langsamem konformationellen Austausch. Von den dabei auftretenden langlebigen Intermediaten weisen wahrscheinlich wenigstens einige offene Konformationen auf, die den Eintritt von *Retinol* in die Kavität erlauben. Dort wird *Retinol* mit hoher Affinität gebunden, die sich in einer Dissoziationskonstante von 0.1 nM widerspiegelt. Ein weiterer, zu beobachtender Schritt scheint die unspezifische Aggregation von *Retinol* an den Komplex wider zu spiegeln. Die Linienformanalyse ermöglichte damit nicht nur die Lokalisation der Portalregion, sondern auch die Aufklärung mehrerer Schritte eines komplexen Bindungsmechanismus.

In der vorliegenden Arbeit wurden zwei komplementäre, sich ergänzende NMR-Techniken verwendet, um die Kinetik der Ligandenbindung an zwei strukturell und funktionell unterschiedlichen Proteinen zu untersuchen. Die Charakterisierung der Mikro- bis Millisekunden-Dynamik der freien Proteine und der Komplexe bei verschiedenen

Ligandenkonzentrationen ermöglichte die Unterscheidung proteineigener Dynamik von Liganden-induzierter Mobilität. Die Linienformanalyse ergab für beide Systeme unerwartet komplexe Bindungsmechanismen. Das Auftreten langlebiger Intermediate mit Lebendauern von mehreren Millisekunden ist für die Funktion beider Proteine essentiell. In der SH2-Domäne werden Konformerengleichgewichte durch die Wechselwirkung mit dem Liganden initiiert, während CRBP-Konformere, die bereits in der apo-Form vorhanden sind, durch die Wechselwirkung kinetisch stabilisiert werden. Die veränderte Dynamik der Proteine zeigt eindeutig eine Wirkung auf die Ligandenbindungseigenschaften, auf die Affinität und auf die Spezifität. Diese Beobachtungen lassen sich im Rahmen des allosterischen Modells von Cooper und Dryden interpretieren. Sie schlugen ein alternatives Modell für allosterische Prozesse vor, das besagt, dass allosterische Prozesse nicht unbedingt auf Konformationsänderungen von Proteinen beruhen müssen, sondern ihre Ursache auch in der Änderung der konformationellen Entropie haben können.

Die detaillierte Untersuchung kinetischer und thermodynamischer Parameter von Proteinen ist essentiell, um unser Verständnis ihrer Eigenschaften zu verbessern. Dank der Entwicklung neuer Techniken werden Kernfragen der Proteinfaltung, der Ligandenbindung und der enzymatischen Katalyse zugänglich. Die Methoden sind selbstverständlich auch für die Untersuchung anderer Biomoleküle wie RNAs, Phospholipide und Polysaccharide einsetzbar. Neben der Befriedigung theoretischen Interesses an grundlegenden Fragen über Proteineigenschaften könnten die Methoden auch praktische Relevanz entwickeln. Das Studium der Mechanismen, wie Intermediate den Umsatz zu funktionellen Komplexen verhindern, ermöglicht einen alternativen Ansatz für die Entwicklung von Arzneistoffen. Die Stabilisierung nicht-funktioneller Zustände stellt eine Möglichkeit dar, therapeutisch interessante Zielmoleküle zu inhibieren. Relaxationsdispersionsexperimente und die Linienformanalyse sind zwei Techniken, die auch in Zukunft interessante Impulse in diese Richtung versprechen.

2 Introduction

Toward a fundamental understanding of the relationship between structure and function of biological macromolecules, the knowledge of the three-dimensional (3D) structure and its time-dependent variation, the dynamics of the molecule, is crucial. The flexibility of biomolecules, proteins in particular, can be coupled closely to their function, as evident from the increasing number of high-resolution structures that show large-scale conformational changes between two different functional states of the protein, e.g. between the active and the inactive conformation or between the apo-form and the conformation with bound ligand. If protein-ligand interactions shall be studied, structures provide detailed information on binding sites and surfaces. However, the two static structures insufficiently explain the determinants of affinity and specificity of the dynamic process. Knowledge of the structures of the free protein and the complex does not include information on the transition between them.

In the past mechanisms of enzymatic turnover were studied extensively employing information obtained e.g. from biochemical assays, isotope replacement and fluorescence measurements, whereas surface plasmon resonance represents a suitable technique for the investigation of ligand binding. However, protein function often involves transitions to low-populated excited states, which are difficult to characterize with the aforementioned methods. Additionally, recent work (Volkman *et al.*, 2001) begun to question the inherent dynamic processes of proteins that contribute to their biological function (Fersht, 1999; Wand, 2001). Current studies on protein dynamics focus on the microsecond to millisecond (μs -ms) time scale (which corresponds to rates of $10^3 - 10^6 \text{ s}^{-1}$), because many biologically relevant processes like enzyme catalysis and ligand binding involve steps with kinetic rates in this range. As was noted by Wand (Wand, 2001), kinetically relevant motion does not necessarily have to be on the time scale of catalysis or binding. If the processes are only weakly coupled, the kinetically relevant motion may be significantly faster than the functional event. It is thus important to study the dynamics of proteins on a large range of time scales. NMR spectroscopy is best suited to provide a wealth of information on the picoseconds to seconds time scale by employing a variety of different experimental techniques as depicted in Figure 1. Motions on the ps-ns time scale significantly contribute to the entropy of the system, whereas μs -ms dynamics include correlated motions and large-scale conformational changes of the molecule.

Recent studies confirm the functional relevance of μs -ms dynamics that can be investigated using Carr-Purcell-Meiboom-Gill (CPMG) (Carr and Purcell, 1954; Meiboom and Gill, 1958) and $T_{1\rho}$ (Deverell *et al.*, 1970; Szyperski *et al.*, 1993; Zinn-Justin *et al.*, 1997; Mulder *et al.*, 1998) relaxation dispersion experiments and line shape analysis (Binsch, 1968; Sandström, 1982; Rao, 1989; Lian and Roberts, 1993; Günther and Schaffhausen,

2002). Experimental data is particularly valuable because molecular dynamics simulation methods still fail to cover this range of time scales.

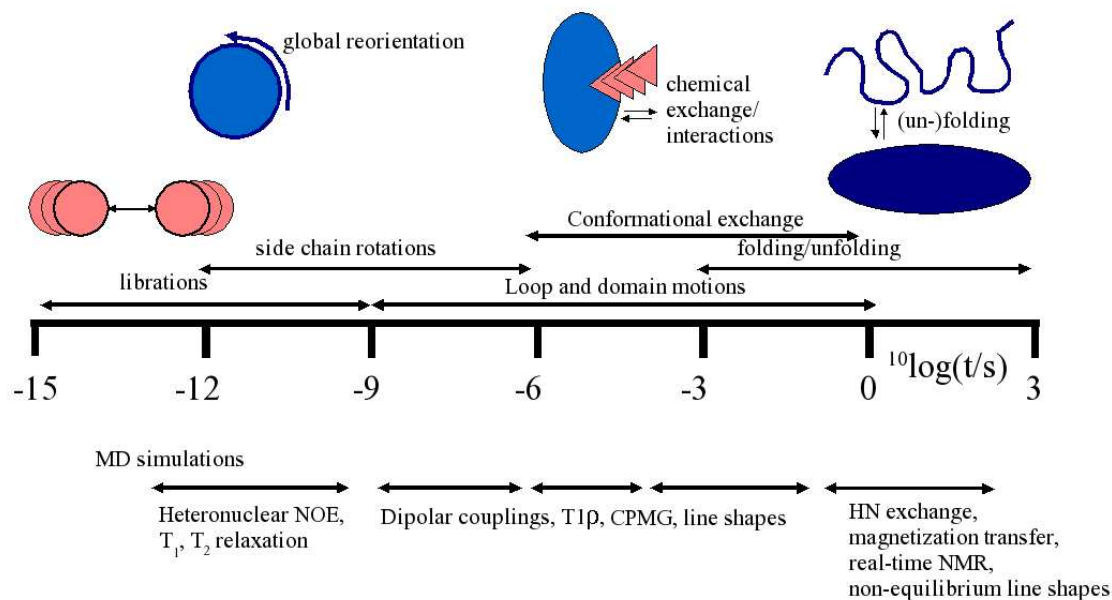


Figure 1: Time scales of protein dynamics accessible by NMR techniques. NMR spectroscopy allows for the characterization of dynamic processes on time scales of picoseconds to hundreds of seconds, corresponding to at least fourteen orders of magnitude. Thus, a large variety of dynamic processes including internal librations, side chain rotations, loop and domain reorientations, folding processes, and intermolecular exchange, such as ligand binding, can be investigated, many of them at atomic resolution. The Figure is adapted from M. Akke.

3 Dynamic Processes on the μ s-ms Time Scale

The basic theory and experimental approaches underlying relaxation dispersion analysis were established decades ago (Carr and Purcell, 1954; Meiboom and Gill, 1958; Carver and Richards, 1972; Jen, 1978). However, advances in heteronuclear NMR spectroscopy of isotopically enriched biomolecules now allow for the sensitive and reliable investigation of exchange phenomena within the protein backbone (Loria *et al.*, 1999a,b; Tollinger *et al.*, 2001; Wang *et al.*, 2001a; Ishima *et al.*, 2004) and side chains (Mulder *et al.*, 2001b, 2002). Many recent NMR studies have provided evidence for dynamics on the μ s-ms time scale in regions of proteins that definitely contribute to *in vivo* function. Thus, the dynamics of macromolecular recognition, ligand binding (Kristensen *et al.*, 2000; Evenäs *et al.*,

2001; Volkman *et al.*, 2001; Mulder *et al.*, 2001a; Lu *et al.*, 2003; Mittag *et al.*, 2003b,a), and catalysis (Eisenmesser *et al.*, 2002; Wang *et al.*, 2001b; Rozovsky and McDermott, 2001; Cole and Loria, 2002) were studied.

Volkman *et al.* showed allosteric behavior in a single-domain signaling protein where phosphorylation stabilizes the active conformation which is already transiently present in the nonphosphorylated state (Volkman *et al.*, 2001). In the case of a cavity mutant of T4 lysozyme that exchanges with an excited state capable of binding small molecules, the dynamic process was analyzed kinetically and thermodynamically with relaxation dispersion experiments at different static magnetic fields and temperatures (Mulder *et al.*, 2001a). Evenäs *et al.* demonstrated that the global rate of interconversion between open and closed states of calmodulin coincides with the estimated calcium off-rate, suggesting that calcium release is triggered by conformational mobility (Evenäs *et al.*, 2001). In contrast, binding of phosphopeptides to a src homology 2 (SH2) domain does not lead to one correlated exchange process with a single off-rate for the protein. Instead binding is characterized by site-specific differences in kinetic rates that can be interpreted as variations in local affinities as presented in this work (Mittag *et al.*, 2003b). In the apo-state of the cellular retinol-binding protein I (CRBP), strong conformational exchange in the portal region leads to the transient opening of the otherwise solvent-shielded cavity to allow high-affinity binding of retinol (Lu *et al.*, 2003; Mittag *et al.*, 2003a). For ribonuclease A (Cole and Loria, 2002), binase (Wang *et al.*, 2001b), triosephosphate isomerase (Rozovsky and McDermott, 2001), and cyclophilin A (Eisenmesser *et al.*, 2002), the rates of conformational exchange involving critical residues coincide with the catalytic rate suggesting that the protein-inherent dynamics are rate-limiting for the catalysis.

3.1 New Methodologies involving Relaxation Dispersion Analysis

3.1.1 Characterizing Structural Transitions Using Relaxation Dispersion Analysis

Protein function correlates with dynamic processes on different time scales and often involves transitions to low-populated excited states that structurally differ from the ground state. Relaxation dispersion experiments at different static magnetic fields and temperatures allow the characterization of kinetic and thermodynamic parameters of these states if they are populated to higher than 0.5 %. The analysis also yields information on structural transitions in the form of chemical shift differences $\Delta\omega$ between exchanging states. The fact that only the magnitude of the chemical shift difference is obtained from relaxation dispersion experiments, exacerbates the translation into conformational changes. To obtain the sign of $\Delta\omega$ requires the analysis of the field dependence of the chemical shift or the comparison of chemical shifts in HMQC and HSQC spectra (Skrynnikov *et al.*, 2002).

The accessibility of the atomic structures of the states undergoing conformational exchange were initially demonstrated by Palmer and coworkers. They were able to assign a conformational exchange process in BPTI to the isomerization of a specific dihedral angle by comparison of the chemical shift difference obtained from relaxation dispersion analysis with both a chemical shift database and chemical shifts calculated from the proposed structure (Grey *et al.*, 2003). For mutants of a Fyn SH3 domain, Kay and coworkers could characterize the full set of kinetic and thermodynamic parameters of a folding intermediate that is present in low population in equilibrium with the folded and the unfolded states (Korzhnev *et al.*, 2004b). The comparison of chemical shifts in all three states allowed the calculation of structural ensembles of the intermediate state by assuming that the chemical shift of the intermediate reflects the number of native contacts of each amide. This approach was originally developed for the calculation of transition state structures from protein engineering Φ values (Vendruscolo *et al.*, 2001; Paci *et al.*, 2002). In addition, the analysis of residual dipolar couplings in terms of structural fluctuations is useful to obtain information on amplitude and directionality of the motion (Tolman *et al.*, 2001; Meiler *et al.*, 2001; Peti *et al.*, 2002). Wang *et al.* have confirmed concordance of structural regions undergoing conformational exchange and structural fluctuations as revealed by residual dipolar couplings (Wang *et al.*, 2001b).

3.1.2 Discrimination of Two-site Exchange from Complex Exchange Phenomena

The general approach still commonly used for the interpretation of experimental relaxation dispersion data assumes a simple two-site exchange model. Often, this assumption is not justified, but the discrimination of two-site exchange phenomena from more complex mixtures of processes is often cumbersome. If the rate constants of individual processes differ significantly by at least one order of magnitude but they are all in the accessible μ s-ms window, a discrimination is possible from single-quantum coherence relaxation dispersion data measured at different magnetic fields (Grey *et al.*, 2003; Korzhnev *et al.*, 2004b).

In this regard, correlated chemical shift modulation of pairs of nuclei (e.g. $^1\text{H}^N$ and $^{15}\text{N}^H$), which can be observed as relaxation dispersion of zero-, double- and multiple-quantum coherences provide additional information (Orekhov *et al.*, 2004; Korzhnev *et al.*, 2004a; Dittmer and Bodenhausen, 2004). A combination of relaxation dispersion experiments of different coherences allows the characterization of the exchange of both nuclei and facilitates the recognition of complex exchange between more than two sites.

3.2 Line Shape Analysis

Line shape analysis of NMR signals, a well-established technique to characterize μ s-ms exchange processes of small molecules, complements the relaxation dispersion approach. Traditionally, line shapes were derived from one-dimensional (1D) NMR spectra (Kern *et al.*, 1995). Application to small molecules was facile, but extensive overlap in ^1H NMR spectra of proteins limited line shape analysis to isolated proton signals. Advances in heteronuclear NMR spectroscopy of isotopically enriched biomolecules now allow the site-specific investigation of exchange in proteins. Line shape analysis is now also applicable to signals of two-dimensional (2D) protein spectra, mostly ^1H - ^{15}N HSQC spectra. Balbach used the analysis of non-equilibrium line shapes of protein signals to study protein folding (Balbach *et al.*, 1996). Recently, it also has been shown that line shape analysis is applicable to the site-specific investigation of protein-ligand interactions (Günther and Schaffhausen, 2002). Protein spectra with varying concentrations of ligands provide kinetic information on the binding process and, even more importantly, on the *mechanism* of the interaction (Chan and Reeves, 1972; Binsch, 1975; Rao, 1989; Günther and Schaffhausen, 2002; Günther *et al.*, 2002). Deviating intensity, shape and chemical shift, of the experimental signals compared to lines expected for simple one-step binding, are used to model populations, frequencies, and lifetimes of additional protein states. Mechanistic information is not easily available from relaxation dispersion data if measured only at one ligand concentration. Indeed, the most complicated system reliably analyzed using relaxation dispersion analysis is exchange between three sites as a two-step sequential model. In contrast, line shape analysis allows for the distinction of sequential and parallel mechanisms (Mittag *et al.*, 2004b). Additionally, information on structural transitions to intermediate states is obtained from chemical shifts of intermediates.

The line width of the resonances in HSQC spectra and chemical shift degeneracy of signals constitute the basic limitations of the method. The kinetic rates must fall within the window of fast to intermediate exchange on the NMR time scale. This window can be expanded by variation of magnetic field strength and temperature. Although the structures of the intermediates usually are not accessible, the visualization of intermediates in spectra provide new and substantial information toward the understanding of protein-ligand interactions.

Through the investigation of interactions of a proteins with various analogs of a ligand, line shape analysis may address basic questions of protein-ligand interactions, such as the affinity and specificity determinants as well as the influence of internal dynamics on binding properties.

3.3 Non-NMR Techniques

A variety of biophysical methods can be used to investigate dynamics of proteins. Fluorescence methods allow the investigation of dynamic processes on a broad range of time scales and require very low protein concentrations. Although site-directed mutagenesis and other techniques allow the introduction of fluorescent labels in addition to naturally occurring tryptophan residues, the number of sites available for fluorescence lifetime methods in proteins is rather low compared to NMR spectroscopy, the latter of which provides at least residue specific kinetic parameters. Instead, certain fluorescence methods exhibit noticeable time resolution. Ultrafast laser technologies can resolve many distinct time steps in dynamic processes (Brunori, 2000).

Microcalorimetry quantitates thermodynamic effects in protein-ligand interactions. Sometimes entropy changes can be correlated with changes in dynamic processes. Entropic effects are especially important for the characterization of allosteric behavior. If intermediates occur in relatively high populations with different equilibrium constants, individual thermodynamic (but of course not kinetic) properties are accessible for characterization.

Time-resolved structural studies by cryogenic x-ray diffraction provides the possibility to obtain atomic-resolution structures of trapped intermediates of enzymes during catalytic turnover. This method is limited by the activity of the enzyme in the crystal, by the usually low concentrations of the transient intermediates, and by the ability to trigger the catalytic process without disrupting the crystal. Very fast reaction initiation can be achieved by femtosecond photoexcitation. On this time scale, even molecular vibrations are synchronized. On longer time scales, the system adjusts to a Boltzman equilibrium, causing chemical reactions to proceed asynchronously. Intermediates are present in many unit cells, but they are vibrationally uncoupled and thus asynchronous. The interpretation of time-resolved experiments is therefore compromised by the speed and the efficiency of the reaction initiation, by the presence of multiple conformational states and by lattice disorder caused by the process itself, which one subjects to observe (Hajdu *et al.*, 2000). Nevertheless, it has been possible to assemble high-resolution snap-shots of Bacteriorhodopsin (Royant *et al.*, 2000), Cytochrome P450 (Schlichting *et al.*, 2000) and Myoglobin (Ostermann *et al.*, 2000) into a 'movie' of the action. However, either the synchronous act spans only a ps-ns time period, or the transition occurs on an unknown time-scale, since the intermediate is trapped artificially.

High-resolution X-ray crystallography allows the determination of anisotropic B-factors and motional models for atomic and collective motions. The rate of the dynamic process is not accessible, but a disordered conformation generally indicates atomic mobility

on a long time scale. Instead, temperature factors are related with rather small fluctuations, which could be simulated on a ps time scale by molecular dynamics (Matoba and Sugiyama, 2003). The potential of this technique is reflected by the possibility to obtain atomic-level structural models of alternative conformations. Admittedly, the populations of conformers must be much higher to be observed in the electron density than for NMR techniques, where conformers with populations down to 0.5 % can be characterized. Furthermore, large-scale mobility on slow time scales is generally difficult to obtain from X-ray analysis because one conformer usually crystallizes preferentially.

4 Chemical Exchange

4.1 Theoretical Background

In a spin system undergoing chemical exchange between different environments due to chemical reactions or conformational transitions, the nucleus exchanges intermolecularly between sites in different molecules or in the second case, the nucleus exchanges intramolecularly between different conformations. In the latter case, no bonds are broken but the conformation of the molecule and therefore also the magnetic environment and the chemical shift of the nucleus is changed. In the case of exchange on the μs - ms time scale, the resulting time dependence of resonance frequencies leads to the dephasing of transverse coherences and the transfer of magnetization between exchanging sites.

Exchange processes of chemically equivalent nuclei can be monitored by NMR spectroscopy as long as they are magnetically distinct. Nuclear spins can be manipulated during the NMR experiment without changing the chemical states of the system because of the weak coupling between spin system and lattice. Therefore, chemical reactions and conformational transitions can be investigated using NMR methods while the system remains in chemical equilibrium (Cavanagh *et al.*, 1995).

Consider the following exchange process between the two sites A and B



where k_{12} is the forward and k_{21} is the reverse reaction rate constant. The reaction rate constants represent the reciprocal lifetimes of the two states A and B:

$$k_{12} = \frac{1}{\tau_a}, k_{21} = \frac{1}{\tau_b}. \quad (2)$$

Indices a and b indicate affiliation to site A or B. The two microscopic rate constants are combined to an overall exchange rate k_{ex} ,

$$k_{\text{ex}} = k_{12} + k_{21}, \quad k_{12} = k_{\text{ex}}p_b, \quad k_{21} = k_{\text{ex}}p_a, \quad (3)$$

and the sum of all populations add to one:

$$p_a + p_b = 1. \quad (4)$$

If sites A and B exhibit different chemical shifts ω_a and ω_b , respectively, the chemical shift difference between the sites will be referred to as $\Delta\omega$. Depending on the ratio of the exchange rate k_{ex} and the chemical shift difference $\Delta\omega$, the line shapes of the signals vary substantially. Figure 2 depicts simulated signals for systems undergoing two-site exchange with varying populations and exchange rates. For equal populations of the two sites A and B ($p_a = p_b = 0.5$, left panel of Figure 2), we expect two separate signals with equal intensities in the absence of exchange (Figure 2e). The linewidths of the resonances are characterized by the transverse relaxation rate constants R_{2a}^0 and R_{2b}^0 ($\text{LW} = R_2/\pi$). In the presence of exchange, the linewidths of the signals increase because of higher effective transverse relaxation rates due to dephasing of the transverse coherences. When the magnitude of the exchange rate approaches the chemical shift difference, the signals are broadened beyond detection. Coalescence occurs at $2(p_a p_b)^{1/2} k_{\text{ex}} \approx \Delta\omega$. For even higher exchange rates, one signal with intermediate chemical shift is observed with successively reduced linewidth. For disproportionate populations (depicted in the right panel of Figure 2), the signal of the minor site is already broadened for relatively low exchange rates. For fast exchange, one single line is observed at the population weighted resonance frequency $\omega_{\text{ex}} = \omega_a p_a + \omega_b p_b$. The ratio of k_{ex} and $\Delta\omega$ determines the so-called NMR time scale:

$k_{\text{ex}} < \Delta\omega$	slow exchange
$k_{\text{ex}} \approx \Delta\omega$	intermediate exchange
$k_{\text{ex}} > \Delta\omega$	fast exchange

As stated above, the transverse coherences can be dephased in the presence of exchange due to the time dependence of the resonance frequencies. The effective transverse relaxation rate constant R_2^{eff} is composed of the relaxation rate in the absence of exchange, R_2^0 , and the exchange contribution R_{ex} :

$$R_2^{\text{eff}} = R_2^0 + R_{\text{ex}}.$$

The exchange contribution depends on the exchange rate k_{ex} , the chemical shift difference between exchanging sites $\Delta\omega$, and the populations p_a and p_b . In the fast exchange limit, R_{ex} is

$$R_{\text{ex}} = p_a p_b \Delta\omega^2 / k_{\text{ex}}. \quad (5)$$

180° pulses can refocus chemical exchange processes with an exchange rate lower than the pulse rate (see also Figure 3). By varying the pulse rate (which is equivalent to the

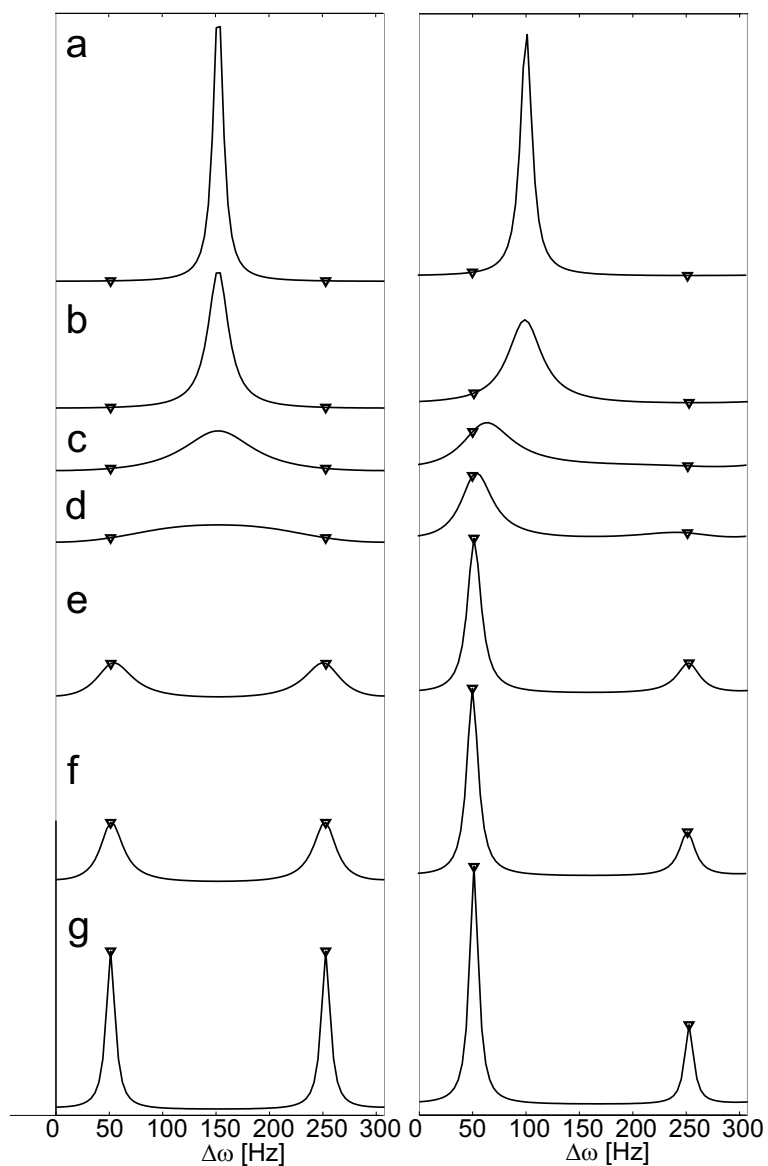


Figure 2: Effect of exchange rate and populations on line shapes of a system undergoing two-site exchange. On the left, the two sites exhibit equal populations, whereas for the right panel the populations equal to 0.75 and 0.25. The exchange rates k_{ex} correspond to (a) 100000 Hz, (b) 10000 Hz, (c) 2000 Hz, (d) 1000 Hz, (e) 200 Hz, (f) 100Hz and (g) 0 Hz from top to bottom, respectively. The frequencies of exchanging sites are labeled with '▽', the frequency difference corresponds to 200 Hz.

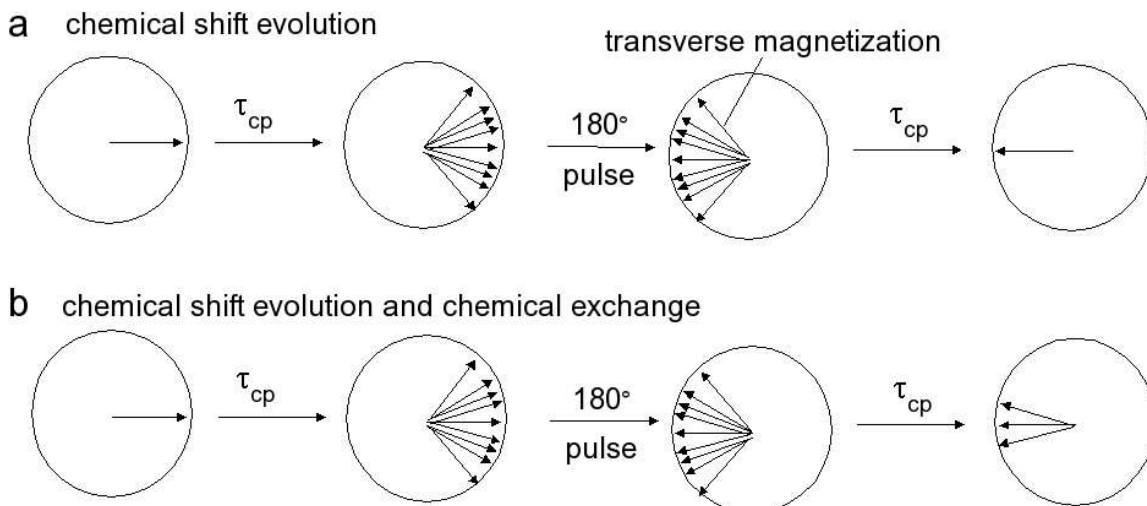


Figure 3: Effect of 180° refocusing pulses on transverse magnetization. Transverse magnetization depicted as arrows in the xy -plane dephases (a) due to the evolution of chemical shift and (b) due to chemical shift evolution and chemical exchange processes. A 180° refocusing pulse reverts the effect of (a) chemical shift evolution and of (b) exchange processes that are slower than the pulsing rate. Faster exchange leads to an accelerated decay of the magnetization and an increased effective transverse relaxation rate R_2^{eff} .

applied refocusing field ν_{cp}) during the relaxation delay T of the CPMG experiment, different fractions of the transverse coherence can be refocused. The resulting field dependence of the effective transverse relaxation rate constant, $R_2^{\text{eff}}(\nu_{\text{cp}})$, is commonly referred to as relaxation dispersion. Recently, relaxation compensated CPMG experiments for the characterization of exchange phenomena of nuclei in the protein backbone (Loria *et al.*, 1999a,b; Tollinger *et al.*, 2001; Wang *et al.*, 2001a; Ishima *et al.*, 2004) and in the side chains (Mulder *et al.*, 2001b, 2002) have been published. Quantification of exchange parameters from experimental relaxation dispersion data requires a mathematical description of the evolution of the magnetization during a CPMG pulse train.

4.1.1 McConnell Equations

The Bloch equations (Bloch, 1946) describe the time dependent evolution of the nuclear magnetization of spin- $\frac{1}{2}$ nuclei in a static magnetic field. To include the effects of two-site exchange in the description of the time-evolution of the magnetization, the Bloch equations must be modified to yield the McConnell equations (McConnell, 1958):

$$\frac{du_a}{dt} = -(\omega_a - \omega_0)v_a - R_{2a}u_a - k_{12}u_a + k_{21}u_b, \quad (6)$$

$$\frac{du_b}{dt} = -(\omega_b - \omega_0)v_b - R_{2b}u_b - k_{21}u_b + k_{12}u_a, \quad (7)$$

$$\frac{dv_a}{dt} = (\omega_a - \omega_0)u_a - R_{2a}v_a - k_{12}v_a + k_{21}v_b - \omega_1 M_{za}, \quad (8)$$

$$\frac{dv_b}{dt} = (\omega_b - \omega_0)u_b - R_{2b}v_b - k_{21}v_b + k_{12}v_a - \omega_1 M_{zb}, \quad (9)$$

where u_j and v_j are real and imaginary parts of the complex magnetization, R_{2j} is the transverse relaxation rate constant, ω_j is the frequency of site j ($j = a, b$), ω_0 is the Larmor frequency and ω_1 is the field strength of an applied transverse magnetic field.

These equations apply if the intensity ω_1 of the spin-echo pulses applied during a CPMG pulse train is sufficiently large and the duration of the pulses t_ω is short:¹

$$\omega_1, \frac{1}{t_\omega} \gg R_{2j}, R_{1j}, k_j, |\omega_j - \omega|, |\omega_{j1} - \omega_{j2}| \quad \text{where } j = a, b \quad (10)$$

To obtain frequency discrimination between positive and negative frequencies, two orthogonal components of the magnetization (u and v) are detected and treated as real and imaginary parts of the magnetization. Complex notation yields

$$G_j = u_j + iv_j. \quad (11)$$

In a CPMG experiment, the decay of the magnetization between pulses is considered. Thus, with $\omega_1 = 0$ equations 6-9 can be rewritten as follows:

$$\frac{dG_a}{dt} = -(R_{2a} + k_{12} - i\delta_a)G_a + k_{21}G_b, \quad (12)$$

$$\frac{dG_b}{dt} = k_{12}G_a - (R_{2b} + k_{21} - i\delta_b)G_b, \quad (13)$$

where $\delta_j = \omega_j - \omega_0$, where ω_j is the chemical shift of species j , and where ω_0 is the angular velocity of the rotating coordinate system.

¹Commonly used π pulses have 50 ms duration corresponding to field strengths of 5000 Hz.

4.1.2 Multi-site Exchange

This scheme can be extended to a more complex chemical system with μ distinct species. Their magnetizations are all in the transverse plane and have magnitudes proportional to the populations of the corresponding species. Assuming the absence of exchange, complex notation according to Bloch yields

$$\frac{d}{dt}G_j = -R_{2j}G_j - i\delta_j G_j. \quad (14)$$

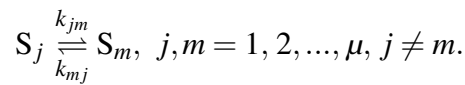
When we introduce the vector \mathbf{G} and the matrix B ,

$$\mathbf{G} = \begin{pmatrix} G_1 \\ G_2 \\ \cdot \\ \cdot \\ G_\mu \end{pmatrix}, \quad B = \begin{pmatrix} -R_{21} - i\delta_1 & & & 0 \\ & -R_{22} - i\delta_2 & & \\ & & \cdot & \\ & & & \cdot \\ 0 & & & -R_{2\mu} - i\delta_\mu \end{pmatrix}, \quad (15)$$

equation 14 can now be replaced by the matrix equation

$$\frac{d}{dt}\mathbf{G} = B\mathbf{G}. \quad (16)$$

Assuming the system undergoes chemical exchange, every species j is converted into any other species m with the rate constant k_{jm} :



The lifetime of the population of the spin system which has changed over from j to m corresponds to $\tau_{mj} = \frac{1}{k_{mj}}$. If two species of the spin system do not exchange, their connecting exchange rate will be zero. We can formulate an exchange matrix C with

$$C = \begin{pmatrix} k_{11} & k_{21} & \cdot & \cdot & k_{\mu 1} \\ k_{12} & \cdot & & & \cdot \\ \cdot & & \cdot & & \cdot \\ \cdot & & & \cdot & \cdot \\ \cdot & & & & \cdot \\ k_{1\mu} & \cdot & \cdot & \cdot & k_{\mu\mu} \end{pmatrix}, \quad (17)$$

where

$$k_{jj} = -\text{Summe}(k_{kj}), \quad j = 1, 2, \dots, \mu. \quad (18)$$

The time dependence of the magnetization \mathbf{G} due to chemical exchange is therefore

$$\frac{d}{dt}\mathbf{G} = C\mathbf{G}. \quad (19)$$

Equations 16 and 19 can be combined into a differential matrix equation describing the time dependent evolution of the transverse magnetization of a spin system undergoing chemical exchange:

$$\frac{d}{dt}\mathbf{G} = (B + C)\mathbf{G} = A\mathbf{G}. \quad (20)$$

For two exchanging sites, expression 20 is equivalent to the McConnell equations (McConnell, 1958) expressed in a general notation for an arbitrary number of species with arbitrary connection. A solution of this differential equation is

$$\mathbf{G}(\theta) = \exp(A\theta)\mathbf{h}, \quad (21)$$

where the initial condition is

$$\mathbf{G}(t_0) = \mathbf{h}, \quad (22)$$

and the new time variable θ with $\theta = t - t_0$ has been introduced. The matrix series $\exp(A\theta)$ can be replaced by the matrix

$$M(\theta) = \exp(A\theta). \quad (23)$$

Equation 21 then becomes

$$\mathbf{G}(\theta) = M(\theta)\mathbf{h}. \quad (24)$$

4.1.3 Recursive Formula

In a CPMG experiment, after an initial $\pi/2$ (90°) pulse, π (180°) pulses are applied to the transverse magnetization with a spacing of $2\tau_{cp}$. Introduction of the subscript n indicates the time interval after the n th π pulse:

$$\mathbf{G}_n(\theta) = M(\theta)\mathbf{h}_n, \quad (25)$$

with $0 \leq \theta \leq 2\tau_{cp}$. Since for $n = 0$ the magnetization after the initial $\pi/2$ pulse is described, $0 \leq \theta \leq \tau_{cp}$. The π pulse converts all components of M to their complex conjugates (indicated by an asterisk). A recursion formula for the integration constants \mathbf{h}_n can be formulated as follows:

$$\mathbf{h}_1 = M^*(\tau_{cp})\mathbf{h}_0^*, \quad (26)$$

$$\mathbf{h}_2 = M^*(2\tau_{cp})\mathbf{h}_1^* = M^*(2\tau_{cp})(M^*(\tau_{cp})\mathbf{h}_0^*)^*, \quad (27)$$

$$\mathbf{h}_{n+1} = M^*(2\tau_{cp})\mathbf{h}_n^*, \quad n > 0. \quad (28)$$

In an illustrative description, \mathbf{h}_n corresponds to the magnetization after the n th π pulse, whereas \mathbf{G}_n represents the magnetization of the spin system between successive π pulses at the time point of the echo formation.

4.1.4 Closed Analytical Expression for Two-site Exchange

To calculate the influence of the refocusing field on the coherence, the recursive formula 28 has to be applied. This equation can either be solved numerically for different values of n or analytically. An approximation for the recursive equation 28 can be obtained by an eigenvalue equation for large numbers of n (Jen, 1978). Carver and Richards were able to formulate a closed expression for the phenomenological transverse relaxation rate constant for two-site exchange (Carver and Richards, 1972):

$$R_2^{\text{eff}}(\nu_{cp}) = 1/2 \left(R_{2a}^0 + R_{2b}^0 + k_{ex} - \frac{1}{2\tau_{cp}} \cosh^{-1} [D_+ \cosh(\eta_+) - D_- \cos(\eta_-)] \right) \quad (29)$$

with

$$\begin{aligned}
D_{\pm} &= \frac{1}{2} \left[\pm 1 + \frac{\Psi + 2\Delta\omega^2}{(\Psi^2 + \zeta^2)^{1/2}} \right], \\
\eta_{\pm} &= \sqrt{2}\tau_{\text{cp}} \left[\pm \Psi + (\Psi^2 + \zeta^2)^{1/2} \right]^{1/2}, \\
\Psi &= (R_{2a}^0 - R_{2b}^0 - p_a k_{\text{ex}} + p_b k_{\text{ex}})^2 - \Delta\omega^2 + 4p_a p_b k_{\text{ex}}^2, \\
\zeta &= 2\Delta\omega (R_{2a}^0 - R_{2b}^0 - p_a k_{\text{ex}} + p_b k_{\text{ex}}).
\end{aligned}$$

The refocusing field is related to the delay $2\tau_{\text{cp}}$ between two 180° pulses in the CPMG pulse train according to $\nu_{\text{cp}} = \frac{1}{4\tau_{\text{cp}}}$. R_{2a}^0 and R_{2b}^0 are the transverse relaxation rate constants of sites A and B in the absence of exchange, respectively. Good approximations can be derived in the fast-exchange limit or for special conditions, such as very unbalanced populations (Luz and Meiboom, 1963; Ishima and Torchia, 1999).

4.2 Numerical Simulation of Relaxation Dispersion Curves

A numerical simulation of the magnetization during CPMG pulse trains is feasible with state-of-the-art computers and allows the exact calculation of the dephasing of coherences during exchange. The evolution of the magnetization can be simulated for any CPMG pulse train using eq. 25. In a typical relaxation dispersion experiment, the dependence of the effective transverse relaxation rate on the refocusing field, $R_2^{\text{eff}}(\nu_{\text{cp}})$, is determined. Thus, in simulations, the evolution of the magnetization for each and every refocusing field requires simulation. This is depicted in Figure 4b for a fast two-site exchange process with a frequency separation of 100 Hz, an exchange rate k_{ex} of 500 s^{-1} , and equal populations $p_a = p_b = 0.5$. The evolution of the magnetization was simulated for a relaxation delay of $T = 60 \text{ ms}$ and 1, 2, 3, 4, 6, 8, 10, 12, 14, 16, 20, 30, 50 or 100 equally spaced echoes. Assuming a mono-exponential decay, the transverse relaxation rate was calculated from the magnitudes of the real parts of the magnetization by

$$R_2^{\text{eff}} = -\frac{1}{T} \ln \frac{I(T)}{I(0)}.$$

A plot of R_2^{eff} against the refocusing field ν_{cp} , the relaxation dispersion, is depicted in Figure 4b.

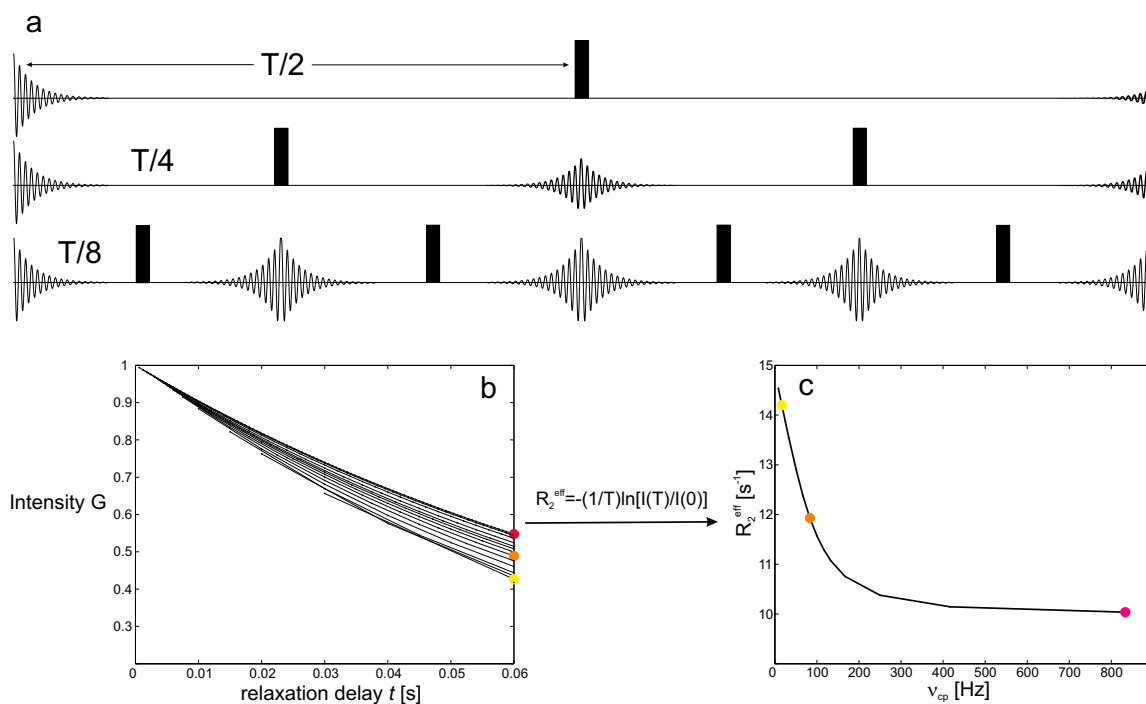


Figure 4: Magnetization during CPMG pulse trains and effect on effective transverse relaxation rates for a fast exchange process with $k_{ex} = 500 \text{ s}^{-1}$, $\Delta\omega = 100 \text{ s}^{-1}$ and equal populations $p_a = p_b = 0.5$. Relaxation rates of the two states in the absence of exchange were set to $R_{2a} = R_{2b} = 10 \text{ s}^{-1}$. (a) CPMG pulse trains of duration T with differently spaced refocusing pulses influencing the amplitude of the echoes. (b) Magnitude of magnetization versus time spent in the transverse plane. The evolution of the magnetization was simulated for $T = 60 \text{ ms}$ with 1, 2, 3, 4, 6, 8, 10, 12, 14, 16, 20, 30, 50 and 100 equally spaced echoes (from bottom to top) during this time. (c) Effective transverse relaxation rates R_2^{eff} calculated from the magnitudes of the magnetization after 60 ms versus the refocusing field ν_{cp} . Colored circles show the influence of the refocusing rate on R_2^{eff} .

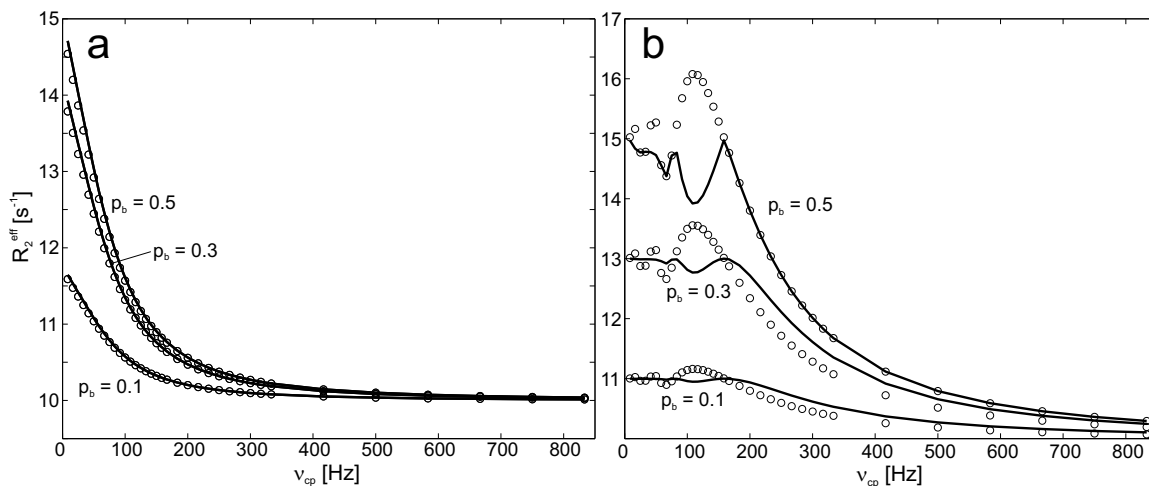


Figure 5: Comparison of theoretical relaxation dispersion curves simulated using eq. 29 (solid lines) and the exact solution of the McConnell equations (circles) (McConnell, 1958). (a) As an example for a fast exchange process, values of $k_{\text{ex}} = 500 \text{ s}^{-1}$, $\Delta\omega = 100 \text{ Hz}$ and populations of one state of 0.1, 0.3 and 0.5 (from bottom to top) were used. (b) For slow exchange on the NMR time scale, parameters were set to $k_{\text{ex}} = 10 \text{ s}^{-1}$, $\Delta\omega = 2000 \text{ Hz}$. Populations of one state were 0.1, 0.3 and 0.5 and relaxation rates of the two states in the absence of exchange were set to $R_{2a} = R_{2b} = 10 \text{ s}^{-1}$.

4.2.1 Comparison with the Analytical Expression

Comparison of relaxation dispersion curves calculated using the analytical expression and curves obtained by numerical simulation of the recursive formula reveals nearly perfect agreement of the approximation and the exact solution in the case of fast exchange. In Figure 5a, relaxation dispersion curves for a fast exchange process with $k_{\text{ex}} = 500 \text{ s}^{-1}$, $\Delta\omega = 100 \text{ Hz}$ and populations of 0.1, 0.3, or 0.5 (from bottom to top, solid lines) calculated using the approximation eq. 29 are compared to the numerical solution of the McConnell equations (shown as circles). For slow chemical exchange with $k_{\text{ex}} = 10 \text{ s}^{-1}$, $\Delta\omega = 2000 \text{ Hz}$ and $p = 0.1, 0.3, \text{ or } 0.5$ (Figure 5b) the approximation 29 and the exact numerical simulation show large differences. The approximation is especially poor at predicting the oscillating parts at low refocusing fields because the sequence of the recursive formula cannot be approximated by an eigenvalue problem ($n = n + 1$) for small numbers of n .

In the case of slow exchange, two separate signals are visible in NMR spectra only one of which contributes to the relaxation dispersion curve in a CPMG experiment. Simulating relaxation dispersion curves using the McConnell equations, one also may select the part of the magnetization of interest. In a slow exchange process, one would select the magnetization that gives rise to the signal in question. In the case of fast exchange, the sum of both magnetizations is selected.

4.3 Analysis of Experimental Relaxation Dispersion Data

Simulation of the magnetization during a CPMG pulse train can be used to fit experimental relaxation dispersion curves. To explore the possibilities and the limits of this approach, relaxation dispersion curves were first simulated using eq. 25 for different sets of parameters and subsequently fitted. Discernment between different sets of parameters that are concordant with a given experimental relaxation dispersion curve requires data from different static magnetic fields. All exchange parameters are independent of B_0 except $\Delta\omega$ (in Hz), which scales proportionally with the field. Thus, twice the number of data points are available to fit the same number of parameters.

In Figure 6, examples of theoretical relaxation dispersion data (depicted as x) at B_0 fields corresponding to ^1H Larmor frequencies of 500 MHz (blue) and 700 MHz (red) are shown. They were fitted to eq. 25 simulating the evolution of the magnetization for each refocusing field. According to eqs. 3 and 4, for a given exchange rate and populations, the two microscopic kinetic rates k_{12} and k_{21} should be discernable and assignable to the corresponding populations. This could be demonstrated successfully for a wide range of different parameter sets. Figure 6a and b show examples for slow and fast exchange. The exchange parameters could be extracted precisely and the two microscopic kinetic rates could be reproduced. In both cases, the transverse relaxation rates of the two sites in the absence of exchange were equal ($R_{2a}^0 = R_{2b}^0$). If these rates differ, a precise extraction of exchange parameters is often not feasible. In Figure 6c, relaxation dispersion curves are depicted which were simulated for $k_{12} = k_{21} = 500 \text{ s}^{-1}$ (thus, $k_{\text{ex}} = 1000 \text{ s}^{-1}$), $p_a = p_b = 0.5$, $\Delta\omega = 300 \text{ Hz}$ (at 700 MHz ^1H Larmor frequency), and $R_{2a}^0 = 20 \text{ s}^{-1}$ and $R_{2b}^0 = 5 \text{ s}^{-1}$. These values could not be reproduced precisely. Nevertheless, the exchange rate k_{ex} obtained by the optimization procedure ($k_{\text{ex}} = k_{12} + k_{21} = 996 \text{ s}^{-1}$) closely resembles the value used for the simulation and the errors of most parameters were in the range of only 2-10%. The value obtained for R_{2b}^0 , in contrast, was 50% too high. To obtain satisfactory results with experimental data that has the additional complication of noise, R_{2a}^0 and R_{2b}^0 should be measured independently in the case of slow exchange.

4.4 Line Shape Analysis of NMR Signals

Line shapes of signals recorded for successive titration steps of a protein with a ligand contain kinetic information. ^1H - ^{15}N HSQC spectra are suitable to monitor the progress of the protein-ligand interaction because of their high dispersion, limited spectral overlap, and the availability of site-specific information. Figure 7a depicts successive ^1H - ^{15}N HSQC spectra of the titration of the N-SH2 domain with MT8 for increasing concentrations of the ligand from blue to red. Chemical shift perturbations in both the proton and

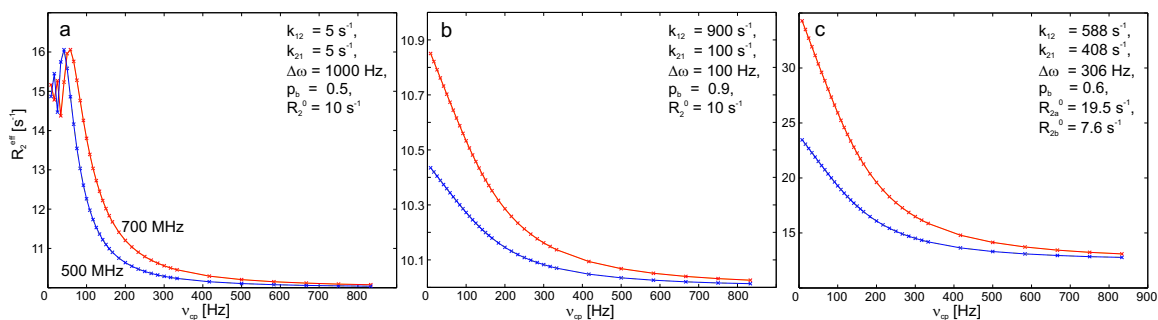


Figure 6: Fitting of theoretical relaxation dispersion data using a numerical approach by simulation of the evolution of the magnetization during the CPMG pulse train for every refocusing field ν_{cp} . Theoretical data points are shown as 'x', fitted curves as solid lines in blue and red (corresponding to ^1H Larmor frequencies of 500 MHz and 700 MHz). The data was simulated using the following parameters: (a) $k_{12} = k_{21} = 5 \text{ s}^{-1}$, $\Delta\omega = 1000 \text{ Hz}$, $p_a = p_b = 0.5$, $R_{2a}^0 = R_{2b}^0 = 10 \text{ s}^{-1}$; (b) $k_{12} = 900 \text{ s}^{-1}$, $k_{21} = 100 \text{ s}^{-1}$, $\Delta\omega = 100 \text{ Hz}$, $p_a = 0.1$, $p_b = 0.9$, $R_{2a}^0 = R_{2b}^0 = 10 \text{ s}^{-1}$; (c) $k_{12} = 588 \text{ s}^{-1}$, $k_{21} = 408 \text{ s}^{-1}$, $\Delta\omega = 306 \text{ Hz}$, $p_a = 0.6$, $R_{2a}^0 = 19.5 \text{ s}^{-1}$, $R_{2b}^0 = 7.6 \text{ s}^{-1}$. Parameters obtained by fitting to eq. 25 are depicted in the upper right corner of individual panels.

the nitrogen dimension can be analyzed quantitatively for individual amino acid residues. As an example, ^1H and ^{15}N cross-sections of the signals of Q415 and K379 are depicted in panels b and c of Figure 7, respectively. The extent of the line broadening throughout the titration reflects the off-rate of the interaction.

Based on the Gutowsky equations (Gutowsky *et al.*, 1953), a theoretical treatment of line shapes in the course of a reaction was described by Sudmeier *et al.* (Sudmeier *et al.*, 1980). For titration spectra recorded under steady-state conditions, the time-evolution of the magnetization does not have to be considered (Anderson, 1954; Günther and Schaffhausen, 2002). The time domain signal under steady-state conditions can be calculated according to an equation by Günther *et al.* (Günther and Schaffhausen, 2002):

$$F(t) = I \exp[(-C + 2\pi i W_0 - R_2)t] \mathbf{P} \quad (30)$$

where

- I is the unity matrix,
- C is a matrix containing the rate constants,
- W_0 is a diagonal matrix with the Larmor frequencies ν_i ,
- R_2 is a diagonal matrix with transverse relaxation rates,
- $R = 1/T_2 = \pi \cdot \text{LW}$ (line width at half height) and
- \mathbf{P} is a column vector with the populations (mole fractions) of the reaction components.

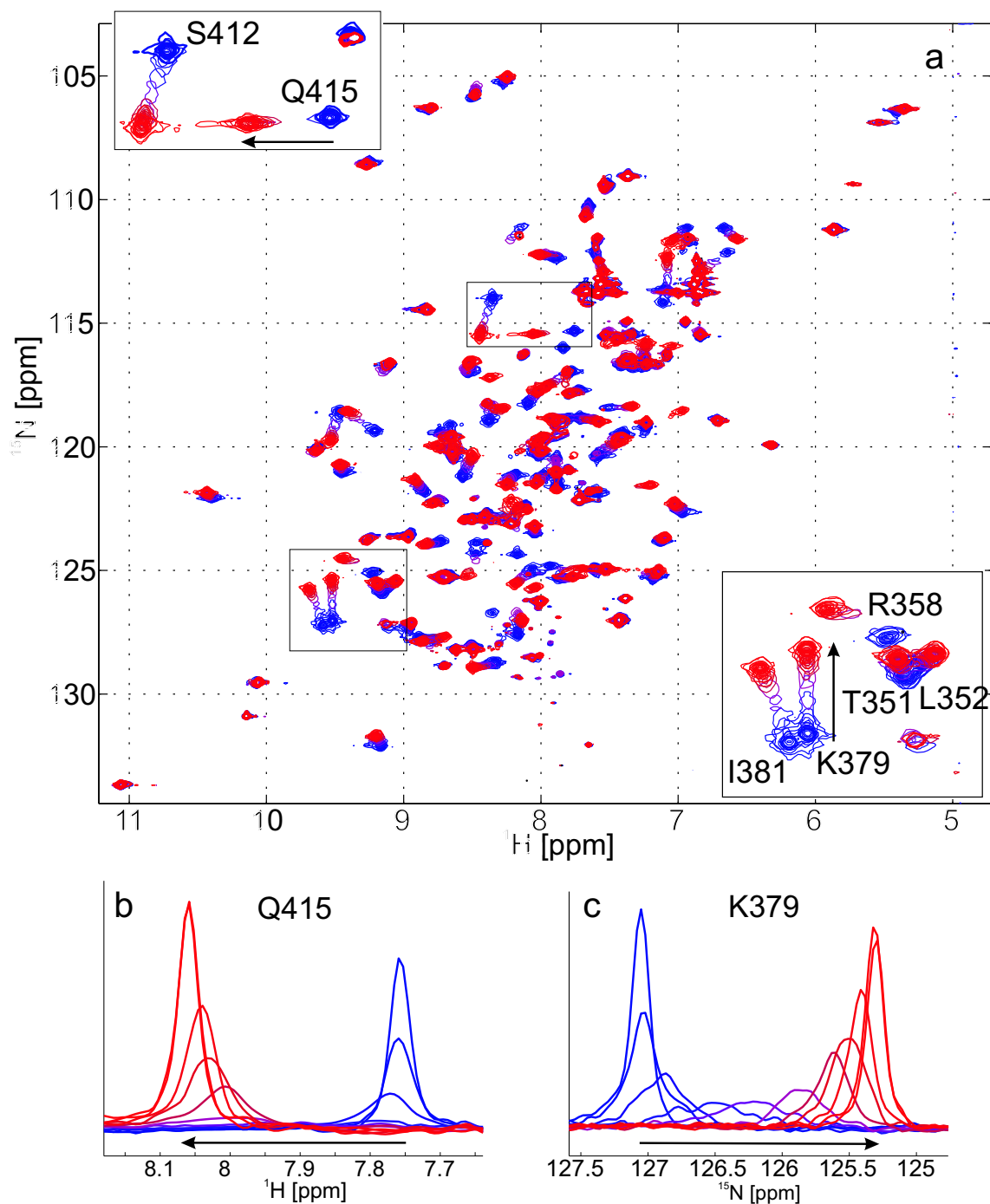


Figure 7: Line shapes of signals from titration spectra contain kinetic information. (a) ^1H - ^{15}N HSQC spectra of the N-SH2 domain in a successive titration with MT8 peptide. Signals of residues involved in the interaction or perturbed by the binding event exhibit chemical shift perturbations. Two sections showing signals of key-residues K379 and Q415 are enlarged in expansions. The extent of the linebroadening in ^1H and ^{15}N cross-sections of signals of (b) Q415 and (c) K379, respectively, contains information on kinetic rates.

Calculation of the time domain signal and subsequent Fourier transformation is much faster than the direct analytical calculation of the frequency domain signal (Binsch, 1968). In addition, the approach suggested by Günther et al. has the intrinsic advantage that typical processing steps such as zero filling or apodization can be incorporated.

4.4.1 Line Shapes for Binding Processes

For reactions such as chemical turnover or binding, the line shapes of NMR signals depend on the relative concentrations of reaction partners. In the typical one-step binding reaction



where P is the free protein, L is the ligand and PL is the complex, the exchange regime is altered for every addition of L during the course of a titration because the exchange rate depends on the concentration of free ligand:

$$k_{\text{ex}} = k_{\text{on}}[L] + k_{\text{off}}. \quad (32)$$

Figure 8 shows line shapes simulated for a titration of a 1mM protein solution with a ligand with a dissociation constant of $K_D = 10^{-6}$ M. Addition of equal amounts of ligand in each step leads to increasing populations of the complex PL as depicted in Figure 9. The line shapes were simulated for equal intrinsic transverse relaxation rates of P and PL, frequency separations of 250 Hz and different off-rates, leading to signals typical for slow exchange on the left ($k_{\text{off}} = 50 \text{ s}^{-1}$), to signals typical for intermediate to fast exchange in the middle ($k_{\text{off}} = 500 \text{ s}^{-1}$), and to signals for fast exchange on the right ($k_{\text{off}} = 2000 \text{ s}^{-1}$).

Experimental line shapes from HSQC spectra of successive titration steps can be simulated using eq. 30 in order to extract the off-rate of the interaction. The simulation method was applied to data for the interaction of the N-SH2 domain of PI3K with an 8 amino acid peptide from polyoma middle T antigen (EEEpYMPME-NH₂, MT8) (Günther *et al.*, 2002). Figures 10a and b show experimental ¹H and ¹⁵N cross-sections (lines with '∇', colored blue to red for increasing concentrations of ligand) of residues E345 and K382 in a titration with MT8 that are typical for the one-step binding scheme of equation 31. Good fits of superimposed simulated signals (depicted as solid lines) that were calculated according to eq. 30 with subsequent Fourier transformation also support this model. Optimal values for the populations of the two states of the protein in each step of the

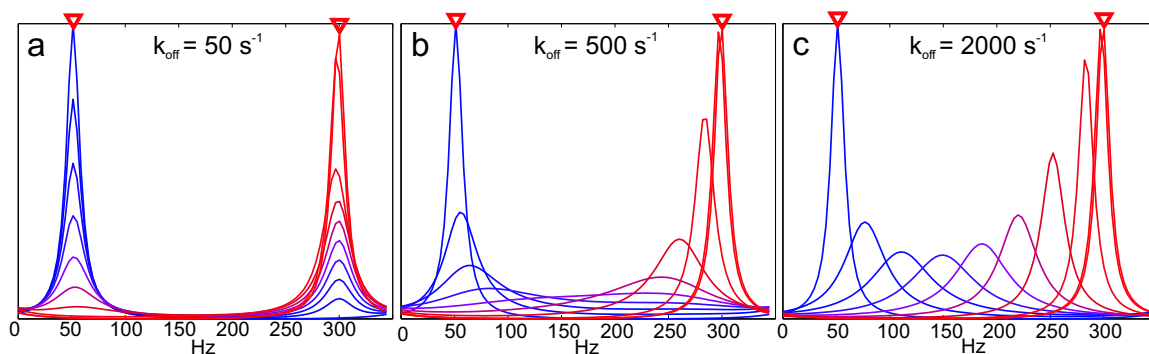


Figure 8: Theoretical line shapes for one-step binding. Simulation of line shapes for subsequent steps of a reaction of the type $P + L \rightleftharpoons PL$ using equation 30 with subsequent Fourier transformation. Populations (mole fractions) of P were calculated for a dissociation constant K_D of 10^{-6} M, a protein concentration of 1 mM and a titration in equal steps until 1.25 equivalents are added (see Figure 9). The signals of P and PL were separated by 250 Hz and the off-rates were set to (a) 50 s^{-1} , (b) 500 s^{-1} and (c) 2000 s^{-1} , respectively. Peak centers of P and PL are marked by red '▽'. The line widths of the signals of P and PL were 15 Hz. The steps in the titration proceed from blue to red. The relative fractions of P for successive steps are $P_P = [1.0 \ 0.865 \ 0.730 \ 0.596 \ 0.461 \ 0.327 \ 0.194 \ 0.069 \ 0.011 \ 0.005]$.

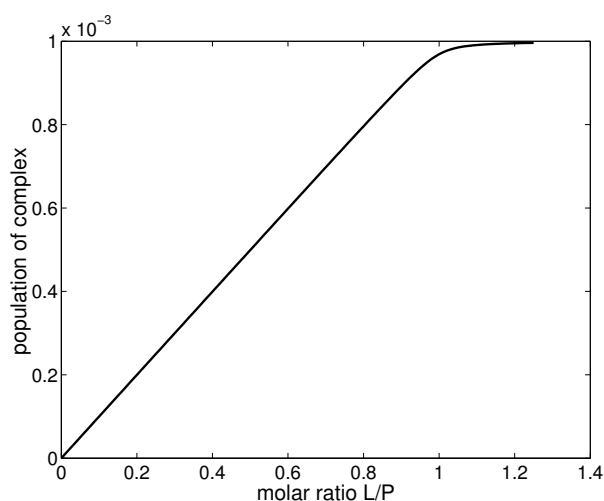


Figure 9: Population of the complex during a ligand titration. Dependence of the population of the complex on the molar ratio of ligand to protein, L/P , for a 1 mM protein solution in a titration with a ligand with a K_D of 10^{-6} M.

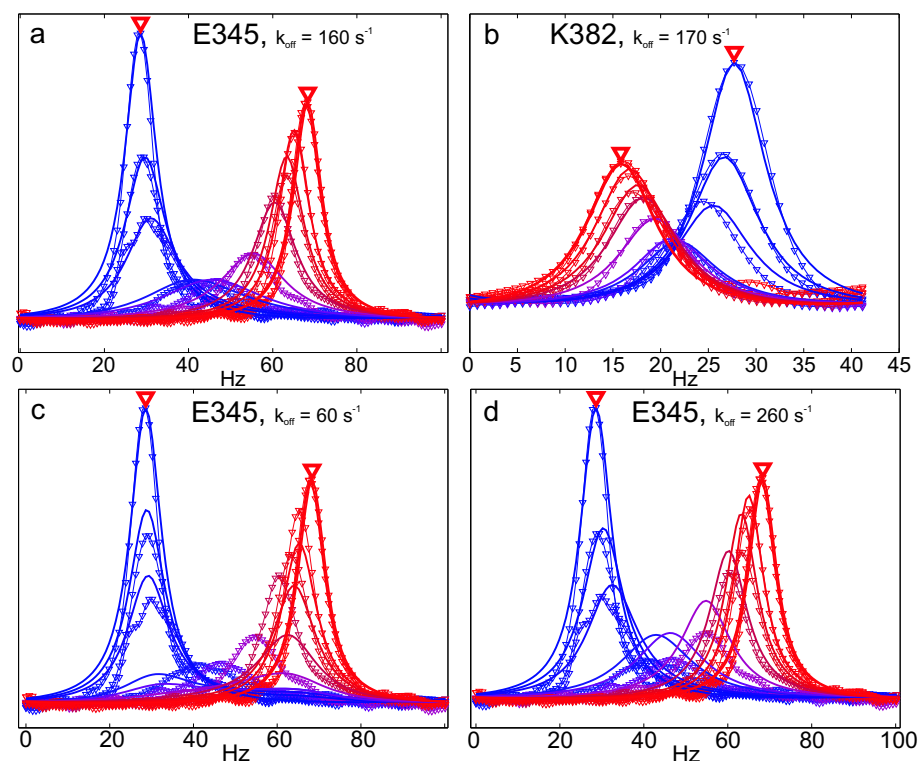


Figure 10: Simulations of experimental titration spectra. (a) ^1H and (b) ^{15}N cross-sections of the signals of E345 and K382, respectively, of the p85 N-SH2 domain in a titration with MT8 peptide (lines with ∇ from blue to red) and simulated lines (solid lines). Experimental lines were derived from ^1H - ^{15}N HSQC spectra recorded on a Bruker DMX500 spectrometer at 303K. Optimal simulation parameters were obtained by manual adjustment of simulated lines to the experimental signals. Simulations were performed using eq. 30 with subsequent application of window functions and Fourier transformations. Although only one dimension is depicted for each residue, the full two-dimensional signal was simulated. Thus, the intensities are scaled accordingly. The calculated off-rates were 160 s^{-1} and 170 s^{-1} , respectively. In panels (c) and (d) ^1H cross-sections of E345 are superimposed with lines simulated for off-rates of 60 s^{-1} and 260 s^{-1} , respectively. Clearly, the optimal off-rate is in between. Peak centers of P and PL are marked by red ∇ .

titration, the line widths and the rate constant of the dissociation were obtained by manual adjustment of the parameters. Figures 10c and d show superimpositions of cross-sections of E345 with line shapes simulated for different off-rates. Slower and faster off-rates lead to poor convergence of experimental and simulated lines. Therefore, an estimate of the off-rate is easily available. However, the exact confidence interval highly depends on the ratio of the chemical shift difference to the off-rate. For very high as well as for very low off-rates, the line shapes vary only slightly with the off-rate. The contribution of the signal-to-noise ratio to the error is only minor (Günther *et al.*, 2002; Mittag *et al.*, 2004b).

Line shape analysis provides kinetic parameters of protein-ligand interactions on a μs -ms time scale although measuring times for 2D spectra extend longer than lifetimes of the studied states. Another particular value of the technique is the possibility to directly visualize kinetic intermediates during the interaction and assign kinetic models that explain

the observed spectra. Examples of different kinetic mechanisms which were simulated can be found in Chapter 10 (Günther *et al.*, 2002; Mittag *et al.*, 2003a, 2004b,a).

4.5 Relaxation Dispersion for Complex Kinetic Models

Eqs. 25 and 30 are generally applicable to various exchange processes. Theoretical line shapes for a sequential two-step binding mechanism are described in Chapter 10 (Mittag *et al.*, 2003a, 2004b,a). The evolution of the magnetization can also be simulated for more complicated kinetic models, allowing interpretation of relaxation dispersion data using sequential and parallel binding schemes.

For the following sequential binding mechanism



the first step represents binding of the ligand to the protein, whereas the second step represents an equilibrium between the intermediate form PL^* and the complex PL , independent of the ligand concentration. The following relations apply:

$$K = \frac{[PL]}{[PL^*]} \quad (34)$$

$$[P][L]k_{12} = k_{21}[PL^*].$$

$k_{12}[L]$ can be combined to an effective rate k'_{12} . The exchange matrix for kinetic model 33 reads

$$C = \begin{pmatrix} -k'_{12} & k_{21} & 0 \\ k'_{12} & -k_{21} - k_{23} & k_{32} \\ 0 & k_{23} & -k_{32} \end{pmatrix}, \quad (35)$$

if exchange between P and PL is not possible. Reaction scheme (33) can be regarded as second order binding followed by an exchange step between an intermediate PL^* and the final product PL . The first step of this reaction will cause successive chemical shift changes for increasing concentrations of L in the case of fast exchange between P and PL^* . The second step is determined by the equilibrium constant K (eq. 34), which in turn depends on general reaction conditions. The resulting line shapes are depicted in Figure

11a for $K = 10$. Interestingly, line shapes for this two-step reaction with a fast off-rate resemble slow exchange line shapes owing to the permanently low concentration of the intermediate species.

Relaxation dispersion curves can be simulated for every set of populations of the exchange process. (A MATLAB script for the simulations can be found in Appendix 9.2.) Figures 11b-d depict examples of relaxation dispersion curves for two field strengths corresponding to the sets of populations of lines (b) 2, (c) 3 and (d) 6 of panel a. Compared to relaxation dispersion curves in Figures 5 and 6, the curves in Figures 11b and c clearly show a change in slope indicative of two processes with different rates. Following the curve from a high to a low refocusing field, the early slope of the line corresponds to a fast process, whereas the steeper slope at low refocusing field is caused by a slower process. In Figure 11d, only the influence of the slow exchange process on the effective transverse relaxation rate R_2^{eff} is clearly observable.

While line shapes help to visualize binding mechanisms, relaxation dispersion analysis will yield more precise rate constants. A combination of both techniques will therefore be beneficial to resolve all distinct steps of a complicated binding mechanism and to assign all microscopic rates.

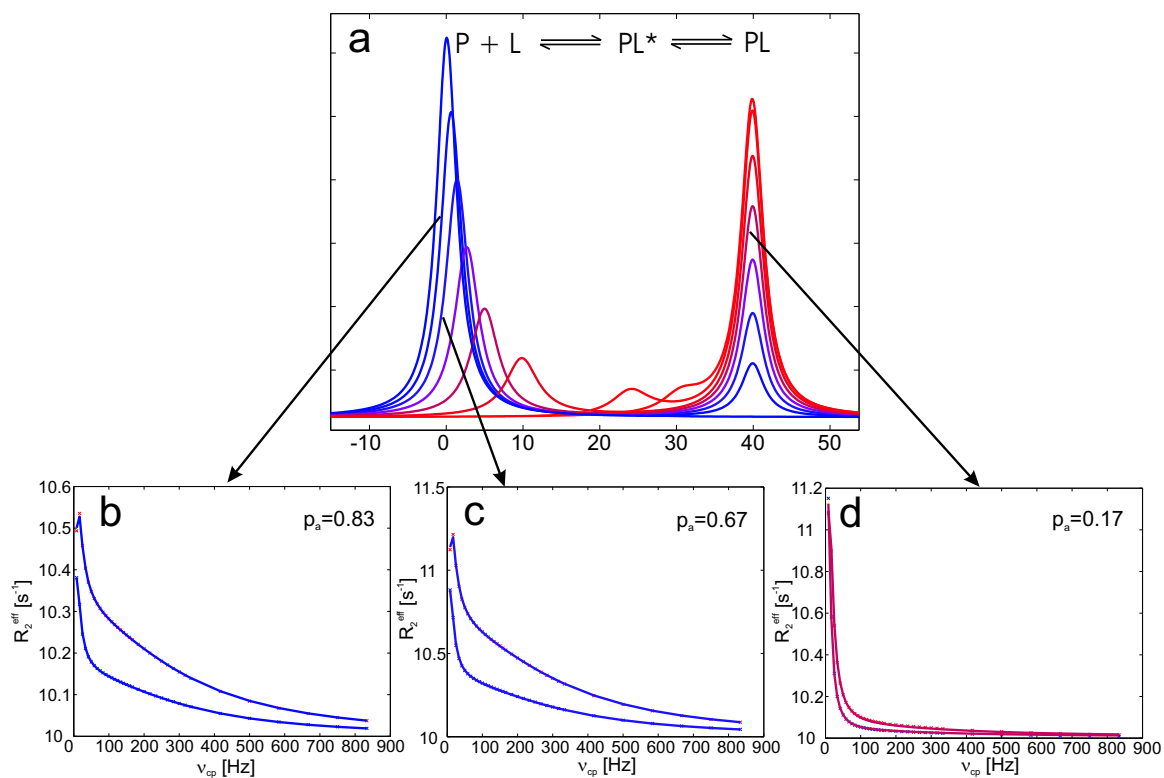


Figure 11: Theoretical line shapes and relaxation dispersion curves for a sequential two-step binding mechanism. The kinetic model is shown in panel a. For the simulation, the off-rate of step 1 was set to $k_{21} = 2000 \text{ s}^{-1}$, the off-rate of step 2 was set to $k_{32} = 10 \text{ s}^{-1}$, frequency differences were 200 Hz and 50 Hz between P and PL^* and PL^* and PL, respectively. For the second step, an equilibrium constant of 10 was used. Populations of P were $P_P = [1, 0.83, 0.67, 0.50, 0.33, 0.17, 0.03, 0]$. Populations of PL^* were calculated according to $P_{PL^*} = \frac{1-P_P}{K+1}$ and populations of PL according to $P_{PL} = 1 - P_P - P_{PL^*}$. For each line of panel (a), theoretical relaxation dispersion curves for two fields were simulated using eq. 25 adjusted for the two-step mechanism. Relaxation dispersion curves at two fields (corresponding to ^1H Larmor frequencies of 500 and 700 MHz) are shown for P_P of (b) 0.83, (c) 0.67 and (d) 0.17. The scales of y-axes are different for the three examples to clarify the characteristics of the curves. A MATLAB script for the simulation of relaxation dispersion curves can be found in Appendix 9.2.

5 Proteins Used as Model Systems in this Work

5.1 SH2 Domains

SH2 domains are independently folding modules of about 100 amino acids that provide otherwise distinct proteins with the ability to specifically bind phosphotyrosine (pTyr) containing protein sequences. The domain was first identified as a functionally important region in the viral oncogene v-Fps by systematic mutagenesis (Sadowski *et al.*, 1986).

v-Fps and other oncogenes from transforming viruses, such as v-Src and v-Abl (Hunter and Sefton, 1980; Sefton *et al.*, 1980; Witte *et al.*, 1980) and the related cellular receptor tyrosine kinases (RTKs), possess tyrosine kinase activity. RTKs dimerize upon activation by a growth factor and transphosphorylate one another (Schreiber *et al.*, 1983). Protein tyrosine kinases were thought to achieve specificity by recognizing short motifs for phosphorylation in their targets and mediating the signal by inducing conformational changes in the target. But interestingly, the search for downstream targets revealed that RTKs are the most abundant pTyr containing proteins in growth factor stimulated cells themselves, raising the question how the extracellular signal is transduced after RTK phosphorylation.

The SH2 domain of v-Fps constitutes a region N-terminal to the kinase domain that is not required for catalytic activity itself, but that modifies both kinase activity and substrate recognition (Sadowski *et al.*, 1986) by binding of pTyr containing protein sequences (Escobedo *et al.*, 1991a; Mayer *et al.*, 1992). Since the domain also is conserved in Src, Abl, and similarly positioned adjacent to the kinase (Src Homology 1, SH1) domain, it was termed SH2.

The discovery of the SH2 domain explained how a single protein from transforming viruses harbors diverse and profound effects such as malignant transformation, changes in cell shape, adhesion, mobility, growth, proliferation, gene expression, metabolism, and cell survival because they serve as scaffolds to recruit signal transduction complexes. Thus, the identification of the SH2 domain was the basis for a new concept of the organization of signal transduction pathways, in which the transduction of highly specific signals is achieved by the assembly of protein complexes through specific interactions of modular proteins (Moran *et al.*, 1990). In the case of SH2 domains, posttranslational phosphorylation regulates the protein-protein interactions.

5.1.1 Structure and Specificity of SH2 Domains

SH2 domains exhibit several features common for many interaction domains such as a cassette-like design, with closely positioned N and C termini, allowing it to be inserted

into another polypeptide chain without blocking its binding surface. Various X-ray and NMR structures of SH2 domains reveal a conserved fold of a central antiparallel β -sheet and two flanking α -helices (see Figure 16a) (Waksman *et al.*, 1992, 1993; Eck *et al.*, 1993a; Hensmann *et al.*, 1994; Nolte *et al.*, 1996; Pintar *et al.*, 1996). The pTyr of phosphopeptide ligands is complexed by two invariant arginines (R340 and R358 in the N-terminal SH2 domain of PI3K) in a conserved pocket between α helix A and the β -sheet.

Specificity of the interaction is achieved by the recognition of the sequence context around the pTyr. Peptide fishing experiments with degenerate phosphopeptide libraries and different SH2 domains demonstrated that each SH2 domain recognizes C-terminal residues to the pTyr (Cantley and Songyang, 1994). This allowed a general classification into four different families according to their phosphopeptide binding preferences. Structures of SH2-peptide complexes show a specific interaction of positions +1 and +3 C-terminal to the pTyr² with residue β D5³ in the central β -sheet of the SH2 domain (Waksman *et al.*, 1992; Eck *et al.*, 1993a). The residue type in position β D5 represents the most important determinant for the specificity of the interaction. Half of all known SH2 domains including the tyrosine kinases of the src-family exhibit a tyrosine or phenylalanine residue in this position, assigning them to group I of SH2 domains. Vav, a representative of group II, has a threonine in position β D5. Group III SH2s, like the N-SH2 domain of PI3K, are characterized by a cysteine or isoleucine in this position. Interestingly, it is possible to change the binding properties of an SH2 domain by mutating β D5 to a different amino acid and thus alter its biological activity (Marengere *et al.*, 1994).

SH2 domains of group I bind phosphopeptides with the general motif [pTyr-hydrophilic-hydrophilic-Ile/Pro], whereas SH2 domains of group III (p85, phospholipase C γ , and SH-PTP2) select the general motif [pTyr-hydrophobic-Xxx-hydrophobic], where Xxx indicates any amino acid type. Individual members of these groups prefer unique sequences, except the Src subfamily (Src, Fyn, Lck, and Fgr), which select the sequence pTyr-Glu-Glu-Ile. The variability of SH2 domain sequences in positions that contact residues +1, +2, and +3 C-terminal to pTyr provides a structural basis for the phosphopeptide selectivity (Waksman *et al.*, 1992; Eck *et al.*, 1993b; Cantley and Songyang, 1994). The N-SH2 domain of p85 of PI3K specifically binds phosphopeptides with the sequence [pTyr-Met/Val-Xxx-Met]. The specificity of the C-SH2 domain is similar. However, it possesses only moderate selectivity for a large, hydrophobic amino acid at the +1 position whereas the selectivity for methionine at +3 is stronger.

In modular protein-protein interactions, specificity is often achieved by a combination of permissive and unpermissive forces that both contribute to the selection of the correct

²Position +1 describes the first residue, +3 the third residue C-terminal to the pTyr.

³Position β D5 describes the fifth residue of β -strand D.

target in the living cell (Zarrinpar *et al.*, 2003). The peptide library approach provided even more than a set of preferred residues at each position of a SH2 binding site. It also identified disfavored amino acids. This is important because selectivity is constituted by high affinity toward the correct target as well as by the exclusion of other potential partners. The identification of preferred SH2 binding sequences permitted the primary sequences of proteins such as RTKs to be scanned for potential SH2 interaction sites, thus allowing the prediction of modular protein-protein interactions.

Although high affinities guarantee high possible biological specificity, very strong interactions can be unfavorable *in vivo* because of their long lifetimes. Such interactions cannot always provide the flexibility required for response to changing extracellular conditions or internal programs. For example, protein-protein interactions that are mediated by posttranslational modifications exhibit relatively low affinities because the binding energy is usually mainly constituted by the modified residue itself. Nevertheless, even the micromolar affinities provide sufficient specificity for the correct interaction. To further overcome low affinity, many signaling complexes use multiple contacts to ensure accuracy of the interaction. Thus, individual interaction domains can be combined in a single polypeptide chain to enhance binding specificity and affinity in multi-protein complexes.

5.1.2 SH2 Function and Mechanisms of Signal Transduction

The association of SH2 domains with their cellular binding partners can elicit various effects. If the target protein is a cell surface receptor in the membrane or a different membrane associated protein, binding of the SH2 domain results in the relocalisation of the soluble cytoplasmic protein and a strong increase in its local concentration. This mechanism is particularly relevant if downstream substrates also associate with the membrane, e.g. for enzymes such as PLC- γ 1, PI3K, GAP and Grb/SOS.

Proteins that bind specifically to protein tyrosine kinases can be preferred substrates of the kinase activity. Due to the increased local concentration, the Michaelis constant for the phosphorylation reduces significantly. For example, p85 and PLC- γ 1 are phosphorylated themselves following stimulation of the cell with growth factors such as platelet derived growth factor (PDGF), nerve growth factor (NGF) or insulin (Kim *et al.*, 1991). In this case, phosphorylation of the target protein exerts the biological effects, whereas the SH2 domain serves only as an adaptor for mediation of the signal.

The association of the SH2 domains of an enzyme with phosphorylated sequences can directly stimulate its activity by the induction of conformational changes, exemplified by PI3K (Backer *et al.*, 1992; Carpenter *et al.*, 1993; Shoelson *et al.*, 1993). The conforma-

tional changes are mediated by residues of the inter-SH2 region (iSH2) (see section 5.2), which directly stimulate the kinase activity of PI3K.

5.1.3 Tandem SH2 Domains

Many modular interaction proteins, such as members of the Syk/ZAP70 family and p85 of PI3K possess two adjacent SH2 domains termed "tandem SH2 domains". Syk family kinases are recruited to cell surface receptors through the interaction of their tandem SH2 domains with tyrosine-phosphorylated sequence motifs called "immunoreceptor tyrosine based activation motifs" (ITAMs). ITAMs typically have the consensus sequence [YXX(L/I)X₇₋₈YXX(L/I)], i.e., two tyrosines spaced by a sequence of 10 or 11 residues containing a hydrophobic residue (L or I) at the third position C-terminal to the phosphotyrosines. The signaling subunits of B- and T-cell receptors and Fc receptors (e.g. of IgE) contain ITAMs. Crosslinking of these receptors leads to the phosphorylation of both tyrosines in the ITAM, transforming it to a high-affinity binding site of members of the Syk/ZAP70 family (Hatada *et al.*, 1995; Flaswinkel *et al.*, 1995; Cambier, 1995; Futterer *et al.*, 1998). Remarkably, the tandem SH2 domains of Syk kinase are able to recognize a variety of doubly phosphorylated ITAMs that vary considerably in the length of the spacer region between the two pTyr. The tandem SH2 domains adapt to these different recognition motifs by varying relative orientations of the two individual SH2 domains (Kumaran *et al.*, 2003). In this case, the preexistence of a conformational equilibrium in the unbound state is crucial for this function.

The spacing of individual tyrosine phosphorylation sites in growth factor receptors varies considerably. In the platelet derived growth factor receptor (PDGFr), tyrosine residues 740 and 751 can be phosphorylated. In the insulin receptor, a six residue-spacer separates the two [YXXM] motifs whereas there is a 20 residue-spacer in IRS-1. Tyrosine residues 315 and 322 can be phosphorylated in the viral middle tumor (MT) antigen.

Such closely spaced phosphorylation sites can either associate with different signaling proteins or enhance the affinity and the specificity toward one target protein. Interaction of two SH2 domains with the same target protein enhances the affinity by three orders of magnitude (Ottinger *et al.*, 1998). The two closely spaced phosphorylation sites of the PDGF receptor that are involved in binding PI3K (pTyr 740 and pTyr 751) activate the enzyme by the association with both SH2 domains (Carpenter *et al.*, 1993). In contrast, pTyr 315 of MT antigen associates with PI3K (Whitman *et al.*, 1985; Kaplan *et al.*, 1986) and Tyr 322, in case of its phosphorylation, mediates the interaction with an SH2 domain of PLC- γ 1 (Su *et al.*, 1995).

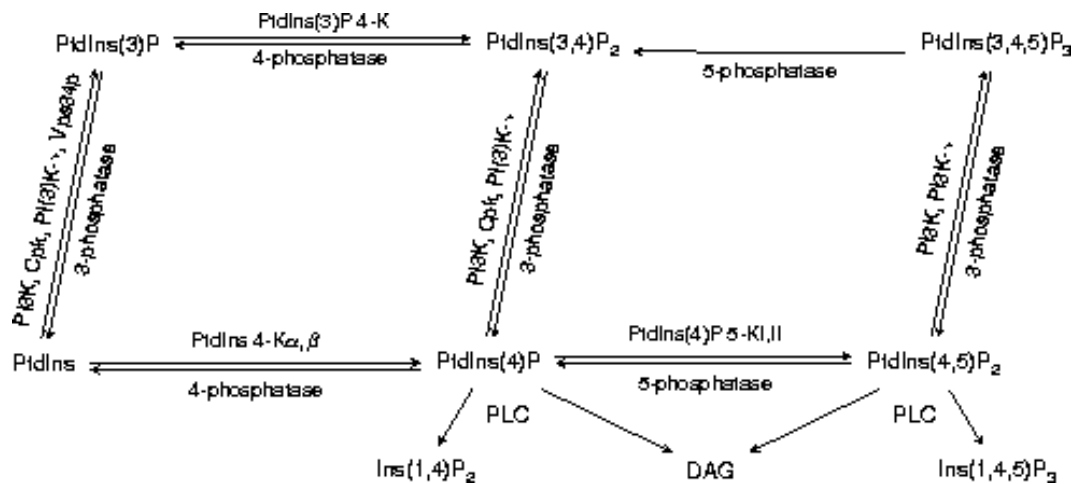


Figure 12: Pathways for phosphoinositide synthesis. The enzymes that synthesize the various phosphoinositides are indicated. Three classes of PI3K enzymes exist: the class I enzymes can use PtdIns, PtdIns(4)P or PtdIns(4,5)P₂ as substrates; class II enzymes phosphorylate PtdIns and PtdIns(4)P; and class III enzymes can only phosphorylate PtdIns. PtdIns(4,5)P₂ is of particular importance: hydrolysis by PLC generates the two second messengers, diacylglycerol (DAG) and Ins(1,4,5)P₃, and phosphorylation by PI3K generates the second messenger PtdIns(3,4,5)P₃. In mammalian cells, at the 3-position phosphorylated inositides are degraded by phosphatases that convert them back to PtdIns, PtdIns(4)P or PtdIns(4,5)P₂. Figure adapted from Toker et al. (Toker and Cantley, 1997).

Diphosphotyrosine sequences can also lead to oligomerization of SH2 domains (Layton *et al.*, 1998). Studies using isothermal titration calorimetry (ITC) showed that a doubly phosphorylated peptide derived from the PDGFR sequence can bind two p85 molecules at high protein-peptide ratios. At equimolar ratios, a 1:1 complex that reduces PI3K activity predominates (O'Brien *et al.*, 2000). These results suggest that the varying activities for alternative binding stoichiometries could be used for regulation of signal transduction in the living cell.

5.2 Phosphatidylinositide 3-kinase

Phosphatidylinositide 3-kinases (PI3Ks) belong to the family of lipid kinases and catalyze the specific phosphorylation of the 3-position of the inositol ring of phosphoinositides (PI). Phosphatidylinositol (PtdIns) constitutes less than 10% of the lipids in eukaryotic membranes. 5% of cellular PI is phosphorylated at the 4-position (PtdIns 4-P) and 5% is doubly phosphorylated at the 4- and 5-positions (PtdIns(4,5)P₂). Only 0.25% of all PIs exhibit a phosphoryl-group at the 3-position, confirming the role of these lipids in the regulation of cellular functions. Indeed, stimulation of cells with growth factors leads to a rapid increase of the concentration of PtdIns phosphorylated at the 3-position.

Members of the PI3K family are divided into three different classes (Vanhaesebroeck

and Waterfield, 1999) (see Figure 12 also for metabolism of PIs). The class I PI3Ks can produce phosphatidylinositol (3,4,5)-trisphosphate (PtdIns(3,4,5)P₃) and are constituted of two proteins, the catalytic 110 kDa subunit (p110) and the 85 kDa regulatory subunit (p85). In the absence of activators, p85 inhibits the catalytic subunit (Carpenter *et al.*, 1990; Escobedo *et al.*, 1991b).

The p85 subunit consists of 724 amino acid residues and has a modular composition mediating modular interactions of PI3K with other proteins. p85 consists of a src homology 3 (SH3) domain, two SH2 domains, and a break cluster region homology (BH) domain. Proline rich sequences flank the BH domain providing binding sites for SH3 domains of downstream targets. The region between the N-terminal SH2 domain (N-SH2) and the C-terminal SH2 domain (C-SH2), referred to as the inter-SH2 region (iSH2), binds the N-terminus of p110 and inhibits its kinase activity in concert with N-SH2. Binding of the SH2 domains to phosphorylated peptide sequences, e.g. in RTKs, activates the kinase activity of p110 presumably through conformational changes of p85. Residues 1-285 of p85 transfer the conformational changes in the protein complex (Rordorf-Nikolic *et al.*, 1995; Yu *et al.*, 1998). In polyoma MT antigen transformed cells as well as upon stimulation with growth factors like PDGF, nerve growth factor (NGF), and insulin, PI3K phosphorylates its own regulatory subunit p85 (Kaplan *et al.*, 1987; Auger *et al.*, 1992; Soltoff *et al.*, 1992).

A number of growth factor receptors with intrinsic or associated protein tyrosine kinase activity stimulate PI3K. Cytosolic proteins that are phosphorylated on tyrosine residues in response to an extracellular signal also can stimulate the enzyme. PI3K activity increases in certain cell types after stimulation with PDGF, insulin, insulin-like growth factor type 1 (IGF-1), colony-stimulating factor 1 (CSF-1), NGF, hepatocyte growth factor (HGF), Steel (stem cell growth factor), and EGF (epithelial growth factor) (Cantley *et al.*, 1991; Stephens *et al.*, 1993; Varticovski *et al.*, 1994). Cells transformed by the oncogenes *v-src*, *v-fms*, *v-abl* or polyoma MT antigen exhibit increased PI3K activity (Cantley *et al.*, 1991).

The SH2 domains of p85 bind phosphorylated tyrosine-sequences as well as PtdIns 3-P, a product of PI3K. Competition of PtdIns 3-P with phosphopeptides, the canonical ligands, represents a negative feedback mechanism terminating the cellular signal (Rameh *et al.*, 1995).

Phosphoinositide phosphatases counteract the activation of class I PI3Ks. "Phosphatase and tensin homolog deleted on chromosome 10" (PTEN) is a tumor suppressor protein in breast cancer and hydrolyzes PtdIns(3,4,5)P₃ to PtdIns(4,5)P₂ (Yamada and Araki, 2001). In contrast, the SH2-domain-containing inositol phosphatase (SHIP) possesses

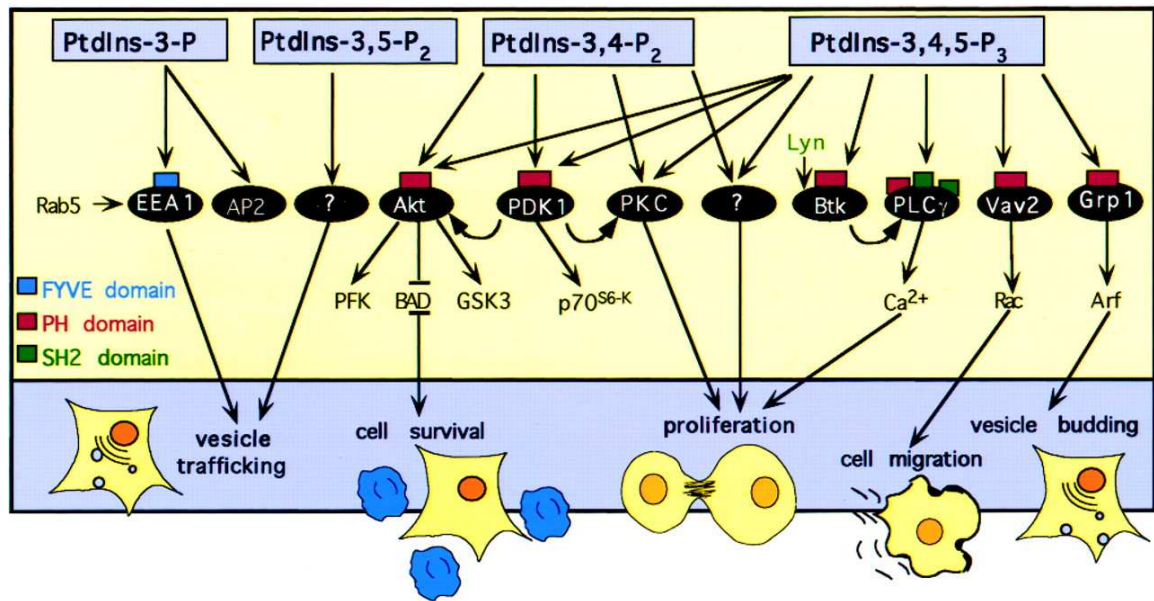


Figure 13: Signal transduction by phospholipid products of PI3K and their target molecules. The different lipid products of PI3Ks are shown at the top of the Figure, and the cellular responses provoked by the 3'-phosphorylated lipids are depicted at the bottom. Direct targets of the lipids are represented as black ovals, the protein domains that mediate the interactions are shown as colored rectangles. The figure is reproduced from Rameh *et al.* (Rameh and Cantley, 1999).

5'-phosphoinositide phosphatase activity and produces PtdIns(3,4)P₂, which activates signaling downstream of PI3K.

5.2.1 Role of PI3K in Cellular Regulation

PI3Ks play a central role in the control of metabolism, proliferation (Fantl *et al.*, 1992; Valius *et al.*, 1993), cell growth, survival (Minshall *et al.*, 1996), migration (Derman *et al.*, 1997; Meili *et al.*, 1999), vesicle trafficking (Wurmser *et al.*, 1999; Corvera *et al.*, 1999), and secretion (Schu *et al.*, 1993) (see Figure 13). Thus, PI3K modulates essential physiological processes and is involved in the pathology of cancer (Vivanco and Sawyers, 2002), inflammation, and cardiovascular diseases. PI3K regulates cellular functions by recruiting PtdIns(3,4,5)P₃-binding proteins to the plasma membrane. Many of these bind to 3-phosphorylated PIs through a pleckstrin homology (PH) domain. FYVE, PX and ENTH domains often interact with PtdIns 3-P (Rameh and Cantley, 1999). Downstream signaling targets of PI3K such as protein kinase C (PKC), PLC γ , and Akt and their effects on the cell are summarized in Figure 13.

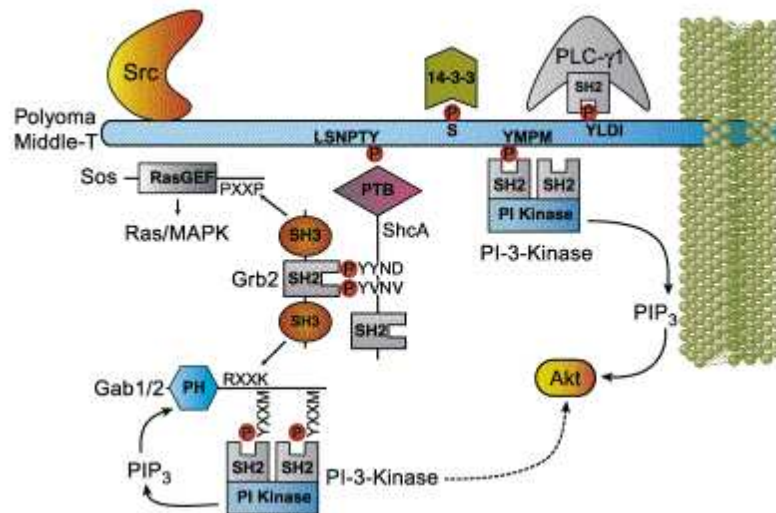


Figure 14: Assembly of a signaling complex around polyoma middle tumor (MT) antigen. MT acts as a scaffold to recruit the tyrosine kinase Src and downstream targets. SH2 domains of various proteins distinguish between different pTyr motifs which leads to the recruitment of PLC- γ 1, ShcA and PI3K and in general to the formation of a signaling network through the reiterated use of modular interactions. The figure is reproduced from Pawson (Pawson, 2004).

5.3 Polyoma Middle Tumor Antigen

Receptors with intrinsic tyrosine kinase activity or with associated cytoplasmic tyrosine kinase subunits mediate the signals received through hormones, cytokines, and antigens to SH2 containing proteins that couple the signals to intracellular effectors such as the Ras GTPase and phospholipid metabolism. Aberrant activation of tyrosine kinases leads to various kinds of cancers. Introduction of a protein that serves as scaffold for the assembly of signal transduction complexes also can transform a cell. The 427 amino acid MT antigen, the major transforming protein of polyoma virus, contains binding sites for various critical signaling proteins and assembles a large complex of proteins such as Src tyrosine kinase, PLC- γ 1, 14-3-3 and PI3K (see Figure 14). The major binding site for PI3K is tyrosine residue 315 which is phosphorylated *in vivo*. The normal composition of signal transduction complexes changes in the presence of the adaptor MT and proliferation is stimulated. Infections with the DNA-virus polyoma can cause tumors in various tissues (Tognon *et al.*, 2003; Reiss and Khalili, 2003).

5.4 The Cellular Retinol-Binding Protein

Intracellular traffic and metabolic utilization of hydrophobic molecules are mediated by specific carriers, small monomeric proteins of approximately 15.5 kDa. The superfamily of intracellular lipid-binding proteins (iLBPs) encompasses the fatty acid-binding proteins

(FABPs) and the carriers of the alcoholic and acidic forms of vitamin A (retinol), the cellular retinol-binding proteins (CRBPs) and the cellular retinoic acid-binding proteins (CRABPs) (Li and Norris, 1996).

5.4.1 Functions of Cellular Retinol-Binding Proteins in the Cell

In different organisms CRBP I, the most widely distributed intracellular carrier of retinol, exhibits distinct tissue distributions. In the adult rat, it is expressed mainly in liver, kidney and in the genital tract (Ong *et al.*, 1994), whereas in humans it is expressed at high levels in gonads, adrenal and pituitary glands (Ong and Page, 1986). In both rat and humans, CRBP II is restricted to the small intestine (Ong *et al.*, 1994). Another remarkable difference between CRBP I and CRBP II is their affinity for *all-trans*-retinol. The K_D of CRBP I is as low as 0.1 nM in neutral aqueous solution, whereas it is about 10 nM for CRBP II corresponding to one hundredfold weaker binding (Li *et al.*, 1991).

These differing affinities, together with the different tissue distributions, point to distinct functions for the two carrier proteins. Some studies suggest a key role in regulating vitamin A homeostasis, as recently confirmed by an *in vivo* study of CRBP-null mice (Ghyselinck *et al.*, 1999). *In vitro* studies have suggested that it is involved in retinol internalization and intercellular transfer (Ottonello *et al.*, 1987; Sundaram *et al.*, 1998), retinol esterification (Ong *et al.*, 1988; Herr and Ong, 1992), retinyl ester hydrolysis (Ottonello *et al.*, 1987; Boerman and Napoli, 1991), and the oxidation of retinol to retinaldehyde in retinoic acid synthesis (Ottonello *et al.*, 1993; Boerman and Napoli, 1996). Retinoic acid represents the active form of vitamin A and plays a key role in cell growth, differentiation, and morphogenesis (Gudas *et al.*, 1994). Recently, it has been shown that CRBP I plays a crucial role in various types of cancer. The occurrence of breast and ovarian cancer has recently been correlated with decreased levels of CRBP I expression (Kuppumbatti *et al.*, 2000, 2001; Esteller *et al.*, 2002; Roberts *et al.*, 2002; Schmitt-Graff *et al.*, 2003).

5.4.2 Retinol Binding to CRBP

The structural motif common to all iLBPs consists of two orthogonal β -sheets, each one containing five anti-parallel β -strands (A to E and F to J), which together form a β -barrel that accommodates the hydrophobic ligand. Two short α -helices cover the open end of the barrel (Banaszak *et al.*, 1994) (see Figure 15 left). The three-dimensional structure of CRBP I, in this text from now on denoted only CRBP, in complex with retinol revealed that *all-trans* retinol is bound in a deeply buried cavity that appears to be fully shielded from the outside solvent (Cowan *et al.*, 1993). While accounting for the high stability of

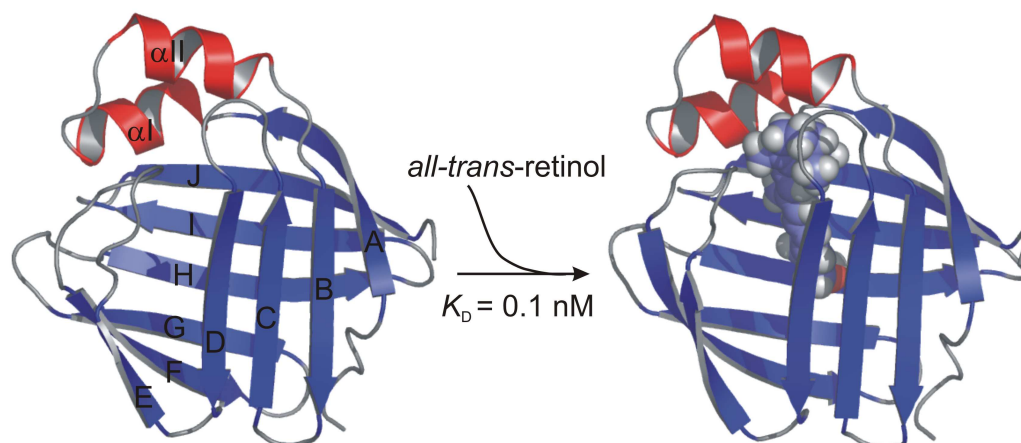


Figure 15: The binding mechanism of retinol to CRBP is not obvious from the structures of the free and the complexed form. CRBP is a ten-stranded β -barrel with a helix-turn-helix motif closing the barrel on one side. Retinol binds in the cavity which is shielded from the outside solvent. Transient opening of the cavity is required for access to the binding site and high-affinity binding. Ribbon diagrams of apo- and holo-CRBP are depicted on the left and right side, respectively. Retinol is shown in a space-filling representation.

the complex, this structure did not provide information on either the mechanism of ligand access to its binding site or the mechanism of ligand release. The solution structure of the protein devoid of retinol (apo-CRBP) was very similar to the structure of the holo-protein (Franzoni *et al.*, 2002). The main difference between the structure ensembles of the apo- and holo-forms was a higher backbone disorder of some segments in the ligand-free protein, including α -helix II, the subsequent linker to β -strand B and the β C- β D and β E- β F turns. This region previously had been identified as a potential portal for ligand access to the binding cavity from comparisons with related fatty acid-binding proteins. A small opening in the surface of intestinal fatty acid-binding protein (I-FABP) could allow ligands access to the cavity (Sacchettini *et al.*, 1989). In the structures of the complexes of adipocyte lipid-binding protein and liver fatty acid-binding protein with their ligand oleate, one end of the bound lipids protrudes into the surrounding solvent (Xu *et al.*, 1993; Thompson *et al.*, 1997).

The investigation of the internal backbone dynamics of CRBP, as obtained from ^{15}N relaxation data (T_1 , T_2 , and heteronuclear nuclear Overhauser effect) at two different fields, indicated several residues with higher mobility on the ps-ns time scale in the apo-protein with respect to the holo-protein (Franzoni *et al.*, 2002) and confirmed the possible involvement of the β C- β D and β E- β F turns in a dynamic mechanism of retinol uptake. However, this observation was not sufficient to explain ligand exchange between the solvent shielded cavity and the sites of retinol uptake and release. Only single residues show significantly reduced S^2 values. The observed modes of ps-ns dynamics do no account

for large scale correlated motions that could open the cavity.

CRBP I is an interesting model to study ligand uptake because its β -barrel structure forms a highly specific binding cavity shielded from the outside solvent. The cavity has to open transiently to allow access to its ligand binding site, though this has never been demonstrated.

6 Summary of Publications

In the following section, the publications that contribute to this work will be reviewed shortly. The aim of this work was to characterize the functional dynamics of proteins during ligand binding. The interaction of the N-terminal SH2 domain of PI3K with phosphopeptides initially served as a model system. To demonstrate the general applicability of the experimental approaches, they were also used to investigate the binding mechanism of retinol to CRBP.

The SH2 protein samples were provided by Prof. Dr. Brian Schaffhausen. The work on CRBP was performed in collaboration with Prof. Dr. Gian-Luigi Rossi and Prof. Dr. Lorella Franzoni, who provided the protein samples and the assignments of apo- and holo-CRBP.

The main contributor to publication 6.2 (Günther *et al.*, 2002) was Ulrich Günther, who performed the titrations and developed the line shape analysis of titration spectra. I contributed at an advanced stage of this publication and performed H/D exchange experiments and CPMG experiments of the free and MT8-complexed wt N-SH2 domain. Titrations for publication 6.3 Mittag *et al.* (2004b) were jointly performed by Ulrich Günther and me.

Line shape analysis was based on work of Ulrich Günther and further extended. Experimental procedures, data analysis and interpretation for publications (Mittag *et al.*, 2003b, 2004b, 2003a, 2004a) and for the unpublished data presented in this thesis were carried out by myself.

The N-terminal SH2 Domain of PI3K as a Model for Protein-Protein Interactions

6.1 Direct Observation of Protein-Ligand Interaction Kinetics

An eight amino acid peptide derived from the binding sequence of polyoma MT antigen and therefore named MT8 (EEEpY₃₁₅MPME-NH₂) was used to probe the effect of ligand binding on the μ s-ms dynamics of the N-SH2 domain. Relaxation dispersion experiments of the free N-SH2 domain, of a N-SH2 sample partially titrated with 1/20 of MT8, and of the N-SH2:MT8 complex permitted the separation of internal dynamics of the protein from dynamics associated with ligand interaction.

The CPMG experiments were performed at two different magnetic fields of 11.7 T and 16.4 T, and the relaxation dispersion curves were fit to a model for exchange between two

sites (eq. 29) for every residue individually. The free N-SH2 domain exhibited limited conformational exchange on the ms time scale in the EF and in the BG loop. These two loops coordinate the residues C-terminal to the pTyr and mediate the specificity of the interaction. In addition, R340, one of the conserved arginine residues in the pTyr binding pocket, exhibited μ s mobility.

In the presence of 1/20th equivalents of MT8, relaxation dispersion experiments demonstrated pronounced chemical exchange in the central β -sheet, in the pTyr binding site, in the EF and in the BG loop. For low concentrations of the free ligand, the exchange rate k_{ex} represents the off-rate of the interaction, k_{off} reflecting the relaxation of the protein back to the free form after release of the ligand. Interestingly, the off-rates differed for different residues, which can be interpreted as varying local affinities. The exchange of a number of residues in the EF loop and in the β -sheet is not only caused by binding and release of the peptide, but in addition by a superimposed conformational exchange of the protein. The free protein is likely to exchange with conformers that are formed by the interaction with the ligand and represent low-populated intermediates on the reaction pathway. The 1:1 complex of N-SH2 and MT8 is rigid on the μ s-ms time scale.

Large differences in kinetic rates of residues adjacent in sequence were observed confirming their individual roles in binding. Nevertheless, residues connected through space by the same side chain interactions exhibited similar rates supporting the possibility of correlated motions in the protein. In this work, CPMG measurements were used to characterize the site-specific functional dynamics of the N-SH2 domain upon ligand binding. The occurrence of intermediates on the binding pathway could be assigned to regions of the protein that mediate specificity of the interaction. A comparison of relaxation dispersion analysis and line shape analysis showed that the combination of both methods is particularly valuable for the interpretation of multi-site exchange, because different sub-processes are better observed in the two different techniques.

6.2 Probing Src Homology 2 Domain Ligand Interactions by Differential Line Broadening

The interaction of the N-SH2 domain with phosphopeptides was probed using line shape analysis of signals of ^1H - ^{15}N -HSQC spectra recorded for increasing concentrations of the ligands. Binding of MT8 was characterized site-specifically for 37 amino acid residues. Off-rates of the interaction varied throughout the structure but agreed with rates from relaxation dispersion experiments. Error estimation of the off-rates demonstrated that the error is dominated by the insensitivity of the line shapes to variations of the rate. The contribution of the signal-to-noise ratio covers only a low percentage of the over-all error.

Several residues, e.g. R340, exhibited lower signal intensities in the free form than in the complex. For the simulation of these line shapes, outward exchange with an undefined species that reduces the signal intensity of one state was assumed. An explanation for the intensity differences might be a reduction of hydrogen exchange rates with water after binding. However, H/D exchange experiments demonstrated that the signal of R340 is in fast exchange with the solvent and cannot be detected immediately after addition of D₂O in either the free or the complexed SH2. CPMG measurements of the free protein shed light onto the problem; although R340 did not exhibit relaxation dispersion, constantly increased relaxation rates independent of the refocusing field indicated exchange on a μ s time scale reducing the signal intensity.

A two-state exchange model sufficed for the interpretation of line shapes of residues of α -helix B, of the whole α -helix A and some residues of the BG loop. In contrast, the signals of some residues of the central β -sheet, of the EF loop, and of the BG loop exhibited shoulders for intermediate ligand concentrations. The complexity of line shapes could be explained assuming a parallel binding mechanism including long-lived intermediates.

To investigate whether the effects observed were specific for binding of MT8, the interaction of the wild type N-SH2 domain with pTyr and with another eight amino acid peptide derived from the PDGFr binding sequence (SVDpY₇₅₁VPML-NH₂) was probed. Additionally, binding of MT8 to the low-affinity mutant I381Y was investigated. Interestingly, only the high affinity-interactions of wt N-SH2 with MT8 and PDGFr peptide led to the formation of multiple protein conformers. Neither in titrations of wt N-SH2 with pTyr nor in titrations of I381Y with MT8 could complex line shapes be observed. The opening of the conformational space of the protein upon encounter with ligand may potentially lead to the formation of binding conformers and may hence be crucial for high-affinity interactions. Based on this assumption, the line shapes of the P427L SH2 that exhibits a mutation in β -strand G were astonishing. In spite of an apparently low affinity for MT8, the signals exhibited four to five signal components each. Assuming one-step binding, off-rates of 100 s⁻¹ to 1000 s⁻¹ could be extracted, which are more in concordance with a micromolar affinity. Apparently, the mutation at the back of the protein leads to destabilization and extensive conformational mobility upon interaction with peptide. If the multiple conformers of this mutant are caused mainly by unproductive attempts of binding that must be reverted before a new encounter can occur, the on-rate of the interaction can be reduced substantially. This model may explain both complex line shapes and low off-rates in spite of a low affinity.

The line shape analysis showed that the interaction of phosphopeptides with the N-SH2 domain involves rearrangements during the binding process. Slow kinetic processes in loops or in regions adjacent to loops determine the overall rate of the protein-ligand interaction.

This work developed line shape analysis as a useful tool for the investigation of protein-ligand interactions. Analysis of 2D protein spectra allows the site-specific assignment of kinetic models to specific residues. The range of rates accessible for quantitative analysis is similar to the range of rates that can be analyzed using CPMG measurements. However, line shape analysis provides mechanistic information and allows the direct visualization of kinetic intermediates.

6.3 Tracing Kinetic Intermediates during Ligand Binding

The mutant P395S, which bears a mutation of Ser 395 in the EF loop to a proline, exhibits reduced affinity for peptides derived from the MT binding sequence (pYM₃PM). In contrast, the affinity for the PDGFR binding sequence (pYV₃PM) is retained. Interestingly, the relevant binding sequences of the peptides differ only in the first position C-terminal to the pTyr. However, the loop exhibiting the mutation site is normally implicated in complexation of the +3-position. Line shape analysis revealed that the mechanism of the interaction depends on the peptide. Populations of the different states, chemical shift differences, and rates of the binding processes could be estimated.

Binding of MT8 occurs with a two-step binding mechanism. Initially, a typical binding process leads to the built-up of an intermediate signal at a ligand/protein ratio of 0.7-0.9. The fast exchange line shapes with a high off-rate indicate instability of the intermediate. A second binding step is required for the formation of the final complex. Since the interaction occurs with a 1:1 stoichiometry, the ligand must be released after the first unproductive binding attempt and recycled for the formation of the complex. The stable intermediate represents a kinetic hindrance for the transition to the product and can be named as a reason for the reduced affinity.

The PDGFR peptide also binds with a two-step binding mechanism. However, in contrast to MT8, the transition to a binding conformer occurs already at low ligand/protein ratios of 0.1. This transition results in a distinct first titration step with changes in intensity and chemical shift of the NMR signal different from the following steps. They in turn correspond to a typical one-step binding mechanism. An initial interaction between P395S and the PDGFR peptide leads to a rearrangement of the protein or stabilizes a conformer from a preexisting equilibrium. However, the intermediate exhibits a long life time. Addition of the ligand seems to reduce the activation energy for the transition of the free protein to the binding conformer.

For the two phosphopeptides, the formation of intermediates with differing stability occurs at different positions of the binding coordinate. These results demonstrated that the specificity of protein-ligand interactions can be regulated kinetically.

6.4 Novel Insights into the Mechanism of Retinol Binding by Cellular Retinol-Binding Protein

This book article describes and compares NMR techniques for the investigation of protein dynamics on the μ s-ms time scale, particularly CPMG experiments and line shape analysis. The article explains the principles of chemical exchange and introduces experimental procedures and data analysis and describes the benefits and limits of relaxation dispersion and line shape analysis. These approaches were used to gain insight into the mechanism of retinol binding by CRBP.

The analysis of the mobility on the μ s-ms time scale of apo-CRBP showed that large portions of the protein, encompassing essentially all β -strands, exhibit conformational exchange with exchange rates between 100 s^{-1} and 1000 s^{-1} . The loop regions, which do not show relaxation dispersion, but have lower S^2 values, seem to be mobile on a faster time scale. The highest exchange contributions are observed for residues from α -helix II, for residues from the turn between the two helices and from turn β C- β D. All these residues frame the putative portal region. Signals of residues in turn β E- β F, which also belong to the portal region, are not detectable because of extensive line broadening. The high degree of conformational flexibility in apo-CRBP, especially around the putative portal region, is almost completely quenched upon retinol binding, indicating that retinol binding markedly reduces the protein conformational flexibility.

A titration of apo-CRBP with retinol and subsequent line shape analysis revealed a complex binding mechanism with distinct sequential steps. The first step is characterized by a high off-rate for all residues and might represent an initial nonspecific interaction of retinol and CRBP. The second slow exchange step sensed by a large subset of residues may represent the rate of retinol dissociation from its specific binding site and account for the high affinity of the carrier for its ligand.

This study of CRBP has provided new insight into the mechanisms of retinol binding to its specific carrier. The complexity of the kinetics of protein-ligand interactions on a per-residue basis had not been observed previously.

6.5 Freezing of Conformers of the Cellular Retinol-Binding Protein by Retinol

The book article "Novel Insights into the Mechanism of Retinol Binding by Cellular Retinol-Binding Protein" encompassed first results of a line shape analysis of a titration of CRBP with retinol. This study has been completed to characterize the mechanism of

retinol uptake into the CRBP cavity on a per-residue basis. A sequence of processes that lead to the transient opening of the portal and to binding of retinol could be resolved.

The analysis confirmed the location of the portal for ligand entry. The investigation allowed a novel view of the processes involved in ligand uptake. In an initial step, retinol binds unspecifically to the surface of the protein. Despite no apparent specificity for this first step, this interaction seems to be important to modulate the microsecond dynamics in the portal region. The conformational exchange seen for *apo*-CRBP is slowed, which allows the ligand to enter the cavity and to bind inside the cavity with high affinity. This time- and residue-resolved mechanism provides basic insights into the core processes required for ligand uptake into protein cavities and proves the importance of intrinsic protein dynamics for protein function.

Additional Unpublished Results

6.6 Complex Interaction of the N-SH2 Domain with a Doubly Phosphorylated Peptide

The major binding site of polyoma MT antigen for the N-SH2 domain of PI3K is Y315 (Whitman *et al.*, 1985; Kaplan *et al.*, 1986), whereas Y322 can support the interaction with PLC γ 1 (Su *et al.*, 1995). Activation of PI3K *in vivo* is much stronger with doubly phosphorylated peptides than with mono phosphorylated ones (Backer *et al.*, 1992; Carpenter *et al.*, 1993; Herbst *et al.*, 1994). One possibility is that closely spaced phosphotyrosines can interact with multiple SH2 domains in the same protein as described for the interaction of ITAM motifs with SH2 domains (Hatada *et al.*, 1995; Mayer, 1995; Futterer *et al.*, 1998). This is possible for PI3K, which possesses two SH2 domains N- and C-terminal of the inter-SH2 region in its p85 regulatory subunit. Binding of two intramolecular SH2 domains to closely spaced phosphotyrosines in a target protein may enhance the affinity and the specificity of the interaction. However, evidence has also been presented that diphosphotyrosine sequences can induce oligomerization of PI3K (Layton *et al.*, 1998).

Typical binding assays measure the ability of phosphorylated peptides to block binding of ^{32}P -labeled tyrosine phosphorylated MT to GST- N-SH2 fusion protein immobilized on glutathione beads (Yoakim *et al.*, 1992, 1994). Interestingly, competition experiments demonstrated that a 15 residue doubly phosphorylated peptide (MT15, EEEpY₃₁₅MPMEDLpY₃₂₂LDIL-NH₂) bound nearly tenfold tighter than a monophosphorylated peptide with the same sequence (EEEpY₃₁₅MPMEDLY₃₂₂LDIL-NH₂) (Weber *et al.*, 2000). For the C-terminal SH2 domain, no enhancement of the affinity was

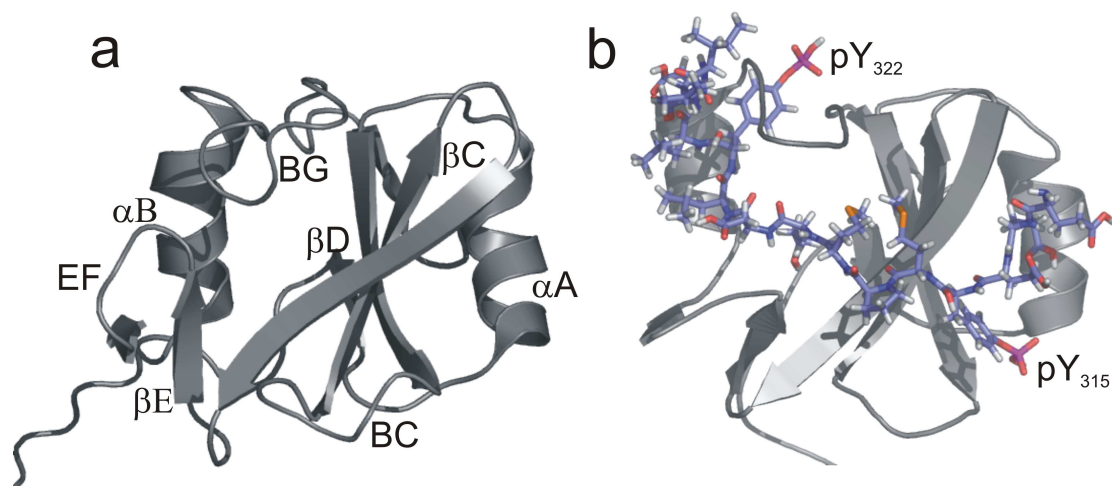


Figure 16: Ribbon diagram of the (a) free N-SH2 domain of PI3K and (b) the complex with a doubly phosphorylated, 15-residue peptide derived from the binding site of MT antigen. (a) The typical SH2-fold encompasses a central antiparallel β -sheet and two flanking α -helices. The annotation of secondary structural elements follows the convention of Eck *et al.* (Eck *et al.*, 1993a). (b) pTyr 315 occupies the conserved primary binding site of the SH2 domain, the residues C-terminal stretch across the central β -sheet. Residues of the large BG loop interact with pTyr 322.

observed. The solution structure of the N-SH2:MT15 complex revealed a novel mode of interaction of an SH2 domain (see Figure 16) (Weber *et al.*, 2000). In addition to the conserved primary phosphotyrosine binding site, the structure revealed an unusual second pTyr binding site formed by residues of the large BG loop. Many target proteins exhibit two closely spaced tyrosine phosphorylation sites that are normally thought to be involved in the recruitment of different signal transduction proteins. Clearly, differential interactions of one doubly phosphorylated target protein with one or two SH2 domains (of the same or different proteins) for different concentration ratios represents a new possibility for the modulation of signals in the living cell.

Temperature dependent line shapes of key residues of the N-SH2 domain in complex with MT15 demonstrated that the protein undergoes temperature dependent conformational exchange between several states.

CPMG measurements and line shape analysis was used to investigate the mechanism of MT15 binding to the N-SH2 (see section 8.1). The interaction of the N-SH2 domain with MT15 shows substantial differences from the previously characterized interaction with MT8. However, it supports our model that initial encounter with ligand induces suitable binding conformers that exhibit high affinity toward the peptide and a long life time. The strong exchange in the SH2 domain at substoichiometric MT15 concentrations arises from a dynamic equilibrium between distinct aggregates of protein and peptide that may differ in relative orientation and stoichiometry of protein and peptide. At low peptide/protein

ratios, two protein molecules compete for one doubly phosphorylated ligand. In the presence of higher peptide concentrations, a transition to 1:1 complexes occurs. In principle, a number of additional complexes with varying stoichiometries are possible, some of which must exhibit a strongly decreased affinity compared to the canonical SH2-phosphopeptide interaction. Recent studies on other protein-protein interactions demonstrated that multiple weak interaction motifs can lead to strong and cooperative binding (Nash *et al.*, 2001). The study of the binding mechanisms of signal transduction complexes in which multiple modules influence the properties of the interaction, stands at the next endeavor.

7 Achievements of this Work and Outlook

In this work, two complimentary NMR techniques were used to investigate the kinetics of protein-ligand interactions of two structurally and functionally different proteins: The N-terminal SH2 domain of Phosphatidylinositide 3-kinase (PI3K) participates in signal transduction pathways and binds tyrosine phosphorylated peptide sequences. CRBP belongs to the family of intracellular lipid binding proteins and stores its hydrophobic ligand retinol in a solvent-shielded β -barrel cavity. Characterization of the μ s-ms dynamics of the free proteins and of their ligand complexes at various ligand concentrations permitted comparison of the inherent dynamics with ligand induced mobility and extraction of the kinetic rates of the interaction. Line shape analysis revealed unexpectedly complex binding mechanisms for both systems. An SH2 domain mutant exhibited differential mechanisms for different ligands with intermediates at differing positions on the reaction pathway, demonstrating that specificity can be determined kinetically. CRBP exhibited a complex binding mechanism encompassing two sequential steps. The occurrence of relatively long-lived intermediates (several milliseconds) constituted an essential property for the function of both proteins. In the SH2 domain, these conformers were induced by encounter with the ligand (Günther *et al.*, 2002; Mittag *et al.*, 2004b), whereas the initial interaction with retinol converted the preexisting fast conformational mobility of apo-CRBP to slow exchange, enabling ligand entry into the cavity of open conformers (Mittag *et al.*, 2004a).

The investigation of intermediate states during binding has opened a new discussion on allosteric regulation and the question whether the allosteric conformational change is already 'presampled' in the ground state (Kern and Zuiderweg, 2003). Cooper & Dryden pointed out that allostery can result from changes in conformational entropy rather than simple changes in average conformation (see Figure 17) (Cooper and Dryden, 1984). Ligand-induced changes in the dynamics of proteins could thereby communicate the allosteric effects between different binding sites without necessarily involving conformational changes of the protein. Although this work does not focus on allostery in its typical definition (binding of one ligand affecting the affinity of another ligand), the results presented in this work can nevertheless be attributed to very similar phenomena. Different proteins with very different ligand binding properties were studied. Interestingly, initial contacts with the ligands can either induce opening of the conformational space of the protein or modify the time scale of conformational exchange inherent to the free protein.

The potential of NMR spectroscopy in protein Biochemistry is derived from its ability to study a wide variety of protein properties, such as structural parameters, protonation states of ionizable groups and dynamics on a large range of time scales. This allows the investigation of protein function in aqueous solution. Relaxation dispersion analysis already

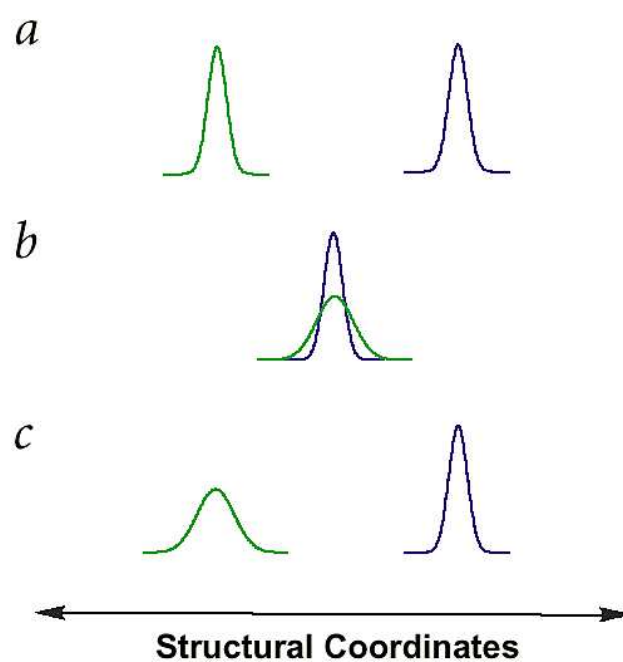


Figure 17: Schematic illustration of allosteric mechanisms. (a) Allostery can be based solely on a change in atomic coordinates of the protein. (b) However, as pointed out by Cooper & Dryden (Cooper and Dryden, 1984), a change in conformational entropy manifested in the dynamics of the protein also provides an alternative rationale for creation of allosteric free energy changes in proteins. Only small changes in the breadth of the conformational distribution would be required if a large number of motional modes are involved. (c) In principle, both mechanisms could be operative. The figure is reproduced from Wand (Wand, 2001).

constitutes an important approach for the study of functionally relevant motions. Line shape analysis represents an additional valuable technique to the broad repertoire of NMR spectroscopy. Its specific advantage is the ability to obtain mechanistic information and to directly visualize kinetic intermediates during ligand binding. Besides providing new insight into basic mechanisms of protein function, the approach may also have important practical implications. Initial results of titrations with a number of proteins suggest that binding intermediates are a common property of proteins differing in structure, function, and ligands. The knowledge that intermediates can retard the transition to a functional complex may lead to new possibilities in drug development. Non-functional states may be trapped by suitable ligands, an alternative concept for the inhibition of therapeutically interesting targets. Furthermore, data on the dynamics on μs -ms time scales and on the occurrence of intermediate forms may be used to guide MD simulations, allowing longer time spans to be simulated by incomplete sampling.

Line shape analysis is easily applicable to small and medium sized proteins. For larger molecules, specific labeling of functionally important residues reduces spectral overlap. Signals with narrow line widths can be obtained by recording TROSY or CRINEPT spectra instead of conventional HSQC spectra. In addition, the approach is applicable to a great variety of biomolecular interactions, including binding of small molecules to RNA aptamers, protein-phospholipid and protein-DNA interactions, and cell communication through polysaccharide moieties.

The detailed analysis of kinetic and thermodynamic parameters characterizing the energy landscape of proteins is essential to understand their biophysical properties. A combination of several new NMR techniques for the characterization of dynamics on relevant time scales opens new avenues to study such properties. The investigation of mechanisms of protein folding, ligand binding and enzyme catalysis will benefit from the development of new experimental techniques and will become even more important and feasible in the future. These approaches may yield significant biological insights into the mode of action in diverse protein systems.

8 Unpublished Results

8.1 Complex Interaction of the N-SH2 Domain with a Doubly Phosphorylated Peptide

Recent structural characterization of the N-SH2 domain in complex with MT15 demonstrated that one doubly phosphorylated peptide binds to one SH2 molecule at equimolar concentrations. Furthermore, multiple signal shoulders in temperature dependent line shapes showed that the complex undergoes slow exchange between several states (Weber *et al.*, 2000). This exchange can arise from conformational mobility as well as from chemical exchange between distinct aggregates of the protein and the peptide. These could differ in relative orientation and stoichiometry.

Relaxation dispersion experiments on the SH2-MT15 complex and on an initial binding state and line shape analysis of titration spectra were used to further investigate the dynamics of the interaction. Experimental procedures were as described in (Mittag *et al.*, 2004b) and (Mittag *et al.*, 2003b).

8.1.1 Results and Discussion

Relaxation dispersion experiments with low concentrations of ligand present in the protein sample were used to monitor the off-rate of the interaction. Figure 18a-f depicts relaxation dispersion curves of several residues chosen as representative examples. E342 (Figure 18a) in α -helix I exhibits flat relaxation dispersion curves, indicating no exchange on the μ s-ms time scale. In contrast, key residues of the interaction experience chemical exchange, e.g. R358, one of the arginines complexating the primary pTyr (Figure 18b). Relaxation dispersion experiments reveal high exchange contributions especially in the β -sheet, in the EF loop, and in the BG loop. T369 (c) and K379 (d) are located in the central β -sheet, which is involved in specific interactions with the three residues C-terminal to pTyr, whereas Y390 (e) and S393 (f) belong to the EF loop.

The amplitudes of the exchange contributions R_{ex} to the transverse relaxation rates are depicted on the ribbon diagram of the N-SH2 in Figure 19a in a colorcode from blue to red for R_{ex} values from 0 s^{-1} - 20 s^{-1} . Interestingly, in β -strand D, residues exhibiting high and low exchange contributions alternate. Those residues which point towards the EF and BG loops (K379, I381, and I383) adopt high values representing the dynamics of the interaction with the peptide. In contrast, S380 and K382 exhibit lower values. This result suggests that exchange monitored on the amide nitrogens reflects motions transferred motions from the side chains that can be correlated through space.

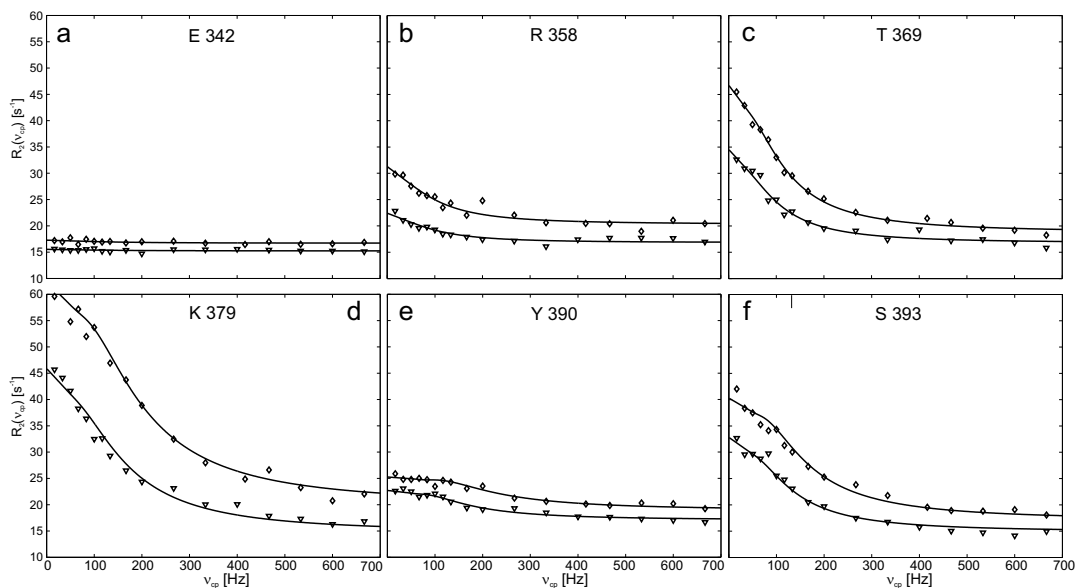


Figure 18: Relaxation dispersion curves of the N-SH2 domain for the initial interaction with MT15. Effective transverse relaxation rates, R_2^{eff} , as a function of the CPMG field strength, ν_{cp} . $R_2^{\text{eff}}(\nu_{\text{cp}})$ of E342 (panel a) does not depend on the CPMG field strength, whereas residues (b) R358, (c) T369, (d) K379, (e) Y390 and (f) S393 exhibit exchange with exchange contributions of 9.8 s^{-1} , 26.1 s^{-1} , 41.1 s^{-1} , 6.2 s^{-1} and 22.4 s^{-1} , respectively. Data recorded at ^1H Larmor frequencies of 700 and 500 MHz are depicted with diamonds and triangles, respectively. The best-fit dispersion curves using a simulation of the full McConnell equations for two-site exchange are shown as solid lines.

The exchange parameters obtained by fitting the relaxation dispersion curves using the full simulation of the McConnell equations 28 on page 28 are listed in Table 1. The exchange rates k_{ex} are depicted on the ribbon diagram of the N-SH2 in Figure 19b with a color code from blue to red for 0 to 1500 s^{-1} . The variations in exchange rates indicate different local life-times of the complexed state of the protein. These differences can be interpreted as differing local affinities of the N-SH2 toward the ligand.

Table 1: ^{15}N Relaxation Dispersion Parameters of Exchanging Residues of the N-SH2 domain in the presence of 1/20 equivalents of MT15

Residue	$R_{\text{ex}} (\text{s}^{-1})^a$	$k_{\text{ex}} (\text{s}^{-1})$	p_a	$\Delta\omega$ (ppm)	$R_2^0 (\text{s}^{-1})$	α
Q 329	4.0	232	0.88	0.27	12.73	1.86
D 330	5.5	428	0.98	1.66	16.08	0.76
I 338	3.9	999	0.98	1.35	13.65	1.62
S 339	19.5	731	0.92	1.19	19.23	1.60
R 340	7.7	723	0.85	0.52	20.26	1.90
N 344	9.8	496	0.95	0.95	16.57	1.47
E 345	8.5	479	0.90	0.55	16.34	1.80

Residue	$R_{\text{ex}} (\text{s}^{-1})^a$	$k_{\text{ex}} (\text{s}^{-1})$	p_a	$\Delta\omega$ (ppm)	$R_2^0 (\text{s}^{-1})$	α
L 347	2.4	360	0.88	0.24	17.22	1.91
R 348	2.7	758	0.92	0.41	17.45	1.91
D 349	2.5	263	0.99	0.89	18.06	0.99
T 354	5.8	554	0.88	0.45	23.55	1.88
V 357	4.1	625	0.90	0.42	18.61	1.89
R 358	9.8	622	0.84	0.53	20.30	1.89
A 360	4.2	1261	0.98	1.42	20.95	1.70
G 366	5.3	654	0.99	2.23	27.06	0.85
Y 368	17.4	642	0.73	0.58	24.62	1.94
T 369	26.1	533	0.90	1.21	18.73	1.39
L 370	6.1	549	0.98	1.25	21.17	1.17
T 371	4.1	916	0.86	0.43	18.26	1.93
L 372	6.3	903	0.88	0.56	18.98	1.91
R 373	5.7	984	0.88	0.56	20.12	1.91
K 374	5.6	1295	0.76	0.47	28.11	1.94
G 375	3.2	1112	0.97	0.93	17.38	1.81
N 378	4.2	995	0.96	0.77	19.96	1.84
K 379	41.1	738	0.92	2.28	19.86	0.97
S 380	3.7	646	0.84	0.33	18.57	1.93
I 381	65.7	941	0.51	1.09	27.97	2.00
K 382	3.2	835	0.98	1.07	17.24	1.66
I 383	22.7	778	0.96	2.45	18.61	0.93
F 384	2.7	630	0.99	1.41	19.54	1.26
R 386	10.2	589	0.95	1.07	19.68	1.49
G 388	4.2	57	0.94	2.51	23.58	0.00
K 389	2.6	138	0.98	1.54	16.06	0.23
Y 390	6.2	489	0.99	2.98	18.90	0.38
G 391	1.9	268	0.99	2.69	18.96	0.18
F 392	19.6	478	0.93	1.23	17.85	1.22
S 393	22.4	546	0.94	1.94	17.03	0.83
D 394	17.4	432	0.95	2.04	19.17	0.57
L 396	11.0	716	0.95	1.15	18.25	1.56
T 397	4.8	1066	0.99	1.88	17.10	1.44
F 398	3.9	421	0.99	3.05	18.07	0.29
N 399	2.5	269	0.97	0.50	18.02	1.45
E 403	1.8	297	0.98	0.57	18.60	1.41
L 404	2.7	470	0.99	1.00	18.09	1.34
I 405	5.4	365	0.96	0.71	20.15	1.49

Residue	R_{ex} (s^{-1}) ^a	k_{ex} (s^{-1})	p_a	$\Delta\omega$ (ppm)	R_2^0 (s^{-1})	α
N 406	8.8	607	0.55	0.36	19.70	1.96
H 407	4.1	550	0.90	0.40	18.70	1.89
Y 408	3.5	437	0.99	1.70	16.43	0.75
S 412	29.0	435	0.92	2.07	19.27	0.55
Q 415	2.9	1083	0.87	0.39	24.70	1.93
Y 416	44.8	2924	0.91	3.07	13.58	1.79
K 419 ^b	~35					
L 420 ^b	~40					
V 422	21.4	1235	0.50	0.76	33.69	1.97
L 425	3.2	1160	0.78	0.34	21.69	1.94

^a $R_{\text{ex}} = R_2(\nu_{\text{cp}} \rightarrow 0) - R_2(\nu_{\text{cp}} \rightarrow \infty)$, $B_0 = 14.1\text{T}$

^b S/N ratio not high enough for reliable optimization of all exchange parameters

Most residues exhibit fast exchange on the NMR time scale as indicated by α values > 1 . However, for residues with large chemical shift differences, such as G366, G388 - D394, Y408, and S412, the exchange is slow as revealed by the ratio of $k_{\text{ex}}/\Delta\omega$ and confirmed independently by the value of α .

Relaxation dispersion curves of residues S339, N344, E345, R358, Y368, T369, K379, I383, F392, S393, D394, N406 and S412 can be fitted *globally*. Chemical shift differences and values of R_2^0 can adopt individual values for each residue, whereas the exchange rate and the populations are treated as global parameters. This analysis reveals a concerted exchange of residues in extended parts of the phosphopeptide binding site with an exchange rate k_{ex} of 648 s^{-1} and a population of the minor site of 3.4 %. However, most exchanging residues of the BG loop region cannot be included into the global fit. They clearly undergo different exchange processes.

NMR line shape analysis of signals in ^1H - ^{15}N HSQC spectra using increasing concentrations of MT15 can directly visualize the mechanism of the binding process. Figure 20 shows ^1H and ^{15}N cross-sections of N344 at two different temperatures. At 303K (depicted at the bottom), the intensities of the signals in intermediate titration steps are too low to account for a simple one-step binding mechanism. This is even more obvious at 308K, where an intermediate signal (marked by a red triangle) builds up in the sixth titration step. Similar line shapes were observed for a large portion of residues. Therefore, NMR line shapes suggest a *two-step binding mechanism*.

As described before, signals of key residues I381, F392, S393 and Y416 are not observable in spectra of the SH2-MT15 complex. However, signals of many other observable residues exhibit complex line shapes. Figure 21 shows ^{15}N cross-sections of K379 and ^1H

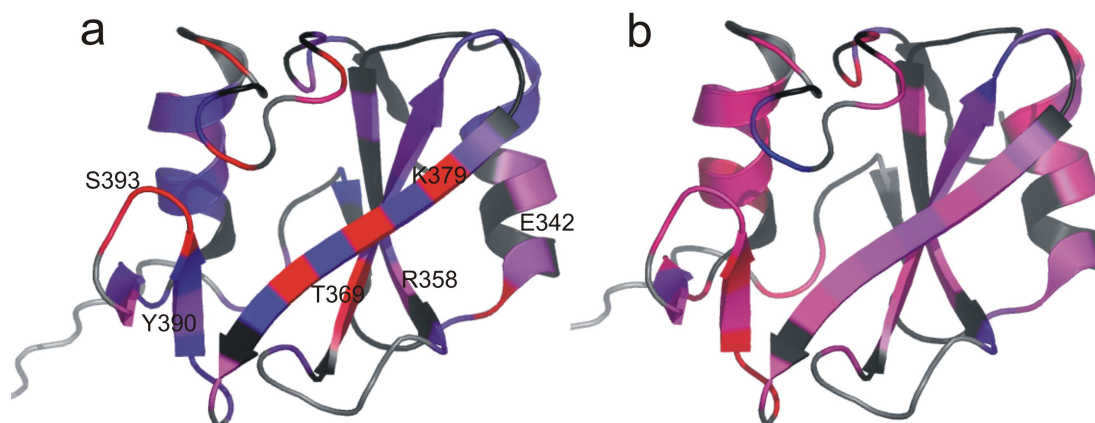


Figure 19: Exchange parameters of the N-SH2:MT15 interaction mapped onto the ribbon diagram. Exchange parameters were derived from relaxation dispersion experiments of the N-SH2 in the initial binding state with MT15 (substoichiometric amount of 1/20). (a) The exchange contributions R_{ex} to the ^{15}N transverse relaxation rate and (b) the exchange rate k_{ex} are depicted by color coding on the ribbon diagram of the SH2 domain. The continuous color scale from blue to magenta to red represents the amplitude of (a) R_{ex} from 0 s^{-1} – 10 s^{-1} – 20 s^{-1} and (b) of k_{ex} from 0 s^{-1} – 750 s^{-1} – 1500 s^{-1} . Residues colored black do not exhibit exchange, residues colored grey could not be analyzed due to missing assignments.

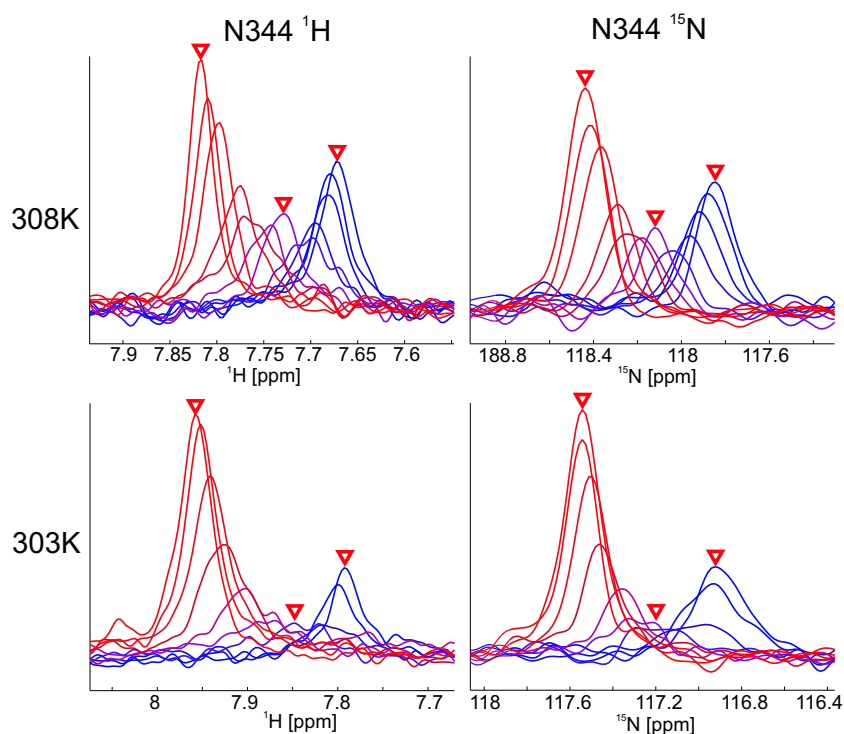


Figure 20: Line shapes of residue N344 at two temperatures demonstrating a two-step binding mechanism. ^1H and ^{15}N cross sections from two-dimensional HSQC spectra of residue N344 for subsequent steps of a titration of the wild type SH2 with MT15 from blue to red. The spectra were recorded at 308K (top) and 303K (bottom). Peak centers of the free form, the intermediate and the complex are labeled with ' ∇ '.

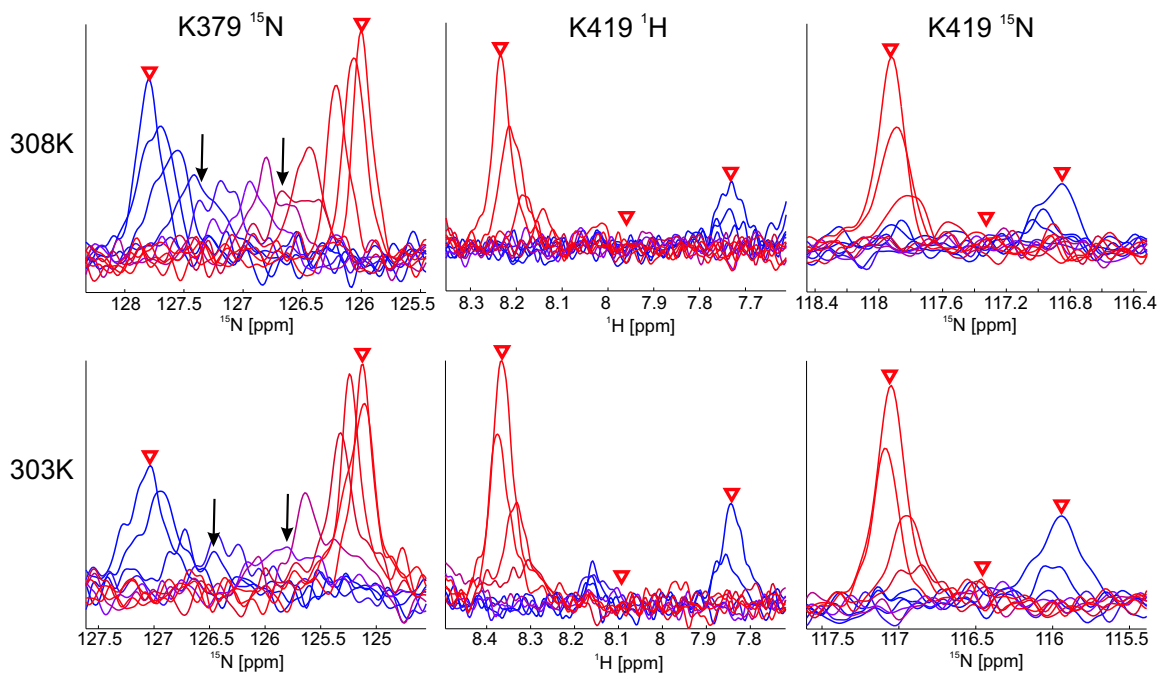


Figure 21: Complex line shapes of signals of the N-SH2 domain in a titration with MT15. ^1H and ^{15}N cross-sections from two-dimensional HSQC spectra in a successive titration with MT15 from blue to red recorded at 308K (top) and 303K (bottom). For residue K379 (left), signals from intermediate titration steps exhibit shoulders (examples marked by arrows) indicating the formation of conformers upon addition of peptide. Cross-sections of K419 are typical for low-populated intermediates. Additionally, some lines exhibit shoulders. The chemical shifts of free protein, complex and the potential chemical shift of intermediate states are marked by ' ∇ '.

and ^{15}N cross-sections of K419. In the case of K379, the signals split at substoichiometric ligand concentrations and exhibit multiple components at both temperatures. Several signal shoulders are marked by arrows and are located at the same positions relative to the signal of the free and complexed protein. The free SH2 and the complex are in fast exchange as indicated by the shifting signals for varying ligand concentrations. In contrast, each signal shoulder represents a conformer in slow exchange. These results could be explained by a parallel binding scheme suggested earlier for the interaction of high-affinity peptides with the N-SH2 domain (Günther *et al.*, 2002; Mittag *et al.*, 2004b).

For K419, the signals disappear for low concentrations of peptide and are restored for equimolar protein:peptide ratios. These line shapes can be explained using a two-step binding mechanism with an intermediate with constantly low populations or very high exchange contributions.

Isothermal titration calorimetry data (unpublished results by V. Rogov) suggest a stoichiometry of 2:1 for the SH2:MT15 interaction. Preparative gel filtration analysis of the sample in intermediate steps of the titration demonstrated the existence of three forms of the protein in equilibrium: the free protein, the 1:1 N-SH2-MT15 complex and an aggre-

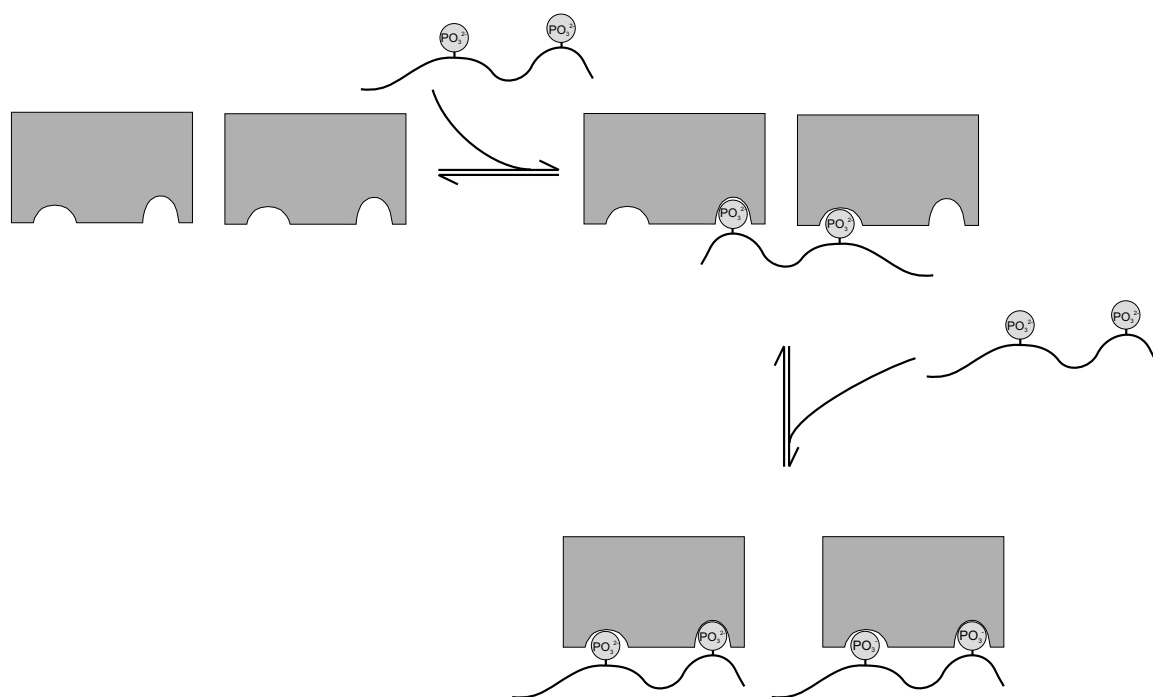


Figure 22: Binding model of the doubly phosphorylated peptide MT15 to the N-SH2 domain. At low peptide concentration two SH2 molecules compete for MT15 resulting in a 2:1 protein-peptide complex. Offering higher peptide concentrations leads to entropically favored 1:1 complexes.

gate of higher molecular mass that corresponds to a 2:1 complex of N-SH2 and MT15. If a rearrangement of a 2:1 complex to a 1:1 complex at higher ligand concentrations is mainly entropically driven, this second binding step cannot be visualized in ITC experiments if the ligand is added to the protein.

The linewidths of NMR signals of the N-SH2:MT15 complex are not greater than those of the free protein, confirming the existence of a 1:1 complex at equimolar concentrations. The low signal intensity and large linewidth of signals in intermediate titration steps observed at 303K (see for example Figure 20 or 21 bottom) is consistent with transient aggregates of higher molecular mass.

The scheme depicted in Figure 22 can explain this data: At low peptide concentrations, one MT15 molecule interacts with two N-SH2 domains through its two phosphotyrosine residues. At higher peptide concentrations, a redistribution of the peptide increases the population of high-affinity 1:1 complexes. The change of stoichiometry from 2:1 to 1:1 is entropically driven. Conformational exchange initiated by the interaction with the ligand is superimposed upon the exchange between alternative complexes. As previously reported for other high-affinity interactions of the wt N-SH2 domain and some mutants, low amounts of ligand lead to the formation of multiple conformers in slow exchange.

8.1.2 Conclusions

The investigation of the interaction of the doubly phosphorylated peptide MT15 with the N-SH2 domain of PI3K demonstrates the potential of the recently introduced methods. A combination of relaxation dispersion experiments and line shape analysis of titration spectra enabled the determination of kinetic rates and provided insight into a complex binding mechanism which was supported by isothermal titration calorimetry and preparative gel filtration.

The interaction of the N-SH2 domain with the doubly phosphorylated peptide MT15 shows substantial differences from the previously characterized interaction with the singly phosphorylated, shorter peptide MT8 (Günther *et al.*, 2002; Mittag *et al.*, 2003b). However, it strongly supports our suggestion that specific ligand binding to the N-SH2 domain induces and requires the formation of long-lived intermediates. The peptide interacts with suitable conformers with high affinity. In the case of MT8, the signals are refocused at high peptide concentrations and the complex is rigid on a μs -ms time scale. In contrast, the MT15 complex exhibits strong conformational exchange even at 1:1 stoichiometry. Signals of key residues such as I381, F392 and S393 vanish during the titration. This conformational mobility may contribute to the entropic advantage of the switch to a 1:1 complex and lead to the tenfold increased affinity of MT15 compared to MT8.

The extensive exchange in the SH2 domain at substoichiometric MT15 concentrations arises from a dynamic equilibrium between distinct aggregates of protein and peptide that may differ in relative orientation and stoichiometry of protein and peptide. Some of these aggregates must be less stable than the usual complex in which the pTyr of the high-affinity peptide sequence is coordinated in the primary pTyr binding pocket. Recent studies on other protein-protein interactions demonstrated that multiple weak interaction motifs can lead to strong and cooperative binding (Nash *et al.*, 2001). Elucidating the dynamics and the mechanisms of protein-protein interactions in which multiple domains ensure the accuracy of the interaction stands at the next endeavor.

References

- Anderson, P. W. (1954) A mathematical model for the narrowing of spectral lines by exchange or motion, *J. Phys. Soc. Jpn.* **9**, 316–339.
- Auger, K. R., Carpenter, C. L., Shoelson, S. E., Piwnica-Worms, H., and Cantley, L. C. (1992) Polyoma virus middle t antigen-pp60c-src complex associates with purified phosphatidylinositol 3-kinase in vitro, *J. Biol. Chem.* **267**, 5408–15.
- Backer, J. M., Myers, M. G., Shoelson, S. E., Chin, D. J., Sun, X. J., Miralpeix, M., Hu, P., Margolis, B., Skolnik, E. Y., and Schlessinger, J. (1992) Phosphatidylinositol 3'-kinase is activated by association with IRS-1 during insulin stimulation, *EMBO J.* **11**, 3469–3479.
- Balbach, J., Forge, V., Lau, W. S., Nuland, N. A., Brew, K., and Dobson, C. M. (1996) Protein folding monitored at individual residues during a two-dimensional nmr experiment, *Science* **274**, 1161–1163.
- Banaszak, L. J., Winter, N. S., Xu, Z., Bernlohr, D. A., Cowan, S., and Jones, T. A. (1994) Lipid-binding proteins: a family of fatty acid and retinoid transport proteins, *Adv. Protein Chem.* **45**, 89–151.
- Binsch, G. (1968) The Study of intramolecular rate processes by dynamic nuclear magnetic resonance, *Top. Stereochem.* **3**, 97–191.
- Binsch, G. (1975) Band-shape analysis, *Academic Press, Dynamic Nuclear Magnetic Resonance Spectroscopy*, , 81.
- Bloch, F. (1946) Nuclear Induction, *Phys. Rev.* **70**, 460–474.
- Boerman, M. H. and Napoli, J. L. (1991) Cholate-independent retinyl ester hydrolysis. Simulation by apo-cellular retinol-binding protein, *J. Biol. Chem.* **266**, 22273–22278.
- Boerman, M. H. and Napoli, J. L. (1996) Cellular retinol-binding protein-supported retinoic acid synthesis, *J. Biol. Chem.* **271**, 5610–5616.
- Brunori, M. (2000) Structural dynamics of myoglobin., *Biophys. Chem.* **86**, 221–30.
- Cambier, J. C. (1995) Antigen and Fc receptor signaling. The awesome power of the immunoreceptor tyrosine-based activation motif (ITAM), *J. Immunol.* **155**, 3281–3285.
- Cantley, L. C., Auger, K. R., Carpenter, C., Duckworth, B., Graziani, A., Kapeller, R., and Soltoff, S. (1991) Oncogenes and signal transduction, *Cell* **64**, 281–302.
- Cantley, L. C. and Songyang, Z. (1994) Specificity in recognition of phosphopeptides by src-homology 2 domains, *J. Cell Sci. Suppl.* **18**, 121–126.

- Carpenter, C. L., Auger, K. R., Chanudhuri, M., Yoakim, M., Schaffhausen, B., Shoelson, S. E., and Cantley, L. C. (1993) Phosphoinositide 3-kinase is activated by phosphopeptides that bind to the SH2 domains of the 85-kDa subunit, *J. Biol. Chem.* **268**, 9478–9483.
- Carpenter, C. L., Duckworth, B. C., Auger, K. R., Cohen, B., Schaffhausen, B. S., and Cantley, L. C. (1990) Purification and characterization of phosphoinositide 3-kinase from rat liver, *J. Biol. Chem.* **265**, 19704–19711.
- Carr, H. Y. and Purcell, E. M. (1954) Effects of diffusion on free precession in nuclear magnetic resonance experiments, *Phys. Rev.* **94**, 630–638.
- Carver, J. P. and Richards, R. E. (1972) General two-site solution for the chemical exchange produced dependence of T₂ upon the Carr-Purcell pulse separation, *J. Magn. Reson.* **6**, 89–105.
- Cavanagh, J., Fairbrother, W. J., Palmer, A. G., and Skelton, N. J., *Protein NMR Spectroscopy: Principles and Practice* (Academic Press, San Diego, CA, 1995).
- Chan, S. O. and Reeves, L. W. (1972) Mechanistic studies of chemical exchange reactions by complete nuclear magnetic resonance line-shape fitting: II. 15-site exchange in binary mixtures of dimethylin dihalides, *J. Am. Chem. Soc.* **95**, 673.
- Cole, R. and Loria, J. P. (2002) Evidence of flexibility in the function of ribonuclease A, *Biochemistry* **41**, 6072–6081.
- Cooper, A. and Dryden, D. T. F. (1984) Allostery without conformational change. A plausible model, *Eur. Biophys. J.* **11**, 103–109.
- Corvera, S., D'Arrigo, A., and Stenmark, H. (1999) Phosphoinositides in membrane traffic, *Curr. Opin. Cell. Biol.* **11**, 460–465.
- Cowan, S. W., Newcomer, M. E., and Jones, T. A. (1993) Crystallographic studies on a family of cellular lipophilic transport proteins. Refinement of P2 myelin protein and the structure determination and refinement of cellular retinol-binding protein in complex with all-trans retinol, *J. Mol. Biol.* **230**, 1225–1246.
- Derman, M. P., Toker, A., Hartwig, J. H., Spokes, K., Falck, J. R., Chen, C. S., Cantley, L. C., and Cantley, L. G. (1997) The lipid products of phosphoinositide 3-kinase increase cell motility through protein kinase C, *J. Biol. Chem.* **272**, 6465–6470.
- Deverell, C., Morgan, R. E., and Strange, J. H. (1970) Studies of chemical exchange by nuclear magnetic relaxation in the rotating frame, *Mol. Phys.* **18**, 553–559.

- Dittmer, J. and Bodenhausen, G. (2004) Evidence for slow motions in proteins by multiple refocusing of heteronuclear nitrogen/proton multiple quantum coherences in NMR, *J. AM. Chem. Soc.* **126**, 1314–1315.
- Eck, M. J., Shoelson, S. E., and Harrison, S. C. (1993a) Recognition of a high-affinity phosphotyrosyl peptide by the src homology-2 domain of p56^{lck}, *Nature* **362**, 87–91.
- Eck, M. J., Shoelson, S. E., and Harrison, S. C. (1993b) Recognition of a high-affinity phosphotyrosyl peptide by the src homology-2 domain of p56lck, *Nature* **362**, 87–91.
- Eisenmesser, E. Z., Bosco, D. A., Akke, M., and Kern, D. (2002) Enzyme dynamics during catalysis, *Science* **295**, 1520–1523.
- Escobedo, J. A., Kaplan, D. R., Kavanaugh, W. M., Turck, C. W., and Williams, L. T. (1991a) A phosphatidylinositol-3 kinase binds to platelet-derived growth factor receptors through a specific receptor sequence containing phosphotyrosine, *Mol. Cell. Biol.* **111**, 125–132.
- Escobedo, J. A., Navankasattusas, S., Kavanaugh, W. M., Milfay, D., Fried, V. A., and Williams, L. T. (1991b) cDNA cloning of a novel 85 kD protein that has SH2 domains and regulates binding of PI3-kinase to the PDGF beta-receptor, *Cell* **65**, 75–82.
- Esteller, M., Guo, M., Moreno, V., Peinado, M. A., Capella, G., Galm, O., Baylin, S. B., and Herman, J. G. (2002) Hypermethylation-associated inactivation of the cellular retinol-binding-protein 1 gene in human cancer., *Cancer Res.* **62**, 5902–5.
- Evenäs, J., Malmendal, A., and Akke, A. (2001) Dynamics of the transition between open and closed conformations in a calmodulin C-terminal domain mutant, *Structure* **9**, 185–195.
- Fantl, W. J., Escobedo, J. A., Martin, G. A., Turck, V., del Rosario, M., McCormick, F., and Williams, L. T. (1992) Distinct phosphotyrosines on a growth factor receptor bind to specific molecules that mediate different signaling pathways, *Cell* **69**, 413–423.
- Feher, V. A. and Cavanagh, J. (1999) Millisecond-timescale motions contribute to the function of the bacterial response regulator protein Spo0F., *Nature* **400**, 289–293.
- Fersht, A., *Structure and Mechanism in Protein Science. A Guide to Enzyme Catalysis and Protein Folding* (Freeman, New York, 1999), 1 edition.
- Flaswinkel, H., Barner, M., and Reth, M. (1995) The tyrosine activation motif as a target of protein tyrosine kinases and SH2 domains, *Semin. Immunol.* **7**, 21–27.

- Franzoni, L., Lücke, C., Perez, C., Cavazzini, D., Rademacher, M., Ludwig, C., Spisni, A., Rossi, G. L., and Rüterjans, H. (2002) Structure and backbone dynamics of apo- and holo-cellular retinol-binding protein in solution, *J. Biol. Chem.* **277**, 21983–21997.
- Futterer, K., Wong, J., Grucza, R. A., Chan, A. C., and Waksman, G. (1998) Structural basis for Syk tyrosine kinase ubiquity in signal transduction pathways revealed by the crystal structure of its regulatory SH2 domains bound to a dually phosphorylated ITAM peptide, *J. Mol. Biol.* **281**, 523–537.
- Ghyselinck, N. B., Bavik, C., Sapin, V., Mark, M., Bonnier, D., Hindelang, C., Dietrich, A., Nilsson, C. B., Hakansson, H., Sauvant, P., Azais-Braesco, V., Frasson, M., Picaus, S., and Chambon, P. (1999) Cellular retinol-binding protein type I is essential for vitamin A homeostasis, *EMBO J.* **18**, 4903–4914.
- Grey, M., Wang, C., and Palmer, A. G. (2003) Disulfide bond isomerization in basic pancreatic trypsin inhibitor: Multisite chemical exchange quantified by CPMG relaxation dispersion and chemical shift modeling, *J. Am. Chem. Soc.* **125**, 14324–14335.
- Gudas, L. J., Sporn, M. B., and Roberts, A. B., *The Retinoids: Biology, Chemistry and Medicine* (Raven Press, N. Y., 1994), 2nd edition, 443–520.
- Günther, U., Mittag, T., and Schaffhausen, B. (2002) Probing Src Homology 2 domain ligand interactions by differential line broadening, *Biochemistry* **41**, 11658–11669.
- Günther, U. L. and Schaffhausen, B. (2002) NMRKIN: Simulating line shapes from two-dimensional spectra of proteins upon ligand binding, *J. Biomol. NMR* **22**, 201–209.
- Gutowsky, H. S., McCall, D. W., and Slichter, C. P. (1953) Nuclear magnetic resonance multiplets in liquids, *J. Chem. Phys.* **21**, 279–292.
- Hajdu, J., Neutze, R., Sjogren, T., Edman, K., Szoke, A., Wilmouth, R., and Wilmot, C. (2000) Analyzing protein functions in four dimensions., *Nat Struct Biol* **7**, 1006–12.
- Hatada, M. H., Lu, X., Laird, E. R., Green, J., Morgenstern, J. P., Lou, M., Marr, C. S., Phillips, T. B., Ram, M. K., and Theriault, K. (1995) Molecular basis for interaction of the protein tyrosine kinase ZAP-70 with the T-cell receptor, *Nature* **376**, 32–38.
- Hensmann, M., Booker, G. W., Panayotou, G., Boyd, J., Linacre, J., Waterfield, M., and Campbell, I. D. (1994) Phosphopeptide binding to the N-terminal SH2 domain of the p85 alpha subunit of Pi 3'-kinase: a heteronuclear NMR study, *Protein Science* **3**, 1020–30, jul.

- Herbst, R., Andrews, G., Contillo, L., Lamphere, L., Gardner, J., Lienhard, G., and Gibbs, E. (1994) Potent activation of phosphatidylinositol-3' kinase by simple phosphotyrosine peptides derived from insulin receptor substrate 1 containing two YMXM motifs for binding SH2 domains, *Biochemistry* **33**, 9376–9381.
- Herr, F. M. and Ong, D. E. (1992) Differential interaction of lecithin-retinol acyltransferase with cellular retinol binding proteins, *Biochemistry* **31**, 6748–6755.
- Hunter, T. and Sefton, B. M. (1980) Transforming gene product of Rous sarcoma virus phosphorylates tyrosine., *Proc. Natl. Acad. Sci. U. S. A.* **77**, 1311–5.
- Ishima, R., Baber, J., Louis, J. M., and Torchia, D. A. (2004) Carbonyl carbon transverse relaxation dispersion measurements and ms- μ s timescale motion in a protein hydrogen bond network, *J. Biomol. NMR* **29**, 187–198.
- Ishima, R. and Torchia, D. A. (1999) Estimating the time scale of chemical exchange of proteins from measurements of transverse relaxation rates in solution, *J. Biom. NMR* **14**, 369–372.
- Jen, J. (1978) Chemical Exchange and NMR T2 Relaxation - The Multisite Case, *J. Magn. Reson.* **30**, 111–128.
- Kaplan, D. R., Whitman, M., Schaffhausen, B., Pallas, D. C., White, M., Cantley, L., and Roberts, T. M. (1987) Common elements in growth factor stimulation and oncogenic transformation: 85 kd phosphoprotein and phosphatidylinositol kinase activity, *Cell* **50**, 1021–9, sep 25.
- Kaplan, D. R., Whitman, M., Schaffhausen, B., Raptis, L., Garcea, R. I., Pallas, D., Roberts, T. M., and Cantley, L. (1986) Phosphatidylinositol metabolism and polyoma-mediated transformation, *Proc. Natl. Acad. Sci. USA* **83**, 3624–3628.
- Kern, D., Kern, G., Scherer, G., Fischer, G., and Drakenberg, T. (1995) Kinetic analysis of cyclophilin prolyl cis/trans isomerization by dynamic NMR spectroscopy, *Biochemistry* **34**, 13594–13602.
- Kern, D. and Zuiderweg, E. (2003) The role of dynamics in allosteric regulation, *Curr. Opin. Struct. Biol.* **13**, 748–757.
- Kim, H. K., Kim, J. W., Zilberstein, A., Margolis, B., Kim, J. G., Schlessinger, J., and Rhee, S. G. (1991) PDGF stimulation of inositol phospholipid hydrolysis requires PLC-gamma 1 phosphorylation on tyrosine residues 783 and 1254, *Cell* **65**, 435–41.
- Korzhnev, D. M., Kloiber, K., and Kay, L. E. (2004a) Multiple-quantum relaxation dispersion NMR spectroscopy probing millisecond time-scale dynamics in proteins: Theory and application, *J. Am. Chem. Soc.* **126**, 7320–7329.

- Korzhnev, D. M., Salvatella, X., Vendruscolo, M., Di Nardo, A. A., Davidson, A. R., Dobson, C. M., and Kay, L. E. (2004b) Characterizing low populated folding intermediates of an SH3 domain by NMR spectroscopy, *Nature* .
- Kristensen, S. M., Siegal, G., Sankar, A., and Driscoll, P. C. (2000) Backbone dynamics of the C-terminal SH2 domain of the p85alpha subunit of phosphoinositide 3-kinase: Effect of phosphotyrosine-peptide binding and characterization of slow conformational exchange processes, *J. Mol. Biol.* **299**, 771–788.
- Kumaran, S., Grucza, R. A., and Waksman, G. (2003) The tandem Src homology 2 domain of the Syk kinase: A molecular device that adapts to interphosphotyrosine distances, *Proc. Natl. Acad. Sci. USA* **100**, 14828–14833.
- Kuppumbatti, Y. S., Bleiweiss, I. J., Mandeli, J. P., Waxman, S., and Mira-Y-Lopez, R. (2000) Cellular retinol-binding protein expression and breast cancer, *J. Natl. Cancer Inst.* **92**, 475–480.
- Kuppumbatti, Y. S., Rexer, B., Nakajo, S., Nakaya, K., and Mira-y Lopez, R. (2001) CRBP suppresses breast cancer cell survival and anchorage-independent growth, *Oncogene* **20**, 7413–7419.
- Layton, M. J., Harpur, A. G., Panayotou, G., Bastiaens, P. I., and Waterfield, M. D. (1998) Binding of a diphosphotyrosine-containing peptide that mimics activated platelet-derived growth factor receptor beta induces oligomerization of phosphatidylinositol 3-kinase, *J. Biol. Chem.* **273**, 33379–33385.
- Li, E. and Norris, A. W. (1996) Structure/function of cytoplasmic vitamin A-binding proteins, *Annu. Rev. Nutr.* **16**, 205–234.
- Li, E., Qian, S. J., Winter, N. S., d'Avignon, A., Levin, M. S., and Gordon, J. I. (1991) Fluorine nuclear magnetic resonance analysis of the ligand binding properties of two homologous rat cellular retinol-binding proteins expressed in Escherichia coli, *J. Biol. Chem.* **266**, 3622–3629.
- Lian, L. and Roberts, J., *NMR of Macromolecules: A Practical Approach*, Practical Approach Series (Oxford University Press, 1993), 1 edition.
- Loria, J. P., Rance, M., and Palmer, A. G. (1999a) A Relaxation Compensated Carr-Purcell-Meiboom-Gill Sequence for Characterizing Chemical Exchange by NMR Spectroscopy, *J. Am. Chem. Soc.* **121**, 2331–2332.
- Loria, J. P., Rance, M., and Palmer, A. G. (1999b) A TROSY CPMG sequence for characterizing chemical exchange in large proteins, *J. Biom. NMR* **15**, 151–155.

- Lu, J., Cistola, D. P., and Li, E. (2003) Two homologous rat cellular retinol-binding proteins differ in local conformational flexibility, *J. Mol. Biol.* **330**, 799–812.
- Luz, Z. and Meiboom, S. (1963) Nuclear magnetic resonance study of the protolysis of triethylammonium ion in aqueous solution - order of the reaction with respect to solvent, *J. Chem. Phys.* **39**, 366–370.
- Marengere, L., Songyang, Z., Gish, G., Schaller, M., Parson, J., Stern, M., Cantley, L., and Pawson, T. (1994) SH2 domain specificity and activity modified by a single residue, *Nature* **369**, 502–505.
- Matoba, Y. and Sugiyama, M. (2003) Atomic resolution structure of prokaryotic phospholipase A2: analysis of internal motion and implication for a catalytic mechanism., *Proteins* **51**, 453–69.
- Mayer, B. J. (1995) Why two heads are better, *Structure* **3**, 977–80.
- Mayer, B. J., Jackson, P. K., Van Etten, R. A., and Baltimore, D. (1992) Point mutations in the abl SH2 coordinately impair phosphotyrosin binding *in vitro* and transforming activity *in vivo*, *Mol. Cell. Biol.* **12**, 609–618.
- McConnell, H. M. (1958) Reaction rates by nuclear magnetic resonance, *J. Chem. Phys.* **28**, 430–431.
- Meiboom, S. and Gill, D. (1958) Modified spin-echo method for measuring nuclear relaxation times, *Rev. Sci. Instrum.* **29**, 688–691.
- Meiler, J., Prompers, J. J., Peti, W., Griesinger, C., and Brüschweiler, R. (2001) Model-free approach to the dynamic interpretation of residual dipolar couplings in globular proteins, *J. AM. Chem. Soc.* **123**, 6098–6107.
- Meili, R., Ellsworth, C., Lee, S., Reddy, T. B., Ma, H., and Firtel, R. A. (1999) Chemoattractant-mediated transient activation and membrane localization of akt/pkb is required for efficient chemotaxis to camp in dictyostelium, *EMBO J.* **18**, 2092–2105.
- Minshall, C., Arkins, S., Freund, G., and Kelley, K. (1996) Requirement for phosphatidylinositol 3'-kinase to protect hemopoietic progenitors against apoptosis depends upon the extracellular survival factor, *J. Immunol.* **156**, 939–947.
- Mittag, T., Franzoni, L., Cavazzini, D., Rossi, G.-L., and Günther, U. L., *Structure, Dynamics and Function of Biological Macromolecules and Assemblies*, chapter Novel insights into the mechanism of retinol binding by cellular retinol-binding protein (IOS Press B. V., Amsterdam, 2003a).

- Mittag, T., Franzoni, L., Cavazzini, D., Schaffhausen, B., Rossi, G.-L., and Günther, U. L. (2004a) Freezing of conformers of the cellular retinol-binding protein by retinol, *in preparation* .
- Mittag, T., Schaffhausen, B., and Günther, U. (2004b) Tracing kinetic intermediates during ligand binding, *J. Am. Chem. Soc.* **126**, 9017–9023.
- Mittag, T., Schaffhausen, B., and Günther, U. L. (2003b) Direct observation of protein-ligand interaction kinetics, *Biochemistry* **42**, 11128–11136.
- Moran, M. F., Koch, C. A., Anderson, D., Ellis, C., England, L., Martin, G. S., and Pawson, T. (1990) Src homology region 2 domains direct protein-protein interactions in signal transduction, *Proc. Natl. Acad. Sci. U. S. A.* **87**, 8622–6.
- Mulder, F. A. A., de Graaf, R. A., Kaptein, R., and Boelens, R. (1998) An off-resonance rotating frame relaxation experiment for the investigation of macromolecular dynamics using adiabatic rotations, *J. Magn. Res.* **131**, 351–357.
- Mulder, F. A. A., Hon, B., Mittermaier, A., Dahlquist, F. W., and Kay, L. E. (2002) Slow internal dynamics in proteins: Application of NMR relaxation dispersion spectroscopy to methyl groups in a cavity mutant of T4 lysozyme, *J. Am. Chem. Soc.* **124**, 1443–1451.
- Mulder, F. A. A., Mittermaier, A., Hon, B., Dahlquist, F., and Kay, L. E. (2001a) Studying excited states of proteins by NMR spectroscopy, *Nat. Struct. Biol.* **8**, 932–935.
- Mulder, F. A. A., Skrynnikov, N. R., Hon, B., Dahlquist, F. W., and Kay, L. E. (2001b) Measurement of slow (us-ms) time scale dynamics in protein side chains by ¹⁵N relaxation dispersion NMR spectroscopy: Application to Asn and Gln residues in a cavity mutant of T4 lysozyme, *J. Am. Chem. Soc.* **123**, 967–975.
- Nash, P., Tang, X., Orlicky, S., Chen, Q., Gertler, F. B., Mendenhall, M. D., Sicheri, F., Pawson, T., and Tyers, M. (2001) Multisite phosphorylation of a CDK inhibitor sets a threshold for the onset of DNA replication., *Nature* **414**, 514–21.
- Nolte, R. T., Eck, M. J., Schlessinger, J., Shoelson, S. E., and Harrison, S. C. (1996) Crystal structure of the PI 3-kinase p85 amino-terminal SH2 domain and its phosphopeptide complexes, *Nature Struct. Biol.* **3**, 364–74.
- O'Brien, R., Rugman, P., Renzoni, D., Layton, M., Handa, R., Hilyard, K., Waterfield, M. D., Driscoll, P. C., and Ladbury, J. (2000) Alternative modes of binding of proteins with tandem SH2 domains, *Prot. Sci.* **9**, 570–579.

- Ong, D. E., MacDonald, P. N., and Gubitosi, A. M. (1988) Esterification of retinol in rat liver. Possible participation by cellular retinol-binding protein and cellular retinol-binding protein II, *J. Biol. Chem.* **263**, 5789–5796.
- Ong, D. E., Newcomer, M. E., and Chytil, F., *The Retinoids: Biology, Chemistry and Medicine*, volume pp. 283-318 (Raven Press Ltd, New Yoek, 1994).
- Ong, D. E. and Page, D. L. (1986) *Am. J. Clin. Nut.* **44**, 425–430.
- Orekhov, V. Y., Korzhnev, D. M., and Kay, L. E. (2004) Double- and zero-quantum NMR relaxation dispersion experiments sampling millisecond time scale dynamics in proteins, *J. Am. Chem. Soc.* **126**, 1886–1891.
- Ostermann, A., Waschipsky, R., Farak, F. G., and Nienhaus, G. U. (2000) Ligand binding and conformational motions in myoglobin, *Nature* **404**, 205–208.
- Ottinger, E. A., Botfield, M. C., and Shoelson, S. E. (1998) Tandem SH2 doamins confer high specificity in tyrosine kinase signaling, *J. Biol. Chem.* **272**, 729–735.
- Ottonello, S., Petrucco, S., and Maraini, G. (1987) Vitamin A uptake from retinol-binding protein in a cell-free system from pigment epithelial cells of bovine retina, *J. Biol. Chem.* **262**, 3975–3981.
- Ottonello, S., Scita, G., Mantovani, G., Cavazzini, D., and Rossi, G. L. (1993) Retinol bound to cellular retinol-binding protein is a substrate for cytosolic retinoic acid synthesis, *J. Biol. Chem.* **268**, 27133–27142.
- Paci, E., Vendruscolo, M., Dobson, C. M., and Karplus, M. (2002) Determination of a transition state at atomic resolution form protein engineering data, *J. Mol. Biol.* **324**, 151–163.
- Pawson, T. (2004) Specificity in signal transduction: from phosphotyrosine-SH2 domain interactions to complex cellular systems., *Cell* **116**, 191–203.
- Peti, W., Meiler, J., Brüschweiler, R., and Griesinger, C. (2002) Model-free analysis of protein backbone motion from residual diplo couplings, *J. AM. Chem. Soc.* **124**, 5822–5833.
- Pintar, A., Hensmann, M., Jumel, K., Pitkeathly, M., Harding, S. E., and Campbell, I. D. (1996) Solution studies of the SH2 domain from the fyn tyrosine kinase: secondary structure, backbone dynamics and protein association, *European Biophysics Journal* **24**, 371–80.

- Rameh, L., Chen, C., and Cantley, L. (1995) Phosphatidylinositol (3,4,5)p3 interacts with sh2 domains and modulates pi 3-kinase association with tyrosine-phosphorylated proteins, *Cell*, 83821–30.
- Rameh, L. E. and Cantley, L. (1999) The role of phosphoinositide 3-kinase lipid products in cell function, *J. Biol. Chem.* **274**, 8347–8350.
- Rao, B. D. (1989) Nuclear magnetic resonance line-shape analysis and determination of exchange rates, *Methods Enzymol.* **176**, 279–311.
- Reiss, K. and Khalili, K. (2003) Viruses and cancer: lessons from the human polyomavirus, JCV., *Oncogene* **22**, 6517–23.
- Roberts, D., Williams, S. J., Cvetkovic, D., Weinstein, J. K., Godwin, A. K., Johnson, S. W., and Hamilton, T. C. (2002) Decreased expression of retinol-binding proteins is associated with malignant transformation of the ovarian surface epithelium., *DNA Cell Biol* **21**, 11–9.
- Rordorf-Nikolic, T., Van Horn, D. J., Chen, D., White, M. F., and Backer, J. M. (1995) Regulation of phosphatidylinositol 3'-kinase by tyrosyl phosphoproteins. Full activation requires occupancy of both SH2 domains in the 85-kDa regulatory subunit, *J. Biol. Chem.* **270**, 3662–3666.
- Royant, A., Edman, K., Ursby, T., Pebay-Peyroula, E., Landau, E., and Neutze, R. (2000) Helix deformation is coupled to vectorial proton transport in the photocycle of bacteriorhodopsin., *Nature* **406**, 645–8.
- Rozovsky, S. and McDermott, A. E. (2001) The time scale of the catalytic loop motion in triosephosphate isomerase, *J. Mol. Biol.* **310**, 259–270.
- Sacchettini, J. C., Gordon, J. I., and Banaszak, L. J. (1989) Crystal structure of rat intestinal fatty-acid-binding protein. refinement and analysis of the escherichia coli-derived protein with bound palmitate, *J. Mol. Biol.* **208**, 327–339.
- Sadowski, I., Stone, J. C., and Pawson, T. (1986) A noncatalytic domain conserved among cytoplasmic protein-tyrosine kinases modifies the kinase function and transforming activity of Fujinami sarcoma virus P130gag-fps., *Mol. Cell. Biol.* **6**, 4396–408.
- Sandström, J., *Dynamic NMR spectroscopy* (Academic Press, 1982).
- Schlichting, I., Berendzen, J., Chu, K., Stock, A. M., Maves, S. A., Benson, D. E., Sweet, R. M., Ringe, D., Petsko, G. A., and Sligar, S. G. (2000) The catalytic pathway of cytochrome p450cam at atomic resolution., *Science* **287**, 1615–22.

- Schmitt-Graff, A., Ertelt, V., Allgaier, H. P., Koelble, K., Olschewski, M., Nitschke, R., Bochaton-Piallat, M. L., Gabbiani, G., and Blum, H. E. (2003) Cellular retinol-binding protein-1 in hepatocellular carcinoma correlates with beta-catenin, Ki-67 index, and patient survival., *Hepatology* **38**, 470–80.
- Schreiber, A. B., Libermann, T. A., Lax, I., Yarden, Y., and Schlessinger, J. (1983) Biological role of epidermal growth factor-receptor clustering. Investigation with monoclonal anti-receptor antibodies., *J. Biol. Chem.* **258**, 846–53.
- Schu, P. V., Takegawa, K., and Fry, M. J. (1993) Phosphatidylinositol 3-kinase encoded by Yeast VPS34 gene essential for protein sorting, *Science* **260**, 88–91.
- Sefton, B. M., Hunter, T., Beemon, K., and Eckhart, W. (1980) Evidence that the phosphorylation of tyrosine is essential for cellular transformation by Rous sarcoma virus., *Cell* **20**, 807–16.
- Shoelson, S. E., Sivaraja, M., Williams, K. P., Hu, P., Schlessinger, J., and Weiss, M. A. (1993) Specific phosphopeptide binding regulates a conformational change in the PI 3-kinase SH2 domain associated with enzyme activation, *EMBO J.* **12**, 795–802.
- Skrynnikov, N. R., Dahlquist, F. W., and Kay, L. E. (2002) Reconstructing NMR spectra of "invisible" excited states using HSQC and HMQC experiments, *J. Am. Chem. Soc.* **124**, 12352–12360.
- Soltoff, S. P., Rabin, S. L., Cantley, L. C., and Kaplan, D. R. (1992) Nerve growth factor promotes the activation of phosphatidylinositol 3-kinase and its association with the trk tyrosine kinase, *J. Biol. Chem.* **267**, 17472–7.
- Stephens, L. R., Jackson, T. R., and Hawkins, P. T. (1993) Agonist stimulated synthesis of phosphatidylinositol(3,4,5)-trisphosphate: a new intracellular signalling system?, *Biochim. Biophys. Acta* **1179**, 27–75.
- Su, W., Liu, W., Schaffhausen, B. S., and Roberts, T. M. (1995) Association of polyomavirus middle tumor antigen with phospholipase c-gamma 1, *J. Biol. Chem.* **270**, 12331–12334.
- Sudmeier, J. L., Evelhoch, J. L., and Jonsson, N. (1980) Dependence of NMR lineshape analysis upon chemical rates and mechanisms: Implications for enzyme histidine titrations, *J. Magn. Reson.* **40**, 377–390.
- Sundaram, M., Sivaprasadarao, A., DeSousa, M. M., and Findlay, J. B. (1998) The transfer of retinol from serum retinol-binding protein to cellular retinol-binding protein is mediated by a membrane receptor, *J. Biol. Chem.* **273**, 3336–3342.

- Szyperski, T., Luginbuhl, P., Otting, G., Güntert, P., and Wüthrich, K. (1993) Protein dynamics studied by rotating frame ^{15}N spin relaxation times, *J. Biomol. NMR* **3**, 151–164.
- Thompson, J., Winter, N., Terwey, D., Bratt, J., and Banaszak, L. (1997) The crystal structure of the liver fatty acid-binding protein, *J. Biol. Chem.* **272**, 7140–7150.
- Tognon, M., Corallini, A., Martini, F., Negrini, M., and Barbanti-Brodano, G. (2003) Oncogenic transformation by BK virus and association with human tumors., *Oncogene* **22**, 5192–200.
- Toker, A. and Cantley, L. (1997) Signalling through the lipid products of phosphoinositide-3-OH kinase., *Nature* **387**, 673–6.
- Tollinger, M., Skrynnikov, N. R., Mulder, F. A. A., Forman-Kay, J. D., and Kay, L. E. (2001) Slow dynamics in folded and unfolded states of an SH3 domain, *J. Am. Chem. Soc.* **123**, 11341–11352.
- Tolman, J. R., Al-Hashimi, H. M., Kay, L. E., and Prestegard, J. H. (2001) Structural and dynamic analysis of residual dipolar coupling data for proteins, *J. Am. Chem. Soc.* **123**, 1416–1424.
- Valius, M., Bazenet, C., and Kazlauskas, A. (1993) Tyrosines 1021 and 1009 are phosphorylation sites in the carboxy terminus of the platelet-derived growth factor receptor b subunit and are required for binding of phospholipase c γ and a 64-kilodalton protein, respectively, *Mol. Cell. Biol.* **13**, 133–143.
- Vanhaesebroeck, B. and Waterfield, M. D. (1999) Signaling by distinct classes of phosphoinositide 3-kinases, *Exp. Cell Res.* **253**, 239–254.
- Varticovski, L., Harrison-Findik, D., Keeler, M. L., and Susa, M. (1994) Role of PI 3-kinase in mitogenesis, *Biochim. Biophys. Acta* **1226**, 1–11.
- Vendruscolo, M., Paci, E., Dobson, C. M., and Karplus, M. (2001) Three key residues form a critical contact network in a protein folding transition state, *Nature* **409**, 641–645.
- Vivanco, I. and Sawyers, C. L. (2002) The phosphatidylinositol 3-kinase AKT pathway in human cancer, *Nat. Rev. Cancer* **2**, 489–501.
- Volkman, B. F., Lipson, D., Wemmer, D. E., and Kern, D. (2001) Two-state allosteric behavior in a single-domain signaling protein, *Science* **291**, 2429–33.

- Waksman, G., Kominos, D., Robertson, S. C., Pant, N., Baltimore, D., Birge, R. B., Cowburn, D., Hanafusa, H., Mayer, B. J., and Overduin, M. (1992) Crystal structure of the phosphotyrosine recognition domain SH2 of v-src complexed with tyrosine-phosphorylated peptides, *Nature* **358**, 646–53.
- Waksman, G., Shoelson, S. E., Pant, N., Cowburn, D., and Kuriyan, J. (1993) Binding of a high affinity phosphotyrosyl peptide the src SH2 domain: crystal structures of the complexed and peptide-free forms, *Cell* **72**, 779–90.
- Wand, A. J. (2001) Dynamic activation of protein function: A view emerging from NMR spectroscopy, *Nat. Struct. Biol.* **8**, 926–931.
- Wang, C., Grey, M. J., and Palmer, A. G. (2001a) CPMG sequences with enhanced sensitivity to chemical exchange, *J. Biomol. NMR* **21**, 361–366.
- Wang, L., Pang, Y., Holder, T., Brender, J., Kurochkin, A., and Zuiderweg, E. (2001b) Functional dynamics in the active site of the ribonuclease binase, *Proc. Natl. Acad. Sci.* **98**, 7684–7689.
- Weber, T., Schaffhausen, B., Liu, Y., and Günther, U. L. (2000) Structure of p85 N-SH2 complexed with a doubly phosphorylated peptide reveals second phosphotyrosine binding site, *Biochemistry* **39**, 15860–15869.
- Whitman, M., Kaplan, D. R., Schaffhausen, B., Cantley, L., and Roberts, T. M. (1985) Association of phosphatidylinositol kinase activity with polyoma middle-T competent for transformation, *Nature* **315**, 239–242.
- Witte, O. N., Dasgupta, A., and Baltimore, D. (1980) Abelson murine leukaemia virus protein is phosphorylated in vitro to form phosphotyrosine., *Nature* **283**, 826–31.
- Wurmser, A. E., Gary, J. D., and Emr, S. D. (1999) Phosphoinositide 3-kinases and their FYVE domain-containing effectors as regulators of vacuolar/lysosomal membrane trafficking pathways, *J. Biol. Chem.* **274**, 9129–9132.
- Xu, Z., Bernlohr, D. A., and Banaszak, L. J. (1993) The adipocyte lipid-binding protein at 1.6-Å resolution. crystal structures of the apoprotein and with bound saturated and unsaturated fatty acids, *J. Biol. Chem.* **268**, 7874–7884.
- Yamada, K. M. and Araki, M. (2001) Tumor Suppressor PTEN: modulator of cell signaling, growth, migration and apoptosis, *J. Cell Sci.* **114**, 2375–2382.
- Yoakim, M., Hou, W., Liu, Y., Carpenter, C. L., Kapeller, R., and Schaffhausen, B. S. (1992) Interactions of polyomavirus middle t with the SH2 domains of the pp85 subunit of phosphatidylinositol-3-kinase, *J. Virol.* **66**, 5485–5491.

- Yoakim, M., Hou, W., Songyang, Z., Liu, Y., Cantley, L., and Schaffhausen, B. (1994) Genetic analysis of a phosphatidylinositol 3-kinase SH2 domain reveals determinants of specificity, *Mol. Cell. Biol.* **14**, 5929–5938.
- Yu, J., Wjasow, C., and Backer, J. M. (1998) Regulation of the p85/p110alpha Phosphatidylinositol 3'-Kinase, *J. Biol. Chem.* **273**, 30199–30203.
- Zarrinpar, A., Park, S. H., and Lim, W. A. (2003) Optimization of specificity in a cellular protein interaction network by negative selection., *Nature* **426**, 676–80.
- Zinn-Justin, S., Berthault, P., Guenneugues, M., and Desvaux, H. (1997) Off-resonance rf fields in heteronuclear nmr: application to the study of slow motions, *J. Biomol. NMR* **10**, 363–372.

9 Appendix

List of Figures

1	Time scales of protein dynamics accessible by NMR techniques.	15
2	Effect of exchange rate and populations on line shapes of a system undergoing two-site exchange.	23
3	Effect of 180° refocusing pulses on transverse magnetization.	24
4	Magnetization during CPMG pulse trains and effect on effective transverse relaxation rates.	30
5	Comparison of theoretical relaxation dispersion curves	31
6	Fitting of relaxation dispersion curves using a numerical approach.	33
7	Line shapes of signals from titration spectra contain kinetic information.	34
8	Theoretical line shapes for one-step binding.	36
9	Population of the complex during a ligand titration.	36
10	Simulations of experimental titration spectra.	37
11	Theoretical line shapes and relaxation dispersion curves for a sequential two-step binding mechanism.	40
12	Pathways for phosphoinositide synthesis.	45
13	Signal transduction by phospholipid products of PI3K and their target molecules.	47
14	Assembly of a signaling complex around polyoma MT antigen.	48
15	The binding mechanism of retinol to CRBP is not obvious from the structures of the free and the complexed form.	50
16	Ribbon diagram of the free N-SH2 domain of PI3K and the complex with a doubly phosphorylated, 15-residue peptide derived from the binding site of MT antigen.	58
17	Schematic illustration of allosteric mechanisms.	61
18	Relaxation dispersion curves of the N-SH2 domain for the initial interaction with MT15.	64

19	Exchange parameters of the N-SH2:MT15 interaction mapped onto the ribbon diagram.	67
20	Line shapes of residue N344 at two temperatures demonstrating a two-step binding mechanism.	67
21	Complex line shapes of signals of the N-SH2 domain in a titration with MT15.	68
22	Binding model of the doubly phosphorylated peptide MT15 to the N-SH2 domain.	69

9.1 Abbreviations, Symbols, and Units

Abbreviations

1D, 2D, 3D	one-, two-, three-dimensional
BH	break cluster region homology
CPMG	Carr-Purcell-Meiboom-Gill
CRBP	cellular retinol-binding protein
GAP	GTPase activating protein
HMQC	heteronuclear multiple quantum coherence
HSQC	heteronuclear single quantum coherence
ITC	isothermal titration calorimetry
ITAM	immunoreceptor tyrosine-based activation motif
MT	polyoma middle T antigen
NMR	nuclear magnetic resonance
PI3K	phosphatidylinositide 3-kinase
PLC- γ 1	phospholipase C- γ 1
p85	regulatory 85 kDa subunit
p110	catalytic 110 kDa subunit
PI	phosphoinositides
PLC	phospholipase C
PtdIns	phosphatidylinositol
PtdIns(3,4,5)P ₃	phosphatidylinositol (3,4,5)-trisphosphate
PtdIns 4-P	phosphatidylinositol 4-phosphate
PtdIns(4,5)P	phosphatidylinositol (4,5)-bisphosphate
pTyr	phosphotyrosine
pY	phosphotyrosine
SH2	src homology 2
SH3	src homology 3
ms	millisecond
μ s	microsecond
ns	nanosecond
PH	pleckstrin homology
ps	picosecond
RTK	receptor tyrosine kinase
wt	wild type

Symbols

$2\tau_{cp}$	duration between two π pulses in CPMG train
$\Delta\omega$	frequency difference
δ_j	chemical shift of species j
v_{cp}	refocusing field
ω_0	Larmor resonance frequency
ω_1	field strength of transverse magnetic field
ω_j	Larmor resonance frequency of species j
θ	time variable
A	relaxation rate, chemical shift, and exchange matrix
B	relaxation rate and chemical shift matrix
B_0	static magnetic field strength
C	exchange matrix
$F(t)$	time domain signal
\mathbf{G}	magnetization vector
G	complex magnetization
\mathbf{G}_n	magnetization at n th echo formation
\mathbf{h}_n	magnetization after n th π pulse
I	unity matrix
K	equilibrium constant
k_{12}	forward reaction rate constant
k_{21}	reverse reaction rate constant
k_{ex}	exchange rate
k_{jm}	rate constant converting species j to m
M_z	longitudinal magnetization
\mathbf{P}	population vector
p_j	population of site j
R_1	longitudinal relaxation rate
R_2	transverse relaxation rate
R_2^{eff}	effective relaxation rate constant
$R_2^{eff}(v_{cp})$	relaxation dispersion
R_{ex}	exchange contribution to transverse relaxation rate constant
T	duration of CPMG pulse train
t	time
u	real part of complex magnetization
v	imaginary part of complex magnetization
W_0	Larmor frequency matrix

Units

Da	Dalton
Hz	Hertz
K	Kelvin
M	mol l^{-1}
l	liter
s	second
T	Tesla

9.2 Matlab Script for the Numerical Simulation of Relaxation Dispersion Curves


```
%Matlab Script for Numerical Simulation of Relaxation Dispersion Curves
```

```
%Two-step mechanism eq. 33.
```

```
%See Figure 11. Simulation of relaxation dispersion curves for the different
```

```
%protein/ligand ratios.
```

```
%
```

```
clear all
```

```
clf
```

```
TD = 1024; %number of points in Time Domain
```

```
TD_wo_zf = TD;
```

```
zf = 1; %factor for Zero Filling
```

```
R2A = 10; %transverse Relaxation Rates for species A
```

```
R2B = 10; % B
```

```
R2C = 10; % C
```

```
r2 = [R2A, R2B, R2C];
```

```
SWH = 120; %Sweep width in Hertz
```

```
K=10; %equilibrium constant
```

```
k21 = 2000; %reverse rate constant of first step
```

```
k23 = 10; %forward rate constant of second step
```

```
pa = [0.999 0.83 0.67 0.5 0.33 0.17 0.03 0.005] %populations of species A
```

```
pb = (1-pa)/(K+1) % B
```

```
pc = 1 - pa - pb % C
```

```
k12 = k21 * pb./pa %forward rate constant of first step
```

```
k32 = k23/K; %reverse rate constant of second step
```

```
B1 = 16.44; %static magnetic field: 700 MHz
```

```
B2 = 11.74; % 500 MHz
```

```
for B=0:1
```

```
    Dw1 = 200; %chemical shift difference of first step
```

```
    dDw1= Dw1 - Dw1*(B2/B1);
```

```
    Dw1 = Dw1 - B*dDw1
```

```
    Dw2 = 50; %chemical shift difference of second step
```

```
    dDw2= Dw2 - Dw2*(B2/B1);
```

```
    Dw2 = Dw2 - B*dDw2
```

```
    W = [0,Dw1,Dw1+Dw2]; %chemical shifts of all three states
```

```
    W/(2*pi) %w = 2*pi*v
```

```
    DW = 1/(SWH); %dwell time
```

```
    AQ = DW * TD; %aquisition time
```

```
    time = linspace(0,AQ,TD); %time vector
```

```
    b=-r2-i*W; %
```

```
    B = diag(b); %see eq. 15
```

```
%define colors for different spectra
```

```
colstep =1/length(pa);
```

```
for n=1:length(pa)
```

```
    ColPal(n,:) = [n*colstep, 0.0, 1-n*colstep];
```

```
end
```

```
for o=1:length(pa)
```

```
    K = [-k12(o) k21 0 %exchange matrix for two-step reaction
```

```
        k12(o) -k21-k23 k32
```

```
        0 k23 -k32];
```

```
    A = B + K; %see eq. 20
```

```
    P = [pa(o), %population matrix
```

```

        pb(o),
        pc(o)];

E = [1,1,1];
G(1) = 1;

g_pulse(:,1) = P*G(1); %initial magnetization

for n = 1 : TD %consider zerofilling of orig data
    F_t(n) = E * (expm(A * time(n))*P); %FIDs in Spalten
end

F_w = real(fftshift(fft(F_t,TD))); %Fourier transformation

freqaxis = linspace((-SWH/2), (SWH/2), TD); %frequency axis
figure(1)
spc_handles(o)=plot(freqaxis,F_w);
hold on
set(spc_handles(o), 'Color', ColPal(o,:))

%Which part of the magnetization shall be selected?
s=input('Fast or slow exchange? \n 0 = fast \n 1 = slow \n');
if (s~=0) & (s~=1)
    disp('Invalid choice!')
    s=input('Fast or slow exchange? \n 0 = fast \n 1 = slow \n');
end
if s==1
    r=input('Choose site 1, 2 or 3: ');
end
TAU=0.06;
echoes=[1:20,22:2:40,40:10:100]; %magnetization will be simulated for these
echo numbers

for m=1:length(echoes)
    clear g_pulse
    clear g_echo
    clear G_all
    g_pulse(:,1) = P*G(1); %initial magnetization
    nechoes = echoes(m); %number of echoes in CPMG pulse train
    tcp=TAU/(2*nechoes); %2tcp = time between successive 180° pulses
    M = expm(A*tcp); %before first 180° pulse only 1tcp
    g_pulse(:,2) = conj(M)*conj(g_pulse(:,1)); %after first 180° pulse
    g_echo(:,1) = M*g_pulse(:,2); %magnetization at first echo
    G_all(1) = g_echo(1,1)+g_echo(2,1);
    N=0;
    if nechoes>1
        M2 = expm(A*2*tcp); %see eq. 23
        for N=1:(nechoes-1)

            g_pulse(:,N+2) = conj(M2)*conj(g_pulse(:,N+1)); %magn after
                successive 180° pulses after 2tcp
            g_echo(:,N+1) = M*g_pulse(:,N+2); %magn during echo
            G_all(N+1) = g_echo(1,N+1)+g_echo(2,N+1);
        end
    end
    clear t

    t_max = [TAU/nechoes:TAU/nechoes:TAU];

    if s==0
        int(m)=real(G_all(N+1));
    elseif s==1

```

```
        int(m)=real(g_echo(r,N+1));
    end
end

vcp = 1./(4*TAU./(2*echoes));           %refocusing field
tau_cp = 1./(4*vcp);
if s==1
    R2 = log(P(r)./real(int))/TAU;      %calculation of relaxation rate...
else                                     %depending on exchange regime
    R2 = log(1./real(int))/TAU;
end

figure(2)
rd_handles(o) = plot(vcp,R2,'x-k');
hold on
set(rd_handles(o),'Color',ColPal(o,:))
set(gca,'XLim',[0 850])
xlabel('v_c_p [Hz'],'FontSize',14);
ylabel('R_2 [s^-1]','FontSize',14);
hold on
keyboard
end
end
```

10 Publications

Direct Observation of Protein–Ligand Interaction Kinetics[†]

Tanja Mittag,[‡] Brian Schaffhausen,[§] and Ulrich L. Günther^{*‡}

Center for Biomolecular Magnetic Resonance, Biocentre N230, J. W. Goethe University, Frankfurt, Marie-Curie-Strasse 9, 60439 Frankfurt, Germany, and Department of Biochemistry, School of Medicine, Tufts University, 136 Harrison Avenue, Boston, Massachusetts 02111

Received May 8, 2003; Revised Manuscript Received July 9, 2003

ABSTRACT: Internal dynamics on the micro- to millisecond time scale have a strong influence on the affinity and specificity with which a protein binds ligands. This time scale is accessible through relaxation dispersion measurements using NMR. By studying the dynamics of a protein with different concentrations of a ligand, one can determine the dynamic effects induced by the ligand. Here we have studied slow internal dynamics of the N-terminal src homology 2 domain of phosphatidylinositol 3-kinase to probe the role of individual residues for the interaction with a tyrosine-phosphorylated binding sequence from polyoma middle T antigen. While slow dynamic motion was restricted to a few residues in the free SH2 and in the SH2 complex, motion was significantly enhanced by adding even small amounts of ligand. Kinetic rates induced by ligand binding varied between 300 and 2000 s⁻¹. High rates reflected direct interactions with the ligand or rearrangements caused by ligand binding. Large differences in rates were observed for residues adjacent in the primary sequence reflecting their individual roles in ligand interaction. However, rates were similar for residues involved in the same side chain interactions, reflecting concerted motions during ligand binding. For a subset of residues, exchange must involve structural intermediates which play a crucial role in high-affinity ligand binding. This analysis supports a new view of the dynamics of individual sites of a protein during ligand interaction.

Protein function strongly depends on changes in three-dimensional structure in response to specific molecular interactions (1). In enzymes, for example, access of the ligand to the catalytic site may require conformational rearrangements to provide a path of entry. Proteins that regulate signal transduction often undergo significant conformational changes in tertiary structure upon ligand binding (2). Protein interactions which involve rearrangements strongly depend on the internal dynamics of the protein. A detailed analysis of protein dynamics will thus provide valuable information for the understanding of protein–ligand interactions. NMR relaxation experiments have proven to be a powerful tool in extracting dynamic parameters at atomic resolution (3, 4). In the past, most relaxation studies concentrated on fast picosecond to nanosecond dynamics. More recently, there has been increased interest in dynamics at a microsecond to millisecond time scale. The inherent dynamics on this time scale are biologically relevant because this is the time scale of many protein–ligand interactions (5). Such slow dynamic processes may involve concerted motions of larger parts of a protein which are relevant for biological function.

NMR spectroscopy provides several possibilities for measuring dynamics on slow time scales. The broadening and shape of protein signals for various ligand concentrations

can be used to determine kinetic rates (6). Chemical exchange rates on a micro- to millisecond time scale can be obtained from relaxation dispersion using Carr–Purcell–Meiboom–Gill (CPMG)¹ sequences. CPMG measurements have previously been used to detect exchange between different conformational states of proteins and have been used to determine kinetic rates involving states with low populations (7, 8). Recently, Eisenmesser *et al.* (9) used CPMG measurements to determine the catalytic turnover rates for individual residues in cyclophilin A by separating the catalytic rate from internal dynamics.

We have been using the N-terminal src homology 2 domain (SH2) of phosphatidylinositol 3-kinase (PI3K) that interacts with phosphotyrosine (ptyr) containing sequences from ligands such as the platelet-derived growth factor (PDGF) receptor or polyoma middle T antigen (MT) as a model to examine protein–ligand interactions using NMR. PI3 kinases are important for cell function (10–18). Interaction of PI3K with middle T ligand is critical for induction of tumors by polyomavirus (19). Intracellular trafficking of PI3K is mediated by the binding of the SH2s to tyrosine-phosphorylated sequences of oncogenes such as MT (20) or receptors such as PDGFR (21, 22). The structure of N-SH2 is known from both NMR and X-ray studies (23–26). As for other SH2s, it can be described as a central antiparallel β -sheet flanked by smaller β -sheets and two α -helices. SH2s

[†] This work was supported by the Large Scale Facility Frankfurt (UNIFRANMR), by a stipend of the Deutsche Studienstiftung (T.M.), and by grants from the National Institutes of Health (B.S.).

^{*} To whom correspondence should be addressed. Telephone: 49-(0)69-79829623. Fax: 49-(0)69-79829632. E-mail: Ulrich.Guenther@em.uni-frankfurt.de.

[‡] J. W. Goethe University, Frankfurt.

[§] Tufts University.

¹ Abbreviations: CPMG, Carr–Purcell–Meiboom–Gill; GST, glutathione *S*-transferase; HSQC, heteronuclear single-quantum coherence; MT, polyomavirus middle T antigen; MT8, EEEpYMPME-NH₂; N-SH2, N-terminal src homology 2 domain of p85; PDGFR, platelet-derived growth factor receptor; PI3K, phosphatidylinositol 3-kinase; ptyr, phosphotyrosine.

bind tyrosine-phosphorylated sequences with specificity being largely determined by the three residues C-terminal to the tyrosine. Our NMR studies have suggested that the structure is interactive in the sense that changes at the ptyr +1 or +3 position C-terminal to the ptyr can have effects throughout the structure (27). Very recently, we have shown how line shape analysis can be used to demonstrate the existence of structural intermediates in the binding process and to measure local off-rates (6 and unpublished data).

Here we use the ability of CPMG measurements to detect motion on the micro- to millisecond time scale to probe the behavior of N-SH2. Separation of internal dynamics and dynamics associated with ligand interaction was achieved by measuring relaxation dispersion for samples with different concentrations of the ligand. We used this information for a kinetic analysis of the interaction of SH2 with a phosphorylated high-affinity peptide derived from the binding site of MT.

MATERIALS AND METHODS

The peptide EEEpY₃₁₅MPME-NH₂ (MT8) was synthesized and HPLC purified by the Tufts Protein Chemistry Facility as described previously (27). The purity was confirmed by NMR spectra and ESI and MALDI mass spectra.

Protein samples were prepared as described previously (27, 29) using 1 L of CELTONE-CN (MARTEK Biosciences Corp.). NMR sample conditions were 0.5 mM ¹⁵N-labeled N-SH2 in 0.1 M KCl (pH 6.8) and a 90% H₂O/10% D₂O mixture in a sample volume of 450 μ L.

All NMR spectra were recorded at 303 K. Relaxation dispersion data were obtained at two static magnetic fields, corresponding to proton Larmor frequencies of 500 and 700 MHz (in some cases 500 and 800 MHz) using a relaxation-compensated CPMG dispersion experiment performed in a constant time manner (8). Spectra were collected as a series of 14–16 two-dimensional (2D) spectra with CPMG field strengths (ν_{cp}) of 17, 33, 50, 67, 83, 100, 117, 133, 167, 200, 233, 267, 333, 400, 500, and 667 Hz. Repeated experiments were performed at 33 and 500 Hz. The constant time period was set to 60 ms; the reference experiment was carried out by omitting the CPMG period. Spectra were acquired with at least 1024 \times 128 complex points. Processing and analysis of the NMR spectra were performed with the use of NMRlab (30).

Chemical exchange on a micro- to millisecond time scale increases the value of R_2 by an amount R_{ex} . The exchange contribution R_{ex} in the measured transverse relaxation time is minimal for fast refocusing rates in CPMG pulse trains. For varying echo times, relaxation dispersion curves are obtained which depend on the chemical shift differences ($\Delta\omega$), the population of the two states, and the exchange rate k_{ex} .

Exchange rates (k_{ex}) were determined by fitting relaxation dispersion curves to the general expression for the phenomenological transverse relaxation rate constant in the case of two-site exchange with $p_B = 1 - p_A$ (31–34):

$$R_2(1/\tau_{cp}) = 1/2 \left\{ R_{2A}^0 + R_{2B}^0 + k_{ex} - \frac{1}{2\tau_{cp}} \cosh^{-1} [D_+ \cosh(\eta_+) - D_- \cos(\eta_-)] \right\} \quad (1)$$

where $2\tau_{cp}$ is the delay between 180° pulses in the CPMG pulse train and

$$D_{\pm} = \frac{1}{2} \left[\pm 1 + \frac{\Psi + 2\Delta\omega^2}{(\Psi^2 + \zeta^2)^{1/2}} \right]$$

$$\eta_{\pm} = \sqrt{2}\tau_{cp} [\pm\Psi + (\Psi^2 + \zeta^2)^{1/2}]^{1/2}$$

$$\Psi = (R_{2A}^0 - R_{2B}^0 - p_A k_{ex} + p_B k_{ex})^2 - \Delta\omega^2 + 4p_A p_B k_{ex}^2$$

$$\zeta = 2\Delta\omega(R_{2A}^0 - R_{2B}^0 - p_A k_{ex} + p_B k_{ex})$$

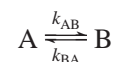
The refocusing field is related to the delay $2\tau_{cp}$ between to 180° pulses according to $\nu_{cp} = 1/(4\tau_{cp})$.

Simulations of eq 1 with different relaxation rates R_{2A}^0 and R_{2B}^0 for the amide nitrogens of sites A and B show only a minor effect on the dispersion curves compared to simulations in which $R_{2A}^0 = R_{2B}^0 = R_2^0$. This effect is most pronounced for very fast refocusing rates ($\nu_{cp} \rightarrow \infty$). However, relaxation dispersion at very high refocusing rates has little influence on the values of k_{ex} , $\Delta\omega$, p_A , and p_B ; it mainly correlates with R_2^0 . Since the difference between transverse ¹⁵N relaxation rates of the exchanging partners is not very high, we have assumed that R_{2A}^0 and R_{2B}^0 are equal. When the chemical shifts of the two states are known, $\Delta\omega$ can be fixed at the value of the chemical shift difference. The chemical shift time regime can be determined from the static magnetic field dependence of the exchange contribution to R_2 . The parameter

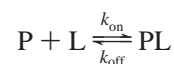
$$\alpha = \left(\frac{B_{02} + B_{01}}{B_{02} - B_{01}} \right) \left(\frac{R_{ex2} - R_{ex1}}{R_{ex2} + R_{ex1}} \right) \quad (2)$$

where R_{ex1} and R_{ex2} are the exchange contributions to the transverse relaxation rate at static magnetic field strengths B_{01} and B_{02} , respectively, equals 1 for intermediate exchange. When $0 < \alpha < 1$, the exchange is slow on the NMR time scale, and when $1 < \alpha < 2$, it is fast. R_{ex} was obtained from the difference in the effective transverse relaxation rate in the absence and presence of a high refocusing field [$R_{ex} = R_2(\nu_{cp} \rightarrow 0) - R_2(\nu_{cp} \rightarrow \infty)$]. Since the time regime detected by relaxation dispersion is determined by the ratio of k_{ex} and $\Delta\omega$ which is determined in a manner independent of α , this parameter is useful in assessing the consistency of the data analysis.

For exchange between two sites



the measured exchange rate k_{ex} equals $k_{AB} + k_{BA}$. If the exchanging sites are the free and the complexed form of a protein



the exchange rate k_{ex} equals $k_{on}[L] + k_{off}$. In the special case where the concentration of the ligand is low, the equilibrium concentration [L] will be minimal for high affinities. Therefore, the measured exchange rate approaches the off-

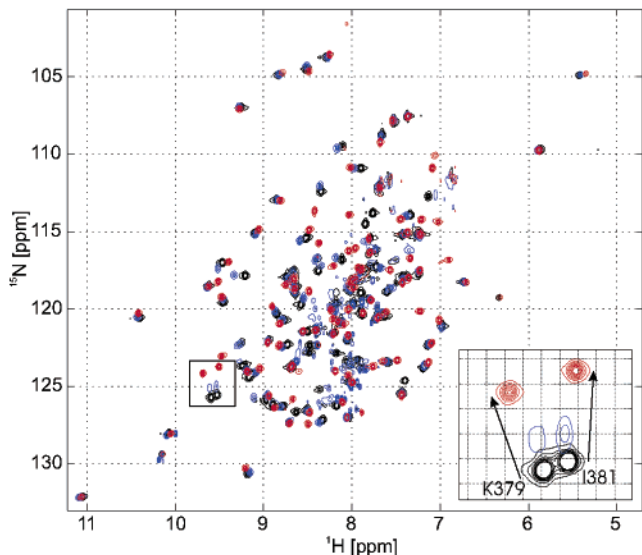


FIGURE 1: ^1H – ^{15}N HSQC spectra of PI3K N-SH2 in the free state (black), an initial binding state with $1/20$ of the stoichiometric amount of the MT8 peptide (blue), and the SH2–MT8 complex (red). In the spectrum recorded for an initial binding state, the resonances are shifted only slightly while lines of K379 and I381 (expansion) are broadened.

rate ($k_{\text{ex}} \approx k_{\text{off}}$), and the free form is usually the only observable species ($p_{\text{F}} \gg p_{\text{PL}}$).

RESULTS

We have characterized motions in N-SH2 associated with the binding of an eight-amino acid peptide EEEpYMPME-NH₂ (MT8) derived from the SH2 binding region of MT antigen. ^{15}N relaxation dispersion was assessed by measuring transverse relaxation rate constants with varying delays between refocusing pulses (relaxation dispersion). This was done for the backbone amides of p85 N-SH2 in three different states: (1) free N-SH2, (2) a saturated N-SH2–MT8 complex, and (3) a partially titrated N-SH2 with only $1/20$ of the stoichiometric equivalent of peptide required for full titration. The corresponding ^{15}N HSQC spectra are shown in Figure 1. Relaxation dispersion curves were analyzed by fitting the data to eq 1 by optimizing k_{ex} , $\Delta\omega$, and the populations of the states. Results of these simulations are presented in Tables 1–4. Differences in relaxation parameters between the three states were used to examine the dynamics of the binding process and to derive the kinetic rates of the interaction.

Exchange in Free SH2. We have analyzed relaxation dispersion for 94 residues for which the resonances were not overlapped in the HSQC spectrum which is shown in black in Figure 1. Examples of typical dispersion curves are shown in panels a and b of Figure 2 for residues D337 and I338. For most residues, the transverse relaxation rate R_2 was not influenced by the refocusing rate, ν_{cp} , of the CPMG sequence. This means there was no contribution from R_{ex} to the transverse relaxation rate R_2 . Most residues in the α -helices and in the β -sheet did not undergo exchange processes. However, we observed small exchange contributions R_{ex} for 15 residues listed in Table 1. The exchanging residues are also depicted in Figure 3a on a ribbon diagram of p85 N-SH2 which is labeled with colors from blue to red for increasing values of R_{ex} .

Table 1: ^{15}N Relaxation Dispersion Parameters of Exchanging Residues of Free SH2

residue	R_{ex} (s^{-1}) ^a	$\Delta\omega_{\text{eval}}$ (ppm)	k_{ex} (s^{-1})	p_{a}	$R_2^0(\nu_{\text{cp}} \rightarrow \infty)$ (s^{-1})	α
Y368	2.3	1.94	894	0.99	15.42	1.24
R373	2.2	0.28	1687	0.5	14.62	1.95
K374	2.0	0.94	91	0.98	18.42	0.18
I383 ^b	5.2	1.77	620	0.99	14.14	0.92
F384 ^b	13.8	0.20	16	0.5	13.76	1.70
Y390	3.8	0.88	815	0.91	13.68	1.72
G391 ^b	2.4	0.73	572	0.98	12.53	1.58
F392 ^b	4.2	1.04	442	0.98	13.81	1.13
S393	2.8	3.16	549	0.99	10.60	0.39
L396 ^b	2.3	4.34	5	0.5	13.17	0.05
T397	2.8	0.19	590	0.5	17.35	1.95
F398	2.8	3.34	6	0.5	12.82	0.03
N399	2.0	0.69	118	0.98	16.02	0.48
N410 ^b	6.0	0.65	487	0.96	21.02	1.59
S412 ^b	1.7	1.56	287	0.99	12.91	0.41

^a $R_{\text{ex}} = R_2(\nu_{\text{cp}} \rightarrow 0) - R_2(\nu_{\text{cp}} \rightarrow \infty)$. ^b Data from 500 and 800 MHz were analyzed.

Table 2: Effective Transverse Relaxation Rates at High and Low Refocusing Field Strengths for Residues with Low Signal-to-Noise Ratios

residue	$R_2(\nu_{\text{cp}} = 667 \text{ Hz})$ (s^{-1})	$R_2(\nu_{\text{cp}} = 17 \text{ Hz})$ (s^{-1})
free SH2		
R340	26.2	27.0
G366	28.2	32.6
D394	20.5	25.0
R409	25.0	24.8
N417	38.6	48.5
V422	17.4	21.8
L424	28.3	31.3
intermediate state		
R409	19.2	23.5
A414	16.3	22.8
V422	21.8	26.1
SH2–MT8 complex		
D394	25.1	28.2
A414	14.8	26.0

The exchange contribution R_{ex} to the total transverse relaxation rate R_2 is a qualitative measure of exchange processes on a micro- to millisecond time scale. Enhanced values of R_{ex} were observed for some residues in the central β -sheet close to the EF loop (I383 in βD and F384 in $\beta\text{D}'$) and for N410 in the BG loop. Interestingly, none of the residues in the ptyr binding pocket exhibited exchange, except R340, one of the arginines involved in the coordination of the ptyr phosphate. For R340 in the ptyr binding pocket, for residues R409, N417, V422, and L424 in the BG loop, and for D394 in the EF loop and one residue in the BC loop (G366), high values of R_2 even at high refocusing rates (Table 2) indicated exchange at a relatively high rate ($k_{\text{ex}} > 2000 \text{ s}^{-1}$). These residues are labeled orange in Figure 3a. Although the exchange contribution must be high in the BG loop, quantitative values for exchange parameters R_{ex} and k_{ex} could not be derived because of the high R_2 and the resulting low signal intensity. High mobility is probably also the reason why resonances of residues S361–H365 from the BC loop cannot be observed in any of our spectra, even at high refocusing rates in CPMG experiments. This view is supported by the exchange contribution observed at the edge of the BC loop for G366.

Table 3: ^{15}N Relaxation Dispersion Parameters of Exchanging Residues of SH2 in the Initial Binding State

residue	R_{ex} (s^{-1}) ^a	$\Delta\omega_{\text{titr}}$ (ppm) ^b	$\Delta\omega_{\text{eval}}$ (ppm) ^c	k_{ex} (s^{-1})	p_a	R_2^0 (s^{-1})	α
D330	4.3	0.04	2.95	843	0.99	13.88	0.78
S339	16.4	0.75		1478	0.65	16.00	1.95
R340	4.6	0.55		1345	0.87	17.11	1.93
E341	1.9	0.22		1252	0.50	12.92	1.95
N344	7.9	0.51		1536	0.50	13.28	1.95
E345 ^d	6.5	0.56		1033	0.87	12.50	—
V357 ^e	3.0	0.28		660	0.50	15.20	—
R358	7	0.51		1252	0.50	16.56	1.96
D367 ^e	4.1	1.31		917	0.97	12.51	—
Y368	17.8	0.32	5.28	1937	0.98	12.75	1.01
T369	28.8	1.21	2.64	766	0.95	19.21	0.79
N378	4.5	0.31		981	0.50	13.42	1.95
K379 ^e	57	1.75		1157	0.67	19.50	—
S380	2.4	0.30	2.15	87	0.97	15.4	0.04
I381 ^e	56	1.48		636	0.74	26.98	—
I383 ^e	25.8	1.81		1706	0.83	16.74	—
F384	4.9	0.44		521	0.91	14.68	1.85
H385	4.1	0.20	2.33	460	0.99	14.18	0.48
R386 ^f	4.9	0.13	1.33	813	0.98	12.78	1.41
Y390	3.5	0.41		1203	0.84	14.28	1.94
G391	3.3	0.16		315	0.50	14.46	1.96
F392	15.9	0.92		1745	0.77	14.78	1.94
S393	6.6	0.39	3.05	518	0.99	12.08	0.37
L396	4.4	0.09	4.67	634	0.99	13.43	0.25
E403	2.8	0.19		355	0.80	15.14	1.93
L404	2.9	0.24		913	0.50	14.48	1.95
N406	8.9	0.65		1806	0.72	12.92	1.95
N410 ^e	40	1.71		1791	0.50	18.70	—
S412	27.9	1.30		2118	0.75	13.08	1.94

^a $R_{\text{ex}} = R_2(\nu_{\text{cp}} \rightarrow 0) - R_2(\nu_{\text{cp}} \rightarrow \infty)$. ^b Chemical shift difference of the amide nitrogen between free N-SH2 and the N-SH2–MT8 complex.

^c Fitted value for $\Delta\omega$, not given when $\Delta\omega_{\text{titr}}$ was used to fit the data.

^d Data from only 700 MHz were used. ^e Data from only 500 MHz were used. ^f Data from 500 and 800 MHz were analyzed.

Table 4: ^{15}N Relaxation Dispersion Parameters of Exchanging Residues of the SH2–MT8 Complex

residue	R_{ex} (s^{-1}) ^a	$\Delta\omega_{\text{titr}}$ (ppm) ^b	$\Delta\omega_{\text{eval}}$ (ppm) ^c	k_{ex} (s^{-1})	p_a	$R_2^0(\nu_{\text{cp}} \rightarrow \infty)$ (s^{-1})	α
R340 ^d	4.2	0.55		399	0.92	25.65	—
E342	1.2	0.03	0.39	46	0.97	12.09	0.46
A351	5.8	0.07	1.46	782	0.98	17.00	1.39
Y368 ^d	2.0	0.32		558	0.85	19.33	—
R373 ^d	3.4	0.17	0.84	297	0.98	18.18	—
K374	1.7	0.26		349	0.94	13.18	1.86
K379	3.7	1.75		1026	0.99	13.00	1.44
S380	2.7	0.30		27	0.89	14.60	0.91
I381	4.4	1.48		648	0.99	14.45	1.20
R386	1.6	0.13	1.83	38	0.96	13.18	0.02
Y390	3.5	0.41		832	0.89	13.53	1.91
S393	2.5	0.39		537	0.94	12.22	1.86
L396	3.0	0.09	1.69	674	0.99	15.69	1.11
V401	3.7	0.25		727	0.58	16.49	1.95
N410	4.3	1.71		967	0.98	16.64	—
S412	3.8	1.30		1323	0.98	14.75	1.75
Y416	20.9	3.40		1518	0.96	19.76	—
L420	4.6	1.91		1329	0.99	13.41	1.56

^a $R_{\text{ex}} = R_2(\nu_{\text{cp}} \rightarrow 0) - R_2(\nu_{\text{cp}} \rightarrow \infty)$. ^b Chemical shift difference of the amide nitrogen between free N-SH2 and the N-SH2–MT8 complex.

^c Fitted value for $\Delta\omega$, not given when $\Delta\omega_{\text{titr}}$ was used to fit the data.

^d Data from only 500 MHz were used.

Exchange in the Initial Binding Step. The successive addition of peptide to N-SH2 causes progressively shifting resonances for 51 of 108 residues (6). Observation of a single set of shifting resonances with a chemical shift reflecting

the populations of both states indicates fast exchange on the NMR time scale ($k_{\text{ex}} \gg \Delta\omega$). This was observed for most residues, although more complicated line shapes with signal shoulders in intermediate titration steps were observed for a subset of residues. These were previously interpreted to represent intermediate conformational states (6). To study the dynamics induced by peptide binding, we added a low concentration ($1/20$ of the stoichiometric equivalent of protein) of the EEEpYMPME-NH₂ peptide (MT8 peptide). The HSQC spectrum of this state is shown in blue in Figure 1. Relaxation rates for many residues of this sample represent a steady state view of the relaxation of the protein from a ligand-bound form to the state of the free protein. Since the exchange partners may also be different conformers of the protein, we have analyzed relaxation dispersion for all 94 residues for which the resonances were not overlapped in the HSQC spectrum. This included many residues for which no ^{15}N chemical shift perturbation was observed in ligand binding for detection of possible intermediates not seen in the titration.

For this low concentration of ligand, the resonances were shifted only slightly from their position in free SH2. It also is important to note that none of the resonances exhibited slowly exchanging signal components. The lines of many residues were broadened as a consequence of exchange initiated by the presence of the ligand (e.g., for residues K379 and I381 which are known to be involved in the binding process and whose amide resonances are depicted in the expansion in Figure 1). For many residues, the exchange contribution R_{ex} was significantly enhanced compared to those of the free and complexed states. This is depicted in Figure 3b where residues which exhibit enhanced exchange are grouped around the tyr binding pocket (S339, R340, E341, V357, and R358), in regions of the central β -sheet which interact with the peptide (N378, K379, S380, I381, I383, F384, H385, and R386), in the EF loop (Y390, G391, F392, S393, and L396), and in the BG loop (R409, N410, S412, and A414). Enhanced exchange for S393 compared to the free SH2 is depicted in panels c and d of Figure 2, which shows the relaxation dispersion curves of S393 in the different states of the protein. The highest exchange contributions were observed in βD for residues K379, I381, and I383, at the tip of the EF loop for F392, and in the BG loop for N410 and S412 (Table 3). For some residues in the BG loop (413–422), high values of R_2 caused intensities that were too low to fit relaxation dispersion curves. However, signal intensities for fast and slow refocusing rates were significantly different, indicating that the low signal intensity was a consequence of a high exchange contribution. This allowed at least a qualitative measure of exchange. Examples for this behavior include R409, A414, and V422 which are labeled orange in the ribbon diagram in Figure 3b. Relaxation rates in the limits of fast and slow pulsing are listed in Table 2. For residues Y408, Q415, Y416, and K419 in BG (labeled in yellow in Figure 3b), no signal was observed after addition of peptide which is another indication of very large amplitude exchange processes, although a quantitative value could not be obtained.

Exchange in the SH2–MT8 Complex. N-SH2 in a stoichiometric complex with MT8 is relatively rigid on a millisecond to microsecond time scale. The exchange process of R340 already observed in free SH2 is preserved, and an

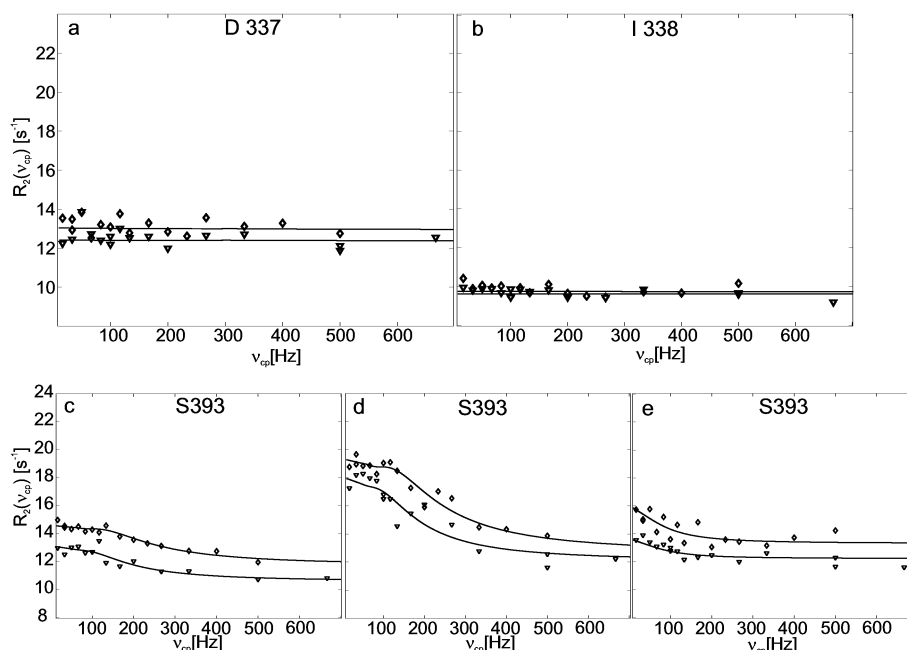


FIGURE 2: Effective transverse relaxation rates, R_2 , as a function of the CPMG field strength, ν_{cp} . The values of R_2 for (a) D337 and (b) I338 of free SH2 do not depend on the field strength (no exchange on a millisecond time scale). Solid lines are straight lines with a value equal to the mean value of R_2 . (c and d) Effective transverse relaxation rates, R_2 , as a function of the CPMG field strength, ν_{cp} , for S393 (c) in free SH2, (d) in the initial binding state, and (e) in the SH2–MT8 complex. The best-fit dispersion curves using eq 1 are shown as solid lines. Data recorded at ^1H Larmor frequencies of 700 and 500 MHz are depicted with diamonds and triangles, respectively.

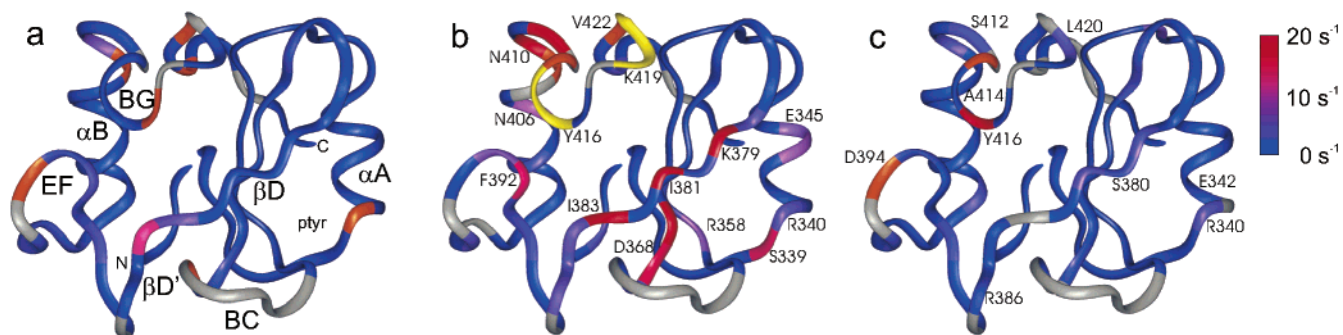


FIGURE 3: Exchange contributions for three different states of N-SH2. The exchange contribution R_{ex} to the ^{15}N transverse relaxation rate is depicted by color coding on the ribbon diagram of the SH2. The continuous color scale from blue to magenta to red (from 0 s^{-1} to 10 s^{-1} to 20 s^{-1}) represents the amplitude of R_{ex} for (a) free SH2, (b) SH2 in the initial binding state, and (c) the SH2–MT8 complex. Residues colored orange exhibit high exchange contributions which could not be quantified. Signals of residues colored yellow disappeared upon addition of ligand. Residues colored gray could not be analyzed due to overlap or missing assignments. The annotation of secondary structural elements follows the convention of Eck *et al.* (35).

additional residue in the ptyr binding pocket, E342, shows exchange (Figure 3c). The final complex behaved in a very different manner from that of the intermediate state. For example, residues in the β -sheet, the EF loop, and the BG loop exhibited very low amplitude exchange compared to the intermediate state.

Strikingly, some residues in the complex exhibited exchange contributions, although ligand binding did not cause any ^{15}N chemical shift change. This behavior was observed for residues E342, A351, R373, R386, and L396 which are labeled red in Figure 4b. Since exchange contributions to R_2 require a chemical shift change $\Delta\omega$, there must be some intermediate with a ^{15}N chemical shift different from that of free SH2. In this case, CPMG measurements can be used to detect exchanging conformers with low populations that cannot be detected in line shapes.

Exchange Rates. As shown in eq 1, relaxation dispersion depends on three important parameters: the population of

exchanging sites, the chemical shift differences between exchanging partners, and the exchange rate k_{ex} . In the previous paragraph, the exchange contribution R_{ex} to R_2 has been described. While R_{ex} provides a qualitative measure of the amount of micro- to millisecond flexibility, k_{ex} , which describes the exchange rate, could be obtained for most exchanging residues. As mentioned earlier, for two-site exchange k_{ex} is defined as $k_{AB} + k_{BA}$, where k_{AB} is the forward reaction rate and k_{BA} is the backward reaction rate.

k_{ex} in Free N-SH2. Exchange rates are mapped on the ribbon diagram of SH2 in Figure 5a using a color scale from blue (0 Hz) to magenta (1000 Hz) to red (2000 Hz). The residues for which exchange rates were calculated are identical to those which exhibited exchange contributions R_e . Exchange rates were low in most parts of free SH2. Most residues in the β -sheet, the EF loop, and the BG loop exhibit exchange rates of $\sim 400\text{--}600\text{ s}^{-1}$ (Table 1). Particularly low exchange rates were observed for K374 in upper βC (91 s^{-1}),

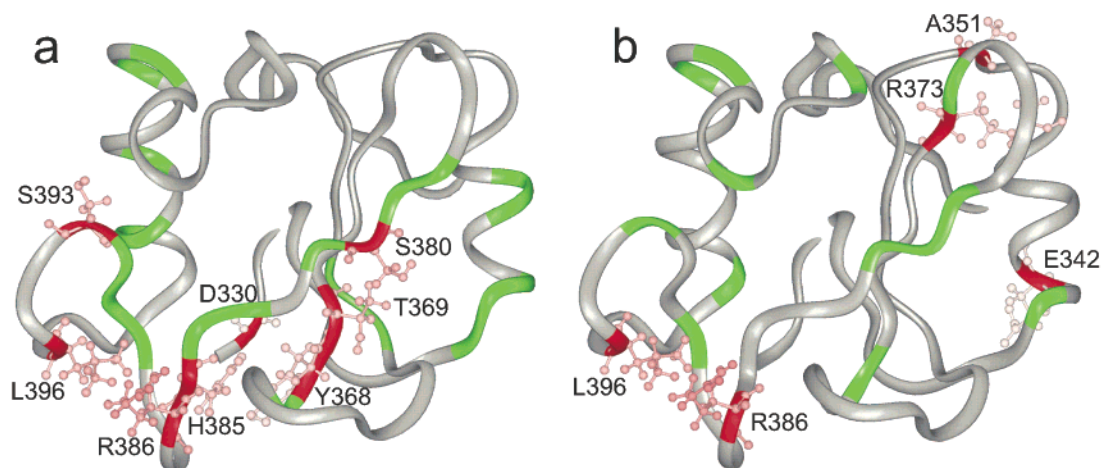


FIGURE 4: Conformational exchange (a) in SH2 in the initial binding state and (b) in the SH2–MT8 complex. The exchange contributions of residues colored green arise from binding and release of the ligand. The exchanging partners are the free and the complexed form of SH2. Their chemical shift difference was assumed in the relaxation dispersion analysis. For residues colored red, the chemical shift difference between the free protein and the complex could not explain the relaxation dispersion curves. Therefore, a different exchange partner must be assumed.

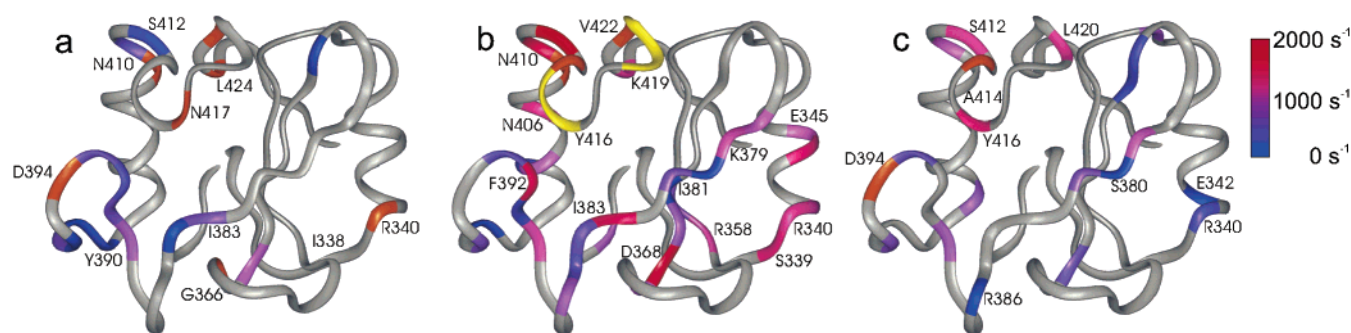


FIGURE 5: Exchange rates in three different states of N-SH2. The exchange rates k_{ex} are depicted by color coding on the ribbon diagram of SH2. A continuous color scale from blue to magenta to red (from 0 s^{-1} to 500 s^{-1} to 1000 s^{-1}) depicts k_{ex} for (a) free SH2, (b) SH2 in the initial binding state, and (c) the SH2–MT8 complex. Residues colored orange exhibit high exchange contributions which could not be quantified. Signals of residues colored yellow disappeared upon addition of ligand. Residues colored gray do not exhibit exchange or could not be analyzed due to overlap or missing assignments.

F384 in $\beta D'$ (16 s^{-1}), and L396 (5 s^{-1}) and F398 (6 s^{-1}) in the EF loop. Y368 in βC next to the BC loop and Y390 in the EF loop exhibited relatively high exchange rates of 894 and 815 s^{-1} , respectively.

k_{ex} in the Initial Binding Step. For exchange of one ligand molecule, k_{ex} also depends on the equilibrium concentration of free ligand $[L]_{eq}$ according to the equation $k_{ex} = k_{on}[L]_{eq} + k_{off}$, where k_{off} is the off-rate and k_{on} is the on-rate. For low concentrations of peptide and high affinities, the calculated exchange rates represent almost pure off-rates; i.e., $k_{ex} \approx k_{off}$. In the case of SH2 and the MT8 ligand, the affinity for the ligand was previously determined in competition binding of MT8 with ^{31}P -labeled MT antigen which gave an IC_{50} value of 8.4 μM (27). For an approximate dissociation constant $K_D (=k_{off}/k_{on})$ of 8 μM , a protein concentration of 0.5 mM, and addition of $1/20$ of the stoichiometric amount of peptide, the concentration of free ligand amounts to 4.3×10^{-7} M, and the occupancy of N-SH2 by MT8 is 4.9%. Only 1.7% of MT8 is not bound to protein.

For exchange induced by the addition of ligand, it is likely that the two exchanging partners are the free and the complexed states of the protein. Therefore, $\Delta\omega$ was set to the values of the ^{15}N chemical shift change of ligand binding if not otherwise indicated (Tables 3 and 4).

Exchange rates k_{ex} for the intermediate state of SH2 were significantly higher than those in free SH2 (Figure 5b). Nineteen residues exhibit exchange rates of 800–2000 s^{-1} , whereas exchange rates of 450–800 s^{-1} were obtained for only six residues. Particularly low exchange rates k_{ex} were obtained for S380 in βD (87 s^{-1}), G391 in the EF loop (315 s^{-1}), and E403 in αB (355 s^{-1}). Y368 next to the BC loop (1937 s^{-1}), I383 in βD (1706 s^{-1}), F392 in the EF loop (1745 s^{-1}), N406 and N410 in αB (1806 and 1791 s^{-1} , respectively), and S412 in the BG loop (2118 s^{-1}) exhibited particularly high exchange rates.

Interestingly, off-rates were often different for adjacent residues. For example, a sequence of residues in βD shows alternating rates. A low value of k_{ex} (87 s^{-1}) was observed for S380, and F382 does not exhibit exchange at all; on the other hand, the exchange rates of K379 (1157 s^{-1}), I381 (636 s^{-1}), and I383 (1706 s^{-1}) were significantly higher. K379, I381, and I383 point in the direction of the αB helix and the BG loop and are directly reflecting the binding reaction, whereas S380 is pointing toward the ptyr binding pocket. The off-rates of residues in the ptyr binding pocket were relatively homogeneous. The two conserved arginine residues coordinating the phosphotyrosine phosphate, R340 and R358, exhibited similar off-rates of 1345 and 1252 s^{-1} , respectively.

Similar off-rates were also observed for adjacent residues S339 and E341 (1478 and 1252 s⁻¹, respectively).

A subset of residues in and adjacent to loop regions (S393 in the EF loop, Y368 and T369 next to the BC loop, and H385, R386, and L396 next to the EF loop labeled in red in Figure 4a) exhibited relaxation dispersions which could not be interpreted adequately using the chemical shift difference between the free and complexed SH2 $\Delta\omega_{P-PL}$. The values of $\Delta\omega$ obtained by optimization of eq 1 are listed in Table 3. Thus, the exchanging partners are not the free, and the complexed protein and the exchange does not arise from binding and release of the ligand. In these cases, the exchange partners for free SH2 are most likely conformers formed upon ligand binding which act as intermediates on the reaction pathway. For all of these residues, the population of the minor state obtained from the simulation was $\leq 5\%$. The value of α was ≤ 1 except for that of R386, indicating exchange in the slow or intermediate time regime.

For those residues where the relaxation dispersion reflects the relaxation of the protein from the complexed to the free state, the parameter α (eq 2) approaches a value of 2, indicating fast exchange on the NMR time scale.

For most residues, the population of the predominant state obtained by fitting eq 1 to the relaxation dispersion data was between 0.8 and 0.99 (Table 3). These values are in concordance with a simple two-state binding reaction and reflect the expected mole fractions. However, for residues S339, E341, V357, and R358 in the ptyr binding pocket, N344 in the α A helix, N378 and K379 in β D, G391 in the EF loop, and L404 and N410 in the α B helix, we obtained populations of the minor state near 50% as obtained by optimization of eq 1. Assuming a one-step binding mechanism where the protein can only appear in a complexed state, the population of the minor state should not exceed 5%. Therefore, significantly enhanced populations of the minor state suggest the existence of protein intermediates stable on this time scale.

k_{ex} in the SH2–MT8 Complex. In the SH2–MT8 complex, the exchange contributions and exchange rates were both generally low compared to those for the sample with a small amount of ligand as depicted in Figure 5c. Exchange rates were in a similar range as those for free SH2. Exceptions were observed for E342 (46 s⁻¹), S380 (27 s⁻¹), and R386 (38 s⁻¹) with low exchange rates, whereas S412, Y416, and L420 in the BG loop exhibit particularly high exchange rates (1323, 1518, and 1329 s⁻¹, respectively).

DISCUSSION

Here we have compared the dynamics of free PI3K N-SH2 to those of the SH2–MT8 ligand complex. Internal motions in SH2 itself could be separated from dynamics induced by the interaction with the ligand by measuring relaxation dispersion in the free protein, the complexed protein, and an intermediate state with a low ligand concentration. This analysis supported the role of some key residues in the EF and BG loop together with residues in the central β -sheet which play a key role in ligand binding. Because we have previously used line shape analysis to examine the same ligand SH2 interaction, this work provides an opportunity to compare the value of the two approaches.

Relaxation dispersion measurements provide a detailed picture of the dynamics induced by SH2–ligand interaction.

Dynamics in the free SH2 are minimal and mainly limited to the loop regions. The highest values of R_{ex} in BG are almost one order of magnitude smaller than those observed with ligand present. However, some residues in BG (orange in Figure 3a) showed low signal intensities with relatively high levels of exchange. These residues (R409, V422, and L424) may have a hinge function for the loop. Missing signals of residues in the BC loop are probably also a consequence of exchange. G366 at the edge of the BC loop exhibited high relaxation rates. Interestingly, the exchange contribution of F384 in β D had the highest value of R_{ex} with a very low exchange frequency. This may reflect the interaction of the F384 side chain with the BC loop. In previous line shape analyses, this residue exhibited conformational averaging when a ligand was present (6). The current analysis suggests that this residue already has a high flexibility on a slow time scale in free SH2.

To measure the dynamics of the interaction of the protein with the ligand, we added a small amount of ligand. Under steady state conditions, it is easily possible to separate the on-rate from the off-rate because the equilibrium concentration of the free ligand is minimal and therefore $k_{on}[L]_{eq}$ becomes negligible. The choice of a low concentration also had the advantage that signal intensities were still sufficiently large to observe signals in CPMG measurements at small refocusing rates. The chemical shift difference between the free and the fully complexed protein should represent the relevant chemical shift difference for the relaxation dispersion effect. Residues for which a good fit could be achieved using $\Delta\omega_{P-PL}$ are labeled green in Figure 4a. However, for a subset of residues, the chemical shift perturbation of ligand binding was too small to fit the relaxation dispersion curves. These residues are labeled red in Figure 4a. Fitting $\Delta\omega$ for these residues yielded small populations for another exchange partner, indicative of an unidentified intermediate on the reaction pathway. These residues are located in loop regions (S393 in the EF loop) and directly adjacent to loop regions (Y368 and T369 next to the BC loop and H385, R386, and L396 next to the EF loop). This supports our previous conclusion from line shape analysis that ligand binding requires the formation of intermediates for some residues (6). Some (D330, Y368, S380, H385, R386, and L396) of these residues for which relaxation measurements suggested intermediates exhibited hardly any chemical shift perturbation. In these instances, intermediates were detected that could not be observed by line shape analysis. For T396 and R386, some exchange was still observed in the complex. Consequently, exchange for these residues must be attributed to some conformational exchange and cannot be attributed to the dynamics of ligand binding. α values between 0 and 1 show that the conformational exchange of these residues is on the slow or intermediate NMR time regime. Signal shoulders in titration spectra further support the existence of slow motions.

The sudden increase in the level of exchange after addition of a small amount of ligand gives an impressive picture of the dynamics in the protein resulting from the ligand interaction. Because there was comparably slow exchange in free SH2 and in the SH2 complex, the high level of exchange observed in the intermediate binding state can be attributed to the relaxation of the protein complex back to free SH2. This is not necessarily the off-rate of the ligand

because the lifetime of the bound state of the protein may be longer than the lifetime of the interaction with the ligand. This may be particularly important if the relaxation to the free state requires complex concerted rearrangements in the protein.

The overall picture of exchange contribution with a small amount of ligand shown in Figure 1b indicates the rearrangements induced by ligand binding and direct ligand interaction. Interestingly, R_{ex} alternates between very high and low values in a sequence of residues from K379 to F384 in β D. Those residues which point toward the BG and EF loops (K379, I381, and I383) adopt high values representing the dynamics of the interaction with the peptide. In contrast, S380 and F384 exhibit lower values and K382 exhibits no exchange. This result suggests that motions observed on the amide ^{15}N reflect motions of side chains which may be correlated through space. For example, the rates of I383 and F384 correlate well with rates in the EF loop and that of K379 correlates with rates in the BG loop, suggesting concerted motion of those residues.

The rearrangement of the BG loop is reflected in high values in the hinge region (N410, S412, A414–Y416, K419, and V422) on each side of the loop. Some residues in the BG loop can no longer be analyzed because of the high dynamics in this loop. Interestingly, F392 at the tip of the EF loop has the greatest exchange contribution in this loop. As previously reported, the EF loop and the BG loop are linked by a stacking interaction of the aromatic side chains of F392 and Y416 in the free protein (26). Upon ligand binding, this interaction is dissolved which is reflected in high exchange contributions for both residues.

Very high exchange contributions were also observed for residues Y368 and T369 in β C, at the edge of the BC loop, which support the role of the BC loop region for the interaction with the ligand (25). Rearrangements in this region of the protein seem to be important for reshaping the ptyr binding pocket for effective high-affinity interaction.

In the ptyr binding pocket, rates of adjacent residues are similar and reflect the off-rate of the ligand in this region. Similar rates are observed for residues S339 and R340, one of the two arginines which coordinate the ptyr phosphate, and E341. Interestingly, the measured rate is similar for R358, the arginine which coordinates the ptyr phosphate from the other side.

In the final complex, Y416 is the only residue which exhibits a large exchange contribution. Y416 had been identified as a residue which undergoes a large movement upon ligand binding (25, 26) and exhibited a large chemical shift perturbation of 3.4 ppm (27). Interestingly, exchange for this and some adjacent residues (N410, S412, and L420) was not completely frozen in the complex. The large chemical shift change upon ligand binding is responsible for the high relaxation dispersion effect.

The off-rates determined here can be compared to off-rates previously determined using line shape analysis (6). Off-rates of S339 [1478 s^{-1} from dispersion analysis vs 1120 (-220 to $+310$) s^{-1} from line shape analysis], R340 (1345 vs 1500 s^{-1}), K379 [1157 vs 930 (-100 to $+120$) s^{-1}], and H385 [460 vs 560 (-80 to $+110$) s^{-1}] obtained from relaxation dispersion analysis and line shape analysis were similar within experimental error. For some residues, however, the results from relaxation dispersion and line shape

analysis did not agree. Line shape analysis yielded values for k_{off} of 550 s^{-1} for F392 and 600 s^{-1} for S412. From relaxation dispersion, we obtained much higher rates, 1745 s^{-1} for F392 and 2118 s^{-1} for S412. These differences may be a consequence of the systematic error made by the assumption of two-state exchange used in the analysis. If the actual mechanism of the interaction involves more than two states, intermediates must be taken into account for the analysis. How does this affect the rates obtained from line shapes and relaxation dispersion? Clearly, intermediates which are not observed will reduce the intensity of the signals for intermediate ligand concentrations. There line shape analysis will yield a rate which is too low. However, relaxation dispersion will show an increased R_2 starting at the highest rate that is involved in a set of parallel processes. In these cases, the rates measured by the CPMG method will always be higher than the rates obtained from line shapes. Interestingly, some of the residues that exhibited very high exchange contributions in the intermediate state exhibited complex lines. K379 and F392 exhibit minor shoulders in one or two lines of the titration, whereas S412 exhibited significantly distorted lines during the titration with disappearing signals. The existence of intermediate states may also be supported by relaxation dispersion curves which could not be fitted using the $\Delta\omega$ from the ligand binding. In these cases, some other conformer must be responsible for the exchange effect. Such conformers may represent intermediates in ligand binding.

There are clearly differences between CPMG and line shape analysis for the examination of molecular dynamics. CPMG is not applied to residues that shift only in the proton dimension (e.g., A360 in the beginning of the BC loop). Line shape analysis clearly emphasizes the complexity of the binding mechanism, while relaxation dispersion gives only rudimentary information about intermediates in ligand binding. However, unlike line shape analysis, CPMG analysis can detect intermediates even if there is no chemical shift difference between free SH2 and the final complex (e.g., D330). Relaxation dispersion analysis also shows conformational exchange in the free protein and in the final complex which cannot be analyzed in line shape analysis.

The overall conclusions from relaxation dispersion and line shape analysis are similar. Both methods provide a direct view of the kinetic events caused by ligand binding at the site of individual amino acids. This analysis supports the role of key regions of the protein such as the ptyr binding pocket and the central β -sheet. An important role of the BG loop and the EF loop is indicated in both analyses. Most importantly, there must be structural intermediates on the binding pathway. In fact, extensive conformational exchange was induced by small amounts of ligand. The nature and location of conformational exchange are important for high-affinity ligand binding. This is a new aspect in the description of protein–ligand interactions which has important theoretical and practical consequences.

ACKNOWLEDGMENT

We thank H. Rüterjans for kindly giving U.L.G. access to his laboratory.

REFERENCES

1. Karplus, M., and McCammon, J. A. (1983) Dynamics of proteins: elements and function, *Annu. Rev. Biochem.* 53, 263–300.

2. Pawson, T. (1995) Protein modules and signalling networks, *Nature* 373, 573–580.
3. Palmer, A. G. (1997) Probing molecular motion by NMR, *Curr. Opin. Struct. Biol.* 7, 732–737.
4. Kay, L. E. (1998) Protein dynamics from NMR, *Nat. Struct. Biol. NMR Suppl.* 5, 513–517.
5. Fersht, A. (1999) *Structure and Mechanism in Protein Science. A Guide to Enzyme Catalysis and Protein Folding*, 1st ed., Freeman, New York.
6. Günther, U., Mittag, T., and Schaffhausen, B. (2002) Probing src homology 2 domain ligand interactions by differential line broadening, *Biochemistry* 41, 11658–11669.
7. Palmer, A. G., Kroenke, C. D., and Loria, J. P. (2001) Nuclear magnetic resonance methods for quantifying microsecond-to-millisecond motions in biological macromolecules, *Methods Enzymol.* 339, 204.
8. Tollinger, M., Skrynnikov, N. R., Mulder, F. A. A., Forman-Kay, J. D., and Kay, L. E. (2001) Slow dynamics in folded and unfolded states of an SH3 domain, *J. Am. Chem. Soc.* 123, 11341–11352.
9. Eisenmesser, E. Z., Bosco, D. A., Akke, M., and Kern, D. (2002) Enzyme dynamics during catalysis, *Science* 295, 1520–1523.
10. Vanhaesebroeck, B., and Waterfield, M. (1999) Signaling by distinct classes of phosphoinositide 3-kinases, *Exp. Cell Res.* 253, 239–254.
11. Dankort, D., and Müller, W. (2000) Signal transduction in mammary tumorigenesis: a transgenic perspective, *Oncogene* 19, 1038–1044.
12. Datta, S., Brunet, A., and Greenberg, M. (1999) Cellular survival: a play in three Acts, *Genes Dev.* 13, 2905–2927.
13. Wurmser, A., Gary, J., and Emr, S. (1999) Phosphoinositide 3-kinases and their FYVE domain-containing effectors as regulators of vacuolar/lysosomal membrane trafficking pathways, *J. Biol. Chem.* 274, 9129–9132.
14. Rameh, L., and Cantley, L. (1999) The role of phosphoinositide 3-kinase lipid products in cell function, *J. Biol. Chem.* 274, 8347–8350.
15. Corvera, S., D'Arrigo, A., and Stenmark, H. (1999) Phosphoinositides in membrane traffic, *Curr. Opin. Cell Biol.* 11, 460–465.
16. Wymann, M., and Pirola, L. (1998) Structure and function of phosphoinositide 3-kinases, *Biochim. Biophys. Acta* 1436, 127–150.
17. Krugmann, S., and Welch, H. (1998) PI 3-kinase, *Curr. Biol.* 8, R828.
18. Fruman, D., Meyers, R., and Cantley, L. (1998) Phosphoinositide kinases, *Annu. Rev. Biochem.* 67, 481–507.
19. Freund, R., Dawe, C. J., Carrol, J. P., and Benjamin, T. L. (1992) Changes in frequency, morphology, and behavior of tumors induced in mice by a polyoma virus mutant with a specifically altered oncogene, *Am. J. Pathol.* 141, 1409–1425.
20. Yoakim, M., Hou, W., Liu, Y., Carpenter, C. L., Kapeller, R., and Schaffhausen, B. S. (1992) Interactions of polyomavirus middle T with the SH2 domains of the pp85 subunit of phosphatidylinositol-3-kinase, *J. Virol.* 66, 5485–5491.
21. Escobedo, J. A., Kaplan, D. R., Kavanaugh, W. M., Turck, C. W., and Williams, L. T. (1991) A phosphatidylinositol-3 kinase binds to platelet-derived growth factor receptors through a specific receptor sequence containing phosphotyrosine, *Mol. Cell. Biol.* 11, 125–132.
22. Kashishian, A., Kazlauskas, A., and Cooper, J. (1992) Phosphorylation sites in the PDGF receptor with different specificities for binding GAP and PI3 kinase *in vivo*, *EMBO J.* 11, 1373–1382.
23. Booker, G. W., Breeze, A. L., Downing, A. K., Panayotou, G., Gout, I., Waterfield, M. D., and Campbell, I. D. (1992) Structure of an SH2 domain of the p85 α subunit of phosphatidylinositol-3-OH kinase, *Nature* 358, 684–687.
24. Hensmann, M., Booker, G. W., Panayotou, G., Boyd, J., Linacre, J., Waterfield, M., and Campbell, I. D. (1994) Phosphopeptide binding to the N-terminal SH2 domain of the p85 α subunit of PI 3'-kinase: a heteronuclear NMR study, *Protein Sci.* 3, 1020–1030.
25. Nolte, R. T., Eck, M. J., Schlessinger, J., Shoelson, S. E., and Harrison, S. C. (1996) Crystal structure of the pi 3-kinase p85 amino-terminal SH2 domain and its phosphopeptide complexes, *Nat. Struct. Biol.* 3, 364–374.
26. Weber, T., Schaffhausen, B., Liu, Y., and Günther, U. (2000) NMR structure of the N-SH2 of the p85 subunit of phosphoinositide 3-kinase complexed to a doubly phosphorylated peptide reveals a second phosphotyrosine binding site, *Biochemistry* 39, 15860–15869.
27. Günther, U., Liu, Y., Sanford, D., Bachovchin, W., and Schaffhausen, B. (1996) NMR analysis of interactions of a Phosphatidylinositol 3'-kinase SH2 domain with phosphotyrosine peptides reveals interdependence of major binding sites, *Biochemistry* 35, 15570–15581.
28. Deleted in proof.
29. Yoakim, M., Hou, W., Songyang, Z., Liu, Y., Cantley, L., and Schaffhausen, B. (1994) Genetic analysis of a phosphatidylinositol 3-kinase SH2 domain reveals determinants of specificity, *Mol. Cell. Biol.* 14, 5929–5938.
30. Günther, U., Ludwig, C., and Rüterjans, H. (2000) NMR-LAB: Advanced NMR data processing in Matlab, *J. Magn. Reson.* 145, 201–208.
31. Luz, Z., and Meiboom, S. (1963) Nuclear magnetic resonance study of the protolysis of triethylammonium ion in aqueous solution: order of the reaction with respect to solvent, *J. Chem. Phys.* 39, 366–370.
32. Carver, J., and Richards, R. (1972) General two-site solution for the chemical exchange produced dependence of T2 upon the Carr-Purcell pulse separation, *J. Magn. Reson.* 6, 89–105.
33. Jen, J. (1978) Chemical exchange and NMR T2 relaxation: the multisite case, *J. Magn. Reson.* 30, 111–128.
34. Davis, D., Perlman, M., and London, R. (1994) Direct measurements of the dissociation rate constant for inhibitor-enzyme complexes via the T1rho and T2 (CPMG) methods, *J. Magn. Reson., Ser. B* 104, 266–275.
35. Eck, M. J., Shoelson, S. E., and Harrison, S. C. (1993) Recognition of a high-affinity phosphotyrosyl peptide by the Src homology-2 domain of p56lck, *Nature* 362, 87–91.

BI0347499

Probing Src Homology 2 Domain Ligand Interactions by Differential Line Broadening[†]

Ulrich Günther,^{*,‡} Tanja Mittag,[‡] and Brian Schaffhausen[§]

Institute of Biophysical Chemistry, J. W. Goethe University, Frankfurt, Biocenter N230, Marie-Curie-Strasse 9, 60439 Frankfurt, Germany, and Department of Biochemistry, School of Medicine, Tufts University, 136 Harrison Avenue, Boston, Massachusetts 02111

Received March 29, 2002; Revised Manuscript Received July 18, 2002

ABSTRACT: Few techniques for probing the role of individual amino acids in interactions of a protein with ligands are available. Chemical shift perturbations in NMR spectra provide qualitative information about the response of individual amino acids of a protein to its interactions with ligands. Line shapes derived from ¹⁵N-HSQC spectra recorded for different steps of a ligand titration yield both kinetic constants and insight into mechanisms by which the ligand binds. Here we have analyzed line shapes for 37 signals of amino acids of the N-terminal src homology 2 domain (N-SH2) of the 85 kDa subunit of phosphatidylinositol 3-kinase (PI3-K) upon binding of phosphotyrosine (ptyr)-containing peptides. Kinetic rates at individual amino acids of the SH2 varied throughout the structure. For a subset of SH2 residues, the fine structure of the NMR line shapes indicated slow motions induced by the presence of small amounts of the ligand. These complex line shapes require one or more additional conformational states on the kinetic pathway. Modeling of the observed ligand interactions suggests a quasi-allosteric initial binding step. N-SH2 mutants with altered ligand affinity or specificity were also examined. Analysis of their line shapes revealed three distinct classes of mutants with different kinetic behaviors.

Differential line broadening of one-dimensional NMR data is a common tool for studying chemical kinetics. It has most often been employed to study chemical exchange or conformational averaging of small organic molecules. For large biomolecules, line shape analysis has been reserved for some isolated signals, such as high-field methyl resonances (1). Isotope-edited two-dimensional NMR spectra offer an increased number of opportunities for analysis of differential line broadening and provide kinetic data for different positions in a protein both because of increased dispersion and because chemical shift perturbations of both nuclei become accessible to analysis. This has made line shape analysis applicable to problems of protein folding (2) and ligand binding kinetics for larger proteins (3). Line shapes recorded for a protein upon ligand binding contain valuable information about the binding rates and mechanism (4, 5). They are most easily interpreted for fast exchange on the NMR time scale for an individual nucleus (here ¹H or ¹⁵N). Sudmeier (6) has shown theoretical line shapes for ligand titrations where line shapes depend on the amount of ligand added. However, line shapes in slow exchange have also been analyzed assuming complex binding mechanisms (3). For quantitative line shape simulations, the proper choice of a suitable kinetic model is crucial. We have recently described

an effective method for calculating line shapes derived from two-dimensional NMR spectra and have demonstrated the complexity of line shapes that can arise from certain kinetic mechanisms (7). Here we have used differential line broadening to study binding kinetics for individual amino acids of the N-terminal SH2¹ domain of the p85 subunit of PI3-kinase (PI3-K).

PI3-K is an enzyme broadly important for trafficking and cell signaling (8–18). Mitogenic signaling (19, 20), vesicle trafficking (21, 22), cell movement (23), rearrangement of cytoskeletal actin (24), and chemotaxis (25) are all normal cell functions where PI3-K plays an important role. Activation is also associated with acute stimulation such as platelet activation by thrombin (26, 27), stimulation of neutrophils by fMet-Leu-Phe (28), and stimulation of phagocytosis (29). PI3-K pathways have important roles in oncogenesis. The original interest in the enzyme came from its association with oncogenes such as v-src and polyoma middle T (MT) (30). Retroviruses expressing mutant forms of PI3-K or its downstream target Akt can induce tumors (31, 32). In the case of middle T, activation of PI3-K is required for tumor formation at sites such as kidney and is critical in others such as breast (33). Besides its role in stimulation of cell growth, PI3-K has a role in preventing apoptosis in a variety of cell types (34, 35). Finally, PI3-K activation is also associated with tumor invasion (36).

[†] This work was supported by the Deutsche Forschungsgemeinschaft, by the NMR Large Scale Facility Frankfurt (UNIFRANMR), by NIH Grants CA34722 and CA50661 (to B.S.), and by a NATO collaborative research grant.

* To whom correspondence should be addressed. Telephone: 49-(0)69-79829623. Fax: 49-(0)69-79829632. E-mail: ugun@bpc.uni-frankfurt.de.

[‡] J. W. Goethe University.

[§] Tufts University.

¹ Abbreviations: HSQC, heteronuclear single-quantum coherence; FID, free induction decay; CPMG, Carr–Purcell–Meiboom–Gill pulse sequence; PDGFr, platelet-derived growth factor receptor; MT, polyoma virus middle T antigen; p85, 85 kDa subunit of phosphatidylinositol 3-kinase; PI3-K, phosphatidylinositol 3-kinase; SH2, Src homology 2 domain; N-SH2, N-terminal src homology 2 domain of p85; ptyr, phosphotyrosine.

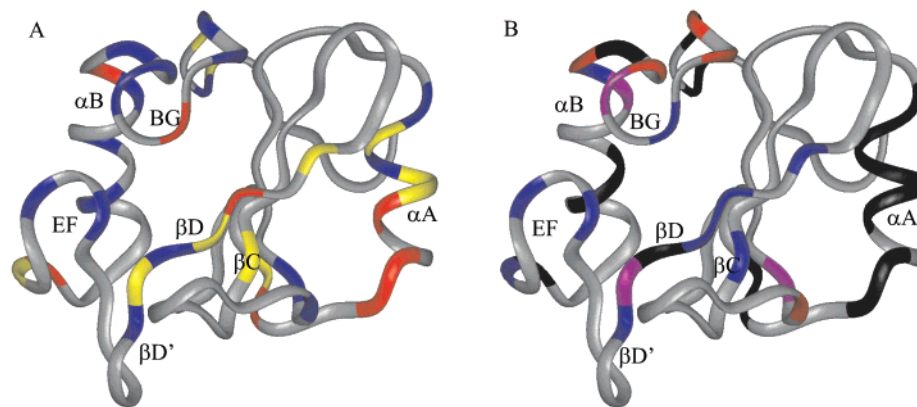


FIGURE 1: Structure of the p85 N-SH2. (A) Colored residues indicate those residues for which line shapes were analyzed from two-dimensional ^{15}N -HSQC spectra. The three colors indicate three regions of lifetimes: $k_{\text{off}} > 1000 \text{ s}^{-1}$ (red), $650 \text{ s}^{-1} < k_{\text{off}} \leq 1000 \text{ s}^{-1}$ (yellow), and $k_{\text{off}} < 650 \text{ s}^{-1}$ (blue). The description of structural elements follows the nomenclature introduced by Eck (68). (B) Colors indicate different types of line shapes for individual residues of the protein. Black is for residues for which line shapes can be described by second-order binding according to $\text{P} + \text{L} \rightleftharpoons \text{PL}$. From blue to violet to red, line shapes show different levels of complexity as described in footnote a of Table 1 [+++ (red), ++ (violet), and + (blue)].

Intracellular trafficking of PI3-K is mediated by the binding of Src homology 2 (SH2) domains. Binding of SH2s to tyrosine-phosphorylated sequences of proteins such as the PDGF receptor (PDGFR) (37–39) or polyoma MT (40) is part of many processes of cell regulation (41–44). In the case of MT, for example, phosphotyrosine residue 315 interacts with the SH2s of the p85 subunit of PI3-K. X-ray diffraction and NMR have established the structure of a number of SH2–tyrosine phosphopeptide complexes (for a review of SH2 structures, see ref 45), including the SH2s of PI3-K (3, 46–50). All SH2s can be described as a central triple antiparallel β -sheet flanked by smaller β -sheets and two α -helices (Figure 1). For most SH2s, the specificity of the interaction with phosphopeptides is determined by the first (+1) and third (+3) residues after the phosphotyrosine (ptyr). In the case of the more N-terminal SH2 of PI3-K (N-SH2), preferred residues at position +1 are M, V, I, and E, while M is the preferred residue at position +3 (51). Different classes of SH2s reveal different patterns of specificity. In some cases, changes in a single amino acid of the protein can alter its specificity. Changing the $\beta\text{D}5$ from I to Y, for example, has been shown to change the specificity of the N-SH2 of PI3-K (52).

The goal of this work has been twofold: to study how SH2s function and to expand the ways NMR analysis can be used to study ligand interactions. We have examined the interactions of tyrosine-phosphorylated peptides matching middle T or PDGF receptor sequences known to bind PI3-K with the N-SH2 of the p85 subunit. Using ^{15}N -labeled protein and ^1H , ^{15}N -HSQC spectra, 37 of 110 amino acids were accessible to differential line broadening analysis. We have compared the behavior of different peptide ligands and mutant SH2s. Qualitative examination of the line shapes shows dramatic differences in the behavior of individual residues. These showed clear evidence for structural rearrangements on a millisecond time scale induced by the binding process. Although such line shapes were too complex to be fully simulated, they provide information about the mechanism of the interaction for individual amino acids. Of particular interest, line shape measurements could be used to distinguish the structural effects of different kinds of mutations. In addition, titration experiments showed that the interactions

of different SH2 residues with the ligand are characterized by different off-rates. This is a form of dynamics measurement that provides information complementary to CPMG measurements (53, 54) that can be used to calculate exchange rates on a microsecond to millisecond time scale.

MATERIALS AND METHODS

The wild-type pGEX3X–GST–N-SH2 construct (amino acids 321–434) and the methods used to produce SH2 for NMR analysis were described previously (55). Binding properties of the mutants P395S and P427L were also reported previously (56). The mutant I381Y (52) was constructed by site-directed mutagenesis using the oligonucleotides 5′-GGGGGAAATAACAAATTATATAAAATATTTCATCGAGAT-3′ and 5′-ATCTCGATGAAATATTTTATATAATTTGTTATTTCCCCC-3′ as previously described (57). ^{15}N -labeled SH2 has been prepared using either rich medium (Celvone U, Martek) or minimal medium prepared with $^{15}\text{NH}_4\text{Cl}$ (Cambridge Isotope Laboratories). Factor Xa (Haematologic Technologies) was used to cleave the SH2 from the fusion protein. The SH2 was further purified by gel chromatography (Superdex 75). The pH of both the SH2 and the ligand solution was adjusted to 6.8 by careful titration with HCl or NaOH. Phosphopeptides were synthesized and HPLC purified by the Tufts Protein Chemistry Facility (55). Peptides that were used were EEEpYMPME-NH₂ from the middle T sequence around the tyrosine phosphorylation site at residue 315 where PI3-K binds and SVDpYVPML-NH₂ from the PDGF receptor sequence at the residue 751 binding site. The purity of peptides was evaluated using MALDI mass spectrometry. The purity of proteins was judged by gel chromatography and the fact that ^1H , ^{15}N -HSQC spectra exhibited a unique set of assigned signals. Concentrations of the protein and peptide were measured by UV absorption at 279 nm [using extinction coefficients of $610 \text{ M}^{-1} \text{ cm}^{-1}$ for ptyr in peptides and $1522 \text{ M}^{-1} \text{ cm}^{-1}$ for tyr in the SH2 (58, 59)]. Concentrated solutions of peptides were made to avoid dilution of the protein upon addition of peptide. The typical volume added in one titration step was 10–15 μL in a total volume of $\sim 250 \mu\text{L}$. After addition of the peptide, the homogeneity of the static magnetic field was readjusted and the tuning of the probe circuit was checked.

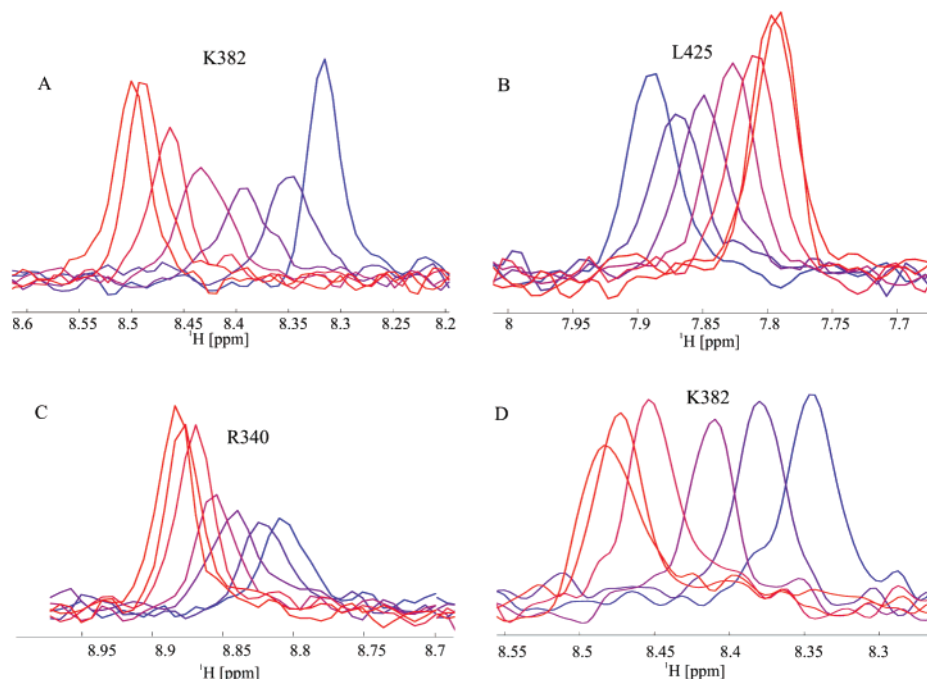


FIGURE 2: Line shapes in the proton dimension of HSQC spectra recorded for a titration of the p85 N-SH2 with EEEpYMPME-NH₂ (MT peptide) (A–C) and phosphotyrosine (D). All titrations proceed from blue (free SH2) to red (SH2 complex).

HSQC spectra were recorded on BRUKER AMX 500 (wild-type SH2) and DMX 500 (SH2 mutants) spectrometers with 2048 data points in the ¹H dimension, and a minimum of 256 increments in the ¹⁵N dimension. Spectra used for line shape analysis in the ¹⁵N dimension were recorded with 700–1024 points in the ¹⁵N dimension. Spectra were processed and line shapes extracted from two-dimensional spectra using NMRLab (60). Gaussian broadening was employed prior to Fourier transformation with LB –5 and GB 0.05 in the incremented dimension and LB –3.0 and GB 0.03 in the recorded dimension.

Line shape calculations were performed as described in ref 7 using software written for MATLAB (The Mathworks). The software was written to calculate the time domain signal for sections of HSQC spectra. Line shapes were fitted assuming second-order binding according to $P + L \rightleftharpoons PL$ using optimization routines available for MATLAB. The accuracy of such simulations depends very much on the rates. For example, in very fast exchange, lines will hardly be broadened and the intensity of lines will hardly be reduced during the titration. For a peak separation of 500 Hz, lines vary little for a k_{off} of $>5000 \text{ s}^{-1}$. For this reason, the rate determined from such line shapes has a large error. A detailed discussion of the error of line shape simulations is found in the Appendix. In this work, we decided to group off-rates in the fast exchange regime into three categories ($k_{\text{off}} > 1000 \text{ s}^{-1}$, $650 \text{ s}^{-1} < k_{\text{off}} \leq 1000 \text{ s}^{-1}$, and $k_{\text{off}} < 650 \text{ s}^{-1}$).

RESULTS

Previous work has identified residues in the p85 N-SH2 that show chemical shift perturbations upon binding of tyrosine-phosphorylated middle T or PDGF receptor peptides (55). These chemical shift changes defined SH2 residues that respond to the binding of the phosphotyrosine (ptyr) or the first residue (+1) or the third residue (+3) C-terminal to the ptyr of the ligand. In binding experiments with a peptide

(EEEpYMPME-NH₂) derived from MT antigen, 51 of 108 SH2 residues showed chemical shift perturbations at least 2–3 times greater than the line width. Because spectral overlap made evaluation of some of these signals impractical, only 37 residues could be analyzed in greater detail. Figure 1A shows a ribbon diagram of the p85 N-SH2 highlighting the 37 residues for which line shapes were studied. All regions of the SH2 are represented, including residues expected to interact with the phosphotyrosine (R340 and R358), with the +1 residue (K379 and I381), and with the +3 residue (I381, F392, and K419) in the ligand peptide as well as residues which are not directly involved in ligand interactions (F384, E345, K346, and L347).

The line shapes of individual residues in the ¹⁵N-HSQC spectra were analyzed by examining cross sections of peaks during titration with ligand. When protein is titrated with ligand, two general types of behavior can be expected for NMR line shapes of signals that have different chemical shifts in the free protein and in the protein complex. In the case of slow exchange on an NMR time scale ($k/\Delta\nu < \pi/\sqrt{2}$), where k is the exchange rate and $\Delta\nu$ the frequency separation of the exchanging signals, the intensities of the two peaks of free and complexed forms will be proportional to the relative amount of free protein and protein complex present in the mixture. No true examples of slow exchange between the free protein and the protein–ligand complex were observed for interactions of the MT peptide with the N-SH2. Complex behavior was observed for E411 because the signal of the free protein showed a minor second component in slow exchange, while only one signal was present in the MT complex (not shown). For fast exchange rates ($k/\Delta\nu > \pi/\sqrt{2}$), a single peak with an intermediate chemical shift is observed at each step in the titration. Examples of this sort of behavior are shown in Figure 2. The intermediate case of coalescence ($k_{\text{coal}}/\Delta\nu = \pi/\sqrt{2}$) will never occur simultaneously for all steps of a titration be-

Table 1: Line Shapes of Signals of the p85 N-SH2 during a Titration with the MT Peptide

amino acid	signal comp ^a	K_{ex}^b	$k_{off} (s^{-1})^d$	amino acid	signal comp ^a	K_{ex}^b	$k_{off} (s^{-1})^d$
W335			950 [-190 + 290]	F392	+	0.9	550 [-60 + 90]
G336		0.8	>2000 ^f	D394	+	0.8	540 [-100 + 170]
S339		0.85	1120 [-220 + 310]	T397	+		950 [-150 + 210] ^e
R340		0.7	>1500 ^f	F398			>2500 ^f
Y343			1900 [-390 + 990]	L404			380 [-120 + 280]
N344		0.85	680 [-110 + 130]	N406		0.88	610 [-210 + 480]
E345			710 [-90 + 120]	R409	++	0.6	260 [-50 + 70]
K346			640 [-90 + 120]	N410	+	0.92	2660 [-410 + 340]
L347			770 [-100 + 140]	E411	+++		-
R348		0.95	250 [-60 + 240]	S412	+++	0.75	600 [-120 + 160] ^e
R358	++		470 ^f	A414	+++	0.65	400 [-60 + 80] ^e
A360	+++		300 ^f	Q415	++	0.85	500 [-60 + 90] ^e
T369	+		980 [-140 + 200]	N417	c		1910 [-660 + 1850]
K379	+		930 [-100 + 120]	K419	+++	0.85	550 [-120 + 150] ^e
I381	+ ^c		1210 [-130 + 170]	D421	+++	0.75	400 [-90 + 140]
K382	+		650 [-90 + 120]	V422		0.75	830 [-180 + 280]
I383			590 [-120 + 200]	L424			480 [-90 + 130]
F384	++		920 [-180 + 260]	L425		0.9	910 [-220 + 380]
H385	+		560 [-80 + 110]				

^a Qualitative classification of line shapes: blank, lines could be simulated assuming a two-state model; +, minor shoulders in one or two lines of the titration; ++, line shapes as described for F384 with shoulders in multiple lines of the titration; +++, significant distortion of lines during the titration with disappearing signals. ^b For K_{ex} , line shapes showed changes in intensity similar to that of R340 that required the consideration of an external equilibrium (7). ^c The line in the first titration step showed a shoulder. A line shape simulation considering this extra feature yields a higher value for k_{off} . ^d Off-rate with error estimation calculated as described in the Appendix in parentheses. ^e Error estimation failed because of the complexity of line shapes. For these lines, off-rates are very uncertain because a two-state mechanism must be questioned. ^f Upper error estimation not possible because the signal is not altered for larger rates.

cause one of the effective rates depends on the ligand concentration (7).

Figure 2A–D shows examples of fast exchange that were observed, where lines (in the ¹H dimension) from a two-dimensional HSQC spectrum are displayed in colors from blue to red for successive steps of the titration. The ribbon diagram of Figure 1B summarizes the residues that showed simple two-state behavior in black. R340 (Figure 2C) represents a variant in this category of signals because the line in the free protein has a significantly smaller intensity than that in the complex. Table 1 lists other residues that showed this type of behavior. Several possible explanations for this behavior have been explored. Relaxation measurements exclude the possibility of an exceptionally high transverse relaxation rate R_2 for this residue (U. Günther, unpublished data). A second possibility is that slow exchange with one or several other conformers that are unable to bind ligand causes the reduced signal intensity of the free state. This is unlikely because CPMG relaxation measurements do not show increased mobility on a millisecond time scale (U. Günther, unpublished results). A plausible explanation would be a reduction in hydrogen exchange rates upon binding. This possibility is generally supported by the observation that most residues for which the intensity of the line in the free state was reduced are located in loop regions which are exposed to the solvent. Also, changes in hydrogen exchange rates have previously been shown for the N-SH2 and interpreted to reflect changes in SH2 stability (61). Hydrogen exchange rates were measured for the free wild-type SH2 and for the SH2 complexed to a MT peptide (Figure 3). Clearly, hydrogen exchange rates are high in loop regions and low in the central parts of the β -sheet. However, the signal of R340 is in fast exchange with the solvent and cannot be detected immediately after addition of D₂O in either the free or the complexed SH2. While none of these results explain the observed changes in signal intensity between the

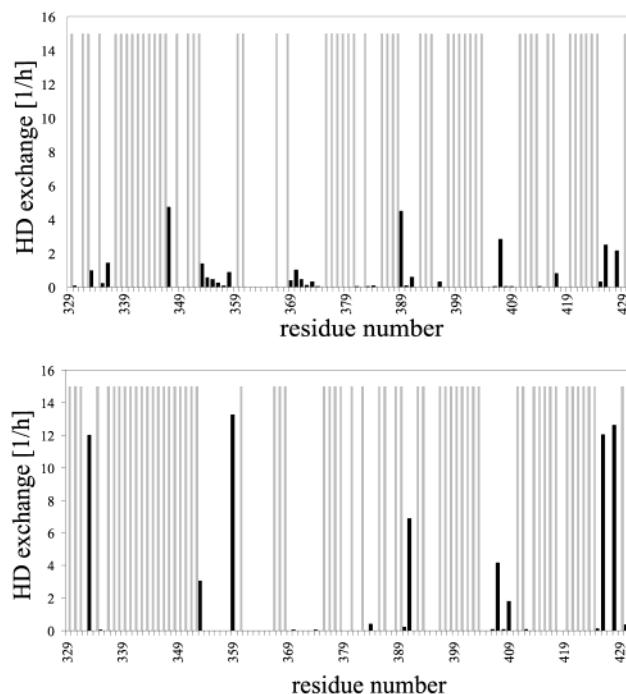


FIGURE 3: Hydrogen exchange rates for the p85 N-SH2 determined by recording HSQC spectra after dissolving the lyophilized protein in D₂O. Free SH2 (top) and SH2 complexed to the MT peptide (bottom). Grey bars indicate residues which exchanged too fast to be observed in D₂O.

free and complexed SH2, we favor the possibility of hydrogen exchange on a faster time scale, not accessible in simple deuterium exchange experiments.

In contrast to residues that showed only a single peak at intermediate chemical shifts during titration, many other residues exhibited more complex line shapes (shown in red on the ribbon diagram of Figure 1B). The most interesting result was the appearance of signal shoulders indicative of multiple long-lived states at some point during the titration

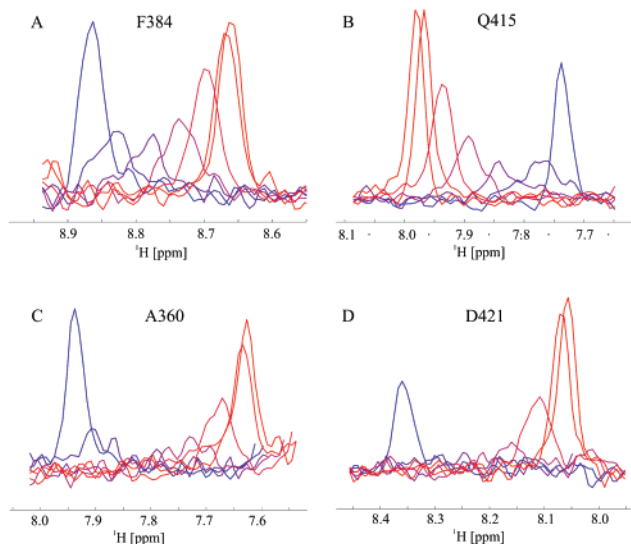


FIGURE 4: Line shapes showing complex behavior for four different residues in a titration of the p85 N-SH2 with the MT peptide. Lines proceed from blue to red for increasing concentrations of the added peptide.

where only a single peak was observed for free or fully complexed SH2. An example of this can already be seen in Figure 2A, where the titration step of K382 (i.e., the third line) showed two minor shoulders.

Figure 4A depicts the striking example of F384, where several titration steps showed signals with two to three shoulders. The shoulders disappeared again in signals toward the end of titration. Q415 (Figure 4B) in the BG loop showed very similar line shapes. Signal component analysis on the FID proves that these signals are periodic in time and thus not noise-related artifacts. An even greater effect was observed for A360 (Figure 4C) and D421 (Figure 4D). Shoulders were clearly observed, for example, in the third and fourth titration steps from the end. In cross sections recorded at an earlier stage of the titration, the heterogeneity induced by ligand binding was so great that the signal was essentially lost. Importantly, none of these residues showed an indication of shoulders in the free SH2. Also, conformational averaging on a slow time scale should also be observed in high R_2/R_1 ratios and in R_2 dispersion determined by CPMG sequences with variable echo times. Neither measurement supports significant millisecond mobility in the free SH2 (U. Günther, unpublished results).

To test whether the effects observed were specific to the middle T ligand, a peptide titration was also carried out for the peptide SVDpYVPML-NH₂, a sequence matching the tyrosine phosphorylation site at residue 751 of the PDGFR receptor. Previous competition experiments showed that this peptide was only slightly lower in affinity than that from MT [$IC_{50} = 13.4$ vs 8.3 mM (55)]. However, peptide selection experiments for the SH2 showed that V is not as favored as M in the +1 position (56). Differences in chemical shift changes upon PDGFR titration changed the subset of residues that could be analyzed. For example, K382 shifted only slightly when the PDGFR peptide was added. Analysis of chemical shift perturbations showed that this peptide had an effect on K379 and L420, two residues which are important for the interaction of the β -sheet and the BG loop. L420, for example, showed a chemical shift in the opposite

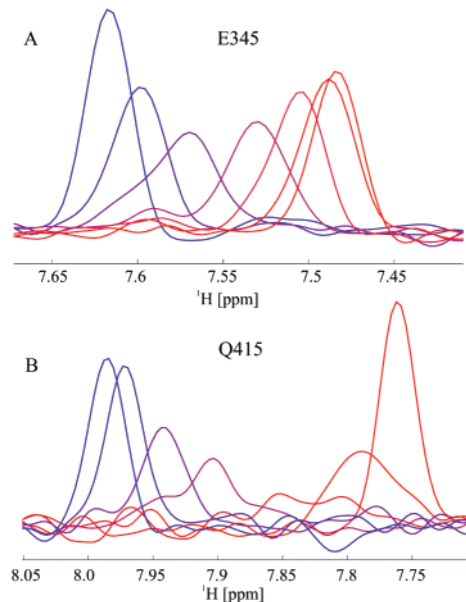


FIGURE 5: Line shapes for the titration of the p85 N-SH2 with the PDGFR peptide (SVDpYVPML-NH₂).

direction when PDGFR peptide was added, but the line shape pattern is the same as for the MT peptide. Despite these differences in the titration, the behavior of the line shapes appeared to be similar. Residues which showed complex behavior for MT also showed complex behavior for PDGFR. Figure 5 shows two examples, E345 and Q415. Line shapes for E345 were close to those expected for two-site exchange. A small shoulder in one titration step suggests that a slow rearrangement may play a role during the titration. The same type of shoulder was also observed for the neighboring residue, K346. Line shapes for Q415 showed complex features similar to those observed for the MT peptide.

Line Shape Analysis Shows Differences among Individual SH2 Residues in Local Off-Rates. Line shapes contain quantitative as well as qualitative information. Protein–ligand interactions characterized by very high off-rates and consequently low affinity show peaks with similar intensities and line widths for different concentrations of ligand in a titration. An example of this type of interaction is shown in Figure 2D for K382 in a titration with ptyr. For the K382–ptyr interaction, very high off-rates were expected for the low affinity of ptyr ($K_D \approx 1$ mM) because $k_{off} = K_D k_{on}$.

High-affinity interactions, such as the interaction of the MT peptide with K382 (Figure 2A), were characterized by line broadening and decreased peak intensities during the titration. Quantitative analysis can be performed on this kind of line shape data using simulated line shapes to estimate k_{off} , the local off-rate, on a residue by residue basis. Line shapes of this type can be simulated assuming a model with second-order binding ($P + L \rightleftharpoons PL$). The mutual effect of line shapes of the two spectral dimensions had to be considered for the calculation because the chemical shifts of both nuclei, ¹H and ¹⁵N, were affected by ligand binding (7). For residues such as R340, the reduced signal intensity of the free state can be handled in line shape simulations by adding an external equilibrium for the free state as described previously (7). This procedure accounts for any type of slow exchange which affects the line shape of the amide ¹⁵N and

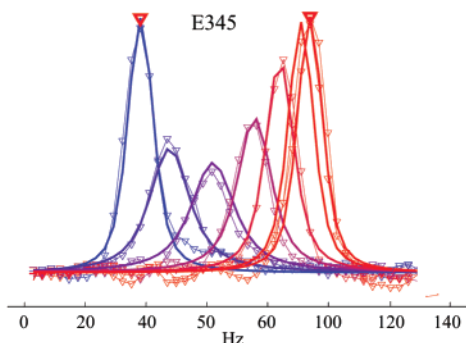


FIGURE 6: Experimental signals (lines with ∇ from blue to red) and simulated line shapes (—) for the E345 residue in a p85 N-SH2–MT titration.

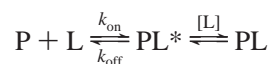
^1H nuclei, including exchange with the solvent or between different conformers. An example of a simulation is shown for the interaction of the MT peptide with E345 (Figure 6). The simulation gave a value of 710 s^{-1} for the off-rate k_{off} . For the MT peptide interaction with K382, a k_{off} of 650 s^{-1} was obtained, consistent with the micromolar affinity of the MT peptide and diffusion-controlled on-rates ($k_{\text{off}}/K_{\text{D}} = 650\text{ s}^{-1}/10^{-6} \approx 10^9\text{ s}^{-1}$). This is equivalent to a lifetime τ_{off} ($=1/k_{\text{off}}$) of $\approx 1.5\text{ ms}$ for the bound state (PL). For the interaction of ptyr with K382, line shape analysis yields a k_{off} value of $>10^4$ (higher rates cannot be distinguished for the chemical shift differences observed for ptyr binding). If diffusion-controlled on-rates are assumed, k_{off} cannot be higher than $K_{\text{D}}k_{\text{on}}$ ($10^{-3} \times 10^9\text{ s}^{-1} = 10^6\text{ s}^{-1}$). The same behavior and similarly high off-rates were observed for all other residues of the SH2 which titrate upon adding ptyr (S339, E345, R358, D359, A360, T369, L370, T371, I381, K382, I383, H385, and F392).

Table 1 lists the results of a line shape analysis for 37 residues titrated with the MT peptide. Lifetimes τ_{off} varied between approximately 0.4 and 4 ms, suggesting that the interaction with the MT peptide is not uniform for all residues of the protein. The line shapes can be roughly classified in three groups: $k_{\text{off}} > 1000\text{ s}^{-1}$, $650\text{ s}^{-1} < k_{\text{off}} \leq 1000\text{ s}^{-1}$, and $k_{\text{off}} < 650\text{ s}^{-1}$. The colors of Figure 1A indicate the calculated off-rates for the 37 residues listed in Table 1. Off-rates of all three categories were observed in different parts of the protein. The differences in off-rates were not connected to ligand interactions in any simple way. Some residues important for ligand binding such as H385 and I383 showed particularly low off-rates (590 and 560 s^{-1}), i.e., long lifetimes of interaction (1.7 and 1.8 ms). Relatively long lifetimes were also observed for residues in the EF loop (F392 and E394). F392 is directly involved in interactions with the peptide. However, D394 is not and points away from the molecule. It seems likely that lifetimes are correlated to concerted rearrangements in the protein. Side chain contacts, for example, between the side chains of F384 and F392, may be important for cross talk between different structural elements of the protein. For one group of adjacent residues, N344, E345, and K346, off-rates were relatively low (640 – 710 s^{-1}), despite the fact that these residues do not play a major role in the interaction with the ligand. Their chemical shift changes must be secondary effects not caused by direct interactions with the ligand. Astonishingly, the off-rate for I381 is $>1000\text{ s}^{-1}$, although this residue is known to interact with the +1 residue of the bound phosphopeptide.

Line Shape Analysis Distinguishes Different Classes of Mutants. Many mutant N-SH2s with differing properties are available for line shape analysis (56). Three, P395S, P427L, and I381Y, were selected to compare to wild type both to understand better the wild-type line shapes and to see how line shape analysis could be used to provide insight into the behavior of the mutants.

I381. The βD5 residue is thought to control specificity at the +1 position. Mutation of βD5 from I381 to Y resulted in a reduced affinity for peptides with a pYMPM sequence and an increased affinity for peptides of the type pYEEI (52). Figure 6 shows representative line shapes for the I381Y mutant, which binds MT with low affinity. The line shapes shown for A360 and for E345 are representative examples of line shapes observed for this mutant which showed typical features for low affinity with very high off-rates. Lines showed no increased line width and therefore no reduced intensity in intermediate signals during the titration. This behavior is the same as that observed for ptyr with wild-type SH2 (Figure 2D). Some reduction in signal intensity in conjunction with some fine structure in line shapes was seen in the first titration step (second spectrum) for A360. However, shoulders in lines were very much reduced, and the amount of reduction of the overall signal intensity is minimal compared to that observed for the wild-type SH2.

P395S, another mutant with altered specificity, is defective in binding MT but is unaffected in its ability to bind the PDGF receptor (56). The mutation is in the EF loop and causes a loss in the ability to select methionine at the +3 position. At the same time, binding experiments established that the mutant prefers valine at +1 whereas the wild type prefers M, V, I, and E, in that order, at the +1 position. This change in selectivity explains why P395S retains the ability to bind PDGFr (pYVPM) while losing affinity for MT (pYMPM). The assignments of P395S and calculated structures will be presented elsewhere (U. Günther, in preparation). Here we show how line shape analysis of titrations with the MT peptide provided insight into the altered behavior of the P395S mutant. With regard to changing the ligand sequence from MT to PDGFr for the wild-type SH2, mutation of the SH2 had some effect on which residues could be subjected to line shape analysis. F392, close to the site of the position 395 mutation, showed a smaller chemical shift perturbation; T397 disappeared completely, and D394 and L396 had relatively weak signals. Titration of P395S with the MT peptide showed striking changes in the nature of the lines from that observed with the wild type. As seen in Figure 8A for I381 in the nitrogen dimension and in Figure 8B for K382 in the proton dimension, the intermediate lines in the titration seemed to “bunch” (black bar) as the titration proceeds. Compared to the behavior of the wild-type SH2, addition of more ligand at intermediate steps for most residues in the titration with the MT peptide results in only a small change in the chemical shift. In Figure 8A, intermediates seemed to be bunched around 124.7 ppm and showed multiple signals in the spectrum of step 7 in the titration at a ^{15}N chemical shift of ~ 124.7 ppm, indicative of a slow exchange process on the reaction pathway:



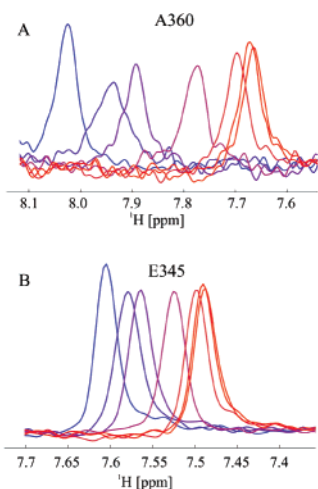


FIGURE 7: Cross sections from HSQC spectra in titrations of the I381Y mutant of the p85 N-SH2 with MT peptide.

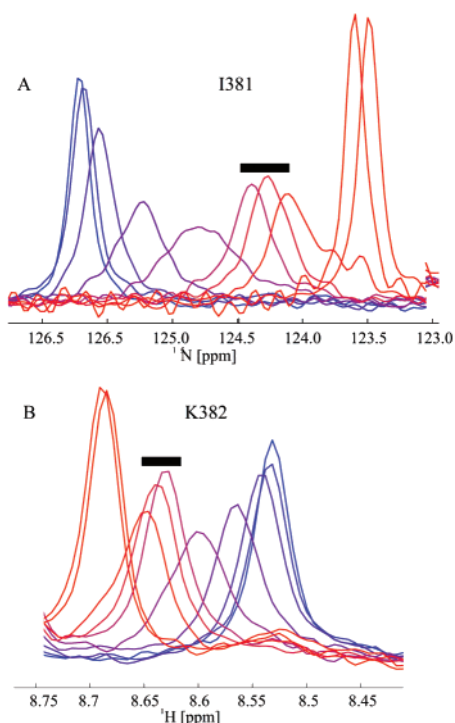


FIGURE 8: Sections from HSQC spectra in a titration of P395S with the MT peptide. Bars indicate signals which are bunched in subsequent spectra of the titration.

The simplest interpretation of this behavior is that the mutant SH2 experiences fast initial binding of L (on a micro-second time scale) associated with chemical shift changes reflecting the PL*/PL ratio followed by a slow conformational rearrangement between PL* and PL. However, the PL*/PL ratio clearly depends on the ligand concentration.

A second feature of the P395S titration was equally striking. Shoulders comparable to those observed for A360 or D421 for the wild-type protein were not observed in the first steps of the titration. This is obviously different than for the wild-type N-SH2 for which multiple shoulders were observed in intermediates in titration with either MT or PDGFr peptides. A reasonable interpretation of this observation is that the intermediates ordinarily seen in the wild type are not induced in the P395S mutant. It seems likely that this failure contributes to the lower affinity.

P427L is a mutant which eliminates binding of either MT or PDGFr (56). It has low affinity for the MT or the PDGFr peptides ($K_D \approx 1$ mM). These results were superficially unexpected because the location of the mutation is in the very end of the SH2, remote from the binding pockets of the SH2. Chemical shifts in HSQC spectra indicated that the mutation causes changes in the N-terminus, in the central β -sheet, in the C-terminal residues of α B, and in BG (Figure 9A). For a large segment in BG, no signals could be identified in either the free protein or the protein–MT complex. This can be ascribed to flexibility in this region of the protein and indicates that the back side contributes stability to the structure.

Figure 10 shows line shapes of P427L for a titration with the MT peptide. For some residues such as R340 (Figure 10A), lines were clearly broadened during the titration despite the low affinity for the peptide. Similar line shapes were observed for other residues in α A (S339 and E345) and in EF (S393 and D394, cyan in Figure 9B). More striking behavior was observed for I381, as shown in HSQC spectra at different stages of a titration with the MT peptide (Figure 10B) and in cross sections in Figure 10C. Cross sections for I381 (Figure 10C) show complex line shapes, a common feature of many residues of P427L. Inspection of line shapes in intermediate spectra during the titration showed that most signals have four to five components. The signal seemed to almost disappear into the background at intermediate stages of the titration. Other residues as shown in red in Figure 9B gave results similar to those for I381. This behavior was completely unexpected for low-affinity binding and was different from the line shapes observed for the low-affinity interaction of ptyr and wild-type SH2.

P427L also showed one additional new feature in its titration. Despite the presence of multiple conformers, most signals move on a straight line in the two-dimensional HSQC spectra with increasing ligand concentrations. However, in P427L we observe at least one signal (F392) where initial chemical shift changes occur in the ^{15}N dimension but the final signal appears with a strong change of both frequencies (0.2 ppm for ^1H and 0.65 ppm for ^{15}N , not shown). The signal seems to move “around a curve” in the two-dimensional HSQC spectrum. This behavior requires multiple long-lived intermediates which are not seen in intermediate spectra during the titration.

DISCUSSION

While structural analysis can elucidate the structure of protein–ligand complexes, understanding the mechanisms by which proteins and ligands interact remains a most challenging problem. Similarly, rationalizing the behavior of mutant forms of proteins is often highly problematic. Here we have used analysis of NMR line shapes to study binding properties of wild-type and mutant SH2s. A major advantage of this approach over other techniques that have been used to study binding kinetics is that differential line broadening using isotope-edited two-dimensional NMR spectra provides kinetic data for different positions in a protein. In addition, the shapes of lines reveal more detailed information about the processes involved in protein–ligand interaction. The N-SH2 of p85 of PI3-K is attractive for these kinds of studies

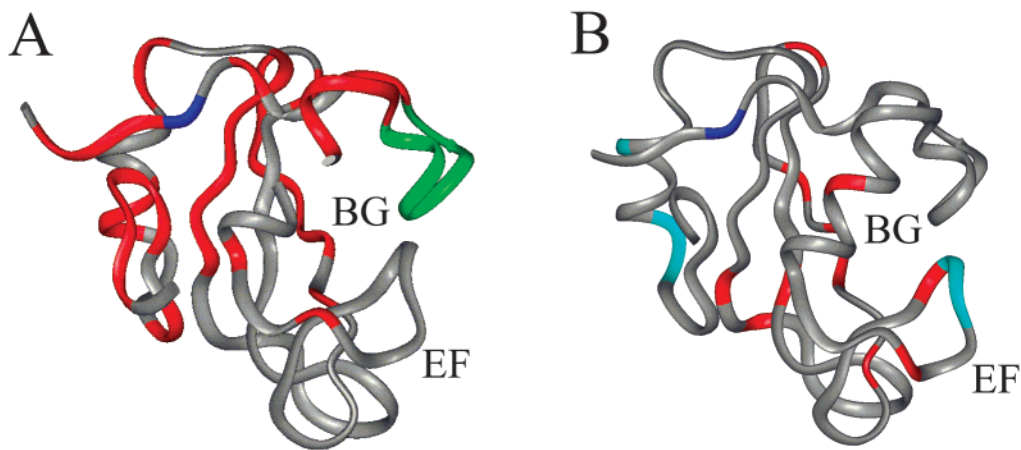


FIGURE 9: Structure of the p85 N-SH2 shown at a 90° angle compared to Figure 1. Colored residues indicate altered chemical shifts in P427L. The mutation site is displayed in blue. (A) Red is for residues for which the chemical shift was altered in P427L compared to that in the wild type. Green is for residues which could not be assigned in the P427L mutant. (B) Types of line shapes for residues which change their chemical shift in the P427L mutant. Red is for signals that exhibit a large number of shoulders in multiple titration steps (e.g., I381). Cyan is for signals showing relatively smooth lines comparable to those of R340 (Figure 10A).

for many reasons. PI3-K is a critical enzyme for cellular signal transduction. Both interesting mutants and ligands are available for studying binding properties. Structural studies using both X-ray and NMR are available for comparison to the results of the line shape analysis. Most importantly, good spectral dispersion permitted analysis of a large number of residues distributed across the surface of the SH2. Essentially all residues that could be titrated showed fast exchange, indicating that off-rates would be on the order of 1000 s^{-1} . Finally, Hensman et al. (3) have studied line broadening for two of these residues (E411 and K379) of a different variant of the p85 N-SH2, pointing to the feasibility of such studies.

Complex Line Shapes. The most striking aspect of the N-SH2 ligand interaction is the existence of multiple species in the intermediate steps of the titration. Heterogeneity induced by ligand binding was observed for many residues across the protein (Figure 1B). This could be seen as shoulders, in the case of F384 or R358, or in the apparent loss of the signal at intermediate steps in the case of A360, Q415, K419, or D421. Most of these residues are located in loop regions or interact with loops through their side chains. For example, the side chain of F384 interacts with F392 in the EF loop. In all, signals for at least 20 of 37 residues exhibited shoulders in intermediate spectra during the titration.

How can the fine structure of intermediate signals in a ligand titration be explained? Somewhat similar effects have been reported previously in one-dimensional spectra for helix-coil transitions of poly- β -benzyl L-aspartate and in ligand binding to RNase or staphylococcal nuclease [see Sykes et al. (4) for a review]. Sample heterogeneity has been suggested as one possible explanation for shoulders in NH and C $^{\alpha}$ peaks in the helix-coil transitions. However, this does not appear to be a likely explanation here. The titrations for the wild-type protein are virtually complete at a 1:1 stoichiometry because of the high affinity. Sequence heterogeneity of the ligand is unlikely because it is not detected via HPLC or MALDI of the peptides and because degradation of the peptide would be expected to lead to peptides with very low affinity (millimolar) and high off-rates.

Alternatively, heterogeneity of the SH2 protein might be possible if, for example, the factor Xa cleavage was not precise. However, this explanation would predict heterogeneity in the starting sample, which was not observed. Also, if this was the reason for peak shapes, effects on many more peaks, not just in loop regions, would be expected. Finally, such heterogeneity would not explain why complexity is different for different residues.

The observation of complex line shapes with multiple shoulders after ligand binding requires one or more conformational intermediates on the reaction pathway. The observation that a ligand can cause conformational equilibria has been made before. Earlier results with RNase (62) and staphylococcal nuclease (63) have suggested conformational equilibria that are affected by ligand binding. That such behavior is observed at some residues and not others suggests that different kinetic mechanisms must be considered for different positions in the SH2. Mutants that exhibited lowered affinity showed changes in this heterogeneity. For example, multiple shoulders were observed for F384 in intermediate spectra in titrations of wild-type SH2 with either MT or PDGFr peptides. However, for the low-affinity mutant P395S or I381Y, shoulders were not observed or their magnitudes significantly reduced in the intermediate steps of titrations. A reasonable interpretation for these observations is that the intermediates ordinarily seen in the wild type are not induced in the mutants. It seems likely that this failure contributes to the lower affinity.

Figure 11 considers some of the possibilities involving multiple conformations for the formation of shoulders in intermediate spectra during a titration. Initially, the idea of either parallel starting conformations (Figure 11A) or parallel intermediates (Figure 11B) might seem attractive. However, parallel starting conformations in slow exchange requires heterogeneity in the free SH2 which was not observed except for E411. The possibility that model 1A is correct but that the concentration of P_1 or P_2 is always too low to be detected can also be ruled out. If $K (=P_i/P)$ is small, the concentration of the binding species P_i will always be low. This will cause line shapes which resemble those observed for slow ex-

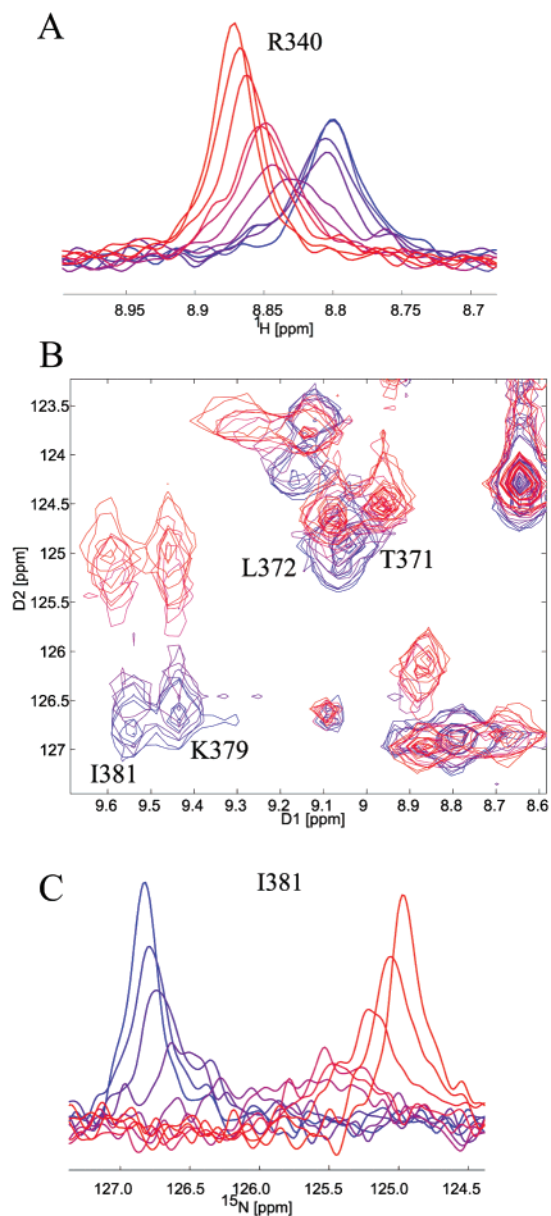
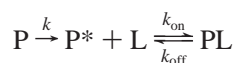


FIGURE 10: (A) Cross sections from HSQC spectra recorded for a titration of the P427L mutant with MT peptide (blue \rightarrow red) for R340. (B) Section from superimposed HSQC spectra for the same titration. (C) Cross sections for I381.

change, as previously shown by the simulation of line shapes for



with only one intermediate (7). This is clearly not the type of line shape observed for residues such as A360, F384, K419, or D421.

An alternative mechanism (Figure 11B) describes a situation where a ligand is bound by P forming different binding products PL_i which are converted into the final product PL. For fast off-rates, peaks will move between the chemical shifts of P and PL_i in the actual binding step. For different species PL_i will convert to PL in a slow step. For this mechanism, the most complex line shapes should occur at the intermediate point where different species PL_i are present. The following conversion of PL_i into PL should

show slow exchange between multiple signals. This is again not what is observed in complex line shapes of the wild-type SH2 binding MT or PDGFr peptides.

Clearly, an additional level of complexity is required to interpret some of the complex line shapes observed in our titrations. One simple possibility is that heterogeneity is induced by an encounter with the ligand (Figure 11C). In this mechanism, the formation of P_i conformations is crucial for high-affinity binding. Although P_0 may still be involved in direct interactions with the ligand (L), binding through P_i will represent major pathways. This amounts to a kind of allosteric model because the formation of binding conformations is induced by initial interaction with ligand. Allosteric effects in a single-domain signaling protein were recently described by Kern et al. by measuring dynamics of exchange between active and inactive conformations for different mutants of the signaling protein NtrC (64).

Such a mechanism explains why line shapes are most complex in the beginning of the titration but show a reduced amount of complexity toward the end where they are dominated by the signal of PL. The initial interaction of the protein and ligand which causes formation of binding conformers P_i must be released during the binding process because the observed stoichiometry is 1:1. In two-dimensional ^{15}N -HSQC spectra, both chemical shifts of intermediates P_i will usually be different from those of P_0 .

Off-Rates. Quantitative calculations indicated that the interactions of individual residues with ligand were characterized by differences in the off-rates (Figure 1A). The distribution of apparent off-rates over the SH2 ranging from approximately 250 to 2500 s^{-1} was clearly not uniform. However, rates are not grouped in distinct regions of the protein. Except for some examples (K382, I383, I385, F392, D394, and T397) where rates of adjacent residues are in a similar range, the role of the rate for an individual residue remains a puzzle. It is, for example, not clear why the off-rate of F398 is more than twice that of its neighbor T397. One possible explanation is that the local off-rate monitored on the backbone NH group represents possible interactions of the side chain (which cause rearrangements of the local geometry, resulting in chemical shift changes). This is a plausible explanation for T397 and F398 because the side chains of the two residues play a completely different role in the protein. T397 is involved in the interaction with the central β -sheet, while F398 points away from the protein.

Detailed interpretation of the differences observed for different residues represents a formidable challenge. It is well-known that line shapes can be used to calculate off-rates for two-state reactions (6). These rates are not necessarily a simple reflection of local contacts between ligand and protein, but rather monitor the response of the protein to the ligand binding. For example, residues such as E345 or K346 that are not directly involved in contacts with the ligand experienced an induced chemical shift change associated with line broadening which reflects the rate of conversion between the fold of the complex and that of the free form. The associated lifetime τ_{off} describes the time the protein spends in the bound state. In this sense, the apparent off-rates must be understood as local dynamics induced by ligand interaction.

The conclusion that the local off-rates represent local dynamics provides a way of reconciling NMR results with

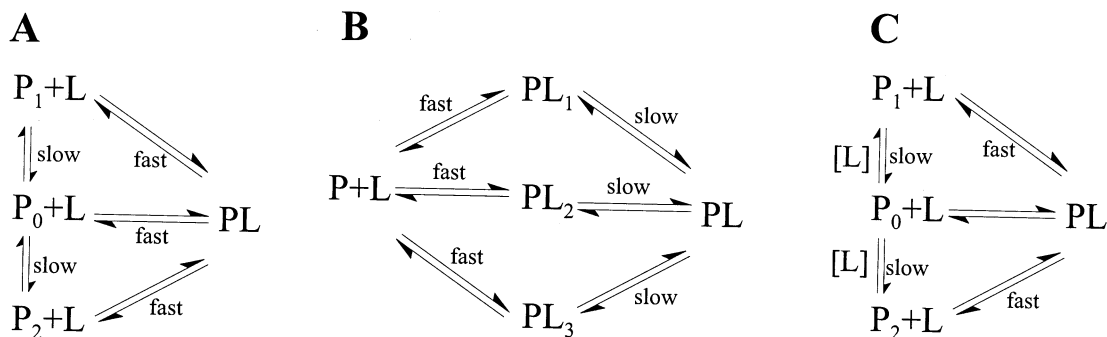


FIGURE 11: Potential mechanisms for SH2 ligand interactions.

those of surface plasmon resonance (SPR) measurements where off-rates of $1.2 \times 10^{-3} \text{ s}^{-1}$ (65) and in a more recent study even 0.6 s^{-1} (66) were reported. Slow rearrangements on a millisecond to second time scale as rate-determining steps for ligand binding may explain this difference because SPR measurements observe the entire process of releasing the peptide. This interpretation is possibly consistent with thermodynamic data of various SH2 constructs which suggested that a conformational change must occur during binding (67). Ladbury et al. assumed that conformational change must be small and limited to loop regions.

From this point of view, relatively high off-rates in the ptyr pocket (red and yellow region in αA in Figure 1A) may be interpreted as fast but low-affinity correlated processes in the ptyr pocket, whereas binding in the ptyr+3 region is characterized by lower off-rates (blue in the EF and BG loop, in βD , and in $\beta D'$). This observation sheds light on the dynamics of the binding process. Most likely, the peptide interacts rapidly with low affinity in the ptyr pocket followed by slower processes in the hydrophobic binding region which are important for high-affinity (lower off-rates).

SH2 Mutants. Each of the mutants studied here exhibited line shapes that could be readily distinguished, not only from those of the wild type but also from each other. The qualitative behavior of the line shapes of wild-type and mutant SH2s clearly showed that altered binding and specificity of mutants must be associated with different types of kinetic mechanisms.

Three different types of behavior were observed. A mutant such as I381Y shows a simple reduction in affinity as shown by higher off-rates. In this regard, it looks much like wild-type SH2 interacting with a poor ligand such as ptyr. There was little change in the qualitative nature of the titrations. Interestingly, the lowered affinity was uniform across the structure, not limited to the region of the mutation.

P427L, a mutant altered in βG near the C-terminus of the SH2, exhibited very different behavior. Here we have observed complex lines with many shoulders all over the protein. Intensities of lines were reduced during the titration. Superficially, these lines resembled line shapes for low off-rates, although the affinity measured by other methods is low. For some residues (e.g., F392), intermediate lines disappeared completely. This reflection of weak binding is quite different from the weak binding of ptyr to the wild-type SH2 or the weak binding of MT to the I381Y mutant where the intensities of the intermediate lines were hardly reduced. Clearly, weak binding in the case of P427L cannot just be ascribed to high off-rates in one-step binding reactions ($P + L \rightleftharpoons PL$, with k_{on} being the forward rate and k_{off} being

the reverse rate). A more complex mechanism involving multiple conformers in intermediate spectra must be involved. One possible explanation may be that off-rates are indeed on the order of $100\text{--}1000 \text{ s}^{-1}$ but on-rates are relatively low. For a K_D of 10^{-3} and a k_{off} of 1000 s^{-1} , the on-rate must be 10^6 , 3 orders of magnitude lower than diffusion-controlled rates. Low on-rates might reflect a low availability of protein conformers suitable for ligand interaction. For example, if in Figure 11C encounter with ligand did not result in formation of suitable species for binding, then the interaction would be poor. Another slightly different interpretation might be nonproductive binding by many conformers in the ensemble. In this case, such nonproductive interactions must be reversed before subsequent interactions with conformers which are more favorable for high-affinity interactions. Such a mechanism would also reduce the apparent on-rate.

Mutation of P395 to S, resulting in lower affinity for the MT peptide, has a different kinetic basis than either the I381Y or P427L mutation. The defect in binding of the MT peptide by the P395S mutant is reflected in the appearance of kinetic intermediates with a distinct chemical shift observed for most residues that serves as a kind of "kinetic knot". In principle, this situation can be described by Figure 11C where P interacts with L to form different intermediates PL_i which convert slowly into the final product. Depending on the ratio of all the rates, intermediates PL_i will build up and the conversion between PL and PL_i will show slow exchange line shapes. This can be interpreted as a kinetic hindrance of binding. A more detailed model along with full structural analysis will be developed elsewhere (U. Günther, manuscript in preparation).

In summary, this work develops an approach to studying the mechanism of protein–ligand interactions using line shape analysis. Line shape analysis is useful to probe processes on a microsecond to millisecond time scale. The range of rates accessible for quantitative analysis is similar to the range of rates which can be analyzed by CPMG measurements. However, line shape analysis has an inherent advantage in that it gives insight into the mechanism underlying an exchange process.

The observed line shapes require that the interactions of the p85 N-SH2 with ligand involve rearrangements during the binding process. Slow kinetic processes in loops or regions adjacent to loops determine the overall rate of the protein–ligand interaction. Since slow exchange in the free SH2 was not observed, we propose a quasi-allosteric model for the interaction with the ligand. The finding that several conformers exist on the binding pathway presents a serious challenge to studies of slow chemical exchange. R_2 dispersion

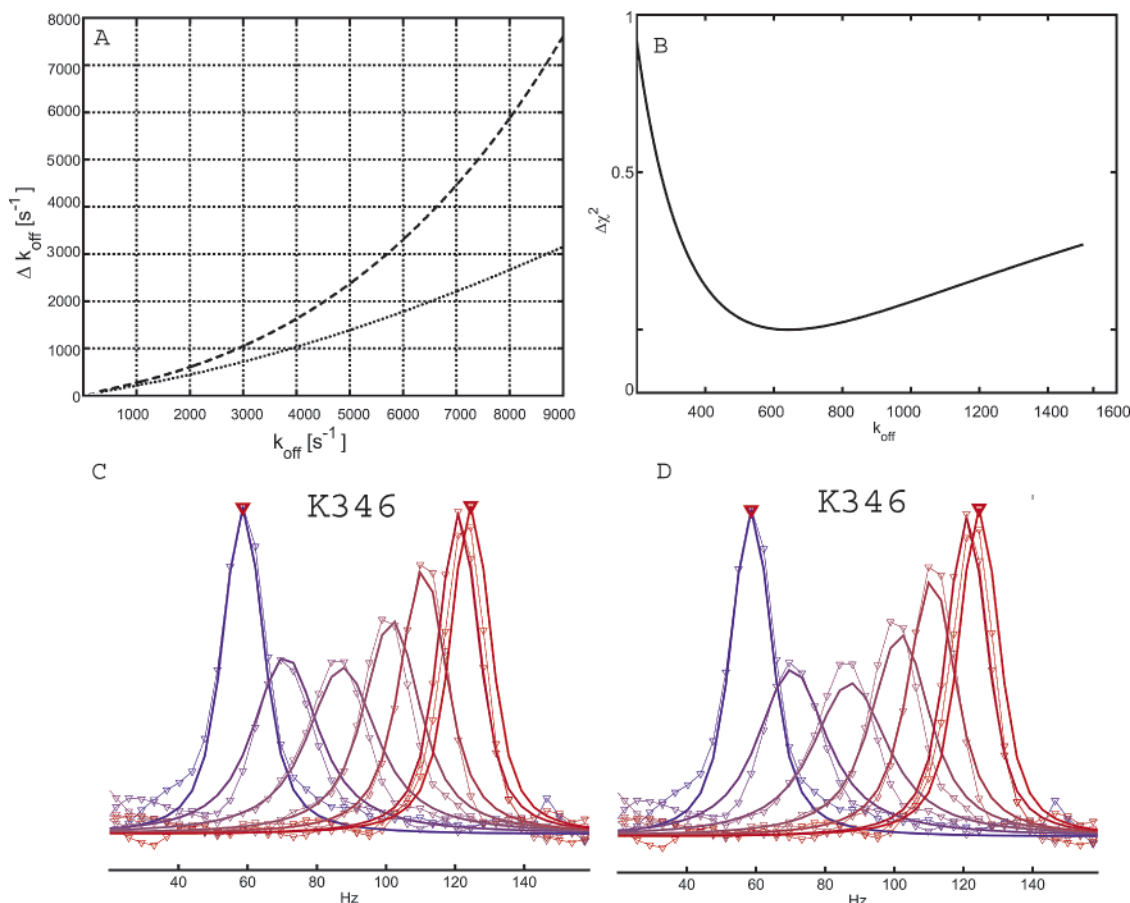


FIGURE 12: (A) Upper and lower error of Δk_{off} for theoretical line shapes simulated for a frequency separation of 150 Hz and a line width of 15 Hz (see the Appendix). (B) $\Delta\chi^2 = \chi_k^2 - \chi_{\text{ref}}^2$ [$\chi_k^2 = \sum(\text{LS}_{\text{sim},k} - \text{LS}_{\text{exp}})^2$ and χ_{ref}^2 is the χ_k^2 for the optimal rate k_{ref}] for K346 calculated as described in the Appendix. (C) Theoretical and simulated line shapes for K346 and a k_{off} of 640 s^{-1} and (D) theoretical and simulated line shapes for K346 and a k_{off} of 550 s^{-1} .

is usually interpreted employing a two-state model. Considering the complexity of mechanisms observed for the p85 N-SH2, such a simplification would clearly not be justified. The study of line shapes in mutants showed that three different mutants with reduced binding affinity revealed completely different line shape patterns reflecting different mechanisms of binding. It will be of considerable interest to see if the complexity of the kinetic mechanism observed here for the N-SH2 is common in the interactions of other proteins with ligands.

APPENDIX

Error Estimation. The error of k_{off} cannot be determined by typically used error estimation protocols, mainly because it is very asymmetric. For high rates, i.e., fast exchange, with little line broadening, curves will be very insensitive to changes in the rate. For lower rates, small changes in rates will cause relatively large changes in line shapes. For the same reason, the upper error is usually larger than the lower error. This is illustrated in Figure 12A which shows a theoretically determined error of k_{off} to higher (dashed line) and to lower (dotted line) off-rates for values of k_{off} between 1 and 8000 s^{-1} . This error was calculated using simulated line shapes for a frequency separation of 150 Hz and an off-rate of 640 s^{-1} . Here the value of χ^2 [$=\sum(\text{LS}_{640} - \text{LS}_k)^2$] for $k = 550 \text{ Hz}$ (χ_{ref}^2) was chosen as an arbitrary standard because the line shapes obtained for this value appeared to be clearly distinct (Figure 12B,C). The calculated error in

k_{off} shown in Figure 12A reflects the change in k_{off} which yields the same χ^2 that was obtained for a k_{off} of 550 s^{-1} . The two curves demonstrate that the upper error increases faster than the lower error. For off-rates around 8000 s^{-1} , the relative error exceeds 100%. These error curves represent the accuracy at which *ideal* line shapes can be simulated for a given set of standard conditions.

Calculation of error estimates for experimental line shapes was based on a similar procedure. One of the underlying problems was the fact that the value of χ^2 [$=\sum(\text{LS}_{\text{exp}} - \text{LS}_{\text{sim},k_{\text{off}}})^2$] depends strongly on artifacts in the spectra. These may include small baseline distortions outside the peak area and signals outside the simulated peaks. Such artifacts do not influence the k for which the minimal χ^2 is observed. However, these χ^2 values obtain almost arbitrary values caused by even small artifacts. They also change significantly depending on the number of experimental data points used in the simulation. For this reason, they do not provide a good error estimate. For this reason, we calculate $\Delta\chi^2 = \chi_k^2 - \chi_{\text{ref}}^2$, where $\chi_k^2 = \sum(\text{LS}_{\text{sim},k} - \text{LS}_{\text{exp}})^2$ and χ_{ref}^2 is the χ^2 for the optimal rate. $\Delta\chi^2$ is very insensitive to the offset and to peaks outside the simulated signals and provides a good relative estimate for the error. As a reference, we use the χ^2 obtained for a k_{off} of 550 s^{-1} for K346. The line shapes for K346 are shown in panels B and C of Figure 12 [$k_{\text{off}} = 640 \text{ s}^{-1}$ (C) and $k_{\text{off}} = 550 \text{ s}^{-1}$ (D)]. The values for upper and lower errors are listed separately in Table 1. It is important to mention that the observed error of experimental lines was

usually very close to the error for theoretical curves without noise. The reason is that the theoretical error is large compared to the influence of noise on peaks in spectra.

ACKNOWLEDGMENT

We thank H. Rüterjans for kindly giving U.G. access to his laboratory.

REFERENCES

- Hoyt, D., Harkins, R., Debanne, M., O'Connor-McCourt, M., and Sykes, B. (1994) *Biochemistry* 33, 15283–15292.
- Balbach, J., Forge, V., Lau, W., Nuland, N., Brew, K., and Dobson, C. (1996) *Science* 274, 1161–1163.
- Hensmann, M., Booker, G. W., Panayotou, G., Boyd, J., Linacre, J., Waterfield, M., and Campbell, I. D. (1994) *Protein Sci.* 3, 1020–1030.
- Sykes, B. D., and Scott, M. D. (1972) *Annu. Rev. Biophys. Bioeng.* 1, 27–50.
- Rao, B. (1989) *Methods Enzymol.* 176, 279–311.
- Sudmeier, J. L., Evelhoch, J. L., and Jonsson, N. (1980) *J. Magn. Reson.* 40, 377–390.
- Günther, U., and Schaffhausen, B. (2002) *J. Biomol. NMR* 22, 201–209.
- Corvera, S., and Czech, M. (1998) *Trends Cell Biol.* 8, 442–446.
- Odorizzi, G., Babst, M., and Emr, S. (2000) *Trends Biochem. Sci.* 25, 229–235.
- Leever, S., Vanhaesebroeck, B., and Waterfield, M. (1999) *Curr. Opin. Cell Biol.* 11, 219–225.
- Rameh, L., and Cantley, L. (1999) *J. Biol. Chem.* 274, 8347–8350.
- Alessi, D., and Downes, C. (1998) *Biochim. Biophys. Acta* 1436, 151–164.
- Fruman, D., Meyers, R., and Cantley, L. (1998) *Annu. Rev. Biochem.* 67, 481–507.
- Shepherd, P., Withers, D., and Siddle, K. (1998) *Biochem. J.* 333, 471–490.
- Hawkins, P., Welch, H., McGregor, A., Eguinoa, A., Gobert, S., Krugmann, S., Anderson, K., Stokoe, D., and Stephens, L. (1997) *Biochem. Soc. Trans.* 25, 1147–1151.
- Cantrell, D. (2001) *J. Cell Sci.* 114, 1439–1445.
- Sotsios, Y., and Ward, S. (2000) *Immunol. Rev.* 177, 217–235.
- Selheim, F., Holmsen, H., and Vassbotn, F. (2000) *Platelets* 11, 69–82.
- Valius, M., and Kazlauskas, A. (1993) *Cell* 72, 779–790.
- Fantl, W. J., Escobedo, J. A., Martin, G. A., Turck, C. W., del Rosario, M., McCormick, F., and Williams, L. T. (1992) *Cell* 69, 413–423.
- Wurmser, A., Gary, J., and Emr, S. (1999) *J. Biol. Chem.* 274, 9129–9132.
- Corvera, S., D'Arrigo, A., and Stenmark, H. (1999) *Curr. Opin. Cell Biol.* 11, 460–465.
- Derman, M. P., Toker, A., Hartwig, J. H., Spokes, K., Falck, J. R., Chen, C. S., Cantley, L. C., and Cantley, L. G. (1997) *J. Biol. Chem.* 272, 6465–6470.
- Wennstrom, S., Hawkins, P., Cooke, F., Hara, K., Yonezawa, K., Kasuga, M., Jackson, T., Claesson-Welsh, L., and Stephens, L. (1994) *Curr. Biol.* 4, 385–393.
- Meili, R., Ellsworth, C., Lee, S., Reddy, T., Ma, H., and Firtel, R. (1999) *EMBO J.* 18, 2092–2105.
- Nolan, R. D., and Lapetina, E. G. (1990) *J. Biol. Chem.* 265, 2441–2445.
- Kucera, G., and Rittenhouse, S. (1990) *J. Biol. Chem.* 265, 5345–5348.
- Traynor-Kaplan, A. E., Thompson, B. L., Harris, A. L., Taylor, P., Omann, G. M., and Sklar, L. A. (1989) *J. Biol. Chem.* 264, 15668–15673.
- Ninomiya, N., Hazeki, K., Fukui, Y., Seya, T., Okada, T., Hazeki, O., and Ui, M. (1994) *J. Biol. Chem.* 269, 22732–22737.
- Kaplan, D., Whitman, M., Schaffhausen, B., Raptis, L., Garcea, R., Pallas, D., Roberts, T., and Cantley, L. (1986) *Proc. Natl. Acad. Sci. U.S.A.* 83, 3624–3628.
- Chang, H., Aoki, M., Fruman, D., Auger, K., Bellacosa, A., Tsichlis, P., Cantley, L., Roberts, T., and Vogt, P. (1997) *Science* 276, 1848–1850.
- Aoki, M., Batista, O., Bellacosa, A., Tsichlis, P., and Vogt, P. (1998) *Proc. Natl. Acad. Sci. U.S.A.* 95, 14950–14955.
- Freund, R., Dawe, C. J., Carroll, J. P., and Benjamin, T. L. (1992) *Am. J. Pathol.* 141, 1409–1425.
- Minshall, C., Arkins, S., Freund, G., and Kelley, K. (1996) *J. Immunol.* 156, 939–947.
- Yao, R., and Cooper, G. M. (1995) *Science* 267, 2003–2006.
- Shaw, L., Rabinovitz, I., Wang, H., Toker, A., and Mercurio, A. (1997) *Cell* 92, 949–960.
- Klippel, A., Escobedo, J. A., Fantl, W. J., and Williams, L. T. (1992) *Mol. Cell. Biol.* 12, 1451–1459.
- McGlade, C., Ellis, C., Reedijk, M., Anderson, D., Mbamalu, G., Reith, A., Panayotou, G., End, P., Bernstein, A., Kazlauskas, A., Waterfield, M., and Pawson, T. (1992) *Mol. Cell. Biol.* 12, 991–997.
- Hu, P., Margolis, B., Skolnik, E. Y., Lammers, R., Ullrich, A., and Schlessinger, J. (1992) *Mol. Cell. Biol.* 12, 981–990.
- Yoakim, M., Hou, W., Liu, Y., Carpenter, C. L., Kapeller, R., and Schaffhausen, B. S. (1992) *J. Virol.* 66, 5485–5491.
- Marengere, L. E., and Pawson, T. (1994) *J. Cell Sci., Suppl.* 18, 97–104.
- Cohen, G., Ren, R., and Baltimore, D. (1995) *Cell* 80, 237–248.
- Schaffhausen, B. (1995) *Biochim. Biophys. Acta* 1242, 61–81.
- Schlessinger, J. (1994) *Curr. Opin. Genet. Dev.* 4, 25–30.
- Kuriyan, J., and Cowburn, D. (1997) *Annu. Rev. Biophys. Biomol. Struct.* 26, 259–288.
- Booker, G. W., Breeze, A. L., Downing, A. K., Panayotou, G., Gout, I., Waterfield, M. D., and Campbell, I. D. (1992) *Nature* 358, 684–687.
- Nolte, R. T., Eck, M. J., Schlessinger, J., Shoelson, S. E., and Harrison, S. C. (1996) *Nat. Struct. Biol.* 3, 364–374.
- Breeze, A., Kara, B., Barratt, D., Anderson, M., Smith, J., Luke, R., Best, J., and Cartledge, S. (1996) *EMBO J.* 15, 3579–3589.
- Siegel, G., Davis, B., Kristensen, S., Sankar, A., Linacre, J., Stein, R., Panayotou, G., Waterfield, M., and Driscoll, P. (1998) *J. Mol. Biol.* 276, 461–478.
- Weber, T., Schaffhausen, B., Liu, Y., and Günther, U. (2000) *Biochemistry* 39, 15860–15869.
- Songyang, Z., Shoelson, S., Chaudhuri, M., Gish, G., Pawson, T., Haser, W., King, F., Roberts, T., and Ratnofsky, S. (1993) *Cell* 72, 767–778.
- Songyang, Z., Gish, G., Mbamalu, G., Pawson, T., and Cantley, L. (1995) *J. Biol. Chem.* 270, 26029–26032.
- Millet, O., Loria, J. P., Kroenke, C. D., Pons, M., and Palmer, A. G., III (2000) *J. Am. Chem. Soc.* 122, 2867–2877.
- Loria, J., Rance, M., and Palmer, A. I. (1999) *J. Biomol. NMR* 15, 151–155.
- Günther, U., Liu, Y., Sanford, D., Bachovchin, W., and Schaffhausen, B. (1996) *Biochemistry* 35, 15570–15581.
- Yoakim, M., Hou, W., Songyang, Z., Liu, Y., Cantley, L., and Schaffhausen, B. (1994) *Mol. Cell. Biol.* 14, 5929–5938.
- Mullane, K., Ratnofsky, M., Culleré, X., and Schaffhausen, B. (1998) *Mol. Cell. Biol.* 18, 7556–7564.
- Zhang, Z., Maclean, D., Thieme-Sefler, A., Roeske, R., and Dixon, J. (1993) *Anal. Biochem.* 211, 7–15.
- Zhao, Z., Zander, N., Malencik, D., Anderson, S., and Fischer, E. (1992) *Anal. Biochem.* 202, 361–366.
- Günther, U., Ludwig, C., and Rüterjans, H. (2000) *J. Magn. Reson.* 145, 101–108.
- Shoelson, S. E., Sivaraja, M., Williams, K. P., Hu, P., Schlessinger, J., and Weiss, M. A. (1993) *EMBO J.* 12, 795–802.
- French, T., and Hammes, G. (1965) *J. Am. Chem. Soc.* 87, 4669–4673.
- Markley, J., and Jardetzky, O. (1970) *J. Mol. Biol.* 50, 223–233.
- Volkman, B., Lipson, D., Wemmer, D., and Kern, D. (2001) *Science* 291, 2429–2433.
- Payne, G., Shoelson, S. E., Gish, G. D., Pawson, T., and Walsh, C. T. (1993) *Proc. Natl. Acad. Sci. U.S.A.* 90, 4902–4906.
- de Mol, N., Plomp, E., Fischer, M., and Ruijtenbeek, R. (2000) *Anal. Biochem.* 279, 61–70.
- O'Brien, R., Rugman, P., Renzoni, D., Layton, M., Handa, R., Hilyard, K., Waterfield, M., Driscoll, P., and Ladbury, J. (2000) *Protein Sci.* 9, 570–579.
- Eck, M. J., Shoelson, S. E., and Harrison, S. C. (1993) *Nature* 362, 87–91.

Tracing Kinetic Intermediates during Ligand Binding

Tanja Mittag,[†] Brian Schaffhausen,[‡] and Ulrich L. Günther^{*†}

Contribution from the J. W. Goethe University, Frankfurt, Center for Biomolecular Magnetic Resonance, Institute of Biophysical Chemistry, Biocenter N230, Marie-Curie-Str. 9, 60439 Frankfurt, Germany, and Department of Biochemistry, Tufts University, School of Medicine, 136 Harrison Avenue, Boston, Massachusetts 02111

Received October 27, 2003; E-mail: Ulrich.Guenther@em.uni-frankfurt.de

Abstract: Specific protein–ligand interactions are central to biological control. Although structure determination provides important insight into these interactions, it does not address dynamic events that occur during binding. While many biophysical techniques can provide a global view of these dynamics, NMR can be used to derive site-specific dynamics at atomic resolution. Here we show how NMR line shapes can be analyzed to identify long-lived kinetic intermediates for individual amino acids on the reaction pathway for a protein–ligand interaction. Different ligands cause different intermediate states. The lifetimes of these states determine the specificity of binding. This novel approach provides a direct, site-specific visualization of the kinetic mechanism of protein–ligand interactions.

Introduction

Enzymology and structural biology have provided insight into the mechanisms of protein function.¹ However, protein interactions are inevitably influenced or controlled by internal protein dynamics that occur on the micro- to millisecond time scale.² The relationship between internal protein dynamics and functions such as catalysis or ligand binding remains poorly characterized. Protein kinetics are often monitored using plasmon resonance and fluorescence methods.^{3–5} While plasmon resonance provides an integrated view of binding kinetics with some information about mechanisms, it lacks the resolution to describe protein behavior at the level of individual residues. Fluorescence methods allow a more detailed view at individual sites of interaction and dynamics on a broad time scale for extremely low concentrations of protein, but detailed molecular interpretation of the results is difficult.

NMR spectroscopy provides several possibilities for measuring dynamics on slow time scales. Recently several groups studied the dynamics of protein ligand interactions on a micro- to millisecond time scale by measuring relaxation dispersion using Carr–Purcell–Meiboom–Gill (CPMG) sequences.^{6,7} The potential of relaxation dispersion experiments has been explored to study site-specific kinetic events in cyclophilin A where the turnover rate could be assigned to an individual amino acid confirming its role for the catalytic function.⁸ Although such

measurements allow a quantitative analysis of localized kinetic rates, the underlying kinetic mechanism remains enigmatic.

Line shape analysis of NMR signals can provide a direct view of the mechanism and the kinetic rates of binding events or exchange processes.^{9–11} Ligand binding and enzymatic catalysis were previously studied by various NMR methods.^{12–15} Line shape analysis of isolated proton signals of the ligand has previously been used to study the catalysis of proline cis/trans isomerization by the isomerase Cyp18.¹⁶ This approach can also be applied to protein signals in two-dimensional (2D) NMR spectra and has been used to study protein folding^{17,18} and more recently to investigate protein–ligand interactions.^{19–21} By the selection of line shapes from 2D spectra of ¹⁵N-labeled proteins, kinetic information was obtained for *individual sites* of the protein.

In this work, we have studied the mechanism of the interactions of the N-terminal src homology 2 domain (N-SH2) of phosphatidylinositol-3-kinase (PI3-K) upon binding of different

[†] J. W. Goethe University.[‡] Tufts University.

- (1) Bruice, T. C.; Benkovic, S. J. *Biochemistry* **2000**, *39*, 6267–74.
- (2) Fersht, A. *Structure and Mechanism in Protein Science. A Guide to Enzyme Catalysis and Protein Folding*, 1st ed.; Freeman: New York, 1999.
- (3) Engelborghs, Y. *Spectrochim. Acta, Part A* **2001**, *57* (11), 2255–2270.
- (4) van Regenmortel, M. H. *Cell. Mol. Life Sci.* **2001**, *58*, 794–800.
- (5) Katsamba, P. S.; Park, S.; Laird-Offringa, I. A. *Methods* **2002**, *26* (2), 95–104.
- (6) Evenäs, J.; Malmendal, A.; Akke, M. *Structure* **2001**, *9*, 185–195.
- (7) Mulder, F. A.; Mittermaier, A.; Hon, B.; Dahlquist, F.; Kay, L. E. *Nat. Struct. Biol.* **2001**, *8*, 932–935.

- (8) Eisenmesser, E.; Bosco, D.; Akke, M.; Kern, D. *Science* **2002**, *295*, 1520–1523.
- (9) Chan, S.; Reeves, L. *J. Am. Chem. Soc.* **1972**, *95*(3), 673.
- (10) Binsch, G. *Dyn. Nucl. Magn. Reson. Spectrosc.* **1975**, 81.
- (11) Rao, B. D. *Methods Enzymol.* **1989**, *176*, 279–311.
- (12) Lacourciere, K. A.; Stivers, J. T.; Marino, J. P. *Biochemistry* **2000**, *39*, 5630–5641.
- (13) Spoerner, M.; Herrmann, C.; Vetter, I. R.; Kalbitzer, H. R.; Wittinghofer, A. *Proc. Natl. Acad. Sci. U.S.A.* **2001**, *98*, 4944–4949.
- (14) Tochtrop, G. P.; Richter, K.; Tang, C.; Toner, J. J.; Covey, D. F.; Cistola, D. P. *Proc. Natl. Acad. Sci. U.S.A.* **2002**, *99*, 1847–1852.
- (15) Volkman, B. F.; Lipson, D.; Wemmer, D. E.; Kern, D. *Science* **2001**, *291*, 2429–33.
- (16) Kern, D.; Kern, G.; Scherer, G.; Fischer, G.; Drakenberg, T. *Biochemistry* **1995**, *34*, 13594–13602.
- (17) Balbach, J.; Steegborn, C.; Schindler, T.; Schmid, F. *J. Mol. Biol.* **1999**, *285*, 829–842.
- (18) Balbach, J.; Forge, V.; Lau, W. S.; Nuland, N. A.; Brew, K.; Dobson, C. M. *Science* **1996**, *274* (5290), 1161–1163.
- (19) Hensmann, M.; Booker, G.; Panayotou, G.; Boyd, J.; Linacre, J.; Waterfield, M.; Campbell, I. *Protein Sci.* **1994**, *3* (7), 1020–30. Jul.
- (20) Günther, U. L.; Schaffhausen, B. *J. Biomol. NMR* **2002**, *22*, 201–209.
- (21) Günther, U.; Mittag, T.; Schaffhausen, B. *Biochemistry* **2002**, *41*, 11658–11669.

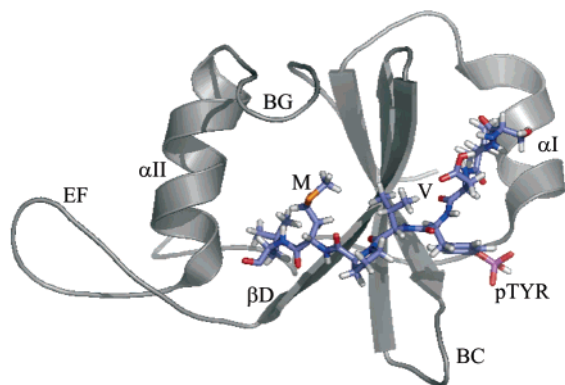


Figure 1. Ribbon diagram of the P395S–PDGFr complex indicating the binding site and the orientation of the bound peptide.²⁸ The ptyr and the positions ptyr + 1 (V) and ptyr + 3 (M) in the ligand are labeled. The annotation of secondary structural elements follows the convention of Eck et al.²⁹

ligands. PI3-K is critical for a broad range of cellular functions including cell growth and survival.^{22,23} The structures of many SH2 domains are known.²⁴ They share common motifs such as a central antiparallel β -sheet flanked by smaller β -sheets and two α -helices. These secondary structural elements are connected by loop regions which are involved in specific ligand interactions. SH2 domains bind phosphotyrosine (ptyr) ligands with ptyr coordinated by two conserved arginines, and they are central to phosphotyrosine signaling pathways.²⁵

The N-SH2 used in this work, P395S, is a mutant of the N-SH2 of PI3-K which appeared in random mutagenesis as a mutant with altered specificity compared to the wild-type N-SH2.²⁶ For this mutant, specificity for the residue immediately C-terminal to the phosphotyrosine (+1) changed from M, V, I, E for wild-type to V, and the specificity for M at +3 seen for wild-type is lost in the mutant.²⁷ As a result, this N-SH2 mutant retains high affinity for the platelet-derived growth factor receptor (PDGFr, PI3-K N-SH2 binding sequence: pYVPM), while having a reduced affinity for the polyomavirus middle T oncoprotein (MT, PI3-K N-SH2 binding sequence: pYMPM). Although the point mutation occurs on a surface loop involved in coordination of the +3 residue, there are differences in structure extending beyond the site of the mutation.²⁸ The binding region of the P395S N-SH2 domain for the peptide derived from PDGFr is depicted in Figure 1. Large parts of the protein are involved in ligand complexation. The ptyr binding pocket is formed by residues in α -helix I, the central β -sheet and the BC loop. The peptide stretches over the β -sheet, where the BG loop is involved in many contacts to the peptide.

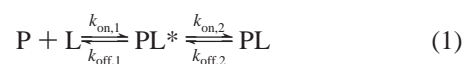
The mechanism of the interactions of the P395S N-SH2 domain with phosphotyrosine-containing ligands has been studied using NMR line shape analysis of two-dimensional ¹⁵N heteronuclear single quantum coherence (HSQC) spectra. We

visualize for the first time *intermediates in ligand binding* for individual amino acids. For different peptide ligands, the lifetime and position of intermediates on the reaction pathway determine the specificity of the interaction. The proposed line shape analysis should be broadly applicable to study protein–ligand interactions of moderately sized proteins.

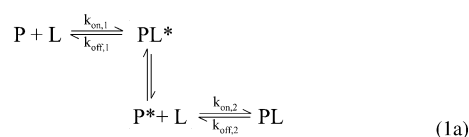
Results and Discussion

In this work, line shape analysis of NMR signals has been used to probe the kinetic behavior of the N-SH2 domain of PI3-kinase upon binding of different phosphotyrosine-containing ligands. Titrations of the P395S N-SH2 mutant for two peptides derived from PDGFr and MT were compared to each other and to titrations of the wild-type N-SH2 domain with the same peptides. The resonances in HSQC spectra of the wild-type N-SH2 recorded for increasing amounts of MT peptide are typical for a simple one-step binding event ($P + L \rightleftharpoons PL$). ¹⁵N cross sections of the signal of S339 (α A1) in the wild-type N-SH2 are depicted in Figure 2a (lines with triangles), where the signal of the free protein is shown in blue. For increasing amounts of peptide, the color changes from blue to red, where red represents the fully complexed protein. Simulations of the line shapes (shown as solid lines) support a one-step binding mechanism.^{20,21}

For P395S, the titration with MT peptide (Figure 2b) showed novel behavior that cannot be explained by one-step binding. As increasing amounts of peptide are added to the free P395S N-SH2 domain (color coding as in Figure 2a), the chemical shifts of the intermediate lines change successively as expected for a binding event that is fast on the NMR time scale. The signals seem to “bunch” between 90 and 100 Hz, and in the eighth step of the titration (at a protein/peptide concentration ratio of 1:0.89), the signal has a large shoulder indicated by an arrow in Figure 2b. This additional complexity in NMR line shapes requires at least one intermediate on the binding pathway that will be denoted PL*. Shifts of the starting signal (blue) are caused by a fast off-rate that averages the signal between the free N-SH2 (P) and the intermediate (PL*) which is generated from the free protein upon association with the ligand (L). The position of the signal between P and PL* reflects changing populations of the two states. The signal shoulder (arrow) indicates slow exchange on an NMR time scale between the intermediate and the final complex (PL, red). These lines were simulated employing the following mechanism:



However, simulations showed that the conversion from PL* to the final product PL also depends on the concentration of the ligand. To account for the 1:1 stoichiometry of the interaction, a more complex mechanism, where L is intermediately released from PL*, must be assumed. The simplest way to summarize this reaction scheme yields a mechanism of the type:



- (22) Fantl, W. J.; Escobedo, J. A.; Martin, G. A.; Turck, C. W.; del Rosario, M.; McCormick, F.; Williams, L. T. *Cell* **1992**, *69* (3), 413–423.
 (23) Valius, M.; Bazenet, C.; Kazlauskas, A. *Mol. Cell. Biol.* **1993**, *13*, 133–143.
 (24) Kuriyan, J.; Cowburn, D. *Annu. Rev. Biophys. Biomol. Struct.* **1997**, *26*, 259–288.
 (25) Cantley, L. C. *Science* **2002**, *296* (5573), 1655–57.
 (26) Yoakim, M.; Hou, W.; Liu, Y.; Carpenter, C. L.; Kapeller, R.; Schaffhausen, B. S. *J. Virol.* **1992**, *66* (9), 5485–5491.
 (27) Songyang, Z.; Shoelson, S.; Chaudhuri, M.; Gish, G.; Pawson, T.; Haser, W.; King, F.; Roberts, T.; Ratnofsky, S. *Cell* **1993**, *72* (5), 767–778.
 (28) Günther, U.; Weyrauch, B.; Zhang, X.; Schaffhausen, B. *Biochemistry* **2003**, *42*, 11120–11127.

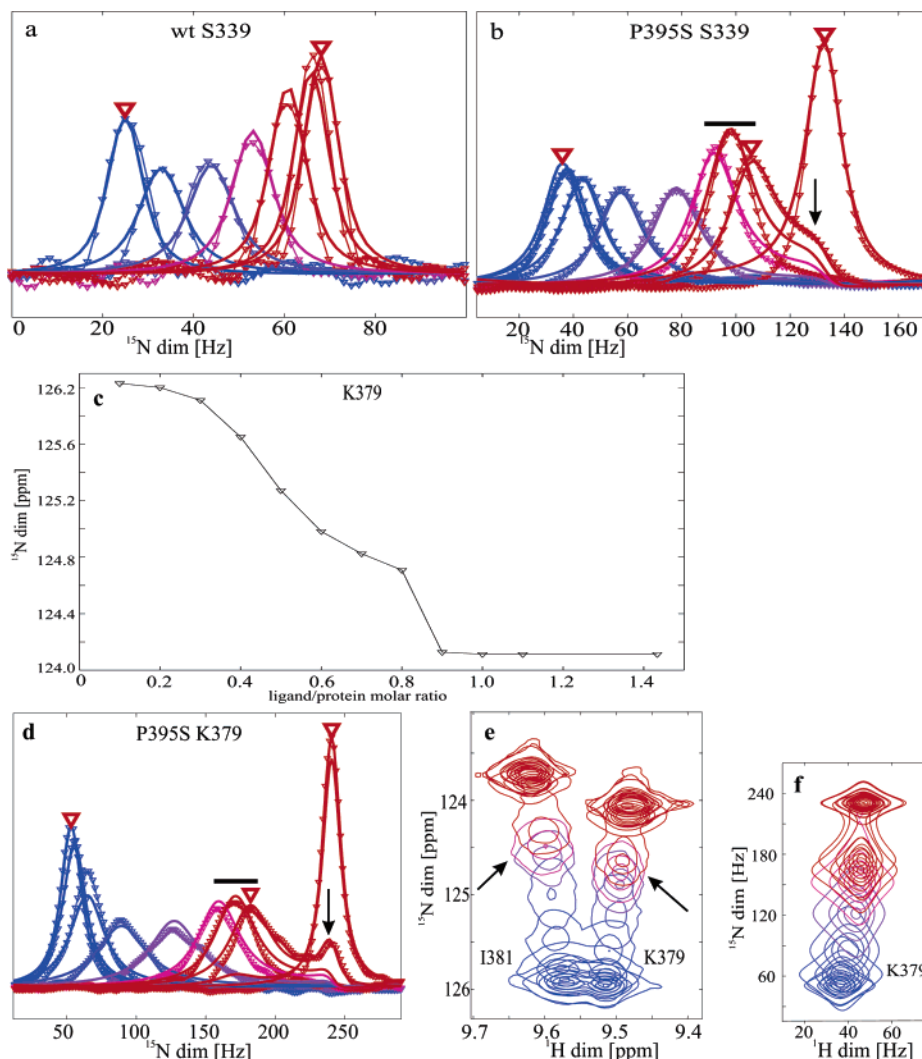


Figure 2. Comparison of line shapes from HSQC spectra of the wild-type N-SH2 with P395S. (a) ^{15}N cross section from two-dimensional HSQC spectra of S339 for subsequent steps of a titration of the wild-type N-SH2 with MT peptide (lines with ∇ from blue to red) and line shapes simulated (solid lines) for a one-step binding model ($\text{P} + \text{L} \rightleftharpoons \text{PL}$). In the same titration for the P395S mutant, “bunching” of signals in ^{15}N slices of (b) S339 and (d) K379 is marked with a solid bar. The simulations are carried out according to the sequential mechanism 1. (c) A binding curve for the ^{15}N dimension of K379 shows intermediate formation at a molar fraction of the ligand of 0.7. (e) Experimental two-dimensional cross peaks of K379 and I381 for sequential steps of a titration show bunching of signals marked with arrows. (f) Simulated two-dimensional signal. Quantitative estimates for the off-rates. P395S S339: $k_{\text{off},1} > 5000 \text{ s}^{-1}$, $k_{\text{off},2} \approx 18[-8 + 8] \text{ s}^{-1}$, $K = k_{\text{on},2}/k_{\text{off},2} \approx 2$. K379: $k_{\text{off},1} \approx 2120[-520 + 820] \text{ s}^{-1}$, $k_{\text{off},2} \approx 26[-10 + 11] \text{ s}^{-1}$, $K = k_{\text{on},2}/k_{\text{off},2} \approx 50$.

The intermediate step in brackets involving a long-lived P^* is not observed in line shapes. Off-rates obtained from NMR line shape simulations represent the reciprocal lifetimes ($\tau = 1/k_{\text{off}}$) of PL^* and PL .

This type of intermediate formation is even more pronounced for residues at the phosphotyrosine + 1 binding site on the central β -sheet such as for residue K379 for which two distinct signals are observed in the eighth titration step (arrow in Figure 2d). Simulations using mechanism 1 provide good fits for both ^{15}N and ^1H cross sections of the signal, and most importantly, the similarity of experimental (Figure 2e) and simulated (Figure 2f) two-dimensional signals validate the model. Quantitative estimates for the off-rates are presented in the caption of Figure 2. In both cases, the off-rate of the second step was more than 1 order of magnitude smaller than the off-rate of the first step.

Intermediate formation upon binding of MT peptide was observed throughout the protein for 24 out of 61 titrating residues labeled magenta on the ribbon diagram in Figure 3a. Residues showing similar kinetics were located in regions of

the protein involved in the ligand interaction including residues in the αB -helix, the EF loop, the central β -sheet, and the ptyr binding pocket (Figure 1). The off-rate of the first step was fast ($500 \text{ s}^{-1} < k_{\text{off},1} < 6000 \text{ s}^{-1}$), while the second step had a low off-rate ($12 \text{ s}^{-1} < k_{\text{off},2} < 35 \text{ s}^{-1}$) and a small equilibrium constant ($2 < K < 50$) favoring the final product PL . The observed variation on off-rates at different sites of the protein represents differences in lifetimes of a particular state in the ligand interaction for individual amino acids.

The large amount of residues which show a two-step kinetic mechanism covers the entire binding region of the binding pocket. Transfer of kinetic events over large parts of the protein is consistent with previous observations which showed that alterations of the peptide in the ptyr + 3 position affects the chemical shifts of the protein resonances in the ptyr pocket. The second binding step must be attributed to a rearrangement which follows ligand binding. The possibility of unspecific interactions at high ligand concentrations suggested by a reviewer can be ruled out because the interaction would be too

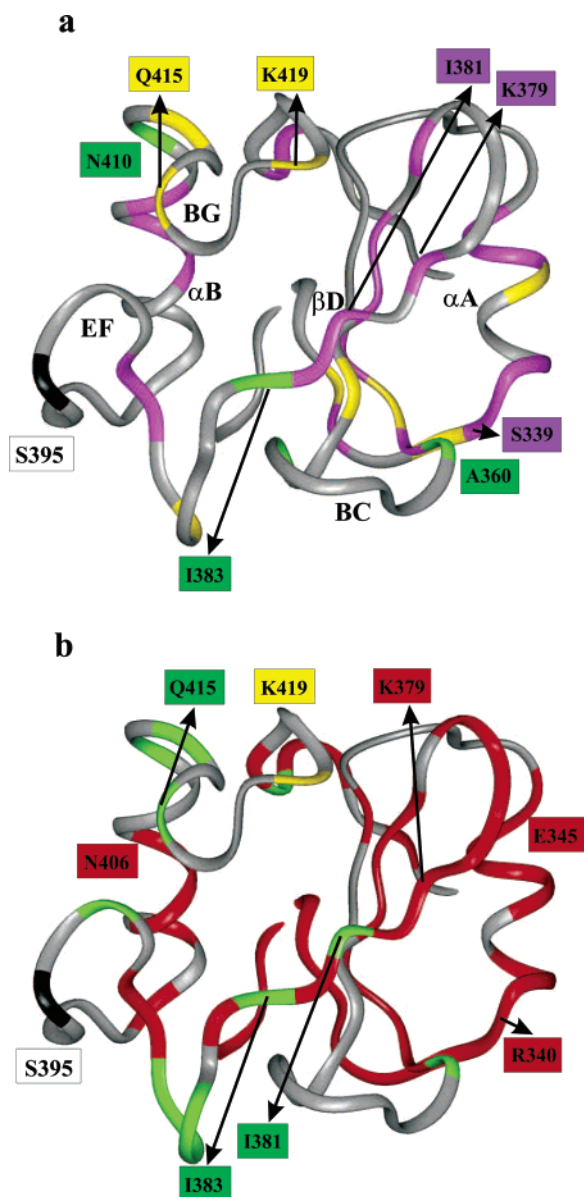


Figure 3. Line shape patterns of residues of the P395S mutant of the p85 N-SH2 domain for titrations with (a) MT peptide and (b) PDGFr peptide mapped onto the structure of the free N-SH2 domain.³⁰ Residues are depicted in different colors according to observed line shape patterns (magenta, model 1a with slow exchange in second step; yellow, model 1a with fast exchange in second step; red, model 2; green, complex line shapes). Key residues mentioned in the text are labeled separately. The mutation site, S395, is shown in black.

weak to cause slow exchange in spectra as observed for many residues (e.g., K379 in Figure 2d). In addition, unspecific binding should be observed after a stoichiometric amount of ligand has been bound to the protein, and unspecific interactions should also be observed for the other ligand and for the wild-type protein.

Ten residues (labeled yellow in Figure 3a) showed different types of line shapes in the titration with MT peptide. The resonances of Q415 represent one example (Figure 4). The concentration of the intermediate is consistently low, and lines shift before and after intermediate formation. As in the first case, it is the interaction with ligand that establishes a binding intermediate. Simulation of two-dimensional line shapes showed that the spectra can be explained by the same sequential model

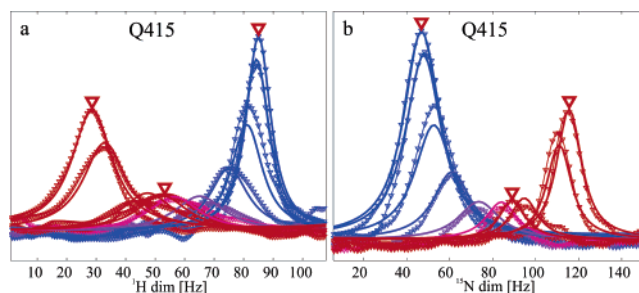
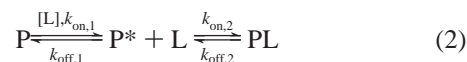


Figure 4. Line shapes from HSQC spectra of the P395S N-SH2 domain in a titration with MT peptide. Cross sections of the (a) ^1H and (b) ^{15}N dimension of signals of Q415 for steps of the titration from blue to red. Experimental lines are shown with ∇ , and simulated signals are shown as solid lines. The simulation of the two-dimensional signal for the sequential reaction 1 yielded the off-rates $k_{\text{off},1} \approx 800 \text{ s}^{-1}$ and $k_{\text{off},2} \approx 600 \text{ s}^{-1}$. The concentration of the intermediate PL* is relatively low. The resonance frequencies of P, PL*, and PL are marked by red triangles.

(eq 1a). However, here the off-rate of the second binding step is much higher causing fast-exchange line shapes for both steps of the reaction ($k_{\text{off},1} \approx 800 \text{ s}^{-1}$ and $k_{\text{off},2} \approx 600 \text{ s}^{-1}$). Essentially, the second binding step requires rearrangements brought about by the first step in a quasi-allosteric fashion. Most of the residues showing this behavior are either in the BG loop or involved in phosphotyrosine coordination including R358, one of the arginines coordinating the ptyr phosphate.

Interaction of the P395S N-SH2 domain with the PDGFr peptide is characterized by a higher affinity and shows very different kinetic properties. Out of 68 titrating residues, 38 show line shapes reflecting a simple one-step binding reaction starting *not* from the signal of the free N-SH2 but rather starting from the second spectrum of the titration series. Line shapes for N406 (Figure 5a and b) show an example of this behavior. The *first step* causes small changes in both dimensions of the spectrum. In the ^1H dimension, the signal in the first spectrum is shifted to lower field with the first addition of ligand (Figure 5a). There is also an increase in intensity. In the ^{15}N dimension of N406, we observe a significantly increased intensity and reduced width of the line with almost no shift in the first titration step in contrast to the following ones. Since only a small volume of 2 μL of peptide dissolved at the same pH and salt concentrations as the protein was added, these effects cannot be caused by dilution, change of salt concentrations, or change in pH.

Instead this behavior of signals requires an intermediate P* which is formed by an initial interaction with ligand L. The subsequent titration starts from the intermediate species P* (labeled with a red ∇ in Figure 5b and c) and shows typical characteristics of a two-site binding between P* and PL. This can be described by a simple mechanism of the form



The line shapes for PDGFr can be well described employing this mechanism. While the first step of this reaction does not necessarily involve specific interactions with the ligand, an encounter with ligand may produce a conformational change or stabilize a conformer of a preexisting equilibrium. This event is necessary for productive binding. The actual role of the ligand in the formation of P* cannot be elucidated from this NMR analysis, but less than 0.1 equiv of PDGFr peptide is required for the conversion while the overall stoichiometry of the

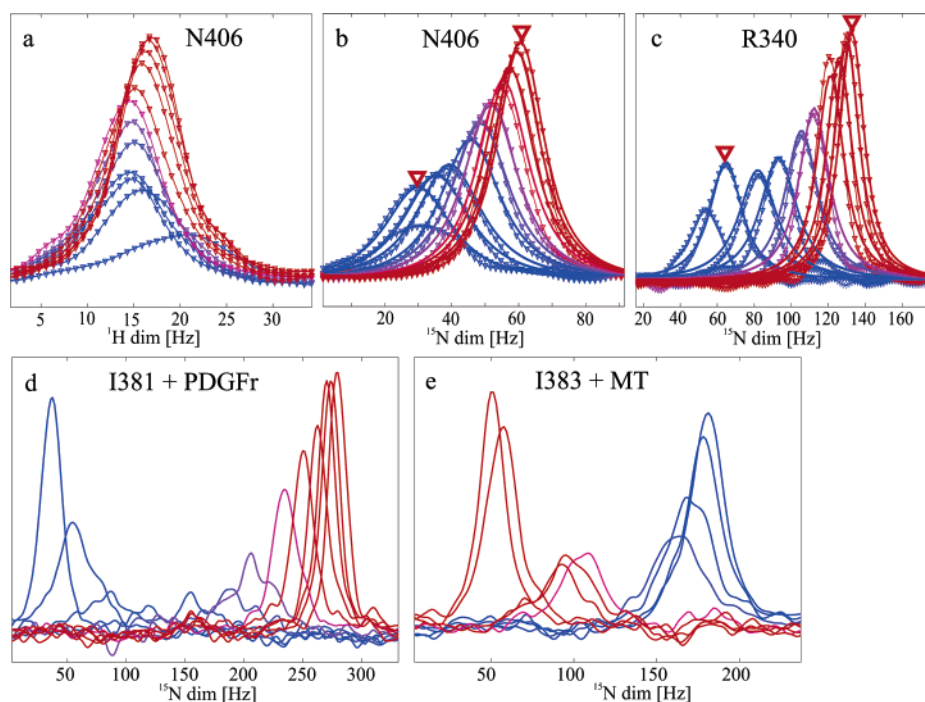


Figure 5. Line shapes from ^1H - ^{15}N HSQC spectra of the P395S N-SH2 domain in titrations with MT and PDGFr peptide. (a–c) P395S N-SH2 interaction with a PDGFr peptide shows rearrangement prior to two-site binding. (a) ^1H and (b) ^{15}N cross sections of N406 in a titration of the P395S N-SH2 with PDGFr peptide. The line shapes can be simulated with a one-step reaction scheme ($\text{P} + \text{L} \rightleftharpoons \text{PL}$) and an off-rate $k_{\text{off}} \approx 1000 \text{ s}^{-1}$ if two-site exchange starts from the second spectrum. (c) In the ^{15}N dimension of R340, the simulation starting from the second spectrum (labeled with a red 5) yields an off-rate of $k_{\text{off},2} \approx 1500 \text{ s}^{-1}$. Experimental lines are shown with ∇ , and simulated signals are shown as solid lines (–) from blue to red for subsequent steps of the titration. (d–e) Complex line shapes indicate the formation of several conformers on the reaction pathway. (d) The ^{15}N cross sections of I381 for subsequent steps of the titration of the P395S N-SH2 with PDGFr peptide exhibit the formation of signal shoulders after addition of ligand. (e) The ^{15}N cross sections of I383 in a titration with MT peptide exhibit several shoulders in intermediate titration steps. Additionally the overall shape of the lines indicate the sequential mechanism 1a.

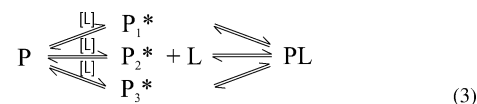
interaction remains 1:1. In this instance, simulations reveal that P^* has a long lifetime and the reverse reaction back to P is unlikely. The off-rate of the second step $k_{\text{off},2}$ is relatively high, as required for fast exchange, and ranges between 200 s^{-1} and 2000 s^{-1} .

Residues showing this type of behavior (labeled red on the ribbon diagram in Figure 3b) were typically located in the α -helices and β -sheets including the arginines R340 (Figure 5c) and R358 which coordinate the phosphotyrosine phosphate. For R340, a distinct first step is observed followed by binding with a relatively high off-rate (1500 s^{-1}) typical for an interaction with relatively low affinity ($K_{\text{D}} = k_{\text{off}}/k_{\text{on}}$). Low off-rates of 320 s^{-1} and 270 s^{-1} indicative of a higher affinity interaction were observed for E345 and K346 in the αA -helix.

An increased intensity after adding PDGFr peptide was observed for many but not for all residues of P395S. The same effect was also observed for the wt N-SH2. The lower intensity of some signals in the free N-SH2 can be attributed to exchange at different time scales. This could be supported by the observation of micro- to millisecond exchange in some positions of the protein³¹ whereas H/D exchange rates did not correlate well with decreased signal intensities. The possibility of concentration-dependent aggregation in the free protein suggested by a reviewer can be ruled out based on line widths of the P395S N-SH2 recorded for different concentrations. The

solution structure of the P395S N-SH2 domain reveals a perturbation of the usual tertiary structure in the small β -sheet and the EF loop, the region around the mutation site.²⁸ The normal fold is partially restored upon ligation. Differences in signal intensities can therefore be attributed to altered exchange properties in the stabilized complex compared to a flexible free protein undergoing conformational exchange.

Even more complex kinetic behavior is observed for some residues. Examples are depicted in Figure 5d and e. Here signals show multiple shoulders corresponding to different long-lived conformers created upon an encounter with ligand. Toward the end of the titration the signal is refocused. Although line shapes are too complex to be simulated, a plausible mechanism is ligand-induced formation of intermediates which can then bind ligand in a parallel reaction scheme. This is shown for the example of three parallel reactions:



Each of these encounters could be of the same type as described by eq 1a or 2.

This kind of line shape was observed for only 4 residues in the MT peptide titration (A360, A366, I383, and N410 shown in green in Figure 3a) and for 10 residues in the titration with PDGFr peptide (A360, G366, I381, I383, S393, N410, S412, Q415, K419, and L424 labeled in green in Figure 3b). Interestingly, I381 showed smooth lines for the titration with

(29) Eck, M. J.; Shoelson, S. E.; Harrison, S. C. *Nature* **1993**, *362*, 87–91.

(30) Weber, T.; Schaffhausen, B.; Liu, Y.; Günther, U. *Biochemistry* **2000**, *39*, 15860–15869.

(31) Mittag, T.; Schaffhausen, B.; Günther, U. L. *Biochemistry* **2003**, *42*, 11128–11136.

MT peptide, similar to those of K379 in Figure 2d and typical for mechanism 1a, but it exhibited complex line shapes in the titration with PDGFr peptide. Signals of A360 and I383 in the titration with MT peptide exhibit the overall shape of lines which can be simulated using mechanism 1. However, the signals of intermediate spectra show shoulders. The signal of A360 also shows complex lines in titrations of the wild-type protein.²¹ For this residue, this behavior may simply reflect a transfer of conformational flexibility from the BC loop. The same effect is also observed in residues in the flexible BG loop which show complex lines (S412, Q415) and reduced intensity (R409, A414).

The results presented here demonstrate the potential of NMR line shape analysis to detect differences in binding mechanisms for different ligands toward the same protein target. There are two major advantages to this approach. One is that, in comparison to methods such as plasmon resonance or fluorescence spectroscopy, a residue specific picture of the binding process is obtained. Almost half of the residues of the N-SH2 could be analyzed individually. Another particular value of this approach is that kinetic rates can be determined by studying steady-state line shapes at different ligand concentrations, although measuring times in NMR spectroscopy are much longer than those lifetimes. In addition, kinetic models both explain the observed spectra and provide quantitative estimations of reaction rates.

The aim of this work was to understand changes in affinity for two different ligands, PDGFr and MT, for the N-terminal SH2 domain of PI3-kinase. Modeling of the two-dimensional NMR signals has provided key insights into the mechanism of the interaction. The high affinity PDGFr peptide ligand induces a stable intermediate N-SH2 on the reaction path to binding. The lower affinity MT peptide generates a different, less stable intermediate. No conformational heterogeneity could be detected in either the free N-SH2 or the final complex.

Line shapes in titrations with the higher affinity PDGFr ligand showed two-site binding after initial rearrangement of the protein or stabilization of a conformer (eq 2). The intermediate formed has a relatively long lifetime (that is a small $k_{\text{off},1}$). For this reason, it must be formed with small concentrations of ligand and there is no direct competition between the two steps of the binding reaction. The intermediate for PDGFr is probably structurally similar to the starting protein because there are only small chemical shift changes between the first spectra. A kinetic hindrance for the conversion from P to the thermodynamically more stable P* must be reduced by addition of ligand.

Line shapes in titrations with the lower affinity MT peptide show the formation of an intermediate with a relatively fast off-rate ($k_{\text{off},1}$), a clear indication that the intermediate lacks stability. Formation of the final product requires a second binding event (see eq 1a). Consequently the first step is an unproductive attempt of a transition to a form which can bind the ligand with high affinity. Since the stoichiometry is 1:1 for the overall interaction, the ligand must be “recycled” for the second binding step. For the MT peptide, a much higher energy barrier must be overcome and the intermediate is not kinetically stabilized. Large chemical shift changes (see intermediates marked in Figure 2) between the intermediate and the free protein suggest significant structural changes.

Additional complexity seen in the line shapes of some residues in the PDGFr titration sheds light on the structural basis

for the observed rearrangements. Residues in β D (I381 and I383) and BG (N410, S412, Q415, and K419) show shoulders in line shapes that cannot occur for two-site binding and that require at least one intermediate each. These signal components reflect the formation of kinetically stable conformers by small amounts of ligand. This must be a concerted rearrangement involving some part of the central β -sheet and the BG loop. This view is supported by the similarity in complexity of line shapes of residues marked green in Figure 3b. Interestingly, these effects can be induced by V but not M in the $\text{tyr} + 1$ position of the ligand. Since formation of intermediates is also seen in these regions in wild-type, they appear to be important for effective binding. The geometry and mobility of the V side chain must be more favorable for inducing these changes.

Conclusions

The mechanism derived here from NMR line shapes of protein signals in ligand titrations describes a novel view of protein–ligand interaction. Despite ongoing efforts to characterize intermediates in protein folding (see ref 32 and references therein), site-specific rearrangements of proteins during ligand binding have only recently been analyzed.²¹

These results demonstrate that specificity in ligand binding is controlled kinetically for the interaction of the N-SH2 mutant P395S with different phosphopeptides. The initial interaction with the higher affinity PDGFr peptide probably induces the formation of an intermediate state which is able to bind ligand with high affinity, whereas an intermediate late on the reaction pathway for binding of MT peptide represents a kinetic hindrance for the conversion to the final product. From initial results of titrations with other proteins, we expect that similar kinetic mechanisms will prove to be common.

Basic limitations of the method are the line width of the resonances in HSQC spectra and chemical shift degeneracy of signals. The kinetic rates must be in the window of fast to intermediate exchange on the NMR time scale. This window can be expanded by the choice of the magnetic field strength. Although the structures of the intermediates are usually not accessible, the visualization of intermediates in spectra provides substantial new information to understand protein–ligand interactions. The existence of these intermediate states may have important practical implications. Sites involved in, or required for, the dynamic changes in ligand binding may represent new targets in the development of therapeutics.

Materials and Methods

Sample Preparation and NMR Spectroscopy. The mutant N-SH2 pGEX3X-GST-N-SH2 construct (amino acids 321 to 434) and the NMR samples were expressed and purified as described previously.^{33,34} ^{15}N -labeled SH2 was prepared using minimal medium with $^{15}\text{NH}_4\text{Cl}$ as a sole source of ^{15}N (Cambridge Isotope Laboratories). Factor Xa (Haematologic Technologies) was used to cleave the N-SH2 from the fusion protein. The N-SH2 was further purified by gel chromatography (Superdex 75) in 0.1 M KCl solution with 0.02% of NaN_3 , pH 6.8. The purity of proteins was judged by gel chromatography and the fact that ^1H – ^{15}N HSQC spectra showed a unique set of assigned signals. Phosphopeptides were synthesized and HPLC purified by the Tufts

(32) Myers, J.; Oas, T. *Annu. Rev. Biochem.* **2002**, *71*, 783–815.

(33) Yoakim, M.; Hou, W.; Songyang, Z.; Liu, Y.; Cantley, L.; Schaffhausen, B. *Mol. Cell. Biol.* **1994**, *14* (9), 5929–5938.

(34) Günther, U.; Liu, Y.; Sanford, D.; Bachovchin, W.; Schaffhausen, B. *Biochemistry* **1996**, *35* (48), 15570–15581.

Protein Chemistry Facility. Their purity was confirmed by NMR spectra and ESI or MALDI mass spectra. Peptides used were EEEpYMPME-NH₂ derived from the known PI3-K binding site of polyomavirus middle T sequence around the tyrosine phosphorylation site at residue 315 (MT peptide) and SVDpYVPML-NH₂ derived from the PDGF receptor sequence at the 751 binding site (PDGFr peptide). The freeze-dried peptides were dissolved in 0.1 M KCl solutions, and the pH was carefully adjusted to 6.8. Concentrations of protein and peptide were measured by UV absorption at 279 nm (using extinction coefficients of 610 L cm⁻¹ mol⁻¹ for ptyr in peptides^{35,36} and an extinction coefficient of 20 735 L cm⁻¹ mol⁻¹ for the N-SH2). The P395S N-SH2 samples had concentrations of 1.0 mM in the titration with MT peptide and 0.5 mM in the case of the titration with the PDGFr peptide. Peptide concentrations were 41 mM for the MT peptide and 12.5 mM for the PDGFr peptide. The typical volume of peptide solution added in one titration step was 1.5 or 2 μL in a total volume of 500 μL. After each addition of peptide, the homogeneity of the static magnetic field was readjusted and the tuning of the probe circuit was checked. The titration was continued until no chemical shift changes were observed in the HSQC spectra, resulting in 9 (MT peptide) and 11 (PDGFr peptide) titration steps. A last addition of one portion of peptide solution confirmed the end of the titration, resulting in a small excess of peptide. ¹H-¹⁵N HSQC spectra were recorded on a BRUKER DMX 500 spectrometer at 303 K with 16 scans and 2048 × 700 points to obtain sufficient spectral resolution for line shape analysis in both dimensions.

Spectra were processed employing qsine window functions, and line shapes were extracted from two-dimensional spectra using NMRLab³⁷ ensuring the careful selection of the slices of the peak maxima. To avoid errors by not selecting the maximum of the signal, sufficient zero filling was used in the line shape simulation process and both dimensions were graphically represented by the simulation program to avoid such errors.

Line Shape Analysis. The details of line shape simulation were reported by Guenther et al.,²⁰ using the software NMRKIN which

calculates the *time domain signal* for sections of HSQC spectra for different kinetic mechanisms assuming steady-state line shapes as described by the equations of Gutowsky and later McConnell.^{38,39} Positions of signals, line widths, populations, and kinetic rates were adjusted iteratively to achieve consistency with experimental data. For the calculations, we assume steady-state conditions wherefore exchange does not have to be simulated during the INEPT transfers. Unlike in the original NMRKIN software, the complete two-dimensional signal is calculated. This is necessary when intermediates appear in cross-peaks of two-dimensional signals. Calculating line shapes in the time domain with subsequent Fourier transformation allowed the use of apodization functions identical to those used for the experimental data. The error of the calculated rates depends on their absolute values.²¹ The kinetic window for which kinetic parameters can be determined precisely from line shapes depends on the chemical shift differences of the species involved in the reaction. The simultaneous simulation of both spectral dimensions improves the quality of the parameter values remarkably because it reduces the degrees of freedom. As reported previously,²¹ the experimental errors of rates are only insignificantly larger than theoretical errors. For off-rate $k_{\text{off},1}$ in the sequential model for K379 in the MT-titration, a theoretical lower error of -520 Hz and an upper error of +820 Hz is obtained, whereas the experimental error is only 2% and 4.3% larger for the lower and upper limit, respectively. We obtain $k_{\text{off},1} = 2120[-530 + 855] \text{ s}^{-1}$. For $k_{\text{off},2} = 26 \text{ s}^{-1}$, the theoretical confidence interval is 17 to 36 s⁻¹, and the experimental confidence interval is 16 to 37 s⁻¹.

Acknowledgment. This work was supported by the European Large Scale Facility Frankfurt and by grants from the NIH to B.S.

Supporting Information Available: Populations of different states as used in the line shape simulations and series of HSQC spectra of the P395S N-SH2 domain in titrations with MT peptide and PDGFr peptide.

JA0392519

- (35) Zhang, Z.; Maclean, D.; Thieme-Sefler, A.; Roeske, R.; Dixon, J. *Anal. Biochem.* **1993**, *211*, 7–15.
(36) Zhao, Z.; Zander, N.; Malencik, D.; Anderson, S.; Fischer, E. *Anal. Biochem.* **1992**, *202*, 361–366.
(37) Günther, U.; Ludwig, C.; Rüterjans, H. *J. Magn. Reson.* **2000**, *145* (2), 201–208.

- (38) Gutowsky, H.; McCall, D.; Slichter, C. *J. Chem. Phys.* **1953**, *21* (2), 279–292.
(39) McConnell, H. M. *J. Chem. Phys.* **1958**, *28*, 430–431.

Novel Insights into the Mechanism of Retinol Binding by Cellular Retinol-Binding Protein

Tanja MITTAG¹, Lorella FRANZONI², Davide CAVAZZINI³,
Gian Luigi ROSSI³ and Ulrich L. GÜNTHER¹

¹*Center for Biomolecular Magnetic Resonance (BMRZ), J.W. Goethe University of Frankfurt, Biocentre N230, Marie-Curie-Str. 9, 60439 Frankfurt, Germany*

²*Department of Experimental Medicine, University of Parma, Via Volturno, 39, 43100 Parma, Italy*

³*Department of Biochemistry and Molecular Biology, University of Parma, Parco Area delle Scienze, 23/A, 43100 Parma, Italy*

Abstract. Protein dynamics on a milli- to microsecond time scale can be characterized by Nuclear Magnetic Resonance techniques, such as Carr-Purcell-Meiboom-Gill experiments and line shape analysis. These approaches were used to gain insight into the mechanism of ligand binding by cellular retinol-binding protein type I, the most widely distributed cytoplasmic carrier of vitamin A. The protein structure comprises a ten-stranded β -barrel and two α -helices enclosing a cavity, fully shielded from the outside medium, both in the presence and in the absence of ligand. Although a comparison of the structures of the apo- and holo-form of this carrier protein could explain the high affinity for vitamin A, the binding mechanism was unknown. Carr-Purcell-Meiboom-Gill experiments revealed extensive conformational mobility in some regions of the apo-protein, particularly in the putative portal region. Line shape analysis gave a novel view of the complexity of the kinetic mechanism of vitamin A binding which involves several steps with vastly different rates.

1 Introduction

Intracellular traffic and metabolic utilization of hydrophobic molecules are mediated by specific carriers, small monomeric proteins of approximately 15.5 kDa. The structural motif common to all intracellular lipid-binding proteins (iLBPs) is a β -barrel, defined by two orthogonal β -sheets, each one containing five anti-parallel β -strands (A to E and F to J), and two short α -helices [1]. The iLBP superfamily encompasses the fatty acid-binding proteins (FABPs) and the carriers of the alcoholic (retinol) and acidic forms of vitamin A, the cellular retinol-binding proteins (CRBPs) and the cellular retinoic acid-binding proteins (CRABPs) [2].

The most widely distributed intracellular carrier of retinol is CRBP type I, which plays a role in the storage of retinol as retinyl-esters, as well as in its mobilization, transport and release to membrane-bound enzymes for metabolic conversion to retinaldehyde, the immediate

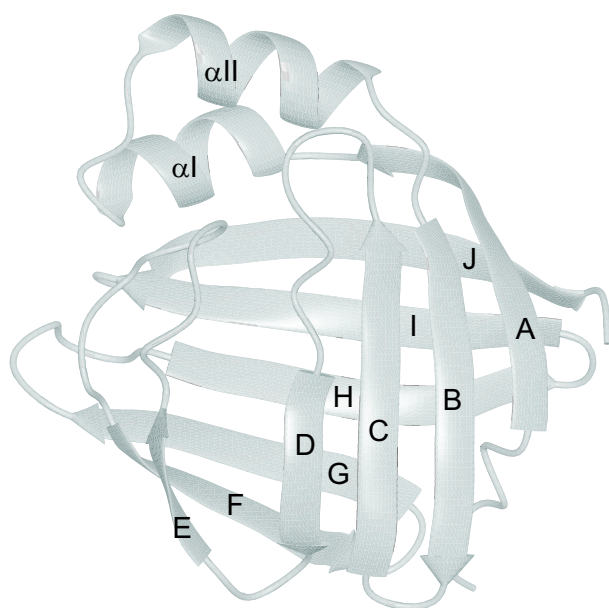


Figure 1: Ribbon diagram of apo-CRBP [7] depicting the β -barrel topology formed by ten antiparallel β -strands (A-J) and a short helix (α I)-turn-helix (α II) motif between β A and β B.

precursor of retinoic acid [3]. The latter metabolite represents the active form of vitamin A involved in cell growth, cell differentiation and morphogenesis [4].

The three-dimensional structure of CRBP, with all-*trans* retinol bound in a deeply buried cavity which appears to be fully shielded from the outside solvent, was determined by X-ray crystallography [5]. Although this structure explained the high stability of the complex ($K_D \sim 0.1$ nM in neutral aqueous solution [6]), it did not provide any information on the mechanism of ligand access to the binding site or the mechanism of ligand release. Information on conformational differences between apo and holo-CRBP was only available after the apo-CRBP structure was determined by NMR spectroscopy [7]. However, not only was the solution structure of the ligand-bound protein (holo-CRBP) very similar to the crystal structure, but also the apo-form structure depicted in Figure 1 was nearly the same. The main difference between the structure ensembles of the apo- and holo-forms was a higher backbone disorder of some segments in the ligand-free protein, including α -helix II, the subsequent linker to β -strand B and the β C- β D and β E- β F turns. This region had previously been identified as a potential portal for ligand access to its binding cavity based on the presence of a small opening in the surface of intestinal fatty acid-binding protein (I-FABP) [8] and the structures of the oleate:adipocyte lipid-binding protein and oleate:liver fatty acid-binding protein complexes which showed that one end of the bound lipid protrudes into the surrounding solvent [9, 10].

Protein function often requires transitions from the ground state to higher energy conformational states. Therefore studying the dynamics of these transitions helps to understand biological functions such as binding of ligands and enzymatic catalysis. NMR techniques provide insight into the dynamic properties of proteins at atomic resolution over a wide range of time scales. Heteronuclear spin relaxation is commonly used to probe dynamics in the picosecond to nanosecond (ps-ns) time regime. It provides information about the overall tumbling of the molecule characterized by the correlation time τ_c and faster intramolecular motion [11].

In the case of CRBP, internal backbone dynamics, obtained from ^{15}N relaxation data (longitudinal relaxation time T_1 , transverse relaxation time T_2 , and heteronuclear nuclear Over-

hauser effect) at two different fields, showed several residues with higher (ps-ns) mobility in the apo-protein with respect to the holo-protein [7] and confirmed the possible involvement of the β C- β D and β E- β F turns in a dynamic mechanism of retinol uptake. However, this observation was not sufficient to explain ligand exchange between the solvent shielded cavity and the sites of retinol uptake and release [7].

Kinetics of internal rearrangements which are important for protein function often occur on a μ s-ms time scale. Ligand interactions may cause either conformational changes or changes of the magnetic environment on this time scale. Usually such slow processes involve concerted motions including more than one residue. NMR provides several methods to study μ s-ms dynamics. Carr-Purcell-Meiboom-Gill (CPMG) experiments [12–16], rotating frame $T_{1\rho}$ relaxation measurements [16–20] and off-resonance ROESY experiments [21] are sensitive to molecular motions or chemical processes on this time scale. Another well-established technique for investigation of μ s-ms time scale kinetic processes is the line shape analysis of NMR signals [22–26]. This has recently been used to obtain valuable information about kinetic mechanisms of interactions in SH2 ligand binding [27] which are not easily available from relaxation dispersion analysis.

1.1 Chemical exchange

The effect of dynamics on a slow time scale will be described by looking at chemical exchange phenomena. Chemical exchange includes conformational exchange and chemical reactions which alter the magnetic environment and therefore the associated chemical shift of nuclear spins. Dynamic processes with reaction rates on a μ s-ms time scale that occur within the course of a single free induction decay (FID) affect the line shape of the corresponding signal (see [22–25] for reviews).

The effect of chemical exchange on the NMR resonance depends on the populations of exchanging partners, exchange rates and chemical shift differences between exchanging partners. This can easily be shown for two-site exchange between two partners A and B:



k_1 and k_{-1} are forward and reverse reaction rate constants. A combined exchange rate

$$k_{\text{ex}} = k_1 + k_{-1} = k_1/p_B = k_{-1}/p_A \quad (2)$$

can be defined. Here p_A and p_B are the equilibrium populations of spins A and B ($p_A + p_B = 1$). Simulated spectra for two-site exchange with unequal populations $p_A = 0.75$ and $p_B = 0.25$ are shown in Figure 2. In the absence of exchange between A and B the spectrum shows two separate signals with resonance frequencies Ω_A and Ω_B , and the linewidths of the resonances are characterized by the transverse relaxation rate constants R_{2A}^0 and R_{2B}^0 ($LW=R_2/\pi$).

In slow exchange, signals remain separated and the line width depends on R_2 and the exchange rates. For increasing exchange rates, lines are broadened until they coalesce at $2(p_A p_B)^{1/2} k_{\text{ex}} \approx \Delta\omega$. For fast exchange at increasing ratios of $k_{\text{ex}}/\Delta\omega$, a single line at the population weighted resonance frequency $\Omega_{\text{ex}} = \Omega_A p_A + \Omega_B p_B$ is observed with successively reduced line width.

The relative values of k_{ex} and $\Delta\omega$ determine whether the exchange is referred to as *fast* or *slow* on the NMR time scale:

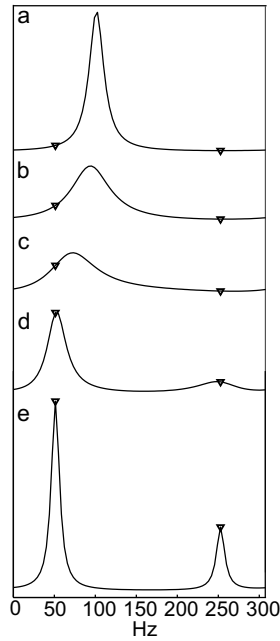


Figure 2: Line shapes of a two-site exchanging system for different exchange rates k_{ex} with unequal populations $p_A = 0.75$ and $p_B = 0.25$. Frequencies of exchanging sites are labeled with '▽'. The frequency difference $\Delta\omega$ is 200 Hz. k_{ex} was set to (a) 10000 Hz, (b) 2000 Hz, (c) 1000 Hz, (d) 200 Hz, (e) 0 Hz.

$$\begin{aligned}
 k_{\text{ex}} \ll \Delta\omega &\rightarrow \text{slow exchange} \\
 k_{\text{ex}} \approx \Delta\omega &\rightarrow \text{intermediate exchange} \\
 k_{\text{ex}} \gg \Delta\omega &\rightarrow \text{fast exchange.}
 \end{aligned}$$

To determine these exchange parameters two methods are commonly used. Relaxation dispersion extracts the exchange contribution from the transverse relaxation rate and allows the analysis of μs -ms exchange. Line shape analysis can also be used to study exchange phenomena and provides a direct view of the mechanism of exchange.

1.2 Relaxation dispersion

The time dependence of the chemical exchange causes an accelerated dephasing of the transverse coherence of the spin reflected in an increased relaxation rate R_2 . The effective relaxation rate R_2 is the sum of the relaxation rate in the absence of exchange, R_2^0 , and the exchange contribution R_{ex} ($R_2 = R_2^0 + R_{\text{ex}}$). The exchange contribution R_{ex} can be separated from R_2^0 because chemical exchange can be refocused by reversing the precession direction of the spins using spin echoes. The most common technique used to refocus chemical exchange is called CPMG, named after its inventors Carr, Purcell, Meiboom and Gill [12, 13]. Refocusing the effect of chemical exchange by a CPMG pulse train has an upper and a lower frequency limit. The lower limit to slow frequencies is determined by the transverse relaxation rate R_2^0 . The fast frequency limit is determined by the smallest possible interval between refocusing pulses and by the length of these pulses. The limits are typically between 2000 s^{-1} and 50 s^{-1} . Faster frequencies are amenable to rotating frame relaxation.

The dependence of R_2 on the refocusing frequency ν_{cp} in CPMG experiments, or the strength of the applied radiofrequency (rf) field in $T_{1\rho}$ experiments, is often called *relaxation dispersion* and allows the quantification of the exchange process. Relaxation dispersion de-

depends on the exchange rate k_{ex} between partners, the populations of the two partners and their chemical shift difference $\Delta\omega$ (because $\Delta\omega$ also determines the dephasing speed).

Solving the modified Bloch or McConnell equations, a general expression for the phenomenological transverse relaxation rate constant in the case of two-site exchange can be obtained [28–31]:

$$R_2(1/\tau_{cp}) = 1/2 \left(R_{2A}^0 + R_{2B}^0 + k_{\text{ex}} - \frac{1}{2\tau_{cp}} \cosh^{-1} [D_+ \cosh(\eta_+) - D_- \cos(\eta_-)] \right) \quad (3)$$

with

$$D_{\pm} = \frac{1}{2} \left[\pm 1 + \frac{\Psi + 2\Delta\omega^2}{(\Psi^2 + \zeta^2)^{1/2}} \right],$$

$$\eta_{\pm} = \sqrt{2}\tau_{cp} \left[\pm \Psi + (\Psi^2 + \zeta^2)^{1/2} \right]^{1/2},$$

$$\Psi = (R_{2A}^0 - R_{2B}^0 - p_A k_{\text{ex}} + p_B k_{\text{ex}})^2 - \Delta\omega^2 + 4p_A p_B k_{\text{ex}}^2,$$

$$\zeta = 2\Delta\omega (R_{2A}^0 - R_{2B}^0 - p_A k_{\text{ex}} + p_B k_{\text{ex}}).$$

The refocusing field is related to the delay $2\tau_{cp}$ between two 180° pulses in the CPMG pulse train according to $\nu_{cp} = \frac{1}{4\tau_{cp}}$. R_{2A}^0 and R_{2B}^0 are the transverse relaxation rate constants of sites A and B in the absence of exchange, respectively. Simplified equations can be derived in the fast-exchange limit or for special conditions such as very unbalanced populations [28, 32].

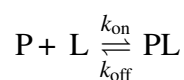
Eq. 3 can be used to simulate relaxation dispersion curves. Examples are depicted in Figure 3 where curves which plot the effective R_2 against the refocusing rate ν_{cp} are shown. These curves demonstrate the limits of this technique: curves for k_{ex} of 0.1 Hz and 10000 Hz are virtually flat and exhibit hardly any dependence on the exchange rate. The high exchange rate of 10000 Hz is only reflected in a higher effective R_2 although R_2^0 was set to 10 s^{-1} in all cases. Exchange parameters are obtained by fitting experimental data to equation 3.

The exchange contribution R_{ex} to the effective relaxation rate R_2 is obtained from the difference of the transverse relaxation rate constants in the absence and presence of a high refocusing field, $R_{\text{ex}} = R_2(\nu_{cp} \rightarrow 0) - R_2(\nu_{cp} \rightarrow \infty)$. The dependence of R_{ex} on the static magnetic field strength B_0 is described by

$$\alpha = \left(\frac{B_{02} + B_{01}}{B_{02} - B_{01}} \right) \left(\frac{R_{\text{ex}2} - R_{\text{ex}1}}{R_{\text{ex}2} + R_{\text{ex}1}} \right) \quad (4)$$

Here $R_{\text{ex}1}$ and $R_{\text{ex}2}$ are the exchange contributions to R_2 at two different static magnetic field strengths B_{01} and B_{02} , respectively. α gives an estimate of the time regime of an exchange process. The value of α is in the range of 0 to 1 in the case of slow exchange, 1 for intermediate exchange and between 1 and 2 for fast exchange. Since the exchange time regime is determined by the ratio of $k_{\text{ex}}/\Delta\omega$, which is obtained independently of α in the data analysis, this parameter is useful to assess the consistency of the data analysis when relaxation dispersion was measured at different field strengths.

For the special case of ligand binding to a protein, the following reaction scheme must be considered:



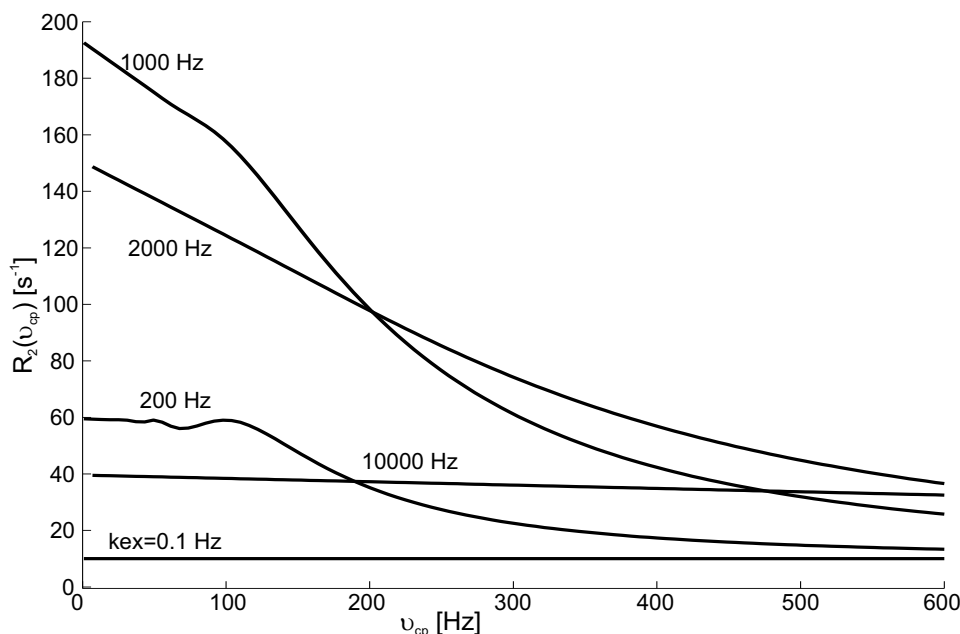


Figure 3: Relaxation dispersion curves simulated according to eq. 3 for the different exchange rates $k_{\text{ex}} = 0.1$ Hz, 200 Hz, 1000 Hz, 2000 Hz and 10000 Hz. R_{2A}^0 and R_{2B}^0 were both set to 10 s^{-1} , the chemical shift difference is $\Delta\omega = 1257$ Hz ($\Delta\nu = \Delta\omega/2\pi = 200$ Hz).

The exchanging sites are the free (P) and the complexed form (PL) of the protein and the exchange rate is given by

$$k_{\text{ex}} = k_{\text{on}}[\text{L}] + k_{\text{off}} \quad (5)$$

Unfortunately $k_{\text{on}}[\text{L}]$ is difficult to determine because the equilibrium concentration of the free ligand is usually unknown. However, for high-affinity interactions the equilibrium concentration $[\text{L}]$ will be small when the concentration of ligand is low [33]. Therefore, the measured exchange rate is approximately the off-rate, $k_{\text{ex}} \approx k_{\text{off}}$. If the off-rate is in a time regime accessible to relaxation dispersion analysis, the kinetics of the interaction can be characterized at atomic resolution. In the case of pure two-state exchange it is also possible to obtain the dissociation constant K_D from titration curves and therefore k_{on} can be calculated.

To a limited degree relaxation dispersion provides information about the presence of intermediates on the reaction pathway because relaxation dispersion depends on the chemical shift difference between the free protein and the complex, $\Delta\omega_{\text{PL-P}}$. When the value of $\Delta\omega$ obtained from a titration of the protein with a ligand is different from that obtained by fitting relaxation dispersion curves, at least one intermediate must be involved in ligand binding.

Using CPMG pulse trains in a ^{15}N heteronuclear correlation experiment, μs -ms dynamics of the backbone and side chains can be determined [16,34,35]. Relaxation dispersion can also be measured for ^{13}C -heteroatoms such as methyl groups in amino acid side chains [36]. Recent applications of these techniques included the investigation of site specific kinetic events in cyclophilin A [37]. There the turnover rate could be assigned to an individual amino acid proving its role for the catalytic function. The potential of relaxation dispersion experiments to study ligand binding in proteins has recently been explored for the case of a SH2 domain, where intermediates on the reaction pathway could be detected [33].

1.3 Line shape analysis

Line shape analysis of signals in NMR spectra is a well-established method to study the kinetics of processes occurring on a μs -ms time scale. In some cases equilibrium constants can be determined. While most former applications of line shape analysis involved small molecules, recent applications show the potential of the technique to study protein-ligand interactions [26, 27]. With very few exceptions, line shapes have been derived from one-dimensional NMR spectra. The degeneracy of chemical shifts in proteins restricts this type of analysis to the study of isolated protons. However, lines can also be obtained from two-dimensional NMR spectra, typically from ^{15}N -HSQC spectra. This approach has been applied by Balbach to study protein-folding [38]. However, line shapes from HSQC spectra can also be employed to study the kinetics of protein-ligand interactions. Here the variation of line shapes as a function of the ligand concentration provides information on the kinetics of the interaction. It is a great advantage of NMR line shape analysis that it provides a qualitative view of the mechanism of reactions as recently demonstrated by Günther *et al.* [26, 27].

A quantitative analysis of line shapes derived from ^{15}N -HSQC spectra in either the proton or nitrogen dimension allows calculation of off-rates for the protein-ligand interaction observed at individual amino acid residues of the protein. A theoretical treatment of line shapes in the course of a reaction was described by Sudmeier *et al.* [39]. The effect of more complex reaction schemes and the use of line shapes derived from two-dimensional spectra were reported more recently [26].

The treatment of the effect of two-site chemical exchange on the magnetization is based on the modified Bloch equations. The time domain signal can be calculated according to an equation by Anderson [40]:

$$F(t) = \mathbf{I} \exp [(-\mathbf{K} + 2\pi i \mathbf{W}_0 - \mathbf{R}_2)t] \mathbf{P}. \quad (6)$$

where

- \mathbf{I} is the unity matrix,
- \mathbf{K} is a matrix containing the rate constants,
- \mathbf{W}_0 is a diagonal matrix with the Larmor frequencies ν_i ,
- \mathbf{R}_2 is a diagonal matrix with transverse relaxation rates,
 $R = 1/T_2 = \pi \cdot \text{LW}$ (line width at half height) and
- \mathbf{P} is a column vector with the populations (mole fractions) of the reaction components.

The calculation of the time-domain signal rather than the frequency domain signal is less time consuming and allows the application of the same apodization functions as used for the experimental data.

For chemical reactions the fate of the line shape depends on the relative concentrations of the reaction partners. The typical course of line shapes in the case of protein-ligand binding



with second order binding and first order release are shown in Figure 4 for increasing concentrations of ligand with colors from blue to red. Such experimental line shapes can be used to determine the kinetics of the reaction.

Line shapes were also used to study more complex binding mechanisms [27]. Here the calculation of the 2D signal by Fourier transformation of the time domain signal simplifies the scaling of intensities of the line shapes when intermediates are involved [41].

Complex sequential reaction mechanisms such as

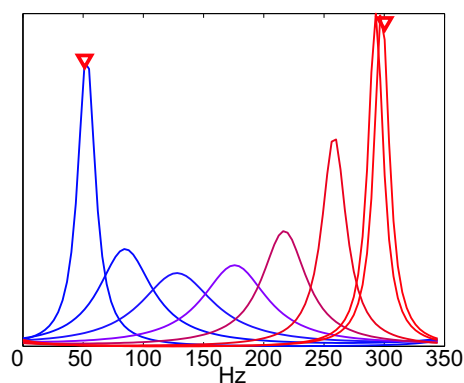


Figure 4: Line shapes simulated for the one-step binding mechanism (7) for increasing populations of the complex from blue to red. The frequency separation was set to 250 Hz, the off-rate k_{off} to 2000 Hz.



and



were recently observed for binding of peptide ligands to SH2 domains [26,27,41]. Reaction (8) can be regarded as second order binding followed by an exchange step between an intermediate PL^* and the final product PL . The first step of this reaction will cause successive chemical shift changes for increasing concentrations of L in the case of fast exchange between P and PL^* . The second step is determined by an equilibrium constant $K = \frac{[\text{PL}]}{[\text{PL}^*]}$ which depends on general reaction conditions. The resulting line shapes are depicted in Figure 5 for different values of the equilibrium constant K . Interestingly, line shapes for a two-step reaction resemble slow exchange line shapes owing to constantly low amounts of the intermediate species. This is demonstrated in Figure 5c.

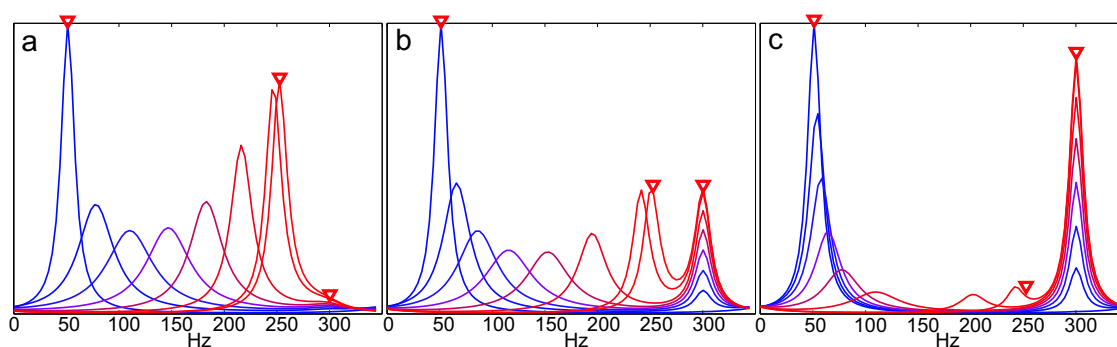


Figure 5: Line shapes simulated for the two-step mechanism (8) for continuously decreasing populations of P from blue to red. The off-rate for the first step of the reaction was 2000 s^{-1} , for the second step the on-rate was set to 10 s^{-1} and the corresponding off-rate was calculated from the equilibrium constant K which was 10, 1.0 and 0.1 in a, b and c, respectively. The locations of the lines of P , PL and PL^* are indicated by ' ∇ '. Frequency separations of P and PL^* were 200 Hz, of PL^* and PL 50 Hz.

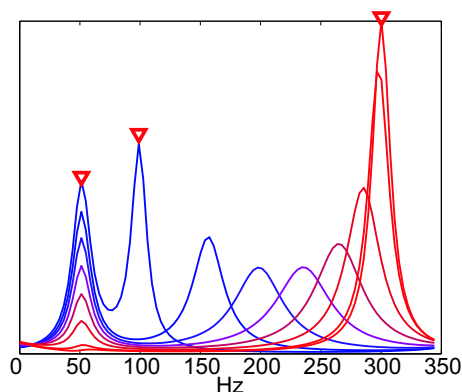


Figure 6: Simulation of line shapes for the two-step mechanism (9) for continuously decreasing populations of P from blue to red. The off-rate for the actual binding step was 2000 s^{-1} . The equilibrium rate $K = \frac{[P^*]}{[P]}$ was set to 1.0. Resonance positions of P, P* and PL are marked by a red '▽'. Frequency separations were 50 Hz between P and P* and 200 Hz between P* and PL.

Similar line shapes are obtained for reaction (9) with the only difference that the exchange step is in the beginning of the reaction followed by ligand dependent titration. A typical spectrum is shown in Figure 6.

2 Results

In order to show the possibilities of the techniques introduced above, relaxation dispersion and titration data of CRBP will be presented.

Binding of retinol to CRBP is a highly enigmatic process despite the wealth of structural information available for the free protein and the protein-ligand complex. Here we present results from NMR relaxation dispersion and from line shape analysis which demonstrate a highly complex kinetic mechanism for the interaction.

2.1 Relaxation dispersion analysis of CRBP

CPMG measurements were performed on the backbone amide resonances of apo-CRBP to characterize its conformational flexibility on the μs -ms time scale on a per-residue basis. The experiments were carried out at 11.7 and 16.4 T, corresponding to proton Larmor frequencies of 500 and 700 MHz, respectively, using a constant relaxation delay [34] to obtain effective transverse relaxation rates R_2 over a wide range of refocusing rates ν_{CP} between 20 and 670 Hz. The relaxation dispersion curves at both fields were fitted to eq. 3 on a per residue basis to obtain exchange rates k_{ex} , chemical shift differences $\Delta\omega$ and populations of the two states involved. 121 of 134 residues in the ligand-free protein were accessible to relaxation dispersion analysis. For the remaining residues no information was available due to spectral overlap or missing assignments. Figure 7a-c depicts the relaxation dispersion curves of residues G46, K40 and S55 in the apo-protein. For G46 the apparent transverse relaxation rate constant, R_2 , is independent of the refocusing frequency in the CPMG pulse train. Therefore G46 does not exhibit a chemical exchange process on a μs -ms time scale. In comparison, R_2 of K40 and S55 shows a strong dependence on the refocusing field. The exchange contributions R_{ex} were determined to be $26.8 \pm 2.4 \text{ s}^{-1}$ and $36.4 \pm 2.6 \text{ s}^{-1}$; the exchange rates k_{ex} were $204 \pm 58 \text{ s}^{-1}$ and $452 \pm 104 \text{ s}^{-1}$, respectively.

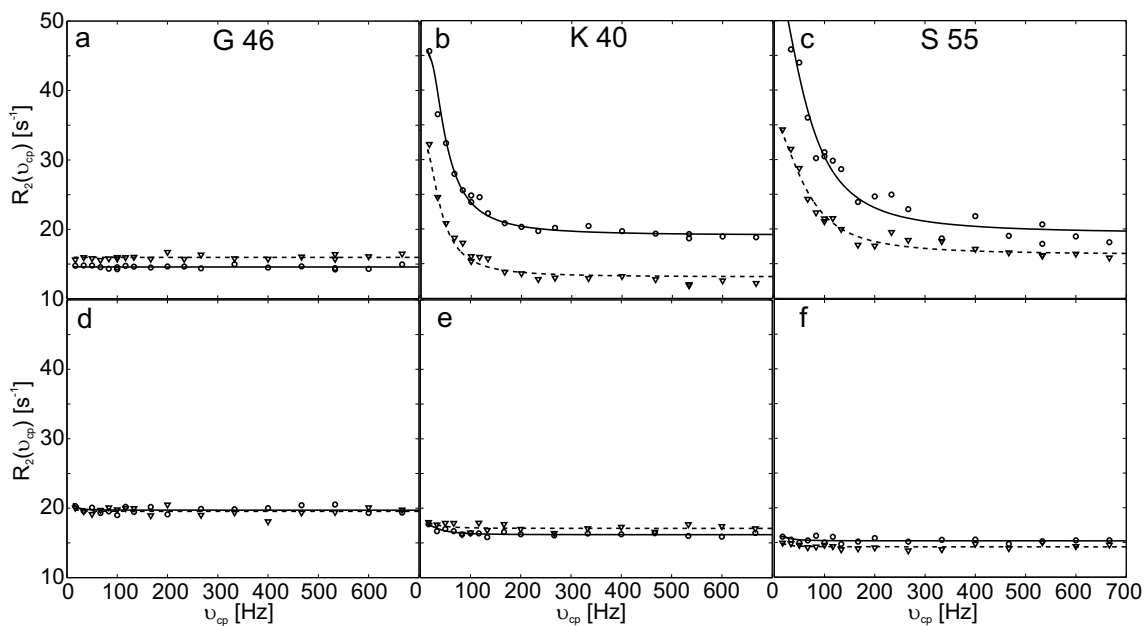


Figure 7: Relaxation dispersion curves of CRBP. Effective transverse relaxation rates, R_2 , are depicted as a function of the refocusing frequency, ν_{cp} , of residues G46 (a, d), K40 (b, e) and S55 (c, f) in apo-CRBP (a-c) and holo-CRBP (d-f). The best-fit dispersion curves using eq. 3 are shown as solid and dashed lines. Data recorded at ^1H Larmor frequencies of 700 and 500 MHz are depicted with circles and triangles, respectively.

Extended regions of CRBP exhibit significant conformational exchange as depicted in Figure 8. This characteristic is reflected in broad lines of signals in ^{15}N -HSQC NMR spectra. Interestingly, most regions of the β -sheet (except part of strands E and F) and most residues in the two α -helices undergo conformational exchange whereas the N-terminus and residues in some turns ($\beta\text{B}-\beta\text{C}$, $\beta\text{D}-\beta\text{E}$, $\beta\text{H}-\beta\text{I}$) are rigid in the μs -ms time scale but undergo motions in the ps-ns time scale. We observe the highest exchange contributions for residues E17 in α -helix I, D24 in the turn between α -helix I and α -helix II, R30, I32 and N34 in α -helix II and S55, T56, F57, R58 and N59 in turn $\beta\text{C}-\beta\text{D}$. All these residues belong to the putative portal. Signals of residues in turn $\beta\text{E}-\beta\text{F}$, which also frame the putative entrance, are not detectable in spectra of apo-CRBP, most likely as a consequence of extensive conformational exchange.

Populations of exchanging states can be obtained by relaxation dispersion analysis. For 26 of the exchanging residues in apo-CRBP the populations of exchanging states are 50% each, which means that they exhibit the same energy. For 52 residues with skewed populations, the average population of the favored state equals 0.88 ± 0.086 .

For most residues the dynamics are in the fast exchange regime indicated by the ratio $k_{ex}/\Delta\omega$ and confirmed by the value of α (eq. 4). The values of exchange rates k_{ex} obtained by fitting the relaxation dispersion curves of exchanging residues to eq. 3 vary by one order of magnitude, between 100 s^{-1} and 1000 s^{-1} , for different residues. The chemical exchange in the protein is not due to one global concerted motion but appears to be more complex. Different residues sense different conformational exchange processes.

The high degree of conformational flexibility in apo-CRBP, especially around the putative portal region, is almost completely quenched upon retinol binding. In Figure 7d-f relaxation dispersion curves of residues G46, K40 and S55 of the holo-protein are depicted. These residues do not undergo an exchange process in the μs -ms time scale. Only residues R58 in turn $\beta\text{C}-\beta\text{D}$ and L74 and D79 in the $\beta\text{E}-\beta\text{F}$ turn exhibit a slight dependence of R_2 on ν_{cp} (indicating a chemical exchange process on the ms time scale). For residues N15, V27, I61,

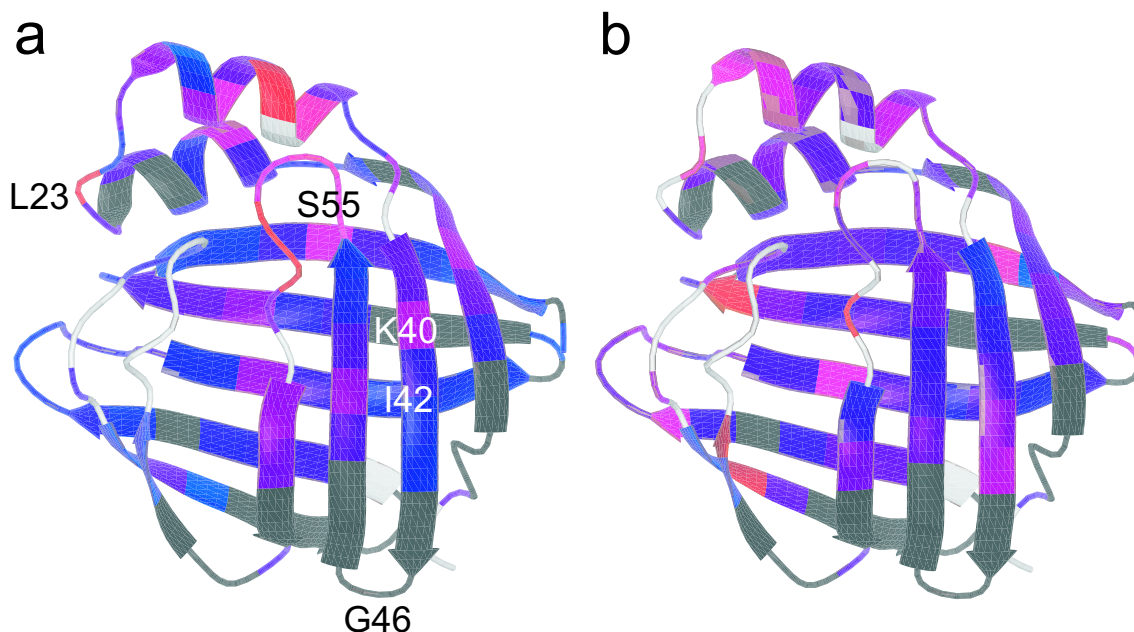


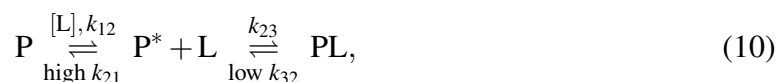
Figure 8: Exchange parameters of apo-CRBP mapped onto the protein ribbon diagram by color coding. The continuous color scale from blue to magenta to red indicates (a) the amplitude of R_{ex} (from 0 s^{-1} to 20 s^{-1} to 40 s^{-1}) or (b) the size of k_{ex} (from 0 s^{-1} to 500 s^{-1} to 1000 s^{-1}). Residues colored black do not exhibit exchange. Residues colored grey could not be analyzed due to spectral overlap, missing assignments or the fact that dispersion curves could not be fitted. The figure was prepared with the program MOLMOL [42].

G76, E100 and G112 faster exchange on a μs time scale is likely because R_2 is enhanced though it does not depend on the refocusing rate.

2.2 Line shape analysis of retinol binding to CRBP

Line shape analysis of signals from $^1\text{H}/^{15}\text{N}$ HSQC spectra recorded for subsequent steps of a titration of CRBP with retinol revealed simple slow exchange between the apo and the holo-form for 19 residues. Figures 9a and b show typical slow exchange line shapes in the ^1H and ^{15}N dimensions of residue I42. Experimental cross-sections are depicted as lines with triangles; simulated lines are solid. The resonance frequencies of the free protein P and the complex PL are indicated by red triangles. In the first spectrum shown in blue only a signal at the resonance frequency of P is observed. For successive titration steps the intensity of the signal of P decreases whereas a signal at the resonance frequency of PL appears, reflecting its increasing population. In intermediate spectra two signals are observed at frequencies of P and PL.

Line shapes of other residues could not be explained with a simple one-step mechanism. In ^{15}N cross-sections of L23 depicted in Figure 9c the signal at the resonance frequency of P shifts for successive titration steps, because of a fast exchange process. However, lines at the right side are still in slow exchange with those at the left side. In fact, line shapes of 20 residues could be described using the following mechanism:



where a fast exchange process with high off-rate is followed by a second event in slow exchange. The second step represents the actual binding though the first step also depends on

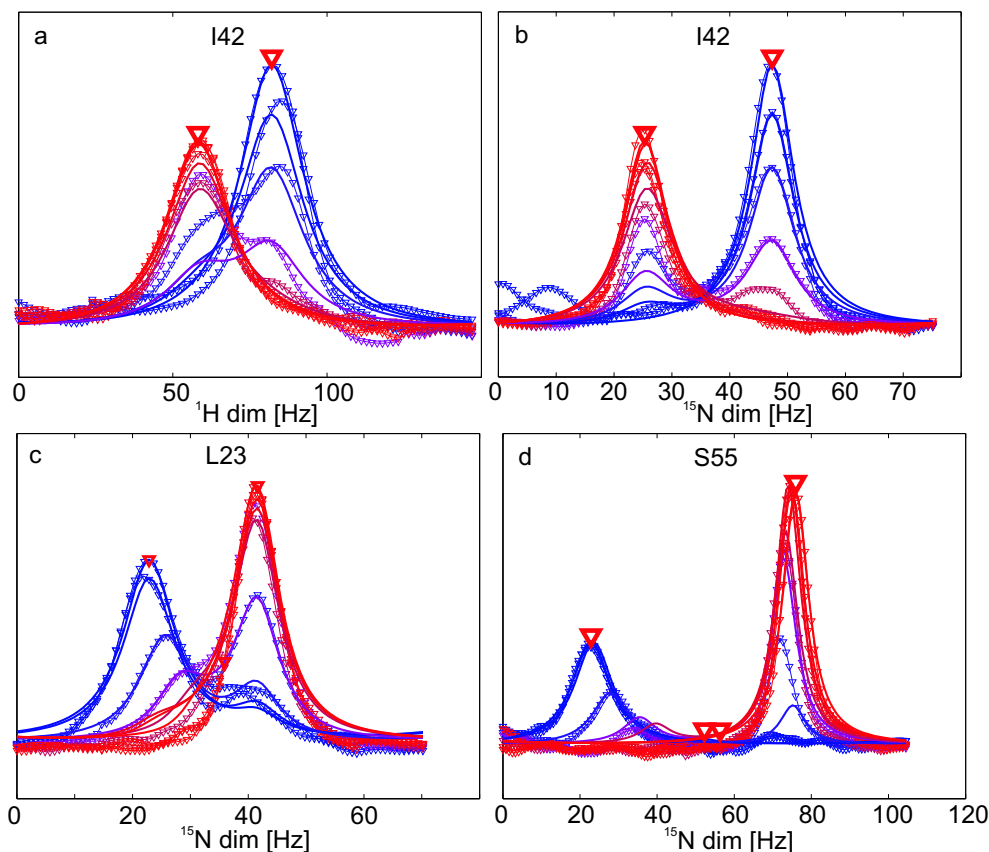
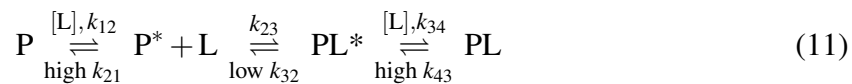


Figure 9: ^1H and ^{15}N cross-sections of signals of CRBP in the titration with retinol (lines with ' ∇ ' from blue to red for subsequent steps of the titration) and simulated lines (solid). (a) ^1H and (b) ^{15}N line shapes of I42 were simulated according to simple one-step binding (eq. 7). ^{15}N cross-sections of (c) L23 and (d) S55 require more complex mechanisms. Resonance frequencies of P, PL and intermediates are marked by red ' ∇ '.

the concentration of ligand (as indicated by [L] above the arrow).

Line shapes of 44 residues showed additional complexity. Figure 9d depicts line shapes for S55; the signal at the resonance frequency of PL also shifts for successive titration steps. A second process in fast exchange must be involved. In this case at least three steps are required to explain the line shapes adequately:



3 Conclusions

Relaxation dispersion experiments and line shape analysis provide novel insights into the conformational flexibility and the binding properties of CRBP. Interestingly, the apo-protein exhibits a high degree of conformational exchange on the μs -ms time scale, while the backbone was found to be rather rigid on the ps-ns time scale [7]. The most pronounced exchange contribution to the ^{15}N transverse relaxation rate, R_{ex} , was observed for residues belonging to α -helix II, the turn between the helices and the turn βC - βD (see Figure 8a). These segments are located in the putative portal region. In contrast, only a few residues show detectable conformational exchange in holo-CRBP, indicating that binding of retinol markedly reduces

the protein conformational flexibility.

Line shapes obtained with increasing amounts of retinol give an even more interesting and unexpected picture. The complexity of line shapes suggests the presence of two, and for many residues three, subsequent kinetic steps in the interaction of retinol with CRBP. The first step is characterized by a high off-rate for all residues and might represent an initial encounter of protein and ligand. The following slower process, observed for most residues, may represent the rate of retinol dissociation from its specific binding site and account for the high affinity of the carrier for its ligand ($K_D = 0.1$ nM). However, for lines in slow exchange, only an upper limit of the off-rate can be determined from line shape analysis, approximately 10 s^{-1} . For some residues we observe a final step with fast exchange line shapes. This may represent a final rearrangement on a μs time scale; however, the role of this step requires further investigation.

The study of CRBP has opened new avenues to gain a deeper understanding of the mechanism of ligand binding to its specific carrier. The complexity of the kinetics of ligand-protein interaction on a per residue basis had not been appreciated previously.

4 Acknowledgements

This work was supported by the Large Scale Facility Frankfurt (UNIFRANMR) and by grants of the Italian Ministry of Education, University and Research (MIUR).

References

- [1] L. J. Banaszak, N. S. Winter, Z. Xu, D. A. Bernlohr, S. Cowan & T. A. Jones (1994) *Adv. Protein Chem.* **45**, 89–151.
- [2] E. Li & A. W. Norris (1996) *Annu. Rev. Nutr.* **16**, 205–234.
- [3] J. L. Napoli (1999) *Prog. Nucleic Acid Res. Mol. Biol.* **63**, 139–188.
- [4] L. J. Gudas, M. B. Sporn & A. B. Roberts (1994) *The Retinoids: Biology, Chemistry and Medicine* (Raven Press, N. Y.) 2nd edition pp. 443–520.
- [5] S. W. Cowan, M. E. Newcomer & T. A. Jones (1993) *J. Mol. Biol.* **230**, 1225–1246.
- [6] E. Li, S. J. Qian, N. S. Winter, A. d'Avignon, M. S. Levin & J. I. Gordon (1991) *J. Biol. Chem.* **266**, 3622–3629.
- [7] L. Franzoni, C. Lücke, C. Perez, D. Cavazzini, M. Rademacher, C. Ludwig, A. Spisni, G. L. Rossi & H. Rüterjans (2002) *J. Biol. Chem.* **277**, 21983–21997.
- [8] J. C. Sacchettini, J. I. Gordon & L. J. Banaszak (1989) *J. Mol. Biol.* **208**, 327–339.
- [9] Z. Xu, D. A. Bernlohr & L. J. Banaszak (1993) *J. Biol. Chem.* **268**, 7874–7884.
- [10] J. Thompson, N. Winter, D. Terwey, J. Bratt & L. Banaszak (1997) *J. Biol. Chem.* **272**, 7140–7150.
- [11] A. G. Palmer (2001) *Annu. Rev. Biophys. Biomol. Struct.* **30**, 129–155.
- [12] H. Y. Carr & E. M. Purcell (1954) *Phys. Rev.* **94**, 630–638.
- [13] S. Meiboom & D. Gill (1958) *Rev. Sci. Instrum.* **29**, 688–691.
- [14] J. P. Loria, M. Rance & A. G. Palmer (1999) *J. Am. Chem. Soc.* **121**, 2331–2332.
- [15] O. Millet, J. P. Loria, C. D. Kroenke, M. Pons & A. G. Palmer (2000) *J. Am. Chem. Soc.* **122**, 2867–2877.
- [16] A. G. Palmer, C. D. Kroenke & J. P. Loria (2001) *Methods Enzymol.* **339**, 204–238.
- [17] C. Deverell, R. E. Morgan & J. H. Strange (1970) *Mol. Phys.* **18**, 553–559.
- [18] T. Szyperski, P. Lugjubuhl, G. Otting, P. Güntert & K. Wüthrich (1993) *Journal of Biomolecular NMR* **3**, 151–164.
- [19] S. Zinn-Justin, P. Berthault, M. Guenneugues & H. Desvaux (1997) *J. Biomol. NMR* **10**, 363–372.

- [20] F. A. A. Mulder, R. A. de Graaf, R. Kaptein & R. Boelens (1998) *J. Magn. Res.* **131**, 351–357.
- [21] J. Schleucher & S. S. Wijemnga (2002) *J. Am. Chem. Soc.* **124**, 5881–5889.
- [22] G. Binsch (1968) *Top. Stereochem.* **3**, 97–191.
- [23] J. Sandström (1982) *Dynamic NMR spectroscopy* (Academic Press).
- [24] B. D. Rao (1989) *Methods Enzymol.* **176**, 279–311.
- [25] L. Y. Lian & J. C. K. Roberts (1993) *NMR of Macromolecules: A Practical Approach* (Oxford University Press) Practical Approach Series 1 edition.
- [26] U. L. Günther & B. Schaffhausen (2002) *J. Biomol. NMR* **22**, 201–209.
- [27] U. Günther, T. Mittag & B. Schaffhausen (2002) *Biochemistry* **41**, 11658–11669.
- [28] Z. Luz & S. Meiboom (1963) *J. Chem. Phys.* **39**, 366–370.
- [29] J. P. Carver & R. E. Richards (1972) *J. Magn. Reson.* **6**, 89–105.
- [30] J. Jen (1978) *J. Magn. Reson.* **30**, 111–128.
- [31] D. G. Davis, M. E. Perlman & R. E. London (1994) *J. Magn. Reson. B* **104**, 266–275.
- [32] R. Ishima & D. A. Torchia (1999) *J. Biom. NMR* **14**, 369–372.
- [33] T. Mittag, B. Schaffhausen & U. L. Günther (2003) *Biochemistry* **42**, 11128–11136.
- [34] M. Tollinger, N. R. Skrynnikov, F. A. A. Mulder, J. D. Forman-Kay & L. E. Kay (2001) *J. Am. Chem. Soc.* **123**, 11341–11352.
- [35] F. A. A. Mulder, N. R. Skrynnikov, B. Hon, F. W. Dahlquist & L. E. Kay (2001) *J. Am. Chem. Soc.* **123**, 967–975.
- [36] N. R. Skrynnikov, F. A. A. Mulder, B. Hon, F. W. Dahlquist & L. E. Kay (2001) *J. Am. Chem. Soc.* **123**, 4556–4566.
- [37] E. Z. Eisenmesser, D. A. Bosco, M. Akke & D. Kern (2002) *Science* **295**, 1520–1523.
- [38] J. Balbach, V. Forge, W. S. Lau, N. A. Nuland, K. Brew & C. M. Dobson (1996) *Science* **274**, 1161–1163.
- [39] J. L. Sudmeier, J. L. Evelhoch & N. Jonsson (1980) *J. Magn. Reson.* **40**, 377–390.
- [40] P. W. Anderson (1954) *J. Phys. Soc. Jpn.* **9**, 316–339.
- [41] T. Mittag, B. Schaffhausen & U. Günther (2003) *submitted* .
- [42] R. Koradi, M. Billeter & K. Wüthrich (1996) *J. Mol. Graph.* **14**, 51–55.

Freezing of Conformers of the Cellular Retinol-Binding Protein by Retinol

Tanja Mittag¹, Lorella Franzoni², Davide Cavazzini³, Brian Schaffhausen⁴, Gian Luigi Rossi³, and Ulrich L. Günther¹

¹*J.W. Goethe University, Frankfurt,*

Center for Biomolecular Magnetic Resonance (BMRZ),

Biocentre N230, Marie-Curie-Str. 9, 60439 Frankfurt, Germany

²*Department of Experimental Medicine, Section of Chemistry and Structural*

Biochemistry, University of Parma, 43100 Parma, Italy,

³*Department of Biochemistry and Molecular Biology, University of Parma, 43100*

Parma, Italy

⁴*Dept. of Biochemistry, Tufts University, School of Medicine, 136 Harrison Avenue,*

Boston, Massachusetts 02111

The cellular retinol-binding protein I exhibits closed conformations that should not bind retinol both in the apo- and in the holo-form. NMR line shape analysis reveals how protein dynamics resolve this apparent paradox by allowing the ligand to access the binding site. Encounter with ligand slows down the dynamics of apo-CRBP and thereby creates long-lived open conformers that allow retinol access to the cavity. The final closed, high affinity complex shows substantially reduced dynamic motion that contributes to high affinity.

Introduction. Although protein-ligand interactions have been at the core of biochemical and biophysical research for decades, little is known about their fundamental mechanisms and the correlation between internal dynamics of proteins and protein functions. New experimental evidence has been spurred by advances in NMR spectroscopy which allow a reliable and sensitive investigation of ligand binding mechanisms on microsecond to millisecond (μs - ms) time scales using lineshape analysis [1,2] and relaxation dispersion [3,4].

Recent NMR studies have tackled allosteric behavior [5], enzymatic turnover [6] and ligand binding [7–11]. An important question is the relevance of inherent motions of the protein for ligand binding, particularly when internal motions are on a different time scale than the kinetics of ligand binding [12]. Furthermore, the common assumption of two-state mechanisms of protein interactions has been questioned. While folding intermediates could be detected for many proteins (see [13] and references therein), two-state models have been used in most analyzes of protein interactions. Recent work has provided evidence for more complex mechanisms, involving sequential binding steps and the generation of slowly exchanging conformers by ligand induced dynamics [2]. In one case binding intermediates were directly observed in NMR line shapes [11].

The cellular retinol-binding protein type I (CRBP I) [14] is a member of the intracellular lipid binding protein (iLBP) superfamily which encompasses the fatty acid binding proteins (FABPs), the carriers of vitamin A derivatives, the cellular retinol binding proteins (CRBPs) and the cellular retinoic acid binding proteins (CRABPs). CRBP I plays a key role in regulating vitamin A homeostasis as recently confirmed by an *in vivo* study of CRBP-null mice [15]. *In vitro* studies have suggested that it is involved in retinol internalization and intercellular transfer [16, 17] retinol esterification [18, 19], retinyl ester hydrolysis [16, 20], and the oxidation of retinol to retinaldehyde in retinoic acid synthesis [21, 22]. It has recently been shown that CRBP I plays a crucial role in various types of cancer. The occurrence of breast and ovarian cancer has been correlated with decreased levels of CRBP I expression [23–27].

CRBP I provides an intriguing problem in protein dynamics. Although several structures of *apo*- and *holo*-CRBP I have been determined using X-ray and NMR spectroscopy [28, 29] (Figure 2 depicts a ribbon diagram of apo-CRBP I), the mechanism of ligand uptake into the β -barrel remains enigmatic. Both forms represent closed conformations with no apparent opening in the surface allowing for ligand binding.

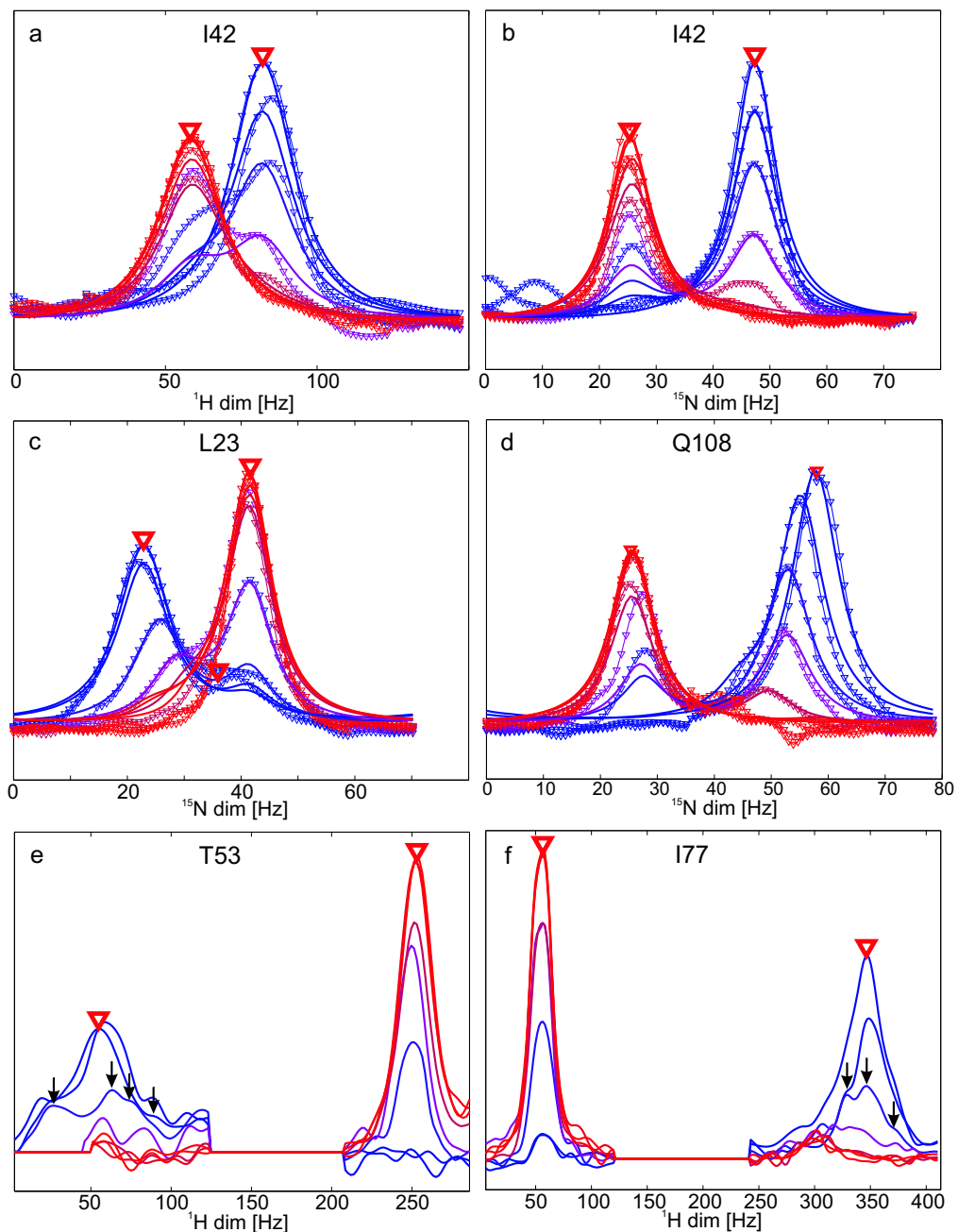
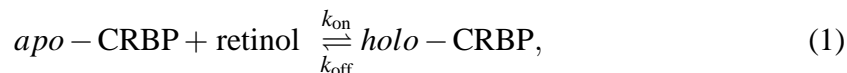


Figure 1: ^1H and ^{15}N cross-sections of signals of CRBP in the titration with retinol (lines with '▽' from blue to red for subsequent steps of the titration) and simulated lines (solid). (a) ^1H and (b) ^{15}N line shapes of I42 were simulated according to simple one-step binding (eq. 1) [30]. ^{15}N cross-sections of (c) L23 and (d) Q108 require the more complex mechanism 2. Resonance frequencies of P, PL and intermediates are marked by a red '▽'. For residues T53 (e) and I77 (f) signals of apo-CRBP show complex line shapes in intermediate steps of the titration with retinol. Signal shoulders in the third spectrum are marked with arrows.

Here we have analyzed the interactions of CRBP I [31] with retinol by analysis of NMR line shapes. Line broadening and shifts of resonances in ^1H - ^{15}N -HSQC spectra of CRBP I recorded for increasing concentrations of retinol were analyzed to extract kinetic parameters and mechanistic information on the binding process [32]. For many residues, we

observe typical slow exchange line shapes that can be simulated employing a two-state binding model:



with second order binding and first order release (k_{on} and k_{off} are forward and reverse reaction rate constants and represent reciprocal life times of *apo*- and *holo*-CRBP). Figures 1a and b show typical signal cross-sections in the ^1H and ^{15}N dimension of the exemplary residue I42 located in βB of CRBP I. The signal of *apo*-CRBP I disappears as the resonance of *the holo*-form increases upon addition of retinol. For this residue, the upper limit for the off-rate is 10 s^{-1} [33] while the on-rate is outside the kinetic window accessible by this analysis. 29 residues colored blue in Figure 2 showed line shapes that could be explained by this two-state mechanism 1.

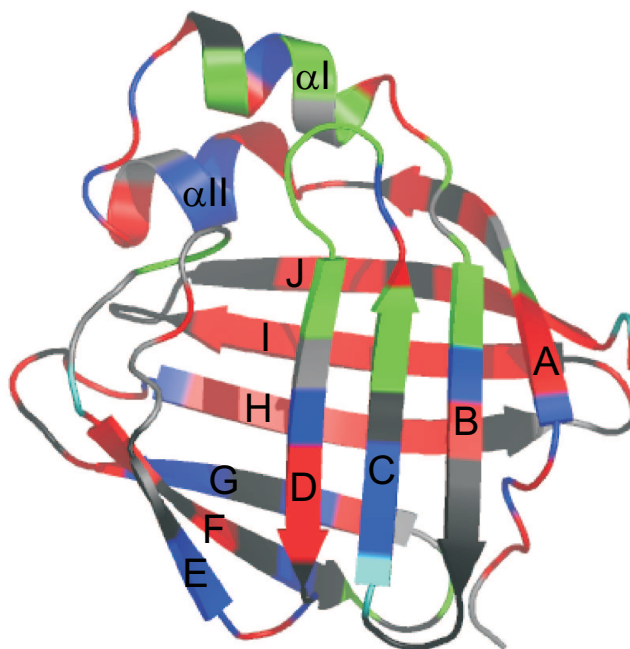
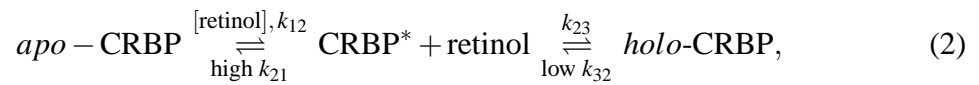


Figure 2: Ribbon diagram of *apo*-CRBP grouping residues according to their binding mechanism as revealed by line shape analysis. black: no perturbation of the chemical shift upon addition of retinol; blue: one-step binding mechanism (1) with signals in slow exchange; light blue: one-step binding mechanism (1) with signals in fast exchange; red: two-step binding mechanism (2); green: complex line shape with shoulders; gray: no mechanism assignable due to missing assignment in one state or severe overlap.

The question remains how such binding occurs if the *apo*-form has no opening to allow

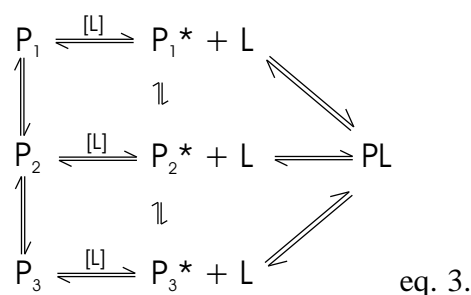
ligand to enter. Closer inspection of the line shapes provides an important clue. Astonishingly, line shapes of many residues showed additional complexity. As an example, line shapes of L23, a residue in the linker region between the two helices, and of Q108, a residue in β H in the core of of the β -barrel, are depicted in Figures 1c and d, respectively. In both cases the resonance frequency of the signal corresponding to apo-CRBP (blue) changes in successive titration steps indicating a fast exchange process ($k_{\text{off}} > 2000\text{s}^{-1}$). In contrast, signals of holo-CRBP (red) do not experience any ligand dependent chemical shift perturbation but altered intensity, typical of slow exchange phenomena. This behavior can be explained well by a two-step binding mechanism:



In this case, a fast exchange process with a high off-rate ($k_{\text{off}} > 2000\text{s}^{-1}$) is sequentially followed by a slow step with a rate $< 10 \text{ s}^{-1}$. The first step, which depends on the ligand concentration represents a low affinity interaction with a high off-rate followed by the the actual ligand uptake with high affinity (low off-rate). This mechanism was encountered for line shapes of 58 residues, colored red in Figure 2 [34].

Considering the very different rates for the two steps of this reaction, the second step must be responsible for the high affinity of CRBP for retinol ($K_D \approx 0.1 \text{ nM}$). Assuming a diffusion controlled on-rate of $\sim 10^9 \text{ s}^{-1}$, an off-rate $< 10\text{s}^{-1}$ is in good agreement with the observed dissociation constant.

A possible "portal region" involving α -helix II and the two turns β C- β D and β E- β F have been previously suggested from comparisons with intestinal fatty acid-binding protein (I-FABP), which has a similar fold as CRBP I, and exhibits a small opening in the crystal structure [35]. For residues in and around this putative portal region, another type of complexity is observed in line shapes of CRBP I. For some residues intermediate spectra exhibit several shoulders indicative of slow conformational exchange. Figures 1e and f show exemplary line shapes of T53 in β C and of I77 in turn β E- β F (shoulders are indicated by arrows). This behavior is best explained by a parallel scheme of the type:



From the close proximity of the signal shoulders an upper limit for the exchange frequency between the different conformers can be estimated to be $< 20s^{-1}$. Interestingly, relaxation dispersion experiments of *apo*-CRBP showed a significant exchange contribution on the ms time scale for those residues [36,37]. This observation suggests that ligand binding causes a transformation of chemical exchange from a millisecond time scale to slow conformational exchange on a sub-second time scale.

Residues exhibiting this type of complex line shapes are labeled green in Figure 2 and are predominantly located around the portal and extending into β -sheets A, B, C, and D. Exceptions are the residues D89 and G91, which are located on the other side of the protein in turn β F- β G. In contrast to the residues showing conformational averaging in the portal region, these residues do not exhibit millisecond exchange in the *apo*-form.

The picture that emerges from these data suggests that interactions with the *apo*-form of CRBP leads to structural changes that then allow specific, high affinity binding. The initial interaction must be non-specific in the sense that the cavity mediating specific binding is inaccessible. This type of interaction can be observed directly for residues that show a third binding step with high off-rate for an excess of retinol. Confirmation for the assumption of an unspecific interaction of retinol with CRBP I was obtained by control experiments where retinol was added to purified *holo*-CRBP I. All the residues which showed a high off-rate response to excess retinol were also involved in the first binding step which precedes ligand uptake detected by initial titrations with ligand.

Analysis of molecular dynamics suggest that the *apo*-form is "poised" to respond to encounter with ligand. A study of of picosecond to nanosecond (ps-ns) dynamics of both protein states revealed few residues with higher mobility in the *apo*-protein located in turns β C- β D and β E- β F and α -helix I and in some loop regions [29,38]. More significant dynamic effects were observed on a micro- to millisecond (μ s-ms) time scale [36,37] for *apo*-CRBP with particularly strong exchange effects in turn β C- β D and α -helix II (Fig. 3a) [39]. The relaxation dispersion analysis showed [40–42] that for most residues one conformational state was occupied by 88%, for a smaller subset of residues two states were populated equally. While most exchange phenomena were in the fast exchange regime on the NMR time scale [43], the rates of exchange varied over a large bandwidth between $100 s^{-1}$ and $1000 s^{-1}$ with particularly high exchange contributions and exchange rates in α -helix II and in turn β C- β D and in the loop residue L23 (red in Fig. 3a). Owing to the broad dispersion of exchange frequencies concerted motions of clusters of residues are unlikely.

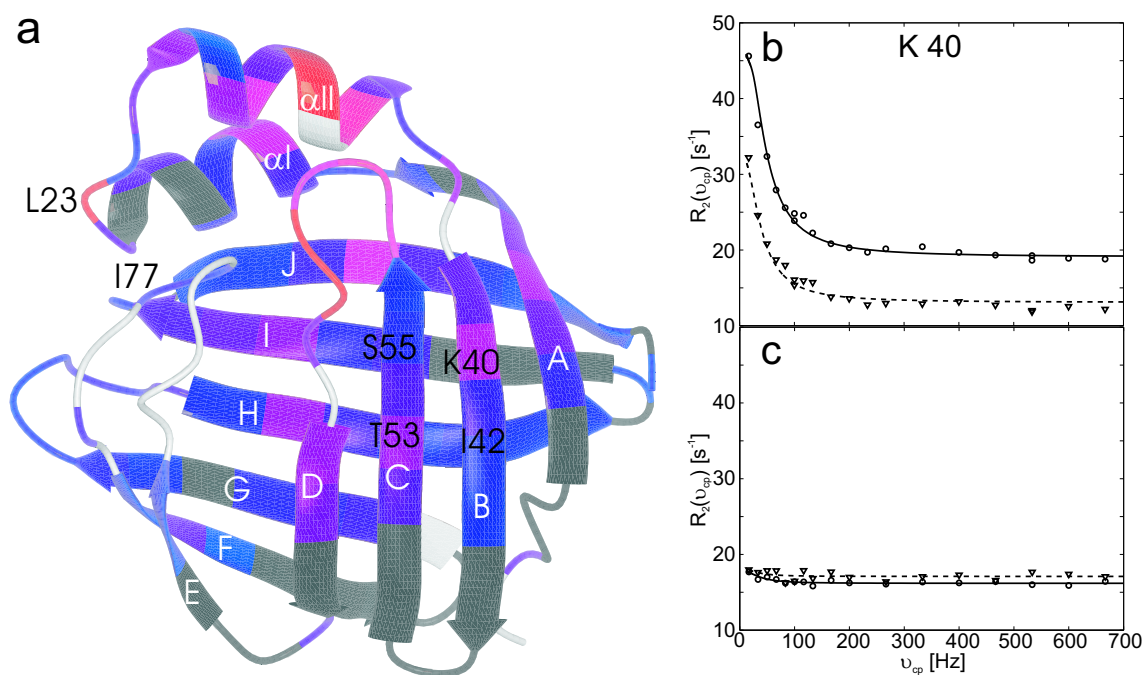


Figure 3: Conformational exchange in *apo*-CRBP which shares the common β -barrel motif of iLBP family members with two nearly perpendicular five-stranded β -sheets (A-E and F-J) and a (α I) helix-turn- (α II) helix motif between β -strands A and B. The internal cavity of the β -barrel contains the highly specific binding site for the hydrophobic ligand. (a) The amplitude of the exchange contribution R_{ex} [44] is mapped on the structure of *apo*-CRBP by a continuous color scale from blue to magenta to red (from 0 s^{-1} to 20 s^{-1} to 40 s^{-1}). Residues colored black do not exhibit exchange. Residues colored gray could not be analyzed [45]. The figure was prepared with the program MOLMOL [46]. (b, c) Relaxation dispersion curves of residue K40 in strand β B in *apo*-CRBP (b) and *holo*-CRBP (c) [42]. The best-fit dispersion curves using the general equation for two-site exchange are shown as solid and dashed lines. Data recorded at 1 H Larmor frequencies of 700 and 500 MHz are depicted with circles and triangles, respectively. K40 exhibits strong exchange in *apo*-CRBP with an exchange contributions R_{ex} of $26.8 \pm 2.4 s^{-1}$. The exchange rate k_{ex} was determined to be $204 \pm 58 s^{-1}$ [47]. The exchange is totally quenched in the complex.

The high degree of conformational flexibility observed in the *apo*-protein is almost completely quenched upon binding of retinol [48]. This suggests that whereas the relevant dynamics for ligand uptake are already present in *apo*-CRBP in absence of the ligand, the dynamic modes that might promote ligand release are not present in the *holo*-form.

Figure 4 classifies residues with respect to their participation in one of the steps of the binding process 2. Residues involved in the first high off-rate interaction of retinol with CRBP are displayed red in Figure 4a. Since most of these residues point away from the β -barrel into the solvent they are ideally suited for initial contact with retinol. Many of these residues, particularly those in the portal region also displayed millisecond mobility in the *apo* protein. Furthermore, a subset of these residues located in the portal region shows slow conformational averaging (green in Figure 4b) for higher concentrations of retinol. This combination of events points to the links between the internal dynamics of

the apo protein and its transformation to slow conformational processes that are required for ligand uptake into the β -barrel. The actual binding step that is responsible for the high affinity of the interaction is sensed by many residues all over the protein including residues, which are part of the β -barrel and residues in the portal region (Figure 4c). Despite the small change between the structures of apo and holo CRBP I the binding of retinol is observed in small chemical shift changes that correspond to alterations of electrostatic charges and steric arrangements. These adjustments may be required to promote the correct binding conformation.

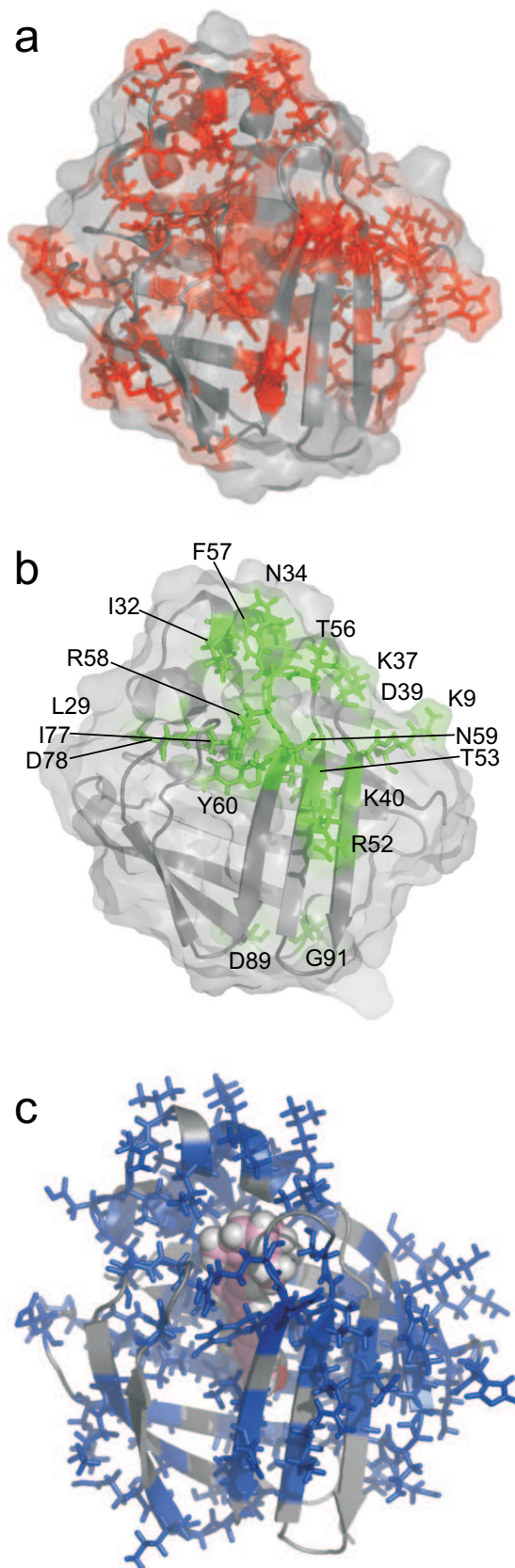


Figure 4: Representations of CRBP depicting residues sensing individual binding steps. (a) Residues labeled red sense a first unspecific interaction with the ligand. (b) Residues labeled green show complicated line shapes with shoulders after the addition of small amounts of ligand. Most of them line the portal, whereas D89 and D91 are located in turn β F- β G at the “bottom” of the β -barrel. (c) depicts residues in blue showing slow-exchange line shapes, which represent the actual high-affinity binding step.

This analysis confirms the location of the portal for ligand entry although slow conformational exchange on the bottom of the β -barrel suggests either an alternative entry point or motions mediated by the retinol molecule in the cavity. The investigation of binding dynamics allows a novel view of the processes involved in ligand uptake. In an initial step, retinol binds non-specifically to the surface of the protein. Despite no apparent specificity for this first step, this interaction is important to modulate the microsecond dynamics in the portal region to slower conformational exchange that allows the ligand to enter the cavity and to bind inside the cavity with high affinity. It is important to note that only residues in the portal region and some additional residues at the bottom of the β -barrel are involved. This new mechanism provides basic insights into the core processes required in ligand uptake into protein cavities and provides a proof for the importance of intrinsic protein dynamics for protein binding.

References

1. U. L. Günther, B. Schaffhausen, *J. Biomol. NMR* **22**, 201 (2002).
2. U. Günther, T. Mittag, B. Schaffhausen, *Biochemistry* **41**, 11658 (2002).
3. A. G. Palmer, C. D. Kroenke, J. P. Loria, *Methods Enzymol.* **339**, 204 (2001).
4. M. Tollinger, N. R. Skrynnikov, F. A. A. Mulder, J. D. Forman-Kay, L. E. Kay, *J. Am. Chem. Soc.* **123**, 11341 (2001).
5. B. F. Volkman, D. Lipson, D. E. Wemmer, D. Kern, *Science* **291**, 2429 (2001).
6. E. Z. Eisenmesser, D. A. Bosco, M. Akke, D. Kern, *Science* **295**, 1520 (2002).
7. V. Feher, J. Cavanagh, *Nature* **400**, 289 (1999).
8. F. A.A. Mulder, A. Mittermaier, B. Hon, F. Dahlquist, L. E. Kay, *Nat. Struct. Biol.* **8**, 932 (2001).
9. J. Evenäs, A. Malmendal, M. Akke, *Structure* **9**, 185 (2001).
10. T. Mittag, B. Schaffhausen, U. L. Günther, *Biochemistry* **42**, 11128 (2003).
11. T. Mittag, B. Schaffhausen, U. Günther, *J. Am. Chem. Soc.* **126**, 9017 (2004).
12. A. J. Wand, *Nat. Struct. Biol.* **8**, 926 (2001).
13. J. Myers, T. Oas, *Ann. Rev. Biochem.* **71**, 783 (2002).

14. The abbreviations used are: CPMG, Carr-Purcell-Meiboom-Gill; CRABPs, cellular retinoic acid binding proteins; CRBP, cellular retinol binding protein; FABPs, fatty acid binding proteins; I-FABP, intestinal fatty acid-binding protein; iLBPs, intracellular lipid binding proteins; rf, radiofrequency.
15. N. B. Ghyselinck, *et al.*, *EMBO J.* **18**, 4903 (1999).
16. S. Ottonello, S. Petrucco, G. Maraini, *J. Biol. Chem.* **262**, 3975 (1987).
17. M. Sundaram, A. Sivaprasadarao, M. M. DeSousa, J. B. Findlay, *J. Biol. Chem.* **273**, 3336 (1998).
18. D. E. Ong, P. N. MacDonald, A. M. Gubitosi, *J. Biol. Chem.* **263**, 5789 (1988).
19. F. M. Herr, D. E. Ong, *Biochemistry* **31**, 6748 (1992).
20. M. H. Boerman, J. L. Napoli, *J. Biol. Chem.* **266**, 22273 (1991).
21. S. Ottonello, G. Scita, G. Mantovani, D. Cavazzini, G. L. Rossi, *J. Biol. Chem.* **268**, 27133 (1993).
22. M. H. Boerman, J. L. Napoli, *J. Biol. Chem.* **271**, 5610 (1996).
23. Y. S. Kuppumbatti, I. J. Bleiweiss, J. P. Mandeli, S. Waxman, R. Mira-Y-Lopez, *J. Natl. Cancer Inst.* **92**, 475 (2000).
24. Y. S. Kuppumbatti, B. Rexer, S. Nakajo, K. Nakaya, R. Mira-y-Lopez, *Oncogene* **20**, 7413 (2001).
25. M. Esteller, *et al.*, *Cancer Res.* **62**, 5902 (2002).
26. D. Roberts, *et al.*, *DNA Cell Biol* **21**, 11 (2002).
27. A. Schmitt-Graff, *et al.*, *Hepatology* **38**, 470 (2003).
28. S. W. Cowan, M. E. Newcomer, T. A. Jones, *J. Mol. Biol.* **230**, 1225 (1993).
29. L. Franzoni, *et al.*, *J. Biol. Chem.* **277**, 21983 (2002).
30. In the first spectrum shown blue, only one signal at the resonance frequency of apo-CRBP is observed. For successive titration steps and addition of the ligand retinol, the intensity of the signal of apo-CRBP decreases whereas a signal at the resonance frequency of holo-CRBP appears reflecting the increasing population of the complex.
31. Protein samples were prepared as described previously. For NMR measurements, samples of 1 mm ¹⁵N-labeled CRBP I were prepared in 0.1 M potassium phosphate buffer (20 mM, pH 6.0, 90D₂O) in a sample volume of 500 μ l.

32. Retinol was solubelized in deuterated methanol (CD_3OD) and added to the ^{15}N -labeled CRBP sample in small steps, typically $5\ \mu\text{l}$ per step. After each addition, a high-resolution sensitivity enhanced $^1\text{H}/^{15}\text{N}$ -HSQC spectrum was recorded with 2048×700 data points at 11.7 T and a temperature of 298 K. In a total, 8 spectra were collected during the titration. For residues which were not subject to chemical shift degeneracy, cross-sections in both spectral dimensions were extracted from all spectra. Line shapes for both dimensions were simulated simultaneously for the set of 8 spectra as described in [1, 11].
33. In the slow-exchange regime, only an upper limit of the off-rate can be assigned because the line shapes depend on the rate only slightly.
34. CD_3OD was added to apo-CRBP in steps of $5\ \mu\text{l}$. High resolution $^1\text{H}/^{15}\text{N}$ -HSQC spectra were recorded with the same specifications as for the titration with retinol. Line shapes were extracted for each residue and compared to the line shapes obtained for the titration with retinol. If direction and extent of chemical shift changes were similar in both titrations the effect was attributed to CD_3OD rather than retinol.
35. J. C. Sacchettini, J. I. Gordon, L. J. Banaszak, *J. Mol. Biol.* **208**, 327 (1989).
36. J. Lu, D. P. Cistola, E. Li, *J. Mol. Biol.* **330**, 799 (2003).
37. T. Mittag, L. Franzoni, D. Cavazzini, G.-L. Rossi, U. L. Günther, *Structure, Dynamics and Function of Biological Macromolecules and Assemblies* (IOS Press B. V., Amsterdam, 2003), chap. Novel insights into the mechanism of retinol binding by cellular retinol-binding protein.
38. Ps-ns mobility was observed for α -helix I, for turns $\beta\text{B}-\beta\text{C}$, $\beta\text{C}-\beta\text{D}$, $\beta\text{E}-\beta\text{F}$, $\beta\text{F}-\beta\text{G}$ and for βI . [29].
39. We observe the highest exchange contributions for residues E17 in α -helix I, D24 in the turn between α -helix I and α -helix II, R30, I32 and N34 in α -helix II and S55, T56, F57, R58 and N59 in turn $\beta\text{C}-\beta\text{D}$. These residues all belong to the putative portal. Signals of residues in turn $\beta\text{E}-\beta\text{F}$, which also frame the putative entrance, are not detectable in spectra of apo-CRBP, most likely as a consequence of extensive conformational exchange.
40. The time dependence of the chemical exchange causes an accelerated dephasing of the transverse coherence of the spin reflected in an increased relaxation rate R_2 . The effective relaxation rate R_2 is the sum of the relaxation rate in the absence of exchange, R_2^0 , and the exchange contribution R_{ex} ($R_2 = R_2^0 + R_{\text{ex}}$). The exchange contribution R_{ex} can be separated from R_2^0 because chemical exchange can be refocused by reversing the precession direction of the spins using spin echoes. The dependence of

R_2 on the refocusing frequency ν_{cp} in CPMG experiments is called relaxation dispersion and allows the quantification of the exchange process. Relaxation dispersion depends on the exchange rate k_{ex} between partners, the populations of the two partners and their chemical shift difference $\Delta\omega$ (because $\Delta\omega$ also determines the dephasing speed).

41. CPMG measurements were performed on the backbone amide resonances of apo-CRBP to characterize its conformational flexibility on the μs - ms time scale. All nmr spectra were recorded at 298 K. Relaxation dispersion experiments were carried out at two static magnetic fields, 11.7 and 16.4 T. A relaxation compensated CPMG experiment was performed in a constant time manner [4] to obtain effective transverse relaxation rates R_2 over a wide range of refocusing rates ν_{cp} . Spectra were collected as a series of 20 2D spectra with CPMG field strengths, ν_{cp} , of 17, 33, 50, 67, 83, 100, 117, 133, 167, 200, 233, 267, 333, 400, 467, 533, 600 and 667 Hz. Repeated experiments were performed at 100 and 533 Hz. The constant time period was set to 60 ms; the reference experiment was obtained by omitting the CPMG period. Spectra were acquired with at least 1024 x 128 complex points. Processing and analysis of the NMR spectra were performed using NMRlab [49].
42. Solving the modified Bloch or McConnell equations, a general expression for the phenomenological transverse relaxation rate constant in the case of two-site exchange can be obtained [50–53]: The refocusing field is related to the delay $2\tau_{cp}$ between two 180° pulses in the CPMG pulse train according to $\nu_{cp} = \frac{1}{4\tau_{cp}}$. The relaxation dispersion curves of both fields were fitted simultaneously to the general equation on a per residue basis, assuming proportionality between $\Delta\omega$ and the static magnetic field to extract the exchange parameters.
43. The exchange regime is indicated by the ratio $k_{ex}/\Delta\omega$ and confirmed by the value of α . The dependence of R_{ex} on the static magnetic field strength B_0 , α gives an estimate of the time regime of an exchange process [54]. In the case of slow exchange, α assumes values between 0 and 1, for fast exchange it is between 1 and 2 and at a value of 1, we encounter intermediate exchange. Since the time regime detected by relaxation dispersion is determined by the ratio of $k_{ex}/\Delta\omega$, which is determined independently of α in the data analysis, this parameter is useful to assess the consistency of the data analysis when relaxation dispersion was measured at different field strengths.
44. The exchange contribution R_{ex} to the effective relaxation rate R_2 is obtained from the difference of the effective transverse relaxation rate constants in the absence and presence of a high refocusing field, $R_{ex} = R_2(\nu_{cp} \rightarrow 0) - R_2(\nu_{mc} \rightarrow \infty)$.

45. 121 of 134 residues in the free CRBP protein were accessible to relaxation dispersion analysis, whereas for the others no information was available due to spectral overlap or missing assignments (as for residues E72-G76 and D79-R80 in the β E- β F turn).
46. R. Koradi, M. Billeter, K. Wüthrich, *J. Mol. Graph.* **14**, 51 (1996).
47. Analysis of relaxation dispersion curves recorded at 500 and 700 MHz showed equal populations for 26 of 78 residues in apo CRBP I. For 52/78 residues skewed populations with a population of 88observed. The role of the *beta*E- and β F loop could not be quantified although significant conformational exchange must be assumed. Fast exchange was found for most residues indicated by the ratio $k_{ex}/\delta\omega$ and confirmed by the value of α .
48. Only residues R58 in turn β C- β D and L74 and D79 in the β E- β F turn exhibit a slight dependence of R_2 on ν_{cp} (indicating a chemical exchange process on the ms time scale). for residues N15, V27, I61, G76, E100 and G112 exchange on a faster μ s time scale is likely because R_2 is enhanced though it does not depend on the refocusing rate.
49. U. Günther, C. Ludwig, H. Rüterjans, *J. Magn. Reson.* **145**, 201 (2000).
50. Z. Luz, S. Meiboom, *J. Chem. Phys.* **39**, 366 (1963).
51. J. P. Carver, R. E. Richards, *J. Magn. Reson.* **6**, 89 (1972).
52. J. Jen, *J. Magn. Reson.* **30**, 111 (1978).
53. D. G. Davis, M. E. Perlman, R. E. London, *J. Magn. Reson. B* **104**, 266 (1994).
54. O. Millet, J. P. Loria, C. D. Kroenke, M. Pons, A. G. Palmer, *J. Am. Chem. Soc.* **122**, 2867 (2000).
55. This work was supported by the European Large Scale Facility Frankfurt (UNIFRANMR), by a stipend of the German National Academic Foundation (T.M.) and by grants from the NIH to B.S.

Lebenslauf

Zur Person

Tanja Mittag, geb. Weber

geb. am 13.06.1977 in Mainz, Deutschland

verheiratet mit Roland Mittag, kaufmännischer Angestellter

Schulbildung

1983 - 1987

Weinbergschule, Grundschule in Hochheim

1987 - 1989

Heinrich von Brentano-Schule, integrierte Gesamtschule in Hochheim

1989 - 1996

Oranienschule, Gymnasium in Wiesbaden

Juni 1996

Abitur mit der Note 1,0

Studium

1996 - 2001

Studium der Biochemie an der Johann Wolfgang Goethe-Universität in Frankfurt

September 1998

Diplom-Vorprüfung

September 2000

Diplom-Hauptprüfung

Sept 2000 - Jan 2001

Diplomarbeit am Institut für Biophysikalische Chemie mit dem Thema "NMR-Struktur der freien N-terminalen SH2-Domäne der p85-Untereinheit der PI3-Kinase und des Komplexes mit einem doppelt phosphorylierten Peptid", Betreuer Prof. Dr. H. Rüterjans

Januar 2001

Diplom mit Auszeichnung

Feb 2001 - heute

Promotion am Institut für Biophysikalische Chemie mit dem Thema "Functional Dynamics of Protein-Ligand Interactions", Betreuer PD Dr. U. Günther

Auszeichnungen

Juni 1996

Auszeichnung des Fonds der Chemischen Industrie für das beste Chemie-Abitur

November 2001

Procter & Gamble Diplom-Förderpreis

Vortrag

April 2004 “Dynamics of protein-ligand interactions” auf der 45. ENC (Experimental Nuclear Magnetic Resonance Conference) in Asilomar, Kalifornien, USA

Stipendien

1999 - 2000 Stipendium der Studienstiftung des deutschen Volkes

2001 - 2004 Promotionsstipendium der Studienstiftung des deutschen Volkes

Lehrerfahrung

2000 - 2002 Organisation des Praktikums “Biophysikalische Chemie für Fortgeschrittene”

2000 - 2003 Betreuung des Versuchs “Lösungsstruktur eines kleinen Peptids mittels 2D-NMR-Spektroskopie”

2001 - 2002 Übungen zur Vorlesung “Biophysikalische Chemie I - Thermodynamik”

Meine akademischen Lehrer waren:

E. Bamberg, L. Banci, J. Bereiter-Hahn, V. Dötsch, E. Egert, J. Engels, K.-D. Entian, H. Fasold, J. Feierabend, K. Fendler, L. Franzoni, C. Griesinger, M. Göbel, U. Günther, K. Hainer, B. Kolbesen, A. Kröger, G. Lambrecht, R. Lancaster, B. Ludwig, H. Michel, W. Müller, R. Prinzing, G.-L. Rossi, H. Rüterjans, B. Schaffhausen, H. Schwalbe, J. Soppa, H. Steiger, C. Winter, H. Zimmermann

Publikationsliste

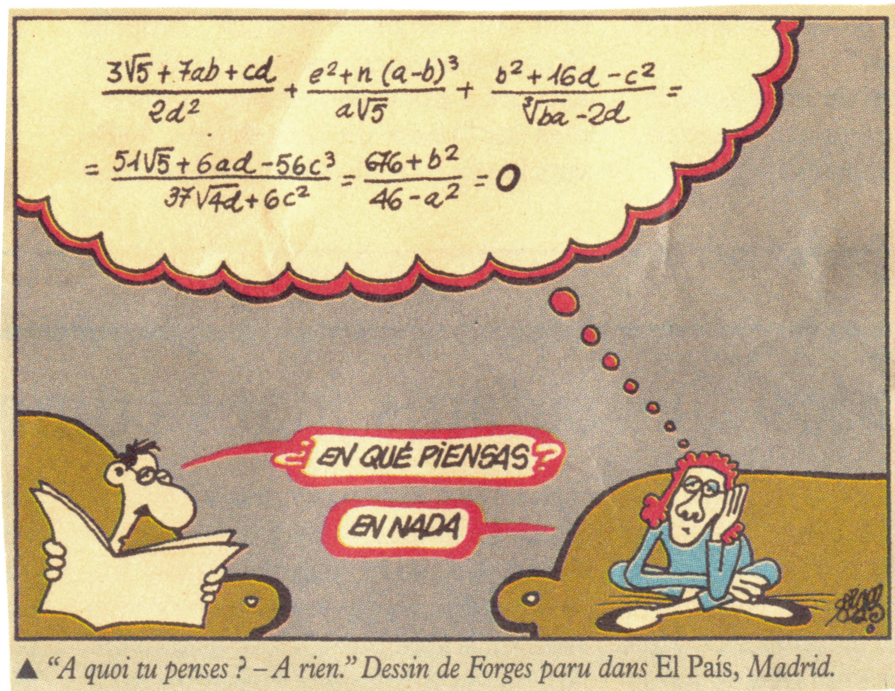
1. **Weber, T.**, Schaffhausen, B., Liu, Y., and Günther, U. (2000) NMR structure of the N-SH2 Domain of the p85 Subunit of Phosphatidylinositide 3-Kinase Complexed to a Doubly Phosphorylated Peptide Reveals a Second Phosphotyrosine Binding Site. **Biochemistry** 39, 15860-15869
2. Günther, U., **Mittag, T.**, and Schaffhausen, B. (2002) Probing Src Homology 2 Domain Ligand Interactions by Differential Line Broadening. **Biochemistry** 41, 11658-11669
3. **Mittag, T.**, Schaffhausen, B., and Günther, U. (2003) Direct Observation of Protein Ligand Interaction Kinetics. **Biochemistry** 42, 11128-11136
4. **Mittag, T.**, Schaffhausen, B., and Günther, U. (2004) Tracing Kinetic Intermediates during Ligand Binding, **J. Am. Chem. Soc.** 126, 9017-9023
5. **Mittag, T.**, Franzoni, L., Cavazzini, D., Rossi, G.-L., and Günther, U. (2004) **Book chapter**: Novel Insights into the Mechanism of Retinol Binding to the Cellular Retinol-Binding Protein, in Structure, Dynamics and Function of Biological Macromolecules and Assemblies (Ed. J. Puglisi), IOS Press, Amsterdam
6. **Mittag, T.**, Franzoni, L., Cavazzini, D., Schaffhausen, B., Rossi, G.-L., and Günther, U. L. (2004) Freezing of Conformers of the Cellular Retinol-Binding Protein by Retinol, in preparation

Eidesstattliche Versicherung

Ich erkläre hiermit an Eides statt, dass ich die vorgelegte Dissertation über “Functional Dynamics of Protein-Ligand Interactions (Funktionelle Dynamik von Protein-Liganden-Wechselwirkungen)” selbständig angefertigt und mich anderer Hilfsmittel als der in ihr angegebenen nicht bedient habe. Ich erkläre weiterhin, dass Entlehnungen aus Schriften, soweit sie in der Dissertation nicht ausdrücklich als solche bezeichnet sind, nicht stattgefunden haben. Ich habe bisher an keiner anderen Universität ein Gesuch um Zulassung zur Promotion eingereicht oder die vorliegende oder eine andere Arbeit als Dissertation vorgelegt.

Frankfurt am Main, den 23. August 2004

Tanja Mittag



vor Jahren von meiner Freundin Marianne erhalten...